


8-2015

ANKYRIN-B AND mTOR COMPLEX 1 IN THE REGULATION OF ELECTRICAL ACTIVITIES IN THE HEART

Henry C. Wu

Henry C. Wu

Follow this and additional works at: http://digitalcommons.library.tmc.edu/utgsbs_dissertations

 Part of the [Cardiovascular Diseases Commons](#), [Circulatory and Respiratory Physiology Commons](#), [Congenital, Hereditary, and Neonatal Diseases and Abnormalities Commons](#), [Disease Modeling Commons](#), and the [Translational Medical Research Commons](#)

Recommended Citation

Wu, Henry C. and Wu, Henry C., "ANKYRIN-B AND mTOR COMPLEX 1 IN THE REGULATION OF ELECTRICAL ACTIVITIES IN THE HEART" (2015). *UT GSBS Dissertations and Theses (Open Access)*. Paper 620.

This Dissertation (PhD) is brought to you for free and open access by the Graduate School of Biomedical Sciences at DigitalCommons@The Texas Medical Center. It has been accepted for inclusion in UT GSBS Dissertations and Theses (Open Access) by an authorized administrator of DigitalCommons@The Texas Medical Center. For more information, please contact laurel.sanders@library.tmc.edu.

ANKYRIN-B AND mTOR COMPLEX 1 IN THE REGULATION OF ELECTRICAL
ACTIVITIES IN THE HEART

by

Henry Wu, B.A.

APPROVED:

Shane Cunha, Ph.D.

Supervisory Professor

Russell Broaddus, M.D., Ph.D.

Mong-Hong Lee, Ph.D.

Ruth Heidelberger, M.D., Ph.D.

Dat Tran, M.D.

APPROVED:

Dean, The University of Texas

Graduate School of Biomedical Sciences at Houston

ANKYRIN-B AND mTOR COMPLEX 1 IN THE REGULATION OF ELECTRICAL
ACTIVITIES IN THE HEART

A DISSERTATION

Presented to the Faculty of The University of Texas Health Science Center at Houston

Graduate School of Biomedical Sciences

In Partial Fulfillment

Of the Requirements

For the Degree of

DOCTOR OF PHILOSOPHY

by

Henry Cheng-Ju Wu, B.A.

Houston, Texas

August 2015

DEDICATION

This thesis is dedicated to my parents, my lovely wife and my other set of parents, my beautiful daughter, and my competitive brother.

To my parents, who instilled in me a strong work ethic, diligence, and perseverance at a young age that have helped me along my life and educational journey especially in trying times. Their constant love, sacrifice, and unquestioned support provided me with the foundation to all of my accomplishments.

To my wife, who always stood by me no matter the circumstances and told me exactly what I needed to hear to get through the difficult times. Her constant encouragement and guidance kept me focused and helped me achieve more than I ever thought I could. And I can never thank her enough for creating the newest member of our family and being the best wife and mother.

To my other set of parents, who work tirelessly to provide my new family with the stability it needs to blossom. Their dedication and belief in me gave me the drive I needed to reach for the stars and pursue all of my dreams.

To my baby daughter, whose toothless smiles made all the long work hours seem insignificant.

Lastly, to my brother, whose amazing achievements always set the standard and inspired me to emulate.

ACKNOWLEDGMENTS

Without all of the support I received throughout this training process, I would not have completed this part of my educational journey. While it is impossible to enumerate everyone who has in one way or the other contributed to the work I have done, I would like to use this opportunity to express my gratitude toward those who have impacted me the most.

First and foremost, I thank Dr. Shane Cunha for offering me an opportunity to get involved in a very exciting project in his lab. He has always been an advocate of my science and work by supporting the experiments I proposed even if the experiments were outside his main research aims. He also constantly reaffirms my qualities as an upcoming medical scientist even when circumstances shake my beliefs and confidence. He spends much time sharing many of his scientific methods with me and exercising my logic with debates on many topics outside of science ranging from politics and government to proper pet care to help mold me into a well-rounded critical thinker. Even though he does not always have an appreciation for a great sense of humor, he nevertheless always manages to have fun intellectual discussions about my methods and results. He inspires me like a mentor, supports me like an uncle, and challenges me like a brother.

I also would like to thank all the faculty members that served on my committees during my graduate school training. Dr. Broaddus, thank you for always being encouraging of my project ideas, supportive of my work, and the chair on my exam committee. Also, seeing your journey from a MD/PhD trainee here at UT Houston to an esteemed professor at MD Anderson helped create an unshakable belief in me that I too can one day complete the MD/PhD training and have a successful career. Dr. Heidelberger, thank you for being my MD/PhD program advisor for the past decade and helping me deal with times of transition. Also, thank you for teaching me how to perform calcium recording on cells during my rotation and allowing me to use the scope for my cardiomyocyte experiments. Dr. Lee, thank you for teaching me mTOR signaling and metabolism that turned out to be an important aspect of my thesis work and thank you for sharing your experiences and meaningful discussions about your work on cancer. I will always remember the analogy you drew between cell cycle and the four seasons. Dr. Tran, thank you for always being there to support me with my progression through graduate school and for letting me use the scope to advance my work. I also will remember and heed your advice for my future on the medical side. Dr. Nathan Bryan, although you have left the institution, the work we did together on the TSC mouse brain may very well lead to the development of my future project ideas.

To other faculty members who have helped my scientific growth at different stages. I thank Dr. Michael Gambello for showing me how to perform animal experiments correctly and use the animal models to propel my science forward. I appreciate the much needed hand-holding in the beginning stage of the graduate school training. Dr. Taegtmeier, thank you for helping me develop a very interesting project that was funded by the institutional center for clinical and translational sciences grant. More importantly, I appreciate your showing me the *in vivo* and *ex vivo* techniques that were critical to the completion of my paper and thesis project. I also want to thank all the faculty members in the Cell and Regulatory Biology program and for their helpful comments and suggestions in group and individual meetings that have contributed to the completion of my thesis.

Finally, I have to thank all the friends I made during my graduate school training who have all taught me something or another in order to help me finish an experiment, accomplish a goal, or simply how to have fun in times of stress. I thank you all for being there to walk the journey with me.

ANKYRIN-B AND mTOR COMPLEX 1 IN THE REGULATION OF ELECTRICAL ACTIVITIES IN THE HEART

Henry Wu, B.A.

Supervisory Professor: Shane Cunha, Ph.D.

The mammalian target of rapamycin complex 1 (mTORC1) activity is paramount in the regulation of electrical activities in the brain and the heart. In the brain, the tumor suppressor gene *TSC2* encodes the protein product tuberin that interacts with hamartin to form a heterodimer Tuberous Sclerosis Complex (TSC) that regulates mTORC1. When *TSC2* is disrupted, mTORC1 activity becomes dysregulated resulting in abnormal electrical activities in the brain manifesting in the form of epileptic seizures. In the heart, mTORC1 activity is triggered by a sustained increase in hemodynamic pressure causing the heart to electrically remodel. A likely candidate serving as the mediator between mTORC1-dependent electrical remodeling in the brain and heart is the adaptor protein ankyrin. In the heart, ankyrin-B targets and maintains the membrane expression of ion channels and transporters that are critical for maintaining calcium ion homeostasis, which underlies normal excitation-contraction coupling. Sustained mTORC1 activity in the heart decreases the expression of ankyrin-B and alters the electrical conductance between the atria and ventricles. These effects are reversed with the administration of

the mTORC1 inhibitor rapamycin. In addition, we identified and characterized two functionally and spatially distinct full-length ankyrin-B isoforms – AnkB-188 and AnkB-212. AnkB-188 selectively interacts with the sodium-calcium exchanger (NCX1) increasing its membrane expression, overall current, and targeting to the sarcoplasmic reticulum/transverse-tubule of neonatal cardiomyocytes. Whereas AnkB-212 does not increase NCX1 membrane expression or current, but uniquely localizes to the sarcomeric M-line. Knockdown of either isoform results in abnormal contraction rhythms *in vitro*, but only the M-line population appears to be regulated by mTORC1. Collectively, the data support the hypothesis that mTORC1 regulates electrical remodeling of the stressed heart by decreasing the expression of the ankyrin-B population at the M-line.

TABLE OF CONTENTS

DEDICATION.....	iii
ACKNOWLEDGMENT.....	iv
ABSTRACT.....	vi
LIST OF FIGURES.....	xiv
LIST OF TABLES.....	
LIST OF ABBREVIATIONS.....	
CHAPTER 1: INTRODUCTION	
1.1 Scope of the Dissertation.....	2
1.2 Hemodynamic Load-Induced Structural and Functional Remodeling.....	5
1.3 mTOR Signaling in the Heart.....	8
1.4 Overactive mTORC1 Underlies Electrical Changes in the Brain.....	12
1.5 Ion Channels and the Adaptor Protein Ankyrin.....	14
1.6 Ankyrin and the Heart.....	18
CHAPTER 2: THE DIFFERENTIAL EFFECTS OF PRENATAL AND/OR POSTNATAL RAPAMYCIN ON NEURODEVELOPMENTAL DEFECTS AND COGNITION IN A NEUROGLIAL MOUSE MODEL OF TUBEROUS SCLEROSIS COMPLEX	
2.1 Introduction.....	23

2.2	Materials and Methods.....	25
2.2.1	Animals.....	25
2.2.2	Rapamycin treatment regimen.....	25
2.2.3	Western analysis, histology and immunohistochemistry..	26
2.2.4	Quantitative analysis.....	26
2.3	Results.....	27
2.4	Discussion.....	50
 CHAPTER 3: mTORC1 ACTIVATION INDUCED ARRHYTHMOGENESIS		
3.1	Introduction.....	55
3.2	Materials and Methods.....	58
3.2.1	Pressure-overloaded model (transverse aortic constriction).....	62
3.2.2	Mouse EKG monitor and analysis.....	63
3.2.3	Isolation of adult mouse cardiomyocytes.....	65
3.2.4	Isolation of neonatal rat ventricular cardiomyocytes.....	66
3.2.5	Tissue and cell protein extraction and quantification.....	68
3.2.6	Immunoblot assay.....	69
3.2.7	Fluorescent immunocytochemistry.....	70
3.2.8	NRVM RNA interference experiments.....	70
3.2.9	Measurements of mRNA expression.....	72
3.2.10	NRVM syncytium contraction recording and analysis.....	72
3.3	Results	
3.3.1	Electrical remodeling in response to chronic load-induced hemodynamic stress <i>in vivo</i>	75
3.3.2	Ankyrin protein expression changes in response to chronic load-induced hemodynamic stress and mTORC1 inhibition.....	77

3.3.3	Effects of <i>in vitro</i> mTORC1 activation on ankyrin-B expression.....	84
3.3.4	<i>In vitro</i> mTORC1 activation alters ankyrin-B subcellular expression.....	86
3.3.5	Physiologic consequences of <i>in vitro</i> mTORC1 activation.....	89
3.4	Discussion.....	91

CHAPTER 4: IDENTIFICATION AND CHARACTERIZATION OF TWO ANKYRIN-B ISOFORMS IN MAMMALIAN HEART

4.1	Introduction.....	97
4.2	Materials and Methods.....	99
4.2.1	Animals.....	99
4.2.2	Human tissue samples.....	99
4.2.3	Isolation and cloning of full-length <i>ANK2</i> transcripts from human ventricular mRNAs.....	99
4.2.4	Quantitative real-time (qt)-PCR analysis of <i>ANK2</i> transcripts.....	103
4.2.5	AnkB-212 antibody generation.....	104
4.2.6	Tissue immunoblot assay.....	104
4.2.7	Cellular fractionation immunoblot assay.....	105
4.2.8	Isolation of neonatal mouse hearts and cultures of neonatal rat ventricular cardiomyocytes.....	105
4.2.9	siRNA construct and NRVM transfections.....	106
4.2.10	Isolation of individual adult mouse cardiomyocytes.....	107
4.2.11	Fluorescent immunocytochemistry and image quantification.....	108
4.2.12	Binding studies.....	108
4.2.13	Patch-clamp recording.....	109

4.2.14	Recording and analysis of NRVM contraction rates.....	110
4.2.15	Statistical analysis.....	111
4.3	Results.....	111
4.3.1	Identification and cardiac expression of ankyrin-B isoforms.....	112
4.3.2	AnkB-188 and AnkB-212 binding to NCX.....	118
4.3.3	AnkB-188 increases NCX membrane expression and current.....	119
4.3.4	AnkB-212 is selectively expressed in heart and skeletal muscle.....	122
4.3.5	Endogenous AnkB-212 is expressed at the cardiomyocyte M-line.....	124
4.3.6	Exogenous AnkB-212 is targeted to the M-line via an interaction with obscurin.....	127
4.3.7	AnkB-188 knockdown decreases the expression and proper subcellular localization of NCX.....	131
4.3.8	AnkB-188 and AnkB-212 knockdown causes different arrhythmic contraction patterns.....	138
4.4	Discussion.....	140

CHAPTER 5: CONCLUDING CHAPTER

5.1	Summary of results and perspectives.....	146
5.2	Future experiments.....	152
	REFERENCES.....	156

APPENDIX: GLUCOSE REGULATION OF LOAD-INDUCED mTOR SIGNALING

A.1	Introduction.....	178
A.2	Materials and Methods.....	179
A.2.1	Rationale for animal models used and overall strategy..	181
A.2.2	Experimental groups.....	182
A.2.3	Isolated working rat heart perfusions.....	182
A.2.4	Cardiac power, oxygen consumption, metabolic rates, metabolite concentrations.....	183
A.2.5	PET and MRI imaging.....	184
A.2.6	Transgenic mice overexpressing cardiac-specific isoform of SERCA2a.....	186
A.2.7	Tissues from failing human hearts.....	187
A.2.8	Western blot analyses.....	188
A.2.9	RNA extraction and qRT-PCR.....	189
A.3	Results.....	189
A.3.1	mTORC1 activation and impaired cardiac power with increased workload.....	189
A.3.2	Oxygen utilization and mitochondrial efficiency were not affected by increased workload or rapamycin treatment.....	193
A.3.3	Glucose 6-phosphate (G6P) and mTOR activation.....	195
A.3.4	G6P-dependent mTOR activation and AMPK downregulation.....	200
A.3.5	Metabolic, structural, and signaling remodeling in response to increased workload <i>in vivo</i>	204
A.3.6	Structural and functional remodeling in response to increased workload <i>in vivo</i>	207
A.3.7	Failing human hearts before and after unloading with a left ventricular assist device.....	210

A.4	Discussion.....	212
A.5	References.....	220
VITA.....		225

LIST OF FIGURES

- Figure 1.1 Conditions leading to physiologic versus pathologic cardiac growth
- Figure 1.2 The mTOR signaling network
- Figure 1.3 Organization of domains of a prototypical ankyrin
- Figure 1.4 Proposed model of mTORC1 regulation of neuronal excitability
-
- Figure 2.1 Prenatal, postnatal and combined rapamycin treatments improved health, weight gain, and longevity
- Figure 2.2 Effects of daily 0.1mg/kg rapamycin treatment regimens on cortical histology and organization
- Figure 2.3 Effects of daily 0.1mg/kg rapamycin treatment regimens on cortical lamination
- Figure 2.4 Effects of daily 0.1mg/kg rapamycin treatment regimens on astrocytes, oligodendroglia and myelination
- Figure 2.5 Effects of 2mg/kg rapamycin i.p. on longevity and weight of Tsc2-hGFAP mice
- Figure 2.6 Effects of rapamycin treatments on learning and memory
- Figure 2.7 Visual and motor control tasks for Morris water maze
- Figure 2.8 Effects of 2mg/kg rapamycin on cortical phosphorylated S6 levels and GFAP expression after behavioral testing
- Figure 2.9 Brain histology after 2mg/kg rapamycin and behavior testing
-
- Figure 3.1 Three different sets of mice were utilized for the *in vivo* experiments
- Figure 3.2 Three different sets of treatment were utilized for the *in vitro* experiments
- Figure 3.3 An example of each of the three parameters measured for each cardiac cycle from the animal EKG recordings.
- Figure 3.4 Example of marker displacement tracking

- Figure 3.5 mTORC1 activity and electrical remodeling in hearts subjected to high workload *in vivo*
- Figure 3.6 Effects of *in vivo* pressure overload on ankyrin-B, -G, and -R
- Figure 3.7 Selective mTORC1 activation reduces ankyrin-B expression *in vitro*
- Figure 3.8 Selective mTORC1 activation changes ankyrin-B expression differently at different subcellular domains *in vitro*
- Figure 3.9 mTORC1 activation leads to arrhythmic contractions of NRVMs *in vitro*
- Figure 3.10 Proposed model for mTORC1 regulation of two subpopulations of ankyrin-B
-
- Figure 4.1 Exon composition and protein domains of ankyrin-B isoforms AnkB-188 and AnkB-212
- Figure 4.2 Relative mRNA expression of AnkB-188 and AnkB-212 in human and mouse cardiac tissues
- Figure 4.3 Both AnkB-188 and AnkB-212 bind NCX
- Figure 4.4 AnkB-188, but not AnkB-212, increases NCX current and membrane expression
- Figure 4.5 Expression of pan-AnkB and AnkB-212 in various tissues
- Figure 4.6 AnkB and AnkB-212 endogenous localizations in adult cardiomyocytes
- Figure 4.7 Expression of pan-AnkB and AnkB-212 in isolated AnkB^{+/-} adult cardiomyocytes
- Figure 4.8 AnkB-212, but not AnkB-188, binds to obscurin
- Figure 4.9 AnkB-212 is targeted to the M-line of cardiomyocytes
- Figure 4.10 AnkB-212 CTD ΔE46 lacks obscurin-binding and M-line targeting
- Figure 4.11 AnkB-188 knockdown decreases the expression of NCX
- Figure 4.12 AnkB-188 knockdown decreases NCX Z-line localization
- Figure 4.13 AnkB-188 and AnkB-212 knockdown precipitates different contraction irregularities

- Figure 4.14 Summary model of the subcellular domain localization of the two full-length ankyrin-B isoforms
- Figure A.1 At high workload, glucose activates mTORC1 and impairs cardiac power in perfused rat hearts
- Figure A.2 Pretreatment with rapamycin has no effect on cardiac efficiency in rat hearts perfused with glucose at high workload
- Figure A.3 Uncoupling protein 3 (UCP3) mRNA and protein levels are not associated with G6P-mediated mammalian target of rapamycin (mTOR) activation
- Figure A.4 In response to high workload, rates of glucose uptake exceed rates of glucose oxidation, hexose 6-phosphate accumulates, and mTOR is activated
- Figure A.5 In the presence of mixed substrates (glucose, NCS, and oleate), G6P levels are increased and mTORC1 signaling is activated at high workload
- Figure A.6 G6P-dependent mTOR activation is associated with downregulation of AMPK
- Figure A.7 Metabolic remodeling and mTOR activation precede structural remodeling in hearts subjected to high workload *in vivo*
- Figure A.8 *In vivo* structural and functional changes accompany metabolic changes in response to pressure overload
- Figure A.9 Mechanical unloading of failing human hearts results in reduced G6P accumulation and reduced mTORC1 activation
- Figure A.10 Proposed mechanism by which G6P accumulation regulates load-induced mTORC1 activation

LIST OF TABLES

Table 4.1	<i>ANK2</i> qt-PCR primer sequences
Table 4.2	siRNA sequences targeting rat <i>Ank2</i>
Table 4.3	Summary of the experiments and findings
Table A.1	<i>Ex vivo</i> perfusion protocols containing four different sets of rats used to study glucose regulated mTOR activation at high workload
Table A.2	Clinical data: samples from failing human hearts
Table A.3	Comparison of baseline and day 1 values for different parameters among TAC mice

ABBREVIATIONS

2DG	2-deoxyglucose
3OMG	3-O-methylglucose
4E-BP1	eukaryotic initiation factor 4E binding protein 1
ACC	acetyl-CoA carboxylase
AMPK	5' AMP-activated protein kinase
Ank	ankyrin
ANK1	ankyrin-R
ANK2/AnkB	ankryin-B
ANK3	ankyrin-G
AIS	axon initial segment
BrdU	bromodeoxyuridine
CA1	cornu ammonis 1
CA3	cornu ammonis 3
CaMKII	calcium/calmodulin-dependent kinase II
CTD	c-terminal domain
DEPTOR	DEP domain-containing mTOR-interacting protein
DD	death domain
DG	dentate gyrus
EDV	end diastolic volume
EF	ejection fraction
eIF-4E	eukaryotic initiation factor 4E
EKG	electrocardiogram
ER	endoplasmic reticulum
ESV	end systolic volume

FDG	2-deoxy, 2[¹⁸ F]fluorodeoxy-glucose
FKBP12	FK506-binding protein 12
G6P	glucose 6-phosphate
GABA	γ-aminobutyric acid
GFAP	glial fibrillary acidic protein
GluN2C	Glutamate receptor inotropic, NMDA 2c
GSK-3β	glycogen synthase kinase 3β
H&E	hematoxylin and eosin
HW/BW	heart weight to body weight ratio
IP	intraperitoneal
IP ₃ R	inositol 1,4,5-trisphosphate receptor
Kir	inward-rectifier potassium channel
K _v	voltage-gated potassium channel
L1-CAM	L1-cell adhesion molecule
LOH	loss of heterozygosity
LVAD	left ventricular assist device
LVEDD	left ventricular end-diastolic dimension
MBD	membrane-binding domain
MBP	myelin basic protein
MF	metformin
mLST8	mammalian lethal with Sec13 protein 8
mTOR	mammalian target of rapamycin
mTORC1	mammalian target of rapamycin complex 1
mTORC2	mammalian target of rapamycin complex 2
mW	milliwatt

MyBP-C	myosin-binding protein C
MZ	marginal zone
NADP	nicotinamide adenine dinucleotide phosphate
Na _v	voltage-gated sodium channel
NCS	non-carbohydrate substrate
NCX1	sodium calcium exchanger 1
NKA	sodium potassium ATPase
NRVM	neonatal rat ventricular (cardio)myocytes
OBD	obscurin-binding domain
Obs	obscurin
p70S6K	ribosomal protein p70 S6 kinase
PET	positron emission tomography
PI3K	phosphatidylinositol-3 kinase
PKB	protein kinase B/Akt
PRAS40	proline-rich Akt substrate 40 kDa
PTEN	phosphatase and tensin homologue
RAPTOR	regulatory associated protein of mTOR
Rheb	Ras homolog enriched in brain
RICTOR	rapamycin-insensitive companion of mTOR
S6	ribosomal protein S6
SA	sinus atrial
SBD	spectrin-binding domain
SC	subcutaneous
SEGA	subependymal giant cell astrocytomas
SERCA2a	sarco/endoplasmic reticulum calcium ATPase

SLM	stratum lacunosum moleculare
SO	stratum oriens
SR/T-tubule	sarcoplasmic reticulum/transverse-tubule
TAC	transverse aortic constriction
TSC	Tuberous Sclerosis Complex
TSC1	hamartin
TSC2	tuberin
UCP3	uncoupling protein 3

CHAPTER 1: INTRODUCTION

1.1 Scope of the Dissertation

This thesis addresses molecular mechanisms of heart failure and arrhythmia. The topic is important because of the two following reasons:

First, heart failure is a leading cause of death and disability in the United States [10]. Over the past several decades, advances in pharmaceutical therapies and acute interventions have decreased the incidence of coronary artery disease and myocardial infarction, yet the prevalence of heart failure has steadily risen. Currently, around 5 million Americans suffer from heart failure, over a million patients are hospitalized because of it, and 300,000 die from consequences of heart failure, with fatal cardiac arrhythmias being a major consequence [11-13]. To put the numbers in perspective, death from heart failure exceeds deaths from all forms of cancer combined [14], and that number is expected to double in the next decade [10].

Second, despite many advances in different areas of cardiovascular medicine and heart disease management shifts from an acute to a chronic setting, symptomatic treatment via inotropic and neurohumoral axis interventions remain the only modalities to face such clinical challenge and the onset of fatal arrhythmias remain unpredictable [15]. With the rising prevalence, there has been a dearth of novel treatment strategies for heart failure and the prevention of the subsequent arrhythmia. This suggests that a different focus in the study of heart failure pathogenesis is necessary for the development of novel therapies.

The development of heart failure is often preceded by cardiac growth manifested as an increase in cardiac mass, or cardiomyocyte hypertrophy. This structural

remodeling temporarily allows for the preservation of cardiac function in response to hypertension, valvular heart disease, or anemia. Over time, the hypertrophied heart no longer compensates against the stressors and the heart progresses into decompensated systolic heart failure, characterized by a loss of functional heart muscle. It is during this stage of the pathology that hearts typically begin to lose their sinus rhythm and progress to arrhythmias. However, the molecular mechanisms that drive the stressed heart to initially hypertrophy and ultimately lose its function and the coordinated contraction remain incompletely understood.

Prior to the progression into heart failure, the stressed heart undergoes a series of characteristic changes. Structurally, hearts hypertrophy and are capable of nearly doubling the mass through hypertrophic remodeling [16]. Modulation of the structural remodeling process therefore is recognized as a potentially novel therapeutic approach for the prevention and treatment of heart failure.

Much effort has been put forth toward the understanding of the structural remodeling process. Studies using microarray gene expression profiling have identified expression changes in calcium handling proteins, sarcomeric proteins, mitochondrial, apoptotic, inflammatory, and extracellular matrix gene clusters [17, 18]. Unfortunately, treatment strategies aimed at normalizing inflammatory reactions and preventing extracellular matrix modifications have not been found to be beneficial [19, 20]. Therefore, a better understanding of the remodeling processes involved in heart failure are necessary to develop a novel targeted approach to reduce the morbidity and mortality associated with heart failure.

The structural remodeling process, specifically hypertrophy of the myocardium, in response to stress dramatically increases the pro-arrhythmic potential. In fact, an important cause of the high mortality and sudden death in heart failure is the insidious onset of potentially fatal cardiac arrhythmias [13]. Therefore, a direct focus on the mechanisms governing the electrical remodeling process is mandatory. Thus, we set out to investigate the molecular and cellular events that regulate the electrical properties of the heart accompanying cardiac hypertrophy and whether there is a point of intervention. Furthermore, we also explored the mechanism by which the prolonged hypertrophic response to stress affects the expression and function of ions handling proteins that establish normal sinus rhythm.

This dissertation provides the evidence in support of the hypothesis that changes in cardiac cellular signaling are required for structural and functional changes in the stressed heart, and sustained pathologic hypertrophic response alters normal rhythm of the heart. The rationale is based on the established and highly conserved pathway – the mammalian target of rapamycin (mTOR) – that integrates the environmental signals such as oxygen availability, energy status of the cell, and nutrient metabolism with cellular growth [21, 22] and its sustained activity promotes the development of abnormal heart rhythms [23, 24]. Specifically, I identified dysregulation of the adaptor protein ankyrin-B – a key protein in proper subcellular targeting and retention of ion channels, transporters, and receptors that regulate the ionic movement – as a novel molecular target under mTOR regulation, and that sustained mTOR activity downregulates expression of ankyrins causing altered expression of ion handling channels and

transporters. The study presents downregulation of ankyrin by mTOR activity as the key linking the chronically stressed myocardium and arrhythmogenesis.

1.2 Hemodynamic Load-Induced Structural and Functional Remodeling

Cardiac hypertrophy is a response to a wide variety of external stimuli. In general there are two types of cardiac hypertrophy: physiologic and pathologic. Physiologic cardiac hypertrophy (i.e. normal growth without structural or functional compromise) occurs in the postnatal period, during pregnancy, or with exercise [25, 26]. On the other hand, pathologic cardiac hypertrophy occurs in response to hypertension, neurohumoral stimulation, or myocardial infarction (Figure 1.1) [16].

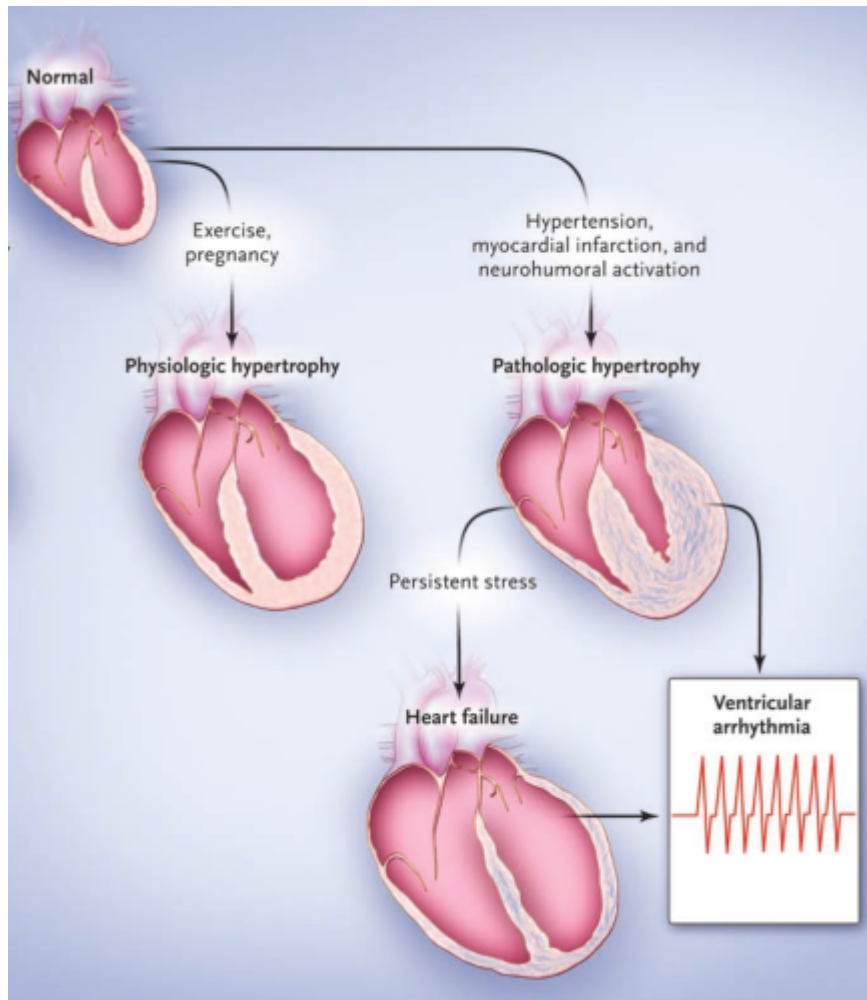


Figure 1.1. Conditions leading to physiologic versus pathologic cardiac growth. Depending on the stimulus, cardiac structural remodeling can be physiologic or pathologic. Physiologic remodeling can be beneficial while pathologic remodeling is associated with decompensated heart failure, ventricular dilation, and electrophysiologic changes leading to malignant arrhythmias. Reproduced with permission from Hill, J.A. and E.N. Olson, *Cardiac plasticity*. N Engl J Med, 2008. 358(13): p. 1370-80, Copyright Massachusetts Medical Society [16].

The process of pathologic cardiac hypertrophy was first identified as a step toward the development of heart failure in the earlier part of the last century [27]. Later, it was recognized that the initial hypertrophy in response to pathologic stressors was first adaptive, but led to systolic dysfunction when the compensation became “inadequate”

[28-30]. The initial adaptive state was in line with Laplace's law which dictated that [wall tension = pressure x radius / (2 x wall thickness)] [26] such that load-induced increases in systolic wall stress was offset by increase in wall thickness [20, 31]. In contrast, the Framingham Heart Study established that left ventricular hypertrophy alone was an independent risk factor for adverse cardiovascular outcomes such as heart failure and arrhythmias. This finding from The Framingham Heart Study suggested the maladaptive role of cardiac hypertrophy that was vastly different from the adaptive nature as suggested by Laplace's law [32, 33]. This begs the question whether cardiac growth is necessary to compensate for the increased cardiac work.

At the cellular level, the heart responds to an increase in workload by post-translational modification of proteins. For example, acute mechanical stress directly activates angiotensin II type 1 receptor and G-protein coupled receptors leading to phosphorylation changes of downstream growth signaling proteins [34-36]. When subjected to an increase in workload chronically, sustained activation of intracellular signaling cascades not only activates cellular growth pathways and leads to hypertrophy, it also changes gene expression, most notably the reactivation of the fetal gene program (e.g. α - to β -myosin heavy chain expression) [16, 37]. In several small animal studies where cardiac hypertrophy was attenuated by inhibition of calcineurin-mediated intracellular growth pathway with cyclosporine showed preservation of systolic function when challenged with hemodynamic stress [38-40]. Similar studies where suppression of other intracellular growth pathways such as GSK-3 β pathway or calcium/calmodulin kinase II have all demonstrated reduced cardiac hypertrophic and preservation of cardiac function in response to pressure overload or β -adrenergic stimulation [41-43]. Inhibition

of pathologic hypertrophic response therefore presents a potential therapeutic avenue for the preservation of cardiac functions.

Since left ventricular hypertrophy is established as an independent risk factor for development of heart failure and arrhythmias, attenuating cardiac hypertrophic response while preserving the contractile performance is a logical approach to prevention and treatment of heart failure. As aforementioned, a number of signaling events take place in the stressed heart to regulate cardiac growth. Thus, a better understanding of how the intracellular signaling events as it relates to changes in electric properties of the heart is essential. Of all the signaling events, the mammalian target of rapamycin (mTOR) pathway is one of the best well-characterized growth signaling cascade to be active in the stressed heart [44-46]. Therefore, a major focus of this thesis is on mTOR activity and proteins responsible for maintaining regular rhythm in the heart.

1.3 mTOR Signaling in the Heart

The evolutionarily-conserved mTOR pathway is part of the insulin signaling that regulate cellular growth and proliferation such as ribosomal biogenesis, protein translation, autophagy, and nutrient metabolism.

mTOR (mammalian *target of rapamycin*) biology was elucidated through the use of the macrolide rapamycin, an antifungal composed of a large macrocyclic lactone ring with deoxy sugars attached that was isolated from a yeast strain *Streptomyces hygroscopicus* found on Easter Island of Rapa-Nui [47]. Rapamycin inhibits cellular growth and proliferation and is now an FDA-approved drug for use as an

immunosuppressant for kidney transplant and prevention of post-angioplasty restenosis [48-50]. Rapamycin has a high affinity for FK506-binding protein 12 (FKBP12) that subsequently inactivates the mTORC1 complex [51] or mTORC2 complex with chronic rapamycin administration [52]. Using rapamycin, mTOR's sensitivity to nutrient availability and ability to mediate protein synthesis was first identified in yeast [53, 54]. Studies in which withdrawal of amino acid from *Drosophila* and mammalian cells with rapamycin administration resulted in decreased mTORC1 activity were demonstrated and the mechanisms by which inhibition occurred were elicited [21]. Nutrient availability, specifically branched-chain amino acids, binds to Rag-Ragulator complex to recruit and directly stimulate mTOR activity [44-46]. In contrast, rapamycin inhibits mTOR activity by complexing with FK506 binding protein 12 (FKBP12), which in turn binds to mTOR's FKBP12-rapamycin binding domain to inhibit its ability to phosphorylate the downstream effectors [55, 56].

mTOR regulates protein translation through phosphorylation of proteins in the translational machinery, and the two most well-characterized downstream targets of mTOR are ribosomal protein p70 S6 kinase-1 (p70S6K1) and eukaryotic initiation factor 4E-binding protein (4E-BP1) [57]. p70S6K1 regulates cell size via phosphorylation of 40S ribosomal protein S6 that is important in translational control of mRNAs containing 5'-terminal oligopyrimidine tract. 4E-BP1 normally binds and inhibits eukaryotic initiation factor 4E (eIF-4E), but the inhibition is relieved with 4E-BP1 phosphorylation by mTOR. eIF-4E then recruits 40S ribosomal subunit to the 5' end of mRNAs [58]. Collectively, mTOR activation results in increased cap-dependent protein translation [59-61].

Further studies on mTOR found that mTOR nucleates two major complexes – mTOR complex 1 (mTORC1) and mTOR complex 2 (mTORC2) [62]. mTORC1 is composed of mTOR, regulatory-associated protein of mTOR (RAPTOR), mammalian lethal with Sec13 protein 8 (mLST8), the proline-rich Akt substrate 40 kDa (PRAS40), and DEP domain-containing mTOR-interacting protein (DEPTOR). mTORC2 is composed of mTOR, rapamycin-insensitive companion of mTOR (RICTOR), protein observed with RICTOR (PROTOR), mLST8, mammalian stress-activated protein kinase-interacting protein 1 (mSin1) [63, 64]. The different components of the two complexes yield distinctly different downstream functions and upstream regulations. mTORC1 activity primarily drives protein translation, cell growth, and cell proliferation whereas mTORC2 regulates cytoskeletal organization via actin reorganization [65]. Another notable difference between the two is that mTORC1 is sensitive to acute rapamycin inhibition and does not change with chronic administration, whereas mTORC2 is not acutely sensitive to rapamycin but is inhibited with chronic rapamycin treatment [66]. The question remains, what roles do the two complexes have in heart growth?

In the unstressed heart, mTORC1 is normally inhibited by its upstream regulator, the tuberous sclerosis complex (TSC) composed of *TSC1* (hamartin) and *TSC2* (tuberin) [67]. In the unstimulated state, N-terminus of tuberin binds hamartin to form a heterodimer coiled-coil complex and the C-terminus of tuberin, the GTPase-activating protein domain, actively inhibits Ras homolog enriched in brain (Rheb) by hydrolyzing Rheb-GTP (active form capable of activating mTORC1) to Rheb-GDP (inactive form) [68-70]. Growth factors (e.g. insulin or insulin-like growth factor 1) or mechanical

stress activates mTORC1 in the insulin signaling pathway by phosphorylating and dissociating the TSC complex in a phosphatidylinositol-3 kinase (PI3K)-dependent manner [71]. Dissociation of tuberin and hamartin suppresses GTPase-activity of tuberin and promotes Rheb-GTP that recruits and activates mTORC1 on the lysosomal surface [72-74].

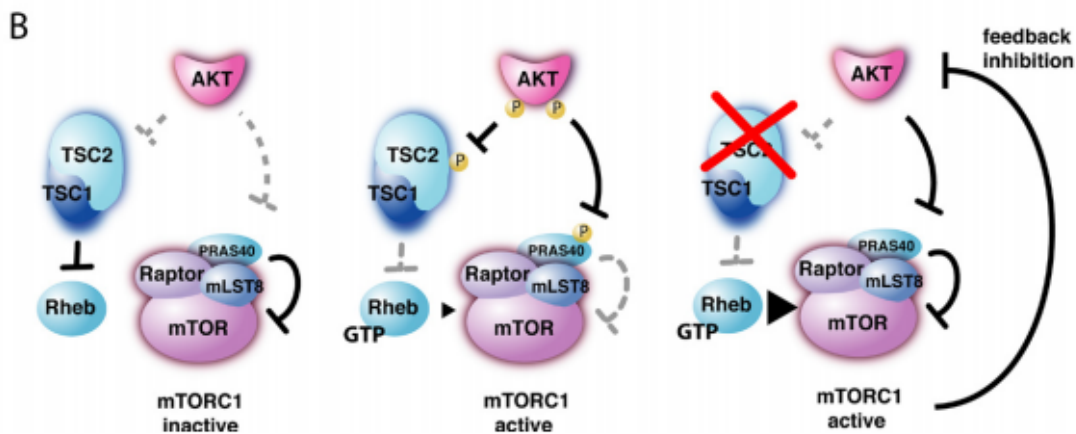
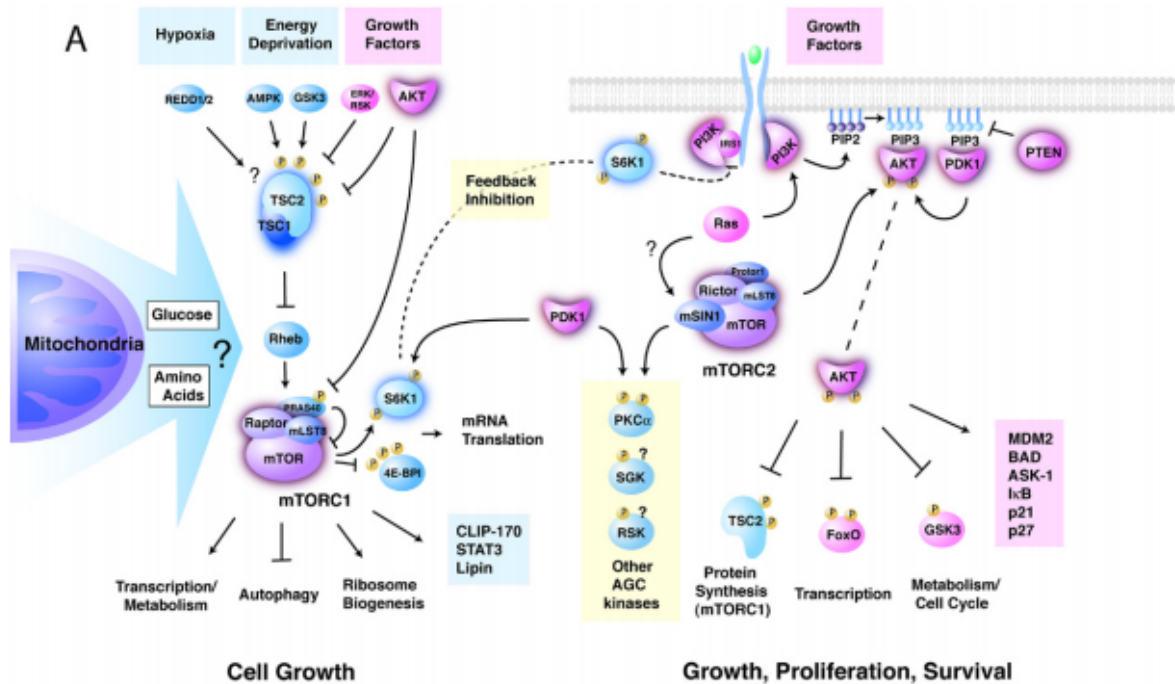


Figure 1.2. The mTOR signaling network. A, mTOR kinase nucleates both the mTOR complex 1 and complex 2. mTOR complex 1 contains RAPTOR, mLST8, PRAS40, and RAGulator complex (not shown in the diagram). mTORC1 drives cellular growth by increasing protein translation and decreasing degradation. B, When Akt is in active, TSC complex inhibits Rheb and PRAS40 inhibits mTORC1. Upon activation, Akt promotes mTORC1 activity by inhibiting the TSC complex and PRAS40. When TSC complex becomes genetically inactivated, strongly elevated Rheb activity greatly increases mTORC1 activity despite negative feedback inhibition by Akt and PRAS40. Reproduced with permission from Guertin, D.A. and D.M. Sabatini, *Defining the role of mTOR in cancer*. Cancer Cell, 2007. 12(1): p. 9-22 [9]. Permission number: 3673841346160.

Collectively, given the sensitivity of insulin signaling to environmental cues and its role in cell growth and proliferation, mTORC1 activity intimately provides and plays a major role in the cardiac hypertrophic response to hemodynamic stress.

1.4 Overactive mTORC1 Underlies Electrical Changes in the Brain

Chronically stressed heart with hypertrophic phenotype exhibits changes in electrocardiogram (EKG) recording [75]. But prior to changes in the EKG, the hypertrophic phase is characterized by numerous signaling pathway changes [76-82]. Prior to the investigation of mTORC1 pathway regulating the electrical changes in the heart, it is prudent to start by exploring the relationship between mTORC1 in the brain, another electrically active organ.

The activation of the mTORC1 pathway in the central nervous system is highly associated with the recurrence of seizures [83]. Genetic mutations of the mTOR pathway components such as phosphatidylinositol-3 kinase (PI3K), phosphatase and tensin homologue (PTEN), Akt/PKB, and mTOR all display unprovoked seizures in animal models [84-88]. But the involvement of mTORC1 in seizure development goes

beyond genetic manipulation of the pathway. Chemical or electrical stimulation and post-traumatic brain injury in rodent models have all elicited recurrent seizures marked by increased mTORC1 activity, and treatment with rapamycin either attenuated the severity or the frequency of seizure activities [89-93]. Furthermore, early data using rapamycin for medically intractable seizures have had promising results leading to current larger scale clinical trials [94].

A notable disease that typifies hyperactive mTORC1 in the brain is tuberous sclerosis complex (TSC). TSC is an autosomal dominant disease caused by germline mutations in either of the tumor suppressor genes, *TSC1* or *TSC2*. As shown in figure 1.2B, inactivation of either gene leads to the inactivation of the TSC complex and hyperactivation of the mTORC1 pathway that promotes the neuropathological changes in the central nervous system characterized by the formation of tubers [95-97]. Tuber formation is a result of abnormal neuronal migration and cellular hypertrophy [98, 99] and has been shown to be the likely origin of recurrent seizures [100, 101], a process whereby the brain is functionally altered and generates abnormal electrical signals. The presence and the number of cortical tubers highly correlate to the degree of seizure severity and number of occurrences, which are one of the most defining and devastating neurologic consequences manifesting in many of the patients afflicted with TSC [102-105].

The mechanism by which overactive mTORC1 remodels electrical properties of neurons that cause recurrent seizures remains perplexing. Much attention has been focused on the inappropriate neuronal migration and synaptogenesis in unprovoked epilepsy [98, 106-108]. But recently, changes in ion handling proteins secondary to

mTORC1 overactivation are beginning to be identified. Functional and expression changes of ion channels and receptors at the cellular level such as voltage-gated potassium channels, glutamate and GABA receptors that result in spontaneous abnormal neuronal firing have been characterized [109-111]. Specifically, neurons with overactive mTORC1 exhibit decreased expression and currents in two inward-rectifier potassium channels (Kir2.1 and Kir6.1) – ATP-sensitive channels that play a role in neuronal repolarization – and an increased expression and currents through the excitatory GluN2C NMDA receptors [109, 112]. Altogether, the net results are lowered threshold for neuronal firing and increased frequency of action potential firing. The expression and current changes are reversible by either inhibiting mTORC1 directly or by modulating downstream effectors of mTORC1 *in vivo* and *in vitro*. These same neurons also exhibit increased spontaneous firing as a result of decreased repolarizing current [109, 112].

The effects of mTORC1 on ion channels, and therefore the electrical properties of the neurons, are clear, but the mechanistic regulation of the channels remains elusive.

1.5 Ion Channels and the Adaptor Protein Ankyrin

Ion channels and transporters require proper interaction with adaptor protein such as ankyrin to facilitate their proper membrane localization and functioning. Ankyrins are a family of intracellular adaptor proteins that interact, transport, and (implicit in the name) anchor membrane proteins at their proper subcellular domains to the underlying cytoskeletal structure [8]. Three independent *ANK* genes (*ANK1*, *ANK2*, and *ANK3*)

make up the ankyrin family and each has a unique function and subcellular localization to facilitate the proper formation of the cellular architecture and biogenesis of distinct membrane domains [113].

The ankyrin proteins vary vastly in size, but a canonical ankyrin protein has four domains: 1.) membrane-binding domain, 2.) spectrin-binding domain, 3.) death domain, and 4.) C-terminal domain (Figure 1.3). Contrary to the naming scheme, the membrane-binding domain does not directly bind to the plasma membrane, but instead binds to a variety of membrane-bound proteins such as ion channels, transporters, and cell adhesion molecules [114-116]. The spectrin-binding domain is where interaction with the underlying cytoskeletal structure occurs. The death domain and the C-terminal domain together are thought to comprise the “regulatory domain” because of their intramolecular association with the membrane binding domain that likely specifies ankyrin’s affinity for different binding partners.

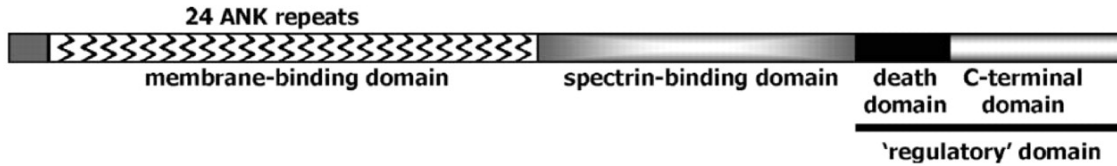


Figure 1.3. Organization of domains of a prototypical ankyrin. 24 ANK repeats comprise the membrane-binding domain that is responsible for interactions with other proteins. Each ANK repeat is composed of an α -helix- β -hairpin loop- α -helix and the exposed tip of β -hairpin loop is where protein binding takes place. The spectrin-binding domain is where ankyrin binds to the underlying cytoskeleton spectrin, thereby “anchoring” the interacting membrane protein. The regulatory domain modulates ankyrin’s intramolecular association and targets ankyrin to specific subcellular domains. Reproduced with permission from Cunha, S.R. and P.J. Mohler, *Cardiac ankyrins: Essential components for development and maintenance of excitable membrane domains in heart*. *Cardiovasc Res*, 2006. 71(1): p. 22-9 [8]. Permission number: 3673851380495.

Because of ankyrin’s ability to bind with multiple partners simultaneously, it is therefore within the ankyrin’s capability to facilitate the formation of large membrane protein complexes to create specialized membrane domains and tether them to the underlying cytoskeleton. An example of the protein complex formed by an ankyrin protein is the interactions between neuronal ankyrin-G with voltage-gated ion channels, cell adhesion molecules (neurofascin-186 or L1-CAM), and the underlying cytoskeleton β IV-spectrin at the axon initial segment (AIS) and nodes of Ranvier [117, 118].

The divergence of the regulatory domain within the same and between different ankyrin products confers different functions of ankyrins by specifying their subcellular localizations and interactions with different binding partners [119, 120]. The functionally distinct and different spatially-localized ankyrins are central in the establishment of neuronal polarity and ion channel clustering at the axon initial segments,

nodes of Ranvier, and paranodes that work in concert to establish membrane excitability and saltatory conduction [121-123].

Neuronal excitability begins at the axon initial segment (AIS), a site of integration from many dendritic signals that result in the initiation of action potentials. Action potentials are generated by clusters of voltage-gated sodium channels and repolarized by voltage-gated potassium channels that are concentrated at the AIS and nodes of Ranvier [118, 124]. Studies have attributed the clustering of the voltage-gated ion channels at the AIS to their interactions with ankyrin-G. Furthermore, in an ankyrin-G null murine model, not only is the clustering of voltage-gated sodium channels at the AIS is disturbed, deficits in action potential initiation and rate of firing are observed [117, 118, 125-127]. Although these studies showed decreased action potential generation and frequency when the binding sites are disrupted by knockdown or point mutations, a recent report showed that lithium-pilocarpine-induced epilepsy in a murine model caused ankyrin-G-dependent changes in the expression of voltage-gated sodium channels [128]. The role ankyrin plays in modulating neuronal excitability by way of their interactions with the ion channels is evident.

Likewise, in the context of the recurrent seizures and decreased voltage-gated potassium channels and currents observed in animal models of TSC, the potential changes in ankyrin expression or localization secondary to dysregulated mTORC1 activity may underlie the molecular pathway leading to increased excitability in the central nervous system of Tsc2-hGFAP described in chapter 2 (Figure 1.4).

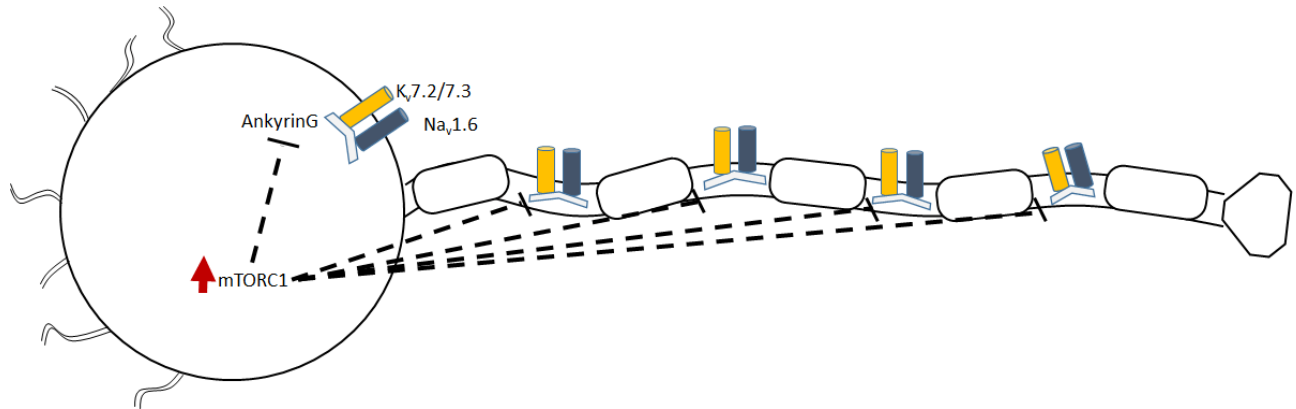


Figure 1.4. Proposed model of mTORC1 regulation of neuronal excitability. Action potential is generated at the axon initial segment (intersection between the soma and the axon) and propagated through the nodes of Ranvier (denoted by the areas in between the myelin sheaths) by the voltage-gated sodium channels ($\text{Na}_v1.6$). Repolarization of the action potential is mediated by the voltage-gated potassium channels ($\text{K}_v7.2/7.3$). Maintenance of $\text{Na}_v1.6$ and $\text{K}_v7.2/7.3$ at their proper subcellular domains is mediated by the adaptor protein ankyrin-G and its expression is likely regulated by mTORC1. Rectangular boxes along the axon represent the myelin sheaths.

1.6 Ankyrin and the Heart

Like the neurons, cardiomyocytes are intrinsically electrically active. Whereas neuronal activity is measured by generation and firing frequencies of action potentials, cardiomyocyte performance is measured by the generation of action potentials, contraction strength and rhythm. These properties of the cardiomyocytes are related as every beat of the heart begins with the generation of an action potential that travels down the sarcoplasmic reticulum/transverse-tubule (SR/T-tubule) to depolarize the voltage-gated calcium channels (or dihydropyridine receptor) causing a calcium-induced calcium release via the ryanodine receptor [129]. This calcium release in turn causes a mechanical contraction by the cardiomyocyte, and, by cell-to-cell electrical coupling at intercalated discs, leads to the contraction of the entire myocardium. Collectively, this is

termed “excitation-contraction coupling” and links the electrical stimulus to a mechanical response [130, 131].

Normal excitation-contraction coupling, similar to neuronal depolarization and repolarization, requires the precise targeting and maintenance of integral membrane proteins at specialized membrane domains. While adaptor proteins such as ankyrin help establish important subcellular domains for action potential generation and propagation in neurons, ankyrin coordinates and establishes identity and functions of SR/T-tubule junction and intercalated discs - important subcellular domains of cardiomyocytes – for the proper conversion of electrical signal to mechanical force. Specifically, ankyrin-B in the heart functions at the SR/T-tubule by targeting and retaining the sodium-calcium exchanger (NCX) and sodium potassium ATPase (NKA) [2, 4]. Loss-of-function ankyrin-B mutations at the cellular level that disrupt interactions with its binding partners lead to decreased NCX and NKA membrane expression and reduced half-life, elevated sarcoplasmic reticulum calcium content, and increased duration of calcium sparks [2, 4, 5, 132, 133]. At the clinical level, the missense mutations have been linked to various arrhythmias – or abnormal rhythms of contraction - that include but not limited to bradycardia, atrial fibrillation, idiopathic ventricular fibrillation, catecholminergic polymorphic ventricular tachycardia, prolonged ventricular repolarization (type IV long QT syndrome), and sudden cardiac death [3-5, 134, 135]. QT interval is the time it takes for the heart to depolarize then subsequently repolarize fully and correlates directly with the increase in the duration of calcium transients observed at the cellular level.

Interestingly, ankyrin-B populations are observed at two distinctly different functional subcellular domains of the cardiomyocyte: one at the SR/T-tubule and the other at the M-line. While many studies have focused on the function of ankyrin-B at the SR/T-tubule, very little is known about the function of ankyrin-B population at the M-line, a site where myosin heavy chain is organized [136]. However, the existence of two ankyrin-B populations at two functionally divergent subcellular domains cannot be attributed to a single isoform despite the multivalent properties of ankyrin proteins. Also, the majority of the studies dealing with ankyrin-B are focused on its binding partners exclusively localized at the SR/T-tubule (e.g. NCX, NKA, and IP₃R) that are completely absent at the M-line. Given that ankyrin-B is expressed at the SR/T-tubule and the M-line, we speculate that there exists more than one ankyrin-B isoform in cardiomyocytes that contribute to the maintenance of the excitation-contraction integrity.

Cardiac expression of multiple ankyrin-B isoforms is a likely hypothesis since alternative-splicing of ankyrin genes has been well-documented. For example, multiple isoforms of ankyrin-G has been identified in the brain [137, 138], muscles [139-141], and heart [142-144]. Multiple isoforms of ankyrin-B have also already been identified in the brain that play a role in neurite outgrowth and control growth cone navigation [145-149]. Yet neurologic clinical manifestation of loss-of-function ankyrin-B remains unreported at this time.

Multiple mutations in ankyrin-B have been associated with cardiac arrhythmias. Interestingly, individual mutations have been linked to diverse groups of arrhythmias. Previous studies examining the molecular basis of ankyrin-B dysfunction have been unable to account for how a single mutation could manifest as atrial fibrillation,

bradycardia, and idiopathic ventricular fibrillation. Findings from these studies were interpreted with the false assumption that the heart expresses one isoform of ankyrin-B. Our hypothesis that the heart expresses multiple ankyrin-B isoforms provides a more fitting explanation for the diversity of arrhythmias resulting from ankyrin-B dysfunction. In Chapter 4, I describe the identification and functional characterization of two novel ankyrin-B isoforms in mammalian heart. This work provides the foundation for future experiments to re-evaluate arrhythmia-associated mutations in the context of endogenously expressed ankyrin-B isoforms.

Different sets of arrhythmias also manifests throughout different stages of heart failure [13]. Multiple, signaling, functional, structural remodeling occur simultaneously in the hypertrophic heart [16]. From Chapter 4, we identify and characterize multiple ankyrin-B isoform expressions and localization in cases of primary cardiac arrhythmias. Using that as platform to interrogate electrical changes in secondary cardiac hypertrophy in Chapter 3, I demonstrate that ankyrin-B expression decreases in a murine model of cardiac hypertrophy via overactivation of the mTORC1 pathway by increased hemodynamic load. Furthermore, I demonstrate a link between mTORC1 activation and reduced ankyrin-B expression at the sarcomeric M-line. Changes in ankyrin-B expression may induce arrhythmia in the hypertrophic heart by disrupting the proper subcellular localization and function of the sodium calcium exchanger and/or other calcium ion handling proteins. In sum, this chapter lays out a molecular path that may in part account for arrhythmogenesis associated with secondary cardiac hypertrophy.

CHAPTER 2: THE DIFFERENTIAL EFFECTS OF PRENATAL AND/OR POSTNATAL RAPAMYCIN ON NEURODEVELOPMENTAL DEFECTS AND COGNITION IN A NEUROGLIAL MOUSE MODEL OF TUBEROUS SCLEROSIS COMPLEX

Acknowledgement: The study presented in this chapter was written collaboratively with the first author Dr. Sharon W. Way, who also contributed significantly to acquisition of the data presented in this chapter

Way, S.W., N.S. Rozas, H.C. Wu, J. McKenna, 3rd, R.M. Reith, S.S. Hashmi, P.K. Dash, and M.J. Gambello, *The differential effects of prenatal and/or postnatal rapamycin on neurodevelopmental defects and cognition in a neuroglial mouse model of tuberous sclerosis complex*. Hum Mol Genet, 2012. **21**(14): p. 3226-36

Reprinted with permission to use in thesis/dissertation from Oxford University Press.
License numbers: 3601191233661 and 3601191093209

2.1 Introduction

Tuberous sclerosis complex (TSC) is a tumor suppressor disorder caused by heterozygous mutations in either the TSC1 (hamartin) or the TSC2 (tuberin) genes [150, 151]. Loss of heterozygosity of either gene [152, 153] and activation of the mTORC1 kinase [152, 154] are important molecular features associated with TSC pathology. Although TSC affects multiple organs, neurodevelopmental defects result in the most substantial morbidity and mortality. Tubers, subependymal nodules and subependymal giant cell astrocytomas (SEGAs) represent common TSC neurodevelopmental abnormalities [155, 156] and are associated with intellectual disability, autism and epilepsy. The prevention and management of these developmental brain lesions are major challenges in caring for patients.

The hamartin and tuberin heterodimer inhibit the rapamycin-sensitive mTORC1 signal transduction pathway that controls translation, proliferation and cell growth [57, 157, 158]. Preclinical trials have demonstrated significant rescue of many neurologic defects using rapamycin [95-97, 159, 160], a macrolide that, upon binding to the intracellular binding protein FKBP12, inhibits the ability of the mTORC1 kinase to signal to its downstream effectors. These studies have paved the way for several human clinical trials that have recently resulted in the approval of everolimus, a rapamycin derivative, for the treatment of SEGAs [161, 162]. Nonetheless, the ability of rapamycin to rescue perinatal defects remains largely untested. A recent report demonstrated a promising effect of one dose of prenatally-administered rapamycin on the longevity of a Tsc1-Nestin mouse model of TSC [159]. Here, we substantially extend those studies by comparing and contrasting the histological and behavioral effects of different perinatal

rapamycin treatment regimens in the previously reported Tsc2-hGFAP neuroglial mouse model of TSC [98]. Using the Tsc2-hGFAP mouse model, we have shown that the loss of Tsc2 in radial glial progenitor cells recapitulates many brain manifestations of TSC. Tsc2-hGFAP animals have cortical and cellular hypertrophy, heterotopias, defects in lamination and myelination, astrogliosis and die at about one month of age [98]. These defects are a combination of prenatal and postnatal neurodevelopmental abnormalities and thus provide a good model for the study of perinatal treatment of TSC. Using the Tsc2-hGFAP model, we sought to systematically determine the most effective treatment regimens to rescue neurodevelopmental defects. We show that combined rapamycin treatment resulted in almost complete rescue of neuronal and glial pathologies, while prenatal or postnatal treatment alone yielded less complete but significant improvements in brain histology. Surprisingly, the animals treated with combined therapy did not perform as well as postnatally treated animals on learning and memory tasks. mTORC1 activity is critical for dictating the overall growth of differentiating neuronal stem cells and postmitotic neurons [163, 164], axon guidance [165] and dendritic arborization [166]. Therefore, overt inhibition of mTORC1 during neurodevelopment may disrupt proper axon guidance and dendritic arborization leading to subsequent deficit in learning and memory in adulthood. These results show that rapamycin can rescue perinatal neurodevelopmental defects and support the cautious design of trials that will assess early rapamycin treatment of TSC-affected children.

2.2 Materials and Methods

2.2.1 Animals

Tsc2-hGFAP mice (*Tsc2ko/flox;hGFAP-Cre*) were generated and genotyped as previously described [98]. All protocols were approved by the University of Texas Health Science Center at Houston Animal Welfare Committee.

2.2.2 Rapamycin treatment regimen

Rapamycin (MP Biomedicals) was dissolved in 100% methanol at 1.0 mg/ml for storage at -20°C. Before use, rapamycin was diluted with PBS and administered intraperitoneally at 0.1 mg/kg daily. Prenatal treatment was conducted by administering rapamycin to pregnant dams from embryonic day 12.5 (E12.5), the approximate day of hGFAP-Cre expression in radial glial progenitors, until delivery (prenatal group). Postnatal treatment started at birth (P0) and ended at weaning (P21) (postnatal group). A third group was treated prenatally from E12.5 and then after birth until weaning (pre+post = combined group). One group of treated animals was used for histologic analysis, and another group was observed for longevity.

For behavior testing, animals were switched from 0.1 mg/kg rapamycin daily to 2 mg/kg rapamycin three times a week between P35 and P44 as daily 0.1 mg/kg was no longer sufficient to suppress seizure activities of the Tsc2-hGFAP mice two weeks past weaning. We used 2 mg/kg because this dose was able to extend the lives and maintain the health of the Tsc2-hGFAP mice without runting them (Figure 2.5). Rapamycin has a

half-life of 4.5 hours in blood [167] so that it is virtually eliminated completely from the body at the end of every 24-hours post injection, the alternate inhibition and activation of mTORC1 every other day appears to achieve therapeutic effects.

2.2.3 Western analysis, histology and immunohistochemistry

Brain lysates were made from P21 animals and analyzed as previously described [98]. Briefly, P21 mice were anesthetized with 2.5% avertin and transcardially perfused with cold PBS followed by 4% paraformaldehyde. Hematoxylin and eosin staining and immunohistochemistry were performed as previously reported [98]. Antibodies used were: phosphorylated (Ser 240/244) S6 (1:100, Cell Signaling), Cux1 (1:50, Santa Cruz), BrdU (1:50, Becton Dickinson), GFAP (1:400, Sigma), NeuN (1:100), MBP (1:200) (Millipore), Olig2 (1:200) (Millipore) and CC1 (1:100, Calbiochem). Antibodies used for western analysis were: tuberin (1:500), hamartin (1:500), α -tubulin (1:2000), S6 (1:500), pS6 (S240/244) (1:500), pS6 (S235/236) (1:500) from Cell Signaling.

2.2.4 Quantitative analysis

Three sections from three mice of each group were used for all quantitation. Sections were matched and a standard area was used for counting. ANOVA was used for analysis of data. The log-rank test was used to compare survival curves. For BrdU analysis, the cortex was divided equally into 10 bins, and a standardized width was used for counts. Learning and memory testing experimenters were blind to the treatment

groups. Animals were trained in two variations of the hidden platform version of the Morris water-maze task: 1-day version and a 7-day version [168-171]. For 1-day training protocol, animals were given 12 consecutive trials (4 min inter-trial interval) in 1 day and a probe test 24 h later. For the 7-day protocol, animals were given four training trials a day (4 min inter-trial interval) for six consecutive days. A probe trial was given 48 h later. Movement within the maze was monitored by a video camera linked to tracking software. Analysis of data was done with unpaired, two-tailed Student's t-test (number of platform crossings and path length) and repeated-measure ANOVAs (learning curves and quadrant preference). Context discrimination testing was done as previously described [172]. Briefly, animals were pre-exposed (no shock) to two contexts that shared certain features (horizontal grid floor, background noise, animal handling to and from the room) while differing in others (differently spaced grids, scent, distal cues, floor shape and color). Animals were given one trial a day of 3 minutes in each chamber with a minimum of 3.5 h between trials. In the shock chamber, animals were given a 2 s, 0.75 mA shock given at 148 s, while no shock was given in the safe chamber. Discrimination of the two contexts was assessed by comparing the time spent freezing (monitored in 2 s intervals) in each chamber during a test trial done on day 4 during which no shock was given. Analysis of the data was done with paired, two-tailed Student's t-test. Data were considered significant at $P < 0.05$.

2.3 Results

To examine whether rapamycin could rescue some or all defects in Tsc2-hGFAP mice, we designed three rapamycin treatment regimens to target prenatal and/or postnatal developmental abnormalities (Figure 2.1A). We optimized a rapamycin dosage (0.1 mg/kg i.p. daily) that suppressed mTORC1 activity as measured by levels of phosphorylated ribosomal protein S6 (Figure 2.1B and C), but did not kill embryos or retard postnatal growth. This dose is 10–50-fold lower than that used in other studies involving TSC mouse models [95-97, 159]. Rapamycin treatment was stopped at birth in the prenatal group or at postnatal day 21 (P21) in the combined and postnatal groups. Animals were either sacrificed for brain histology or observed for longevity.

In all treatment groups, rapamycin improved the health of Tsc2-hGFAP mice (Figure 2.1D, E, F). The postnatal and combined treatment groups were healthy and appeared indistinguishable from controls at P21, but began to die from seizures at about P40 (Figure 2.1F). These results along with our longevity study presented in Figure 2.5 further demonstrated that rapamycin treatment must be continued to prevent death in mutant animals as shown in other models [96, 97]. Nonetheless, the median age of survival of both postnatal and combined groups was significantly longer than untreated mutants. Prenatal treatment had a modest effect on postnatal health, and did not significantly alter the median survival. These attenuated effects of prenatal treatment are likely due to the reactivation of mTORC1 after the cessation of treatment at P0 as demonstrated by increased phosphorylated S6 (pS6) immunostaining (Figure 2.2A).

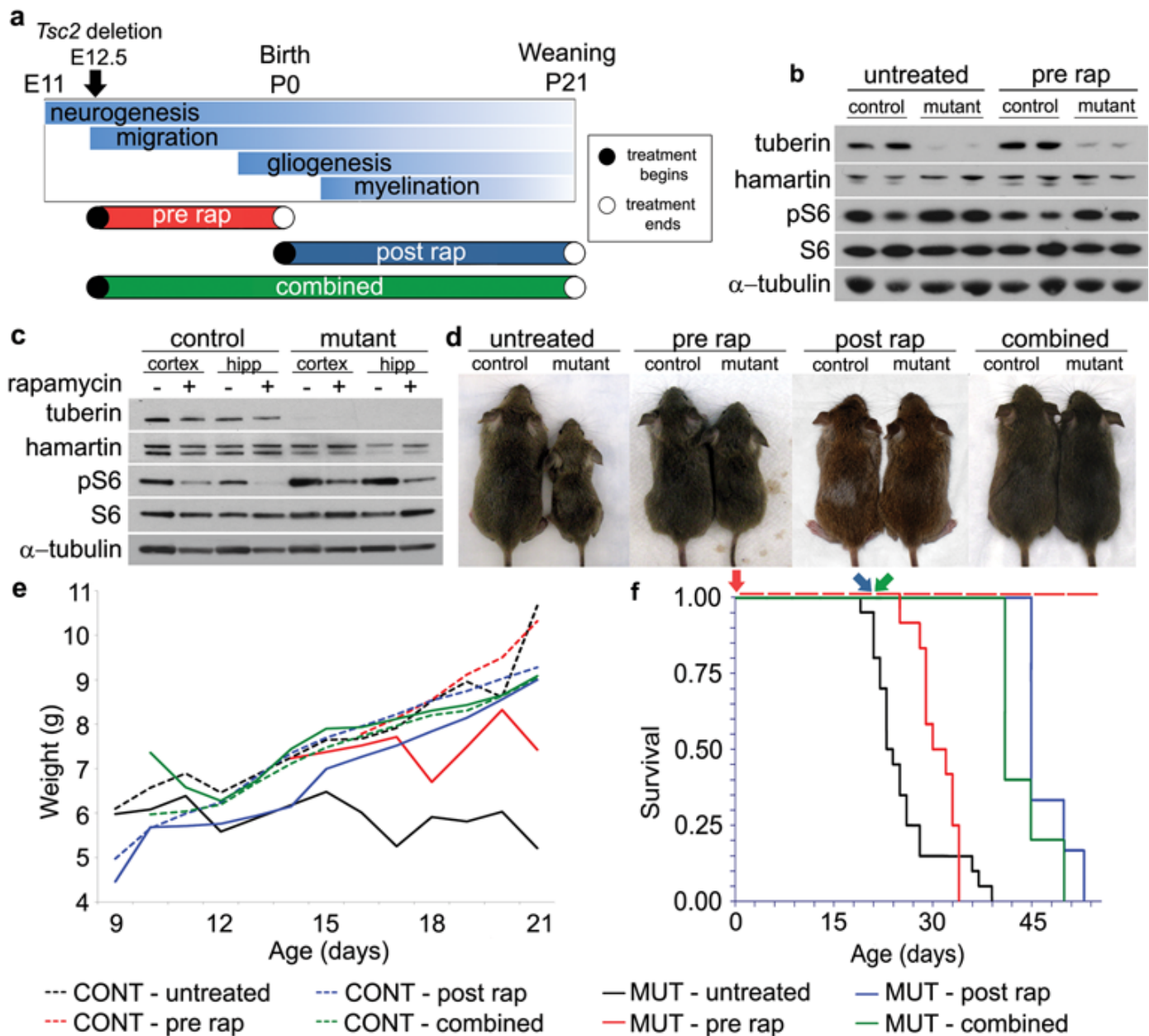
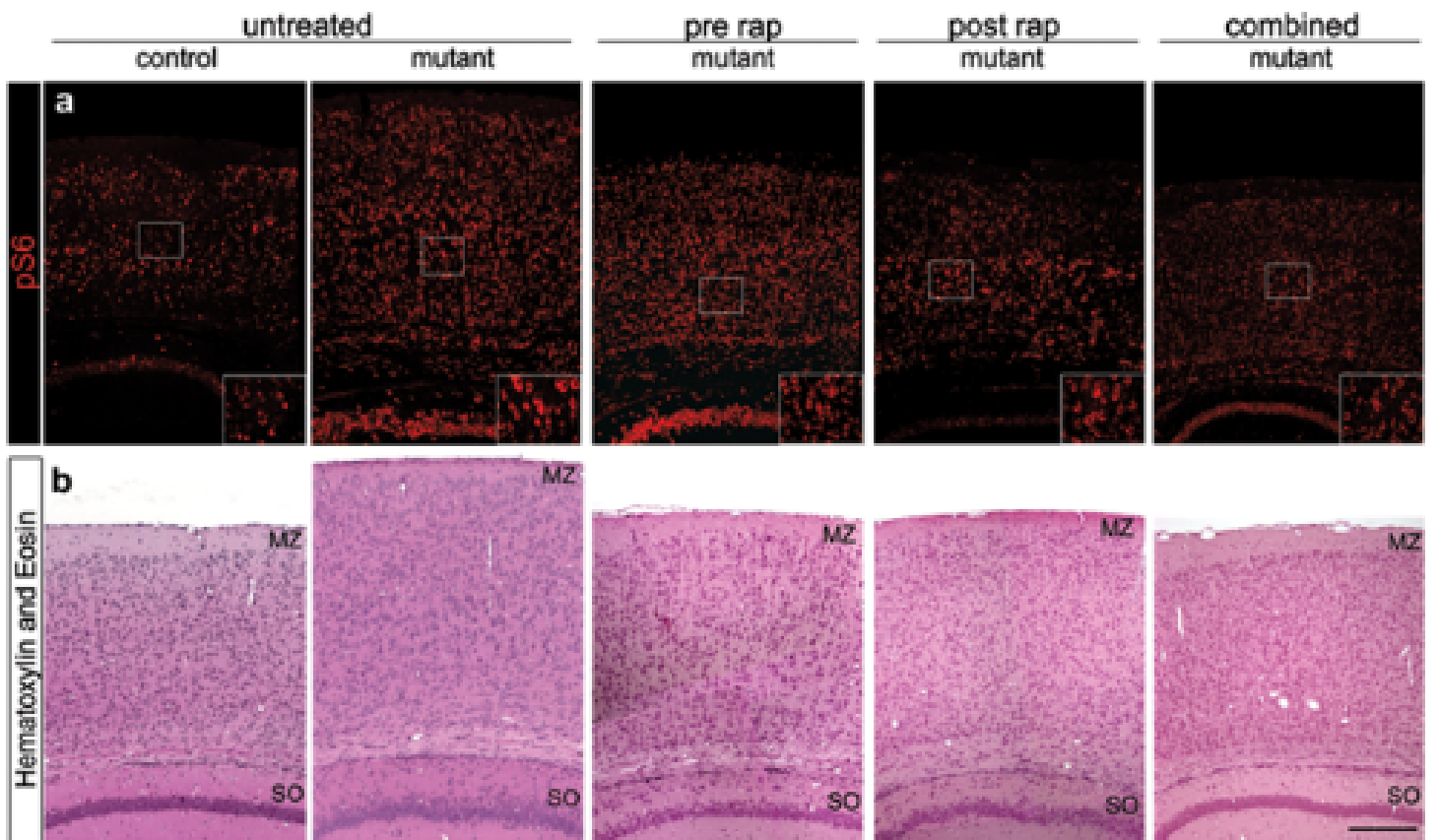


Figure 2.1. Prenatal, postnatal and combined rapamycin treatments improved health, weight gain and longevity. A, Rapamycin treatment regimens and their relationship to brain development. Prenatal treatment was from E12.5-birth (P0); postnatal treatment from P0 to weaning (P21); combined treatment from E12.5 to P21. In the cohorts used for histology and longevity studies, prenatal treatment stopped at birth (open circle), postnatal and combined treatments were stopped at P21 (open circle). B, Brain lysates from newborn animals after 0.1 mg/kg prenatal rapamycin treatment from E12.5 to birth were analyzed by immunoblotting. The levels of phosphorylated S6 (pS6), an indicator of mTORC1 activation, were decreased in the lysates of the rapamycin-treated Tsc2-hGFAP (mutant) animals, although not to control levels. Total S6 was unaffected. C, Immunoblots of cortical and hippocampal lysates from P21 mice treated with 0.1 mg/kg i.p. rapamycin from P0 to P21. Levels of pS6 in the untreated Tsc2-hGFAP cortex and hippocampus were increased. Treatment reduced mutant pS6 levels to approximately untreated control levels. Total levels of S6 remained unchanged. Based on these results, daily 0.1 mg/kg i.p. was used for further experiments. D, Control and Tsc2-hGFAP mutant mice at P21 after the different rapamycin treatment regimens. E, Graph demonstrating an improvement in weight gain for all rapamycin regimens compared with untreated Tsc2-hGFAP mice (solid black line). Rapamycin treatment regimens had no effect on weight gain in control animals. F, The Kaplan–Meier survival plots of untreated and all treatment regimens after the cessation of rapamycin. Colored arrows correspond to day of rapamycin cessation for specific groups. Median age of death: MUT-untreated P23 (n = 20); MUT-prenatal P31 (n = 12; $P = 0.08$); MUT-postnatal P45 (n = 6; $P < 0.001$); MUT-combined P41 (n = 5; $P = 0.0001$).

Phosphorylation of S6 in the brains of the postnatal and combined treatment groups at P21 (Figure 2.2A) was decreased compared with untreated mutants, consistent with the immunoblot analysis used to optimize the dose of 0.1 mg/kg (Figure 2.1C). Further histologic analysis demonstrated significant reduction in cortical enlargement and cellular hypertrophy in all three treatment groups (Figure 2.2B, D, F, G). The effects of combined treatment on cortical and hippocampal organization were most striking (Figure 2.2B, C, E). Prenatal and combined treatment restored the cell sparse marginal zone (MZ) that was thinner and less defined in the untreated and postnatal treated brains (Figure 2.2B). The hippocampal pyramidal layer of the combined treatment group was well organized and almost indistinguishable from control (Figure 2.2C and E). Prenatal and postnatal treatment also improved hippocampal organization, although the CA1 and CA3 regions remained somewhat disorganized. All untreated

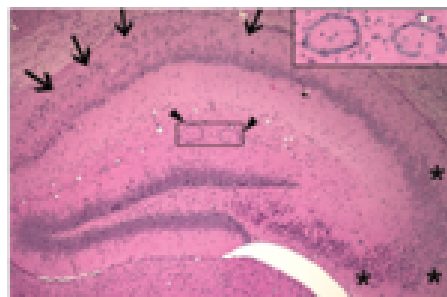
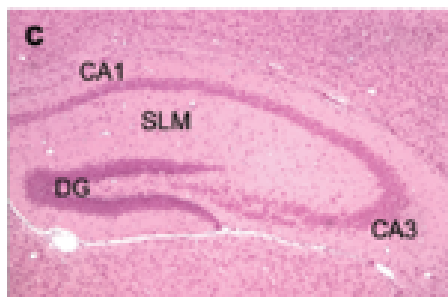
Tsc2-hGFAP animals have distinctive ring heterotopias in the stratum lacunosum moleculare (SLM) (Figure 2.2C). No heterotopia was seen in the prenatal or combined treatment samples. Small heterotopias were seen in two out of seven postnatal-treated animals. We then examined ectopic NeuN-positive cells in the stratum oriens (SO) to assess how rapamycin affected the abnormal position of these cells. Postnatal and combined treatments reduced the number of ectopic cells in the SO, but combined treatment reduced the number of ectopic cells to almost control levels (Figure 2.2E and H). These results demonstrate that rapamycin can correct the abnormal migration of Tsc2-deficient neurons. The additive effect of pre- and postnatal rapamycin treatment on hippocampal organization is consistent with the *in utero* and postnatal development of this structure [173].



untreated

control

mutant



pre rap

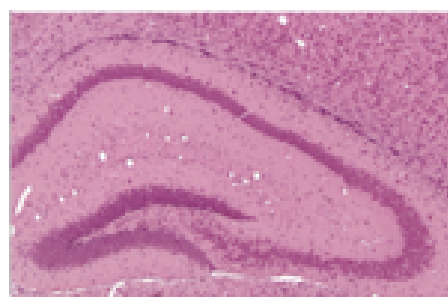
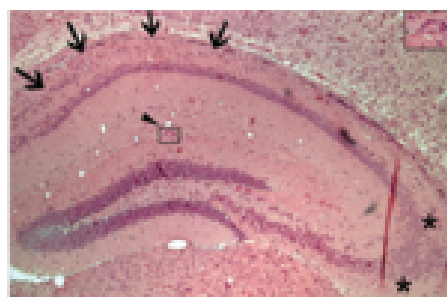
post rap

combined

mutant

mutant

mutant



untreated

pre rap

post rap

combined

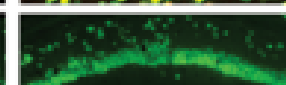
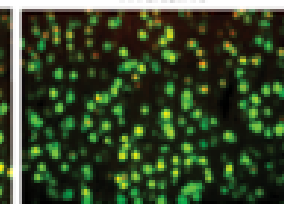
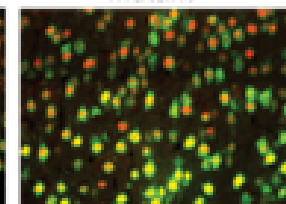
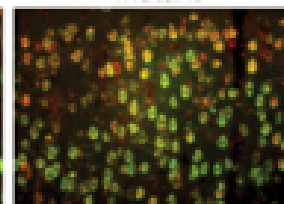
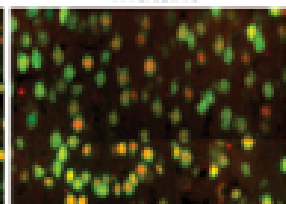
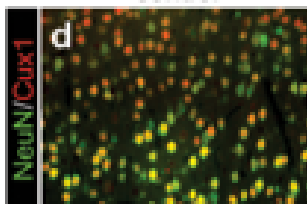
control

mutant

mutant

mutant

mutant



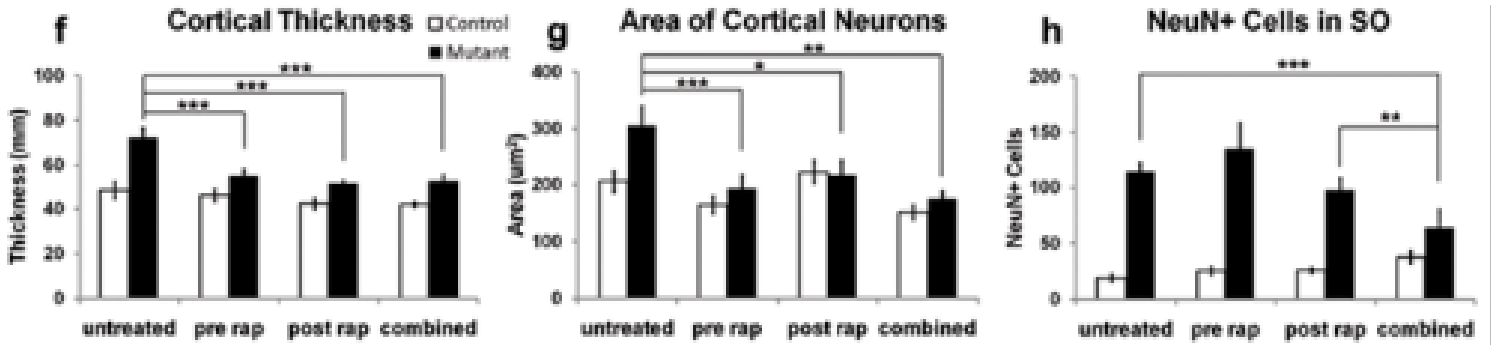
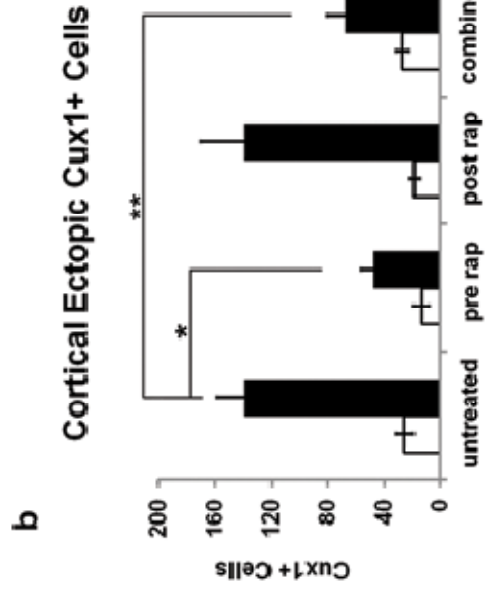
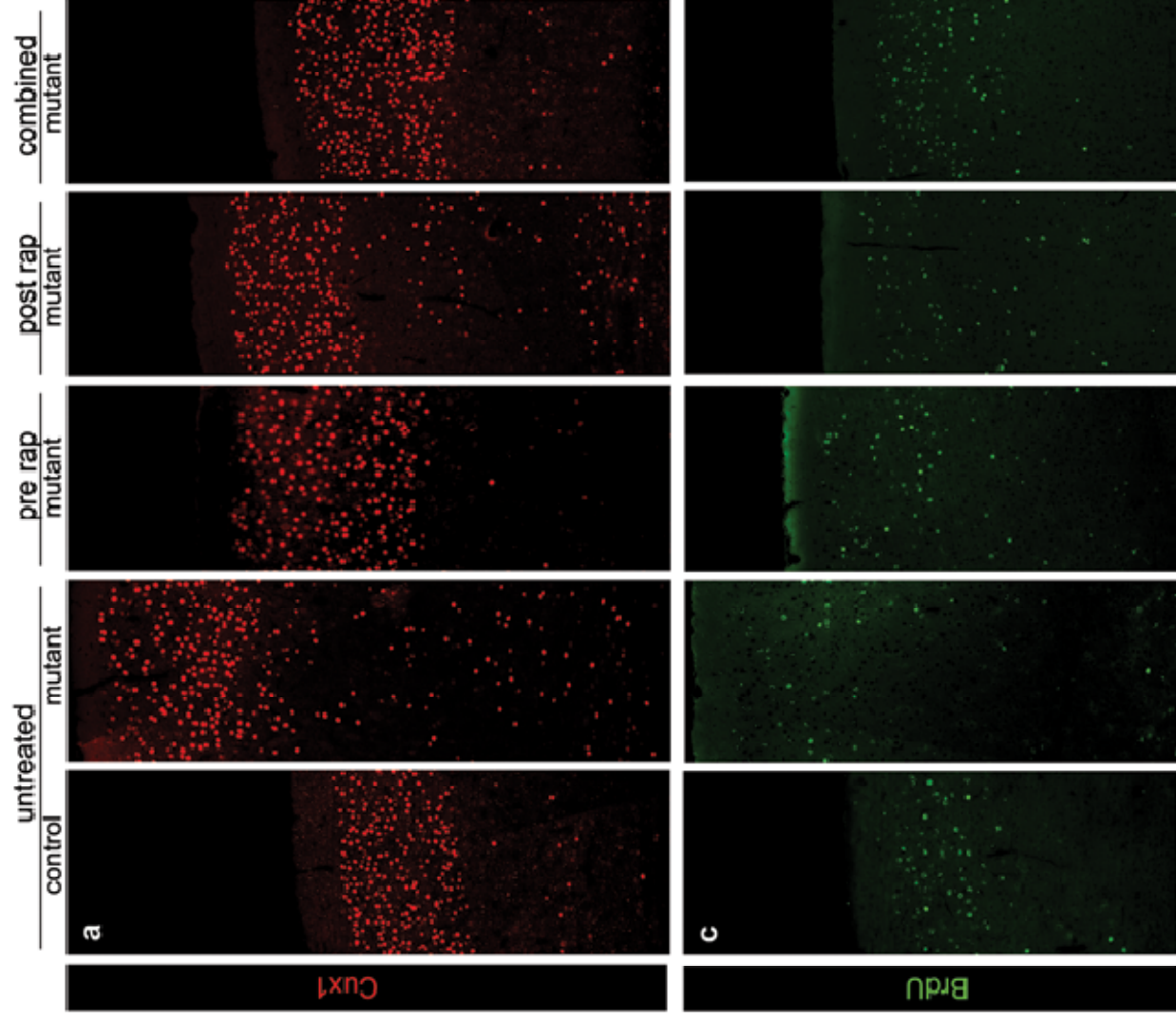


Figure 2.2. Effects of daily 0.1 mg/kg rapamycin treatment regimens on cortical histology and organization. A, Cortical and hippocampal phosphorylated S6 (pS6) immunohistochemistry. Untreated Tsc2-hGFAP brains at postnatal day 21 demonstrated an increased pS6 signal compared with control. Postnatal and combined treatments decreased the intensity of pS6 staining in Tsc2-hGFAP brain consistent with suppression of mTORC1. In the prenatally-treated brains, pS6 expression was comparable with untreated Tsc2-hGFAP levels, suggesting reactivation of mTORC1 during the period of no treatment from P0 to P21. B, H&E staining of the cerebral cortex. Note the well-formed MZ in the brains from prenatal and combined treated Tsc2-hGFAP mice. C, H&E staining of hippocampus. Combined treatment resulted in a mutant hippocampus that was almost identical in organization to the control. The CA1 and CA3 regions were indistinguishable between control and combined treatment groups, but remain somewhat split and disorganized (arrows and asterisks) in the prenatal and postnatal groups. The ring heterotopia in the SLM of the mutant mice (arrowheads and insets) were absent in prenatal and combined treatments, and were occasionally seen in the postnatal group (two out of seven animals examined; 15/15 untreated Tsc2-hGFAP mice have ring heterotopias). D, Higher magnification of cortical layers II/III showing NeuN immunohistochemistry of enlarged neurons of the untreated mutant and the rescue of cell size by the various treatments. E, NeuN immunohistochemistry of the CA1 region of the hippocampus. Note the ectopic cells in the SO of untreated Tsc2-hGFAP mice that are decreased in number in postnatal treatment, and almost disappear in combined treatment brains. F, Bar graph showing the rescue of cortical thickness in all treatment regimens ($***P < 0.001$). The thickness of the control cortex was unaffected by the different rapamycin regimens. G, Bar graph showing the rapamycin rescue of neuronal hypertrophy ($*P < 0.05$; $**P < 0.01$; $***P < 0.001$). Control neuronal size was not significantly affected by rapamycin. H, Bar graph showing the number of ectopic neurons in the SO of the hippocampus in different treatment groups. Combined treatment had the greatest effect on reducing the number of ectopic neurons in the SO ($**P < 0.005$; $***P < 0.0005$). Data represent mean +SEM. MZ, marginal zone; SLM, stratum lacunosum-moleculare; SO, stratum oriens; DG, dentate gyrus.

To examine the effects of rapamycin on cortical lamination, we performed immunohistochemistry to detect the layer II–IV-specific transcription factor Cux1 [174] (Figure 2.3A and B). Both prenatal and combined rapamycin decreased the number of

ectopic Cux1-positive cells in cortical layers V and VI of Tsc2-hGFAP mice. Postnatal treatment had little effect on the distribution of Cux1-positive cells. These results suggest that *in utero* administration of rapamycin can rescue the abnormal migration of cortical neurons to appropriate layers of the cortex. To further assess the effect of rapamycin on neuronal migration, we analyzed the fate of cortical neurons born at E15.5 using BrdU birthdating (Figure 2.3C and D). In control mice, the majority of BrdU labeled neurons at E15.5 appear in the upper cortical layers. More BrdU-labeled neurons are present in the lower cortical layers of the untreated mutant, suggesting that the loss of Tsc2 affects the migration of some late-born neurons. Prenatal treatment increased the distribution of BrdU-labeled cells toward more superficial layers, whereas postnatal and combined treatments resulted in a BrdU distribution that was most similar to controls. These demonstrate that rapamycin can alter the abnormal migration of Tsc2-deficient neurons during both prenatal and postnatal cortical development.



d Cortical BrdU+ Cell Distribution

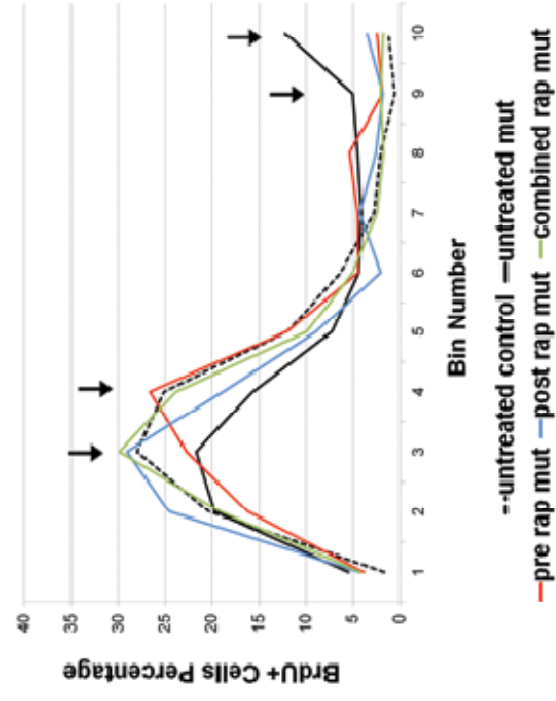
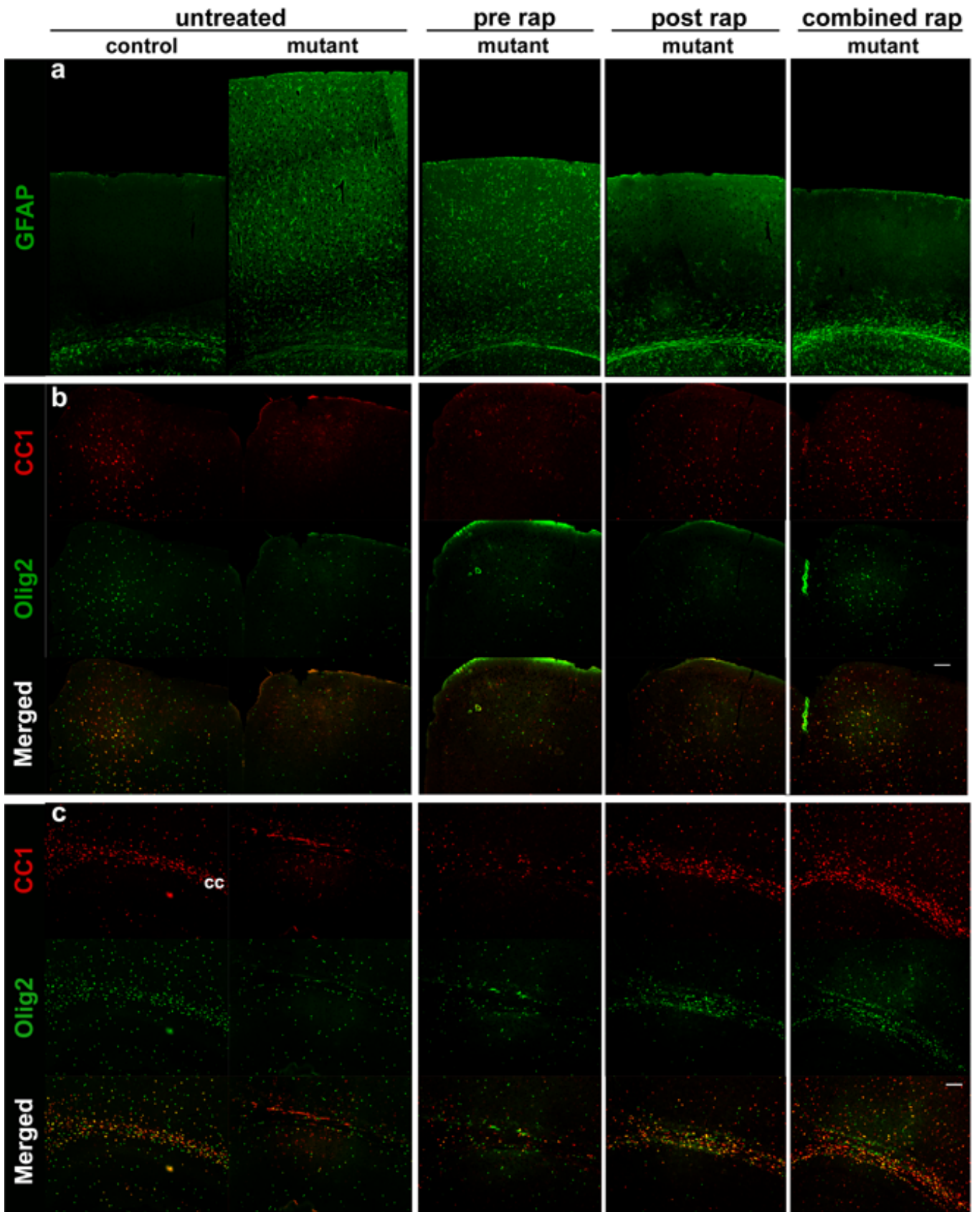


Figure 2.3. Effects of daily 0.1 mg/kg rapamycin treatment regimens on cortical lamination. A, Cux1 immunohistochemistry. Note the ectopic Cux1-positive cells in the deep cortical layers of the untreated Tsc2-hGFAP brain. B, Bar graph of ectopic Cux1-positive cells. Prenatal and combined rapamycin treatment significantly reduced the number of ectopic Cux1 cells in layers V and VI ($*P < 0.05$; $**P < 0.005$). C, BrdU immunohistochemistry at P21 showing cortical cells BrdU-labeled at E15.5. D, Histogram showing distribution of E15.5 BrdU-labeled cells in different treatment groups. Bin 1 is at the pial surface and bin 10 is at the ventricular zone. Untreated Tsc2-hGFAP mice have more BrdU-labeled neurons in the lower bins 9 and 10. All treatments increased the proportion of BrdU-labeled cells in the more superficial bins. Arrows indicate significant differences between control and untreated, and among treatment regimens. Data represent mean \pm SEM. MZ, marginal zone.

oligodendrocytes and myelination were examined. Untreated Tsc2-hGFAP mice at P21 showed a decreased number of mature cortical and callosal oligodendrocytes (Figure 2.4B, C, E, and F). Prenatal rapamycin treatment had little effect on mature oligodendrocyte number. Postnatal and combined treatments significantly restored the number of mature oligodendrocytes in both the cortex and corpus callosum of mutant animals. These results are consistent with the late embryonic and postnatal maturation of oligodendroglia [175]. Cortical myelination is also a postnatal event. Accordingly, we observed substantial rescue of myelination defects in only the postnatal and combined treatment groups (Figure 2.4D).



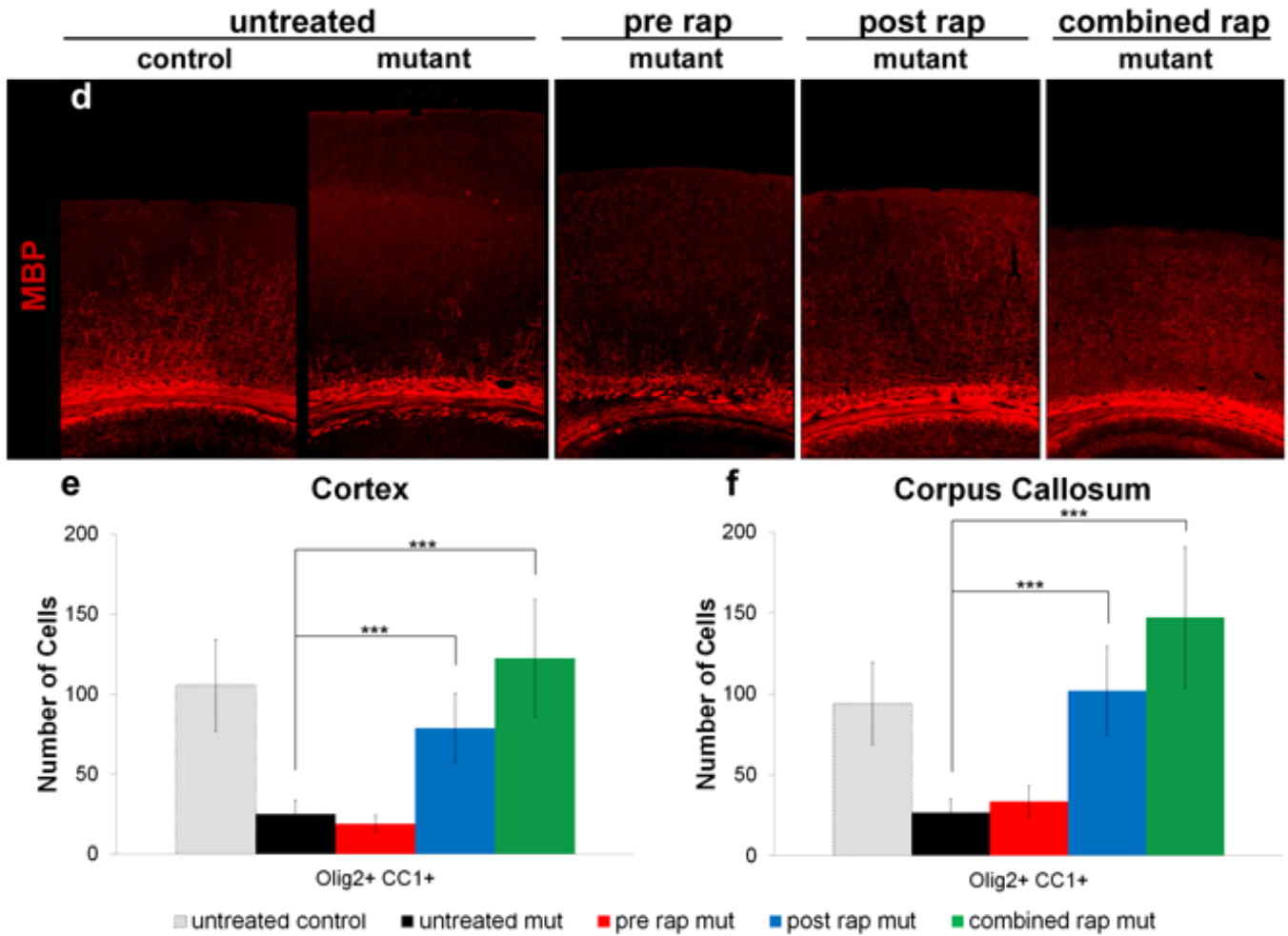


Figure 2.4. Effects of daily 0.1 mg/kg rapamycin treatment regimens on astrocytes, oligodendroglia and myelination. A, Glial fibrillary acid protein (GFAP) immunohistochemistry. Prominent astrogliosis in untreated mutant was defined by increased cortical GFAP expression. Postnatal and combined rapamycin treatment normalized GFAP expression. Prenatal treatment had little effect on the upregulation of GFAP. B and C, CC1 and Olig2 immunohistochemistry to identify mature oligodendroglia in the midline cortex (B) and lateral corpus callosum (C). Many mature oligodendroglia were found in the control midline cortex and corpus callosum. In the same structures of the untreated Tsc2-hGFAP, there was a marked decrease in mature oligodendrocytes. Postnatal and combined treatments restored the cortical oligodendrocyte distribution to control levels ($***P < 0.001$), whereas prenatal treatment had little effect. D, Myelin basic protein (MBP) immunohistochemistry. MBP distribution in the cortex is almost absent from untreated Tsc2-hGFAP mice. Postnatal and combined treatment demonstrated significant restoration of the normal MBP pattern. Data represent means \pm SEM.

While haploinsufficiency for Tsc1 and Tsc2 is associated with modest behavioral deficits [95, 176, 177], the consequences of LOH on behavior have been more difficult to assess due to the lethality associated with many of these mouse models [98, 107, 108]. We found that 2 mg/kg intraperitoneal injection of rapamycin three times a week beginning at P10 was able to maintain the health and extend the lifespan of Tsc2-hGFAP mice as long as treatment continued (Figure 2.5). We reported weights of the animals for three reasons: 1.) untreated mutants or prenatal rapamycin treated mutants all appear physically runted by postnatal day 23, 2.) it is unknown how increased mTORC1 activity in the brain reduces body weight but it is possible that hypothalamic mTORC1 activation suppresses appetite [178], and 3.) seizure activities may cause a reduction in weight but it is difficult to assess subclinical seizures. Therefore, to assess if histologic rescue in the combined and postnatal groups led to improved brain function, postnatal and combined treatment groups were switched from 0.1 mg/kg daily to 2 mg/kg rapamycin three times a week between postnatal days 35 and 44 to maintain their health and permit behavioral analysis (Figure 2.6A). Behavior testing was initiated after the first four doses of rapamycin and spanned P42–P120 (1.5–4 months). After the completion of behavioral testing, brains were isolated for histologic analysis.

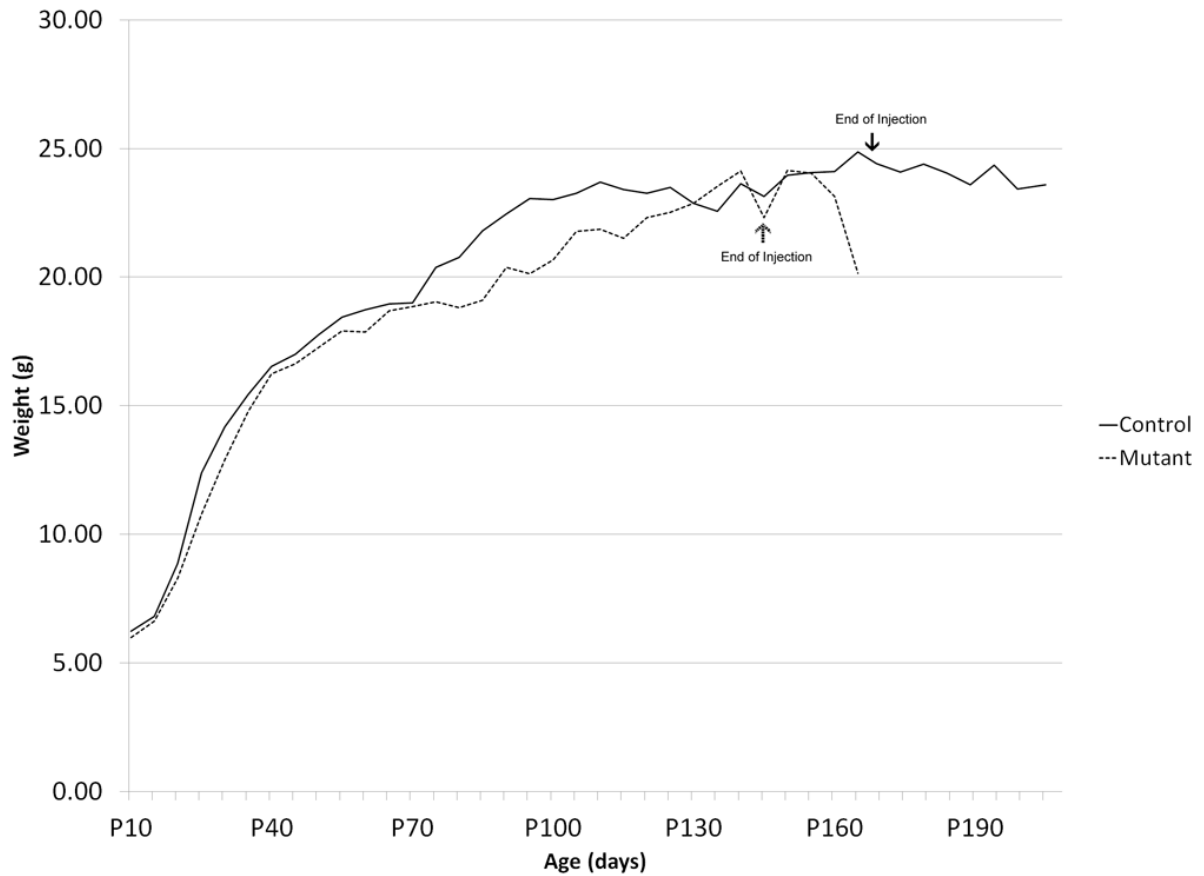


Figure 2.5. Effects of 2mg/kg rapamycin i.p. on longevity and weight of Tsc2-hGFAP mice. Tsc2-hGFAP animals were treated with 2mg/kg rapamycin three times a week starting at postnatal day 10. This regimen extended the life and health of the Tsc2-hGFAP mice so that they were indistinguishable from control mice. Mutant animals began to die from seizures approximately 2 weeks after rapamycin was discontinued.

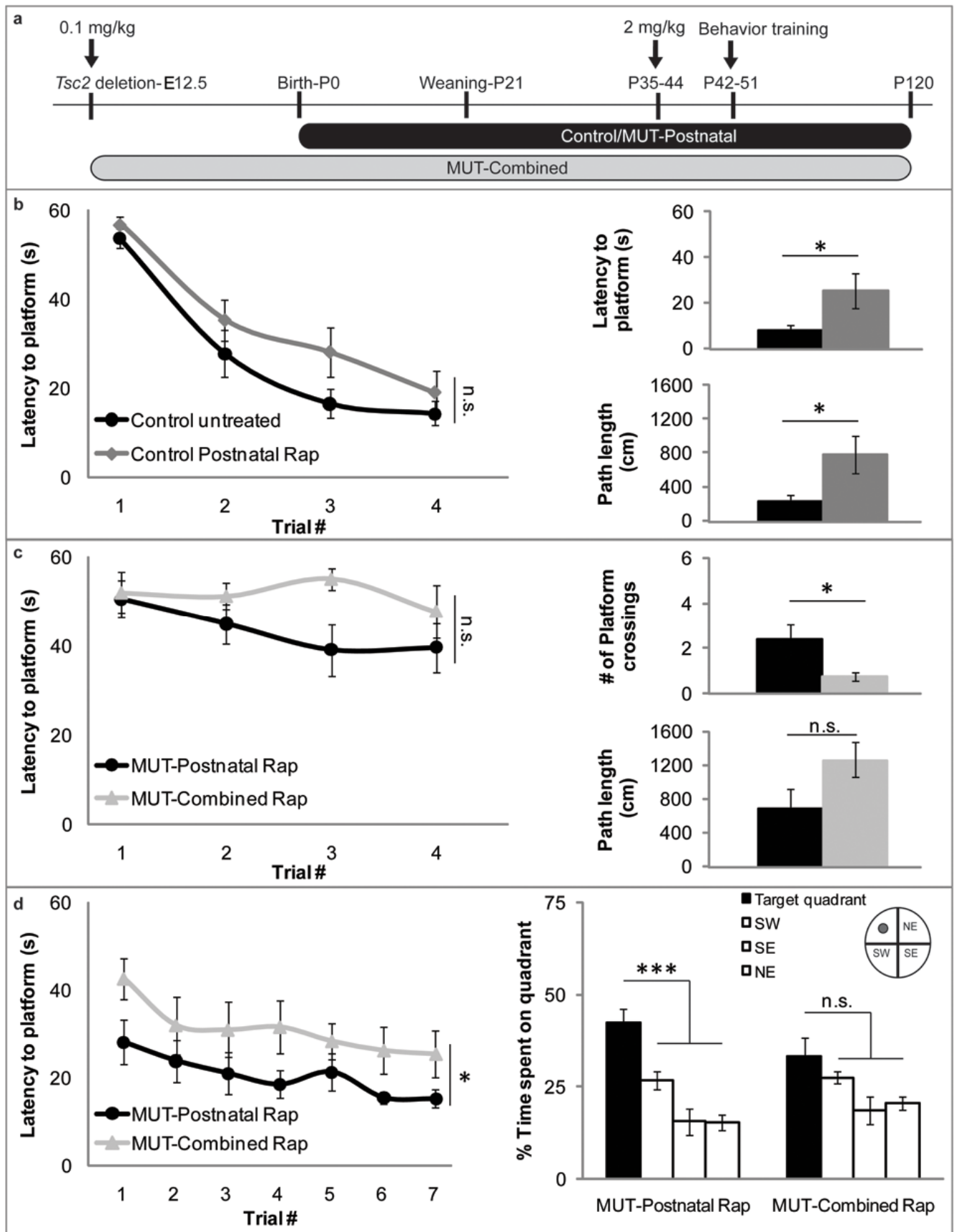
Spatial memory, which is sensitive to the manipulation of the TSC2-mTOR cascade, was tested using a modified 1-day version of the Morris water maze task [168, 169, 179]. Consistent with this, control mice treated with 2 mg/kg rapamycin had significantly impaired long-term memory as indicated by increased latency ($P = 0.04$) and path length ($P = 0.03$) to cross the previous location of the hidden platform during a

probe trial administered 24 h after training (Figure 2.6B). Untreated mutants were unable to be tested because none survives beyond postnatal day 40. When the performance of the postnatal and the combined Tsc2-hGFAP treatment groups were compared, no significant difference in acquisition was observed (Figure 2.6B versus C, left panels). Probe trials showed a decreased path length and significantly increased number ($P = 0.036$) of platform crossings for the postnatal group when compared with those observed for the combined treatment group, suggesting enhanced memory. As the 1-day paradigm does not typically give rise to strong spatial localization, these animals were given daily training (four trials) for an additional 7 days. Consistent with our probe trial results, the postnatal group showed improved memory for the platform location on day 1 compared with the combined group. This difference was maintained throughout the training ($P = 0.037$), with both groups acquiring the location of the hidden platform at similar rates (Figure 2.6D). When spatial localization was assessed in a probe trial given 48 h after the last day of training, a significant preference for the target quadrant was observed for the postnatal ($P < 0.001$), but not the combined treatment groups ($P = 0.204$). No significant differences in either swimming speed or performance in a visible platform task were observed between the two treatment groups (Figure 2.7).

Heterozygous Tsc2^{+/-} mice have an impaired ability to discriminate between two similar contexts, a deficit that could be lessened by pre-training rapamycin treatment [95].

Untreated control mice can distinguish between two similar contexts after 1 day of training as indicated by significantly more freezing in the context in which a mild foot shock was delivered (Figure 2.6E). In agreement with the previous results, control animals treated with rapamycin were unable to perform this discrimination. When both

rapamycin-treated Tsc2-hGFAP groups were tested after 3 days of training, only the postnatal-treated group was able to distinguish between the two contexts (Figure 2.6F). Altogether, these results show that postnatal rapamycin can enable Tsc2-hGFAP animals to learn and remember. While combined rapamycin treatment produced a most complete histologic rescue, these animals had impaired memory when compared with the postnatal group.



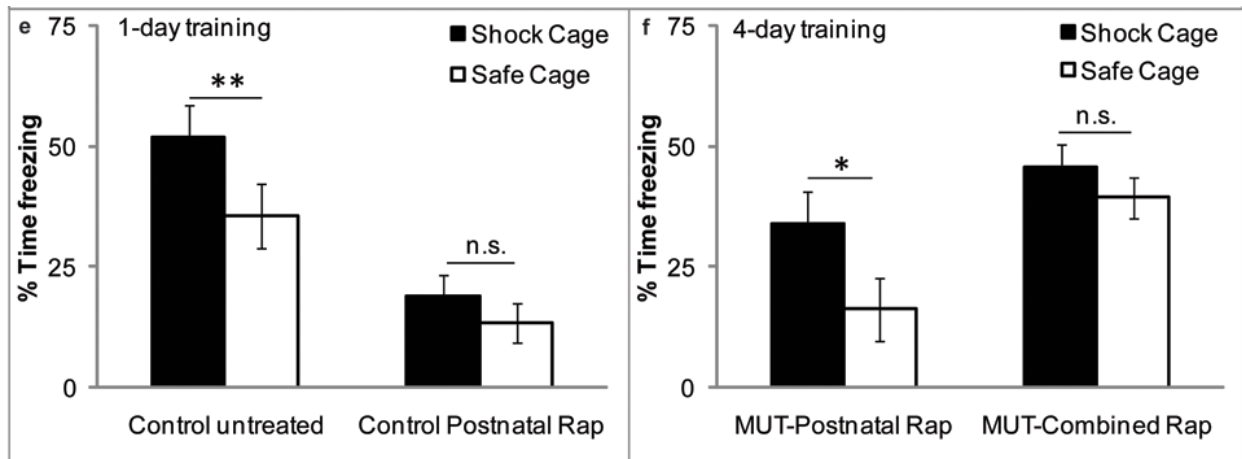


Figure 2.6. Effects of rapamycin treatments on learning and memory. A, Rapamycin treatment regimens and timing for behavior testing. Animals were treated with 0.1 mg/kg rapamycin daily starting at E12.5 (combined group) or birth (postnatal group). Between P35 and P44, rapamycin dosing was changed to 2 mg/kg three times a week to maintain the health of the animals. Treatment continued throughout behavior testing and ended at P120. B, Left panel: latency to platform during a 1-day Morris watermaze training protocol ($n = 10$ control untreated group, $n = 10$ control postnatal rapamycin group; two-way repeated-measures of ANOVA with treatment and trial number as between-subjects factors: $F(1,18) = 2.95$, $P = 0.103$). Right panels: latency to platform and path length traveled during probe trial 24 h after completion of training (two-tailed, unpaired Student's *t*-test; latency to platform $P = 0.04$; path length $P = 0.03$). C, Left panel: latency to platform during a 1-day Morris watermaze training protocol ($n = 8$ for both groups; two-way repeated-measures ANOVA with treatment and trial number as between-subjects factors: $F(1,14) = 3.01$, $P = 0.105$). Right panels: platform crossings and path length traveled during probe trial 24 h after completion of training (two-tailed, unpaired Student's *t*-test; platform crossings $P = 0.036$; path length $P = 0.09$). D, Left panel: latency to platform during a 7-day Morris watermaze training protocol ($n = 8$ MUTpostnatal rapamycin group, $n = 9$ MUT-combined rapamycin group, two-way repeated-measures ANOVA: group main effect $F(1,15) = 5.271$, $P = 0.037$). Right panel: quadrant preference during a probe trial 48 h after training (one-way repeated-measures ANOVA (MUT-postnatal group) and ANOVA on ranks (MUT-combined group) with quadrant as between-subjects factor: $F(3,21) = 12.831$, $P < 0.001$; Chi-square = 4.600, 3 d.f., $P = 0.204$). E, Percent time spent freezing in shock cage or safe cage after 1 day of training in a context discrimination protocol ($n = 10$ both groups; two-tailed, paired Student's *t*-test $P = 0.009$ (control untreated); $P = 0.085$ (control postnatal rapamycin)). F, Percent time spent freezing in shock cage or safe cage after 4 days of training in a context discrimination protocol [$n = 7$ MUT-postnatal rapamycin group, $n = 9$ MUT-combined rapamycin group; two-tailed, paired student's *t*-test $P = 0.014$ (MUTpostnatal rapamycin group); $P = 0.37$ (MUT-combined rapamycin group)]. * $P < 0.05$, ** $P < 0.01$, *** $P < 0.001$. Data represent means \pm SEM.

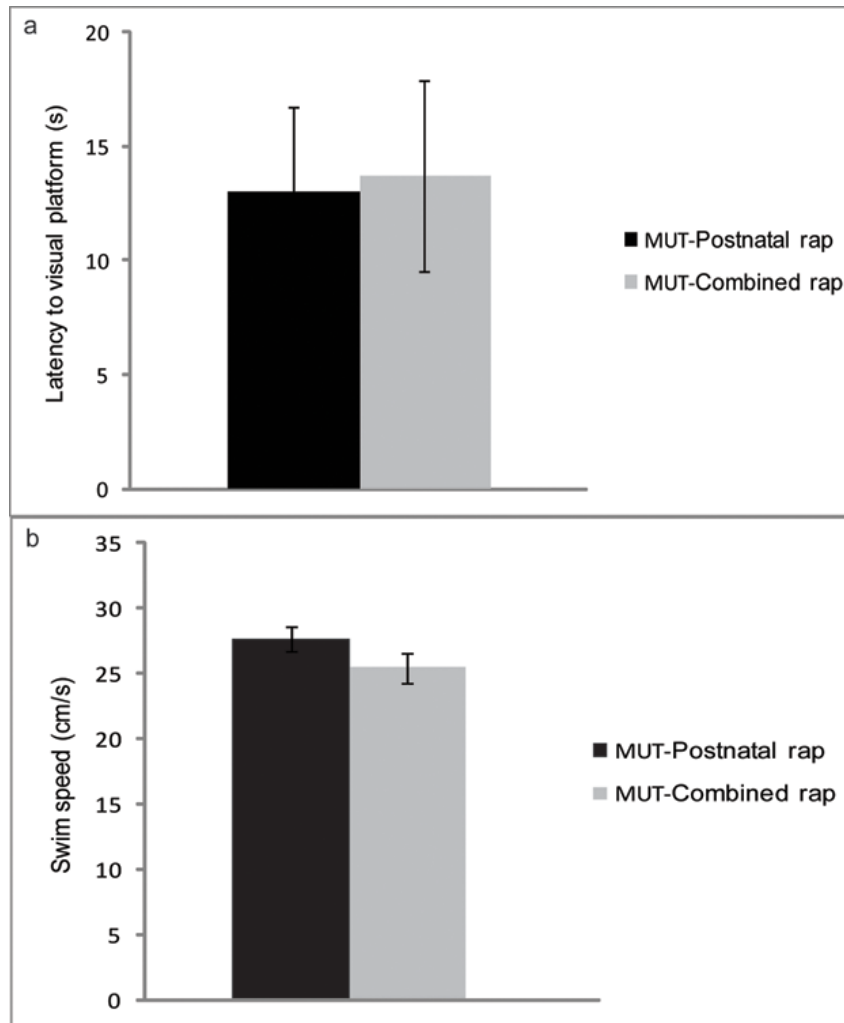


Figure 2.7. Visual and motor control tasks for Morris water maze. A, There was no difference in latency to finding a visual platform between the two mutant groups. B, There was no difference in the swim speed between the two mutant groups. Data represent means \pm SEM.

After the completion of behavioral testing, we analyzed the brains of the postnatal and combined groups to assess if 2.5 months of 2 mg/kg rapamycin treatment changed the brain histology that was observed at P21 after daily 0.1 mg/kg rapamycin. We found increased expression of phosphorylated S6 (240/244) above control levels (Figure 2.8A). While 2 mg/kg rapamycin three times a week was enough to maintain the health of the animals, it was not sufficient to suppress mTORC1 to control levels as we

observed in the P21 brains. We also noted an increase in cortical thickness in the mutant animals compared with controls that would also be consistent with increased mTORC1 activity. The increased pS6 was accompanied by an increase in GFAP (Figure 2.8B), indicative of astrogliosis associated with mTORC1 hyperactivity as has been reported previously [98, 108, 180]. Hippocampal and cortical organization, lamination and myelination were unchanged compared with the histologic analysis observed at P21 after daily 0.1 mg/kg rapamycin in the postnatal and combined groups (Figure 2.9).

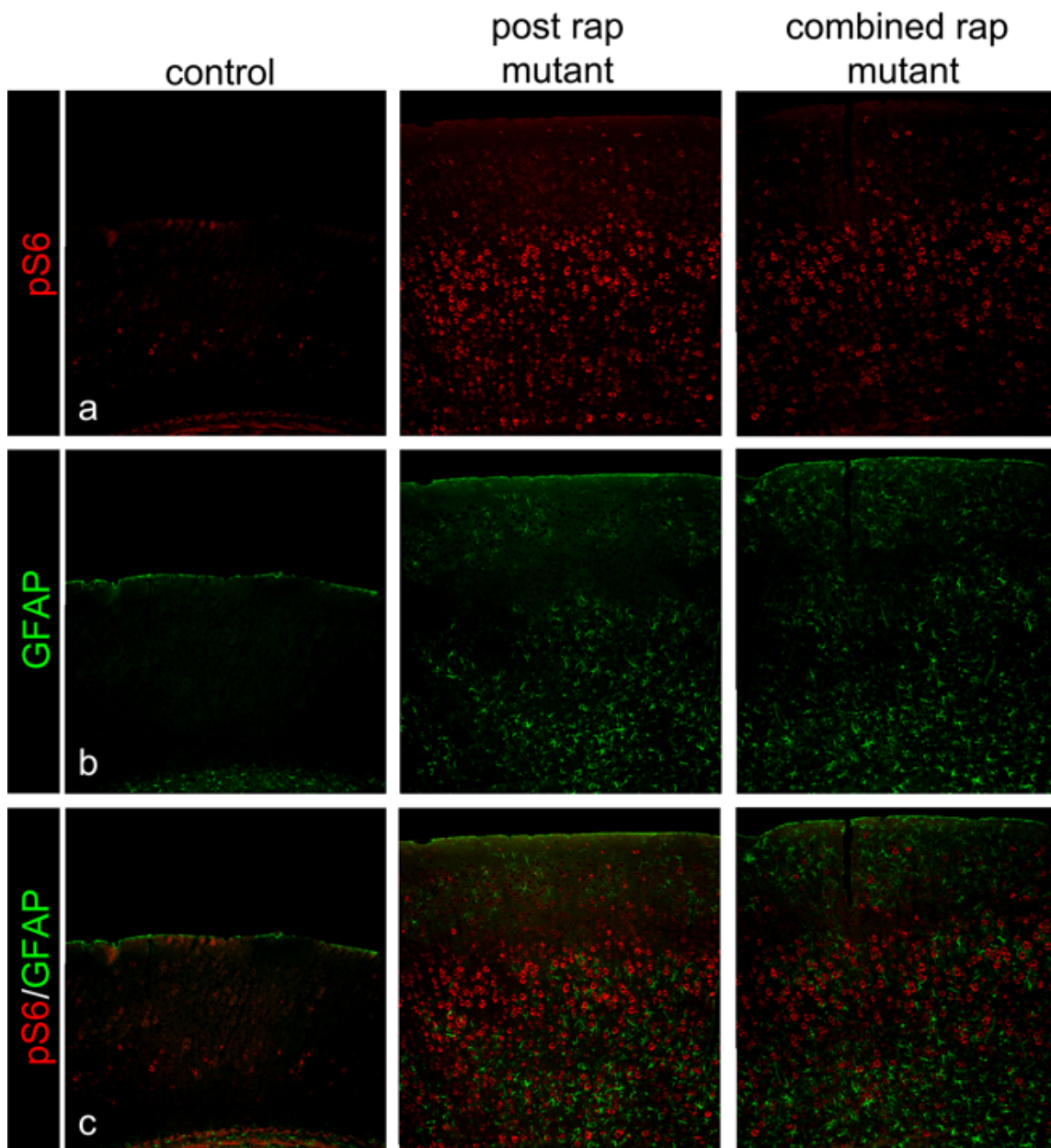
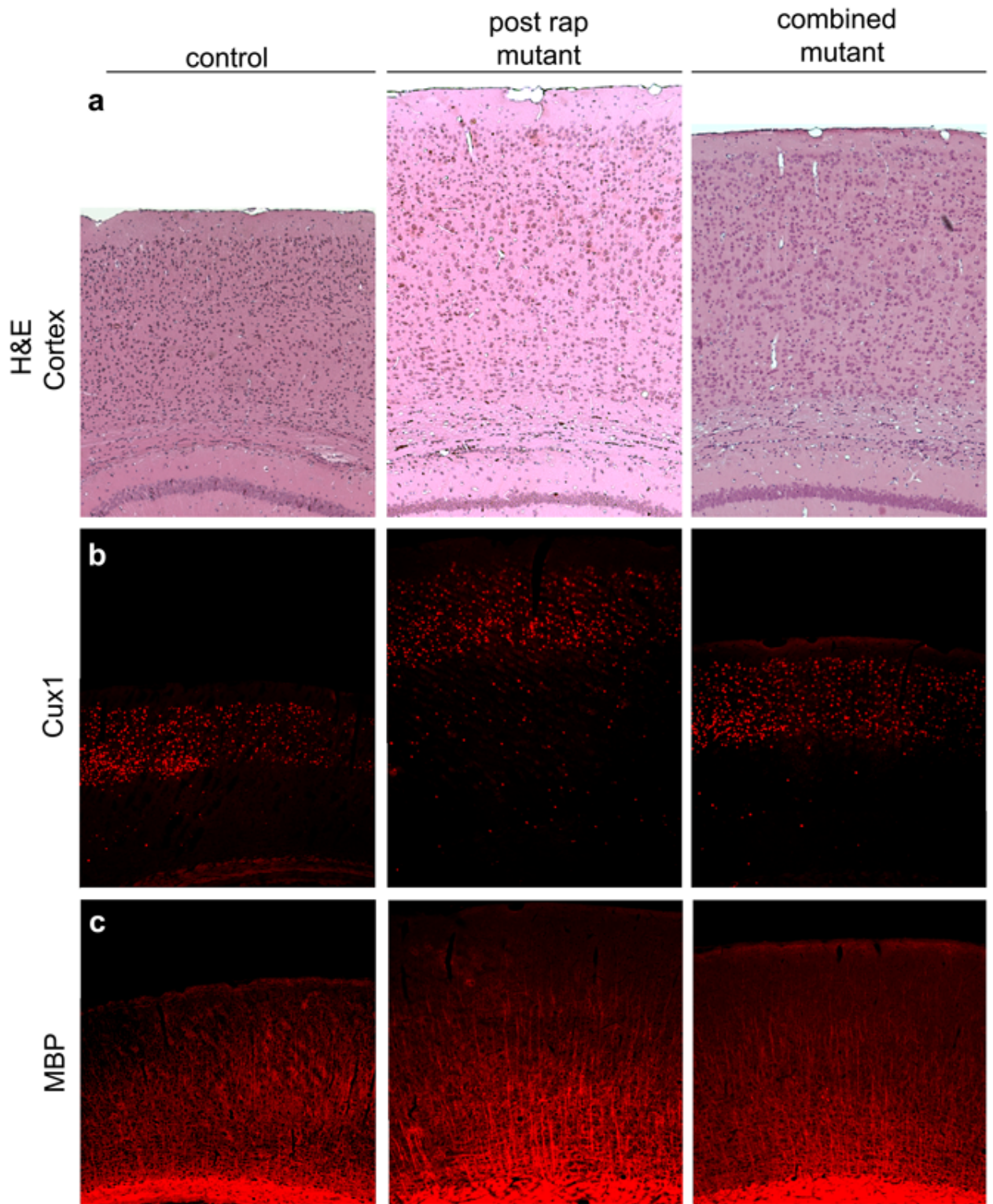


Figure 2.8. Effects of 2 mg/kg rapamycin on cortical phosphorylated S6 levels and GFAP expression after behavioral testing. A, There is increased expression of pS6 levels in the cortex of both the postnatal and combined groups, indicating that 2 mg/kg of rapamycin was not sufficient to maintain the mTORC1 inhibition observed at P21 after 0.1 mg/kg from Figure 2. B, The increased pS6 expression is accompanied by cortical astrogliosis. C, Merge of A and B.



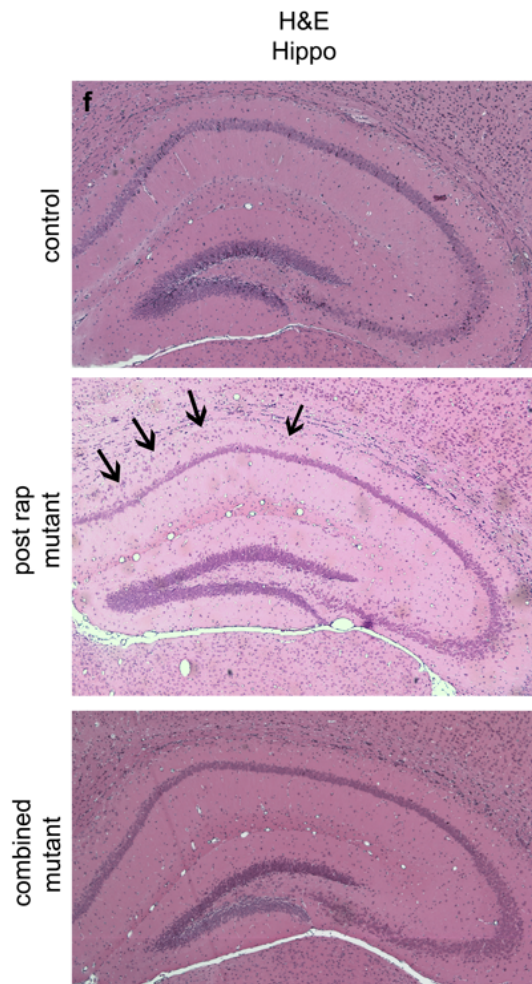
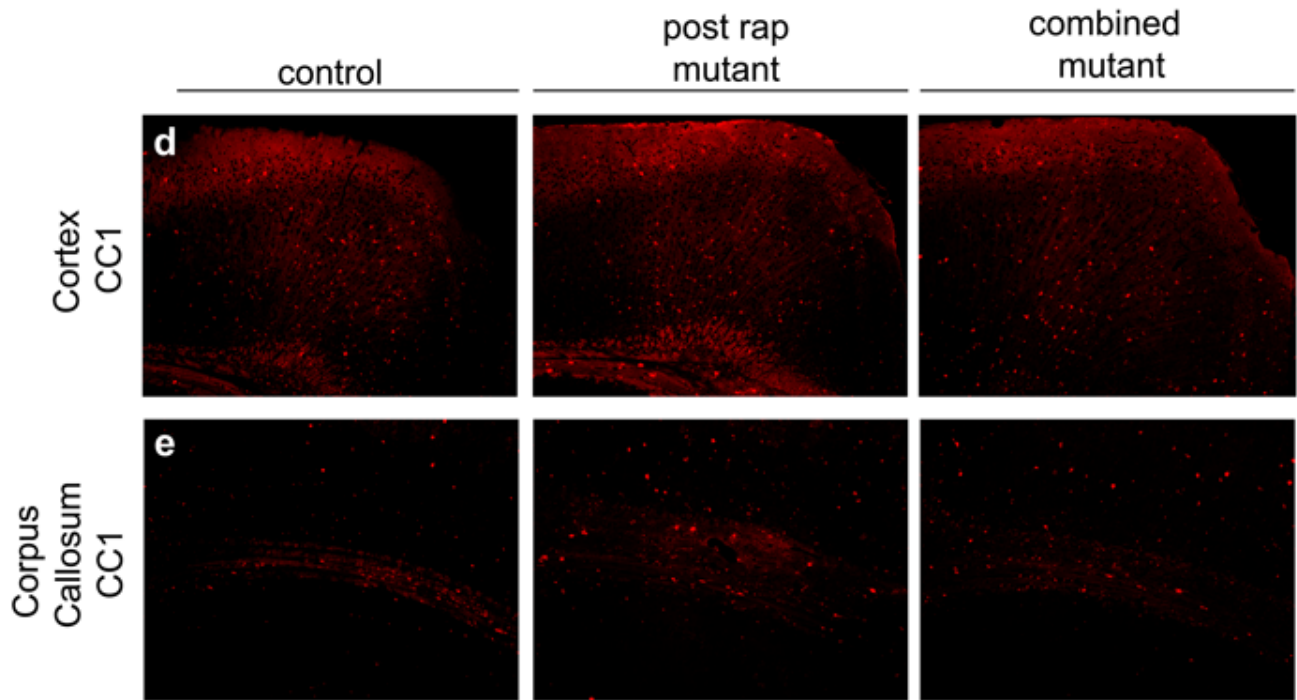


Figure 2.9. Brain histology after 2 mg/kg rapamycin and behavior testing. A, H and E staining of the cortex. The cortex is thicker in the treated mutant animals but appears well organized. The postnatal treated brains are thicker than the combined group. B, Cux1 immunohistochemistry. As seen at P21 after 0.1 mg/kg rapamycin, the mutant brains show organized cortical layers II-IV, but the postnatal group has more ectopic Cux1 positive cells in layers V and VI. C, MBP immunohistochemistry. Myelination is not affected by the 2 mg/kg rapamycin treatment and remains well established. D and E, CC1 immunohistochemistry. Oligodendrocyte distribution does not appear to be affected by the 2 mg/kg rapamycin treatments, though the thickness of the corpus callosum is increased in the mutant brains. F, H&E staining of hippocampus. The hippocampus of the mutant animals remains well organized after the 2 mg/kg treatment, though some ectopic pyramidal cells remain in the stratum oriens of the postnatal group as seen at P21 (arrows).

2.4 Discussion

In this study we demonstrate the prevention of Tsc2-associated neurodevelopmental abnormalities in a neuroglial mouse model of TSC using different perinatal rapamycin treatment regimens. Prenatal, postnatal and combined rapamycin treatment regimens were well tolerated and improved the overall health of Tsc2-hGFAP mice. However, discontinuation of rapamycin at postnatal period ultimately led to death, a finding consistent with previous reports [96, 97]. Of the three regimens tested, the combined treatment was most effective in restoring histologic development of the cortex. However, the observed reductions in cortical and hippocampal developmental pathologies did not correlate with memory function. The postnatal-treated animals performed better than the combined treatment group in two hippocampus-dependent memory tasks.

The combined treatment, which targeted both *in utero* and postnatal neurodevelopment, achieved a remarkable histologic rescue that was almost indistinguishable from untreated control animals. The results of combined treatment were an additive effect of rapamycin on prenatal and postnatal developmental events. For example, the migration of cortical neurons to their appropriate layer is predominantly a prenatal event. Only prenatal and combined treatments were able to rescue the MZ and the distribution of Cux1-positive cells. Postnatal treatment had little effect on antenatal neuronal migration defects. Likewise, postnatal and combined treatments mainly affected developmental defects that are predominantly postnatal or continue through the postnatal period such as oligodendrogenesis, myelination and the later stages of hippocampal development [173, 175]. These results suggest

developmental windows of opportunity for the perinatal rescue of TSC pathology with rapamycin.

The *Tsc2*-hGFAP mutant mice used in this study died postnatally, even if rapamycin treatment was maintained at 0.1 mg/kg given daily (Figure 2.1F). In order to test the consequences of rapamycin treatment on learning and memory, 2 mg/kg rapamycin was administered three times a week during behavioral testing. Although this dosing was not adequate to suppress mTORC1 activation to control levels, it still has a major clinical relevance and suggests that partial mTORC1 inhibition in human TSC patients may be adequate to improve neurologic function.

Although both combined and postnatal groups appeared to learn the 7-day Morris watermaze task, the performance of the postnatal group was found to be significantly improved when compared with the combined treatment group (Figure 2.6C). This improved performance was also observed when long-term memory was assessed, as indicated by increased search times in the immediate vicinity where the platform was previously located. Consistent with this, combined treatment animals were incapable of performing a context discrimination task, suggesting that prenatal rapamycin exposure has subtle effects that significantly affect memory consolidation in this group. As the mTORC1 pathway participates in a number of processes critical for neurodevelopment such as neuronal growth, axon guidance, synapse formation and myelination, disruption of these processes could contribute to the observed memory dysfunction in the combined treatment group [181-184]. Additional ultrastructural and dose–response studies would be needed to assess these possibilities.

The results of these and a previous study raise the feasibility of administering low-dose rapamycin to women carrying a TSC-affected fetus and/or treating TSC-affected children within the first few years of life [159]. Specifically we saw that daily 0.1mg/kg rapamycin treatment had a significant impact on the prenatal mutants but that dose has minimal effects on the adults suggesting a different dose-response curve between fetuses and mothers. Moreover, many TSC-associated functional deficits such as epilepsy and autism spectrum disorders often manifest within the first few years of life [155]. *In utero* medical treatment has precedence. Periconceptual folic acid prevents neural tube defects [185]. Rapamycin is classified as a class C teratogen. Animal studies suggest adverse effects on the fetus at higher doses, but there are no well-controlled human studies. There have been a few reports of pregnant mothers having received rapamycin in the transplant literature [186]. Most of the infants were phenotypically normal; however, no formal follow-up cognitive testing has been done. In spite of these observations, the negative effects of rapamycin on the behavior of the combined treatment group suggests that more preclinical studies need to be done to better assess the neuroanatomic and physiologic consequence of mTORC1 inhibition on the developing mammalian brain. Nonetheless, the postnatal studies are perhaps more encouraging and raise the possibility of clinical trial in infants or young children. Further studies are needed to assess dosages that would be beneficial, but not induce a failure to thrive phenotype as we and others have observed with high doses of rapamycin.

In summary, we demonstrate several novel developmental effects of rapamycin on a neuroglial loss of heterozygosity model of TSC. These results suggest that rapamycin treatment during the early perinatal period might be an opportune interval to

treat developmental disorders caused by mTORC1 dysregulation. Partial mTORC1 rescue in human TSC patients may provide significant therapeutic benefit. Our results will help better design future preclinical and clinical trials for TSC and other mTORopathies.

CHAPTER 3: mTORC1 ACTIVATION INDUCED ARRHYTHMOGENESIS

3.1 Introduction

Mammalian target of rapamycin complex 1 (mTORC1) overactivity has been implicated in many studies to be closely involved with epileptogenesis, a manifestation of the hyperactive electrical signals in the central nervous system [91, 93, 187]. mTORC1 is also a strong candidate for pathologic cardiac hypertrophy and arrhythmias. Many transcriptional, cell signaling, and metabolic changes accompanying mTORC1 signaling and the pathologic remodeling have been identified [188-190]. Prolonged pathologic cardiac hypertrophy causes the heart to eventually decompensate, thus many studies have focused on therapeutic methods to modulate mTORC1 signaling to halt or even reverse the cardiac remodeling process [191-193]. However, the Framingham Heart study identified that left ventricular hypertrophy is not only associated with increased risk of heart failure, but it is also associated with sudden cardiac death due to fatal arrhythmias [11-13].

Mechanisms of arrhythmias in hypertrophied hearts are complex. The most consistent observations in arrhythmias in the hypertrophic myocardium are heterogeneous increases in ventricular contraction and relaxation duration [13]. At the cellular level, the ionic perturbations are often a result of alterations in calcium ion handling proteins leading to prolonged action potential duration and repolarization [194-196]. This remodeling of the electrical property of the myocardium can likely induce arrhythmogenesis by the development of early and/or delayed afterdepolarizations, or abnormal depolarization of cardiomyocyte that affect different phases of cardiac action potential [197]. Early afterdepolarization is depolarization that affects either stage 2 or 3 of a cardiac action potential either because of decreased potassium ion channel

conductance or increased inward calcium current [198, 199]. In contrast, delayed afterdepolarization arises from resting action potential after the completion of repolarization secondary to cytosolic calcium overload [198].

The development of arrhythmias may also arise from changes in gap junction signaling that would delay the propagation of action potentials across the myocardium. The degree of prolonged action potential duration is not uniform throughout the hypertrophic heart. In some animal models, the degree of action potential duration varied between epicardium and endocardium [200, 201]. At the cellular level, action potentials propagate between adjacent cardiomyocytes through the intercalated disc. Connexin 43 is a gap junction protein expressed at the intercalated disc and its retention and function are regulated by several kinases including protein kinase A, protein kinase C, MAPK, and casein kinase [202-208]. Hypertrophic hearts show decreased phosphorylation and localization at the intercalated disc that correlate with slowing of action potential conduction and an increase in overall contraction time [209-212]. Such heterogeneous increase in depolarization duration is likely arrhythmogenic with altered electrical gradients and abnormal repolarization [201]. Indeed, animal studies have shown that dispersed repolarization and refractoriness within the hypertrophied myocardium is susceptible to induced polymorphic ventricular tachycardia or ventricular fibrillation [213-215].

Despite advances in understanding mechanisms of and novel therapeutics for cardiac hypertrophy, the mechanism by which the stressed heart progresses from structural and functional remodeling to electrical remodeling remains elusive [216]. Calcium ion homeostasis is central to establishing normal sinus rhythm and calcium

mishandling is increasingly viewed as central point of disease-related electrical changes [217, 218]. In the hypertrophic heart or the failing heart, calcium-handling channels and transporters such as sarco-endoplasmic reticulum calcium ATPase (SERCA2a) displays reduced expression and function [219, 220] whereas expression of the sodium-calcium exchanger (NCX1) is increased [221]. While NCX1 expression increases in this model of cardiac hypertrophy, the overall NCX1 current density is decreased due to either decreased channel activity or membrane expression.

Calcium transport by NCX1 is a major mechanism of establishing normal calcium homeostasis via removal of intracellular calcium during diastole [222]. NCX1 catalyzes the bidirectional exchange of three sodium ions for one calcium ion and works in concert with sodium-potassium ATPase (NKA) to repolarize the cell. It has been shown *in vivo* and *in vitro* that the cytoskeletal adapter protein ankyrin-B, encoded by the *ANK2* gene, is critical for the proper membrane targeting and functioning of NCX1 and NKA [2, 5, 133]. Recently, it was shown that ankyrin-B expression is altered in cardiomyopathy and regulated by calcium-dependent pathways in similar fashion as SERCA2a and NCX1. Yet, the link between cellular hypertrophic growth signaling and the changes in electrogenic protein expression remain unexplored.

Cardiac hypertrophy is closely linked with cardiac arrhythmias [213-215] and mTORC1 signaling is central in regulating cellular hypertrophic response [193, 223]. We propose that mTORC1 activity links cardiac hypertrophy to arrhythmia via regulation of ankyrin-B expression.

3.2 Materials and Methods

To determine the effects of mTORC1 on cardiac rhythm, we employed both *in vivo* and *in vitro* methods to activate mTORC1. We first used an established *in vivo* model of load-induced cardiac hypertrophy and examined the effects on cardiac rhythms with electrocardiogram (EKG) recordings. EKG recordings and heart tissues were obtained from 3 groups of animals: (1) mice chest cavities were exposed, aorta visualized, but was not constricted (sham); (2) mice chest cavities were exposed, aorta visualized, and was constricted (transverse aortic constriction, or TAC). They were allowed a 1-week recovery period prior to 2-week DMOS vehicle administration; (3) Another group of TAC'd mice were allowed a 1-week recovery period prior to 2-week daily intraperitoneal administration of 2mg/kg rapamycin [stock 1mg/1mL DMSO and diluted in 1x PBS prior to injection] (MP Biomedicals). A baseline EKG recording was obtained in all groups prior to the start of vehicle or rapamycin administration. Figure 3.1 outlines the timeline for the *in vivo* experimental protocol.

We also employed an *in vitro* model of induced mTORC1 activity in primary neonatal rat ventricular myocyte (NRVM) culture. We chose NRVM culture because the dispersed NRVMs spontaneously and rhythmically contract in culture starting 1 day after plating and express cardiomyocyte structures such as transverse-tubules and sarcomeres. Whereas adult mouse cardiomyocytes are difficult to maintain in culture, NRVMs are easier to isolate, culture, and readily transfected. This makes them an ideal model for exploring signaling regulation for cardiomyocytes *in vitro* [224, 225].

Induced mTORC1 activity was achieved by disrupting the direct upstream inhibitor of mTORC1 - the tuberous sclerosis complex (TSC) - via siRNA knockdown of tuberin, a TSC complex constituent containing GTPase activity [73, 226, 227]. We examined the effects of mTORC1 on NRVM contraction rhythm by video recording of the contractions in culture. Figure 3.2 outlines the timeline for the *in vitro* experimental protocol.

All the animal experimental protocol was reviewed and approved by UTHSC Animal Welfare Committee, Institutional Animal Care and Use Committee of Baylor College of Medicine, or both. All animal surgeries were performed by Dr. Corey Reynolds from BCM mouse phenotyping core lab.

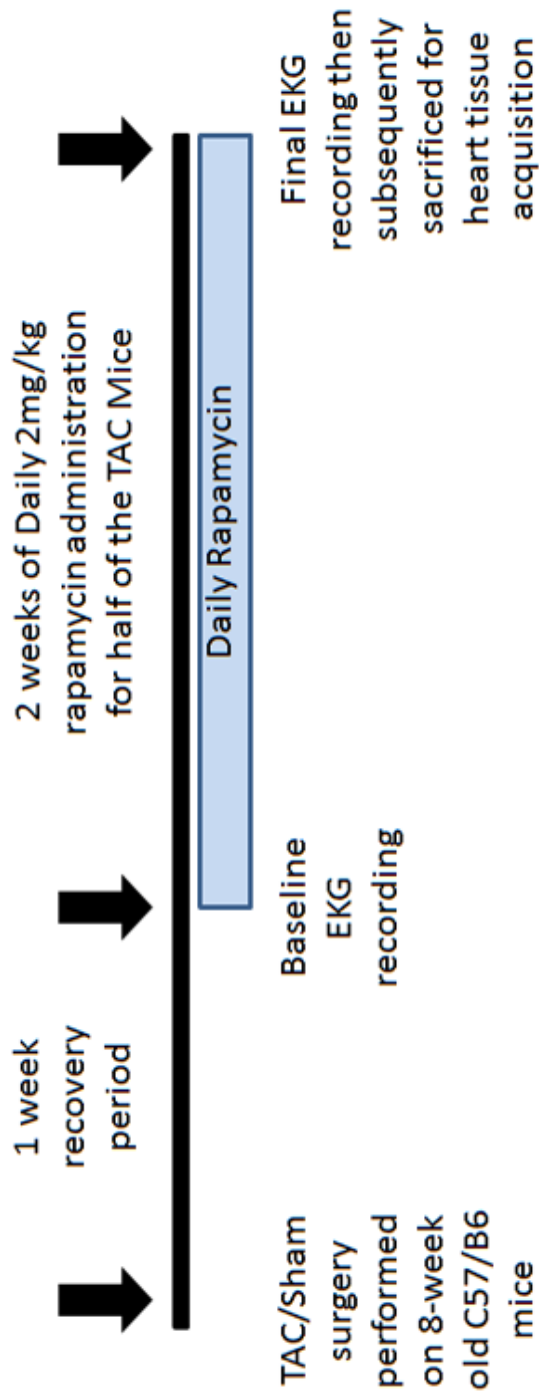


Figure 3.1. Three different sets of mice were utilized for the *in vivo* experiments. Sham mice had EKG recordings obtained at 1 week and 3 weeks post-surgery. Half of the TAC mice had baseline EKG recordings at 1 week post-surgery, subsequent daily vehicle (DMSO) treatment for 2 weeks, and final EKG recordings at 3 week post-surgery. The other half of the TAC mice underwent the exact experimental protocol as the vehicle treated group with the exception of daily 2mg/kg rapamycin treatment instead of vehicle.

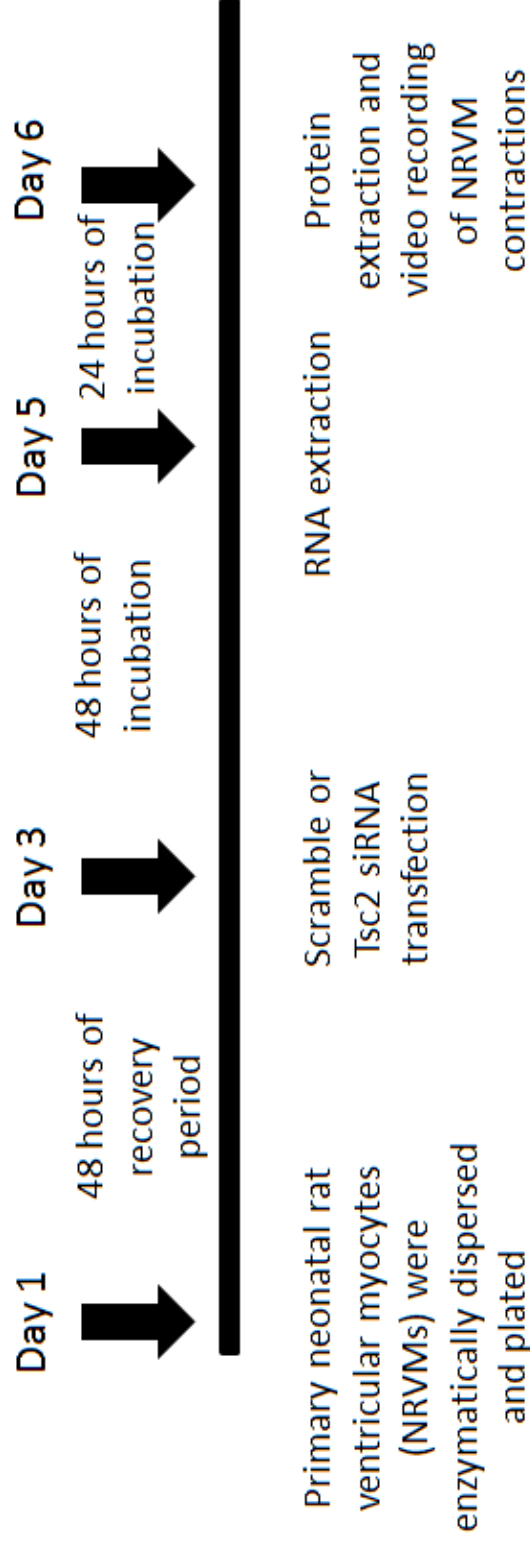


Figure 3.2. Three different sets of treatment were utilized for the *in vitro* experiments: Untransfected, scramble siRNA transfected, and Tsc2 siRNA transfected. Untransfected NRVMs had the culture media replaced at the same time as scramble or Tsc2 siRNA treated cultures. Cultures were transfected with scramble or Tsc2 siRNA on day 3 for 6 hours and subsequently washed and replaced with serum-free culture media. RNA extraction occurred on day 5 to assess knockdown effects prior to day 6 protein extraction and contraction recordings.

3.2.1 Pressure-overload model (transverse aortic constriction)

An animal model of pressure-overload hypertrophy and heart failure was induced by a transverse aortic constriction (TAC). Adult animals (8-week old C57BL/6) will be used in the surgical preparation. Prior to anesthesia each animal will receive a dosage of buprenorphine (0.1-2.5 mg/kg SC). We purchased this agent through Center for Comparative Medicine (Baylor College of Medicine) per animal. The animal was then anesthetized using 2% isoflurane in 100% O₂. The neck and chest areas were prepared by shaving and removing hair, cleansing the skin with surgical soap followed by wiping with 70% ethanol. This procedure was repeated three times. Prior to surgery, all instruments were sterilized in a dry bead sterilizer. The anesthetized animal was placed in a supine position and a 5mm section of the trachea was carefully exposed by mid-neck incision and retraction of muscle tissue. This allowed visualization for insertion of the endotracheal tube which was a polyethylene size 90 tubing beveled on the edge for ease of entrance through the larynx. The tongue was carefully manipulated as the endotracheal tube was inserted into the trachea with visibility through a dissecting microscope, viewing the trachea and entrance of the endotracheal tube. Once the proper position was confirmed, the endotracheal cannula was connected to a volume-cycled rodent ventilator (CWE, Inc.) which runs on supplemental 100% oxygen with a tidal volume approximately 0.15-0.25ml and a respiratory rate of 100-125 breaths per minute. Once steady breathing was established, an incision was made through the ventral chest skin to mid-thorax after which the thorax was opened to mid-sternum. This partial thoracotomy was followed by retracting the sternal edges with a retractor (Fine Science Tools). The thymus was then retracted to expose the transverse aorta. Between

the right innominate and left carotid artery, an aortic constriction was placed by tying a 6-0 suture black braided non-absorbable silk suture) against a 3mm length of 27 gauge needle. After two knots, the 27 gauge needle was promptly removed which yielded a constriction of approximately 0.3mm as the outer diameter of the 27 gauge needle. This produced a 60-80% aortic constriction. The outflow was then briefly (1-2s) pinched off on the respirator to allow re-inflation of the lungs. The retractor was removed and the ribs were drawn together and sutured using 5-0 Prolene (blue monofilament polypropylene suture). Once the chest was closed, the outflow was briefly pinched off again to ensure proper breathing. The skin was then closed using 5-0 non-absorbable monofilament sutures, which will be removed within 10 days post-surgery. Once all sutures were in place, anesthesia was stopped and the animal was allowed to recover and removed from the ventilator. The animal was monitored closely for any abnormal signs of pain or labored breathing before being returned to the animal room. In case of any signs of pain, the animal received another dosage of buprenorphine (0.1-2.5 mg/kg SC) every 6-12 hours when needed. The degree of constriction was evaluated with a Doppler flow study a week after the procedure on the Vevo ultrasound machine.

3.2.2 Mouse EKG monitor and analysis

The mouse was anesthetized with 2% isoflurane mixed with 100% oxygen. Once sedation was obtained, the paws of the mouse were placed on the heated mouse monitor pad (Indus Instruments) in a supine position and the feet were taped to the EKG leads. A rectal probe was inserted for core body temperature monitoring during the procedure.

EKG rhythms were then recorded from the mouse for offline analysis with Adobe Photoshop (version 11.0, San Jose, CA, USA).

For each EKG recording, P-, Q-, R-, S-, and T-waves are identified on a cardiac cycle. The following three parameters that assess the conduction system of the heart are measured: (1) Time between start of the P-wave to start of the Q-wave (P-R interval); (2) start of the Q-wave to end of the S-wave (QRS interval); and (3) start of the Q-wave to end of the T-wave (Q-T interval). The same measurements are made for a total of 3 cardiac cycles per recording and repeated 2-3 times per each condition and animal. See figure 3.3 for illustration of the EKG waveforms and parameters measured.

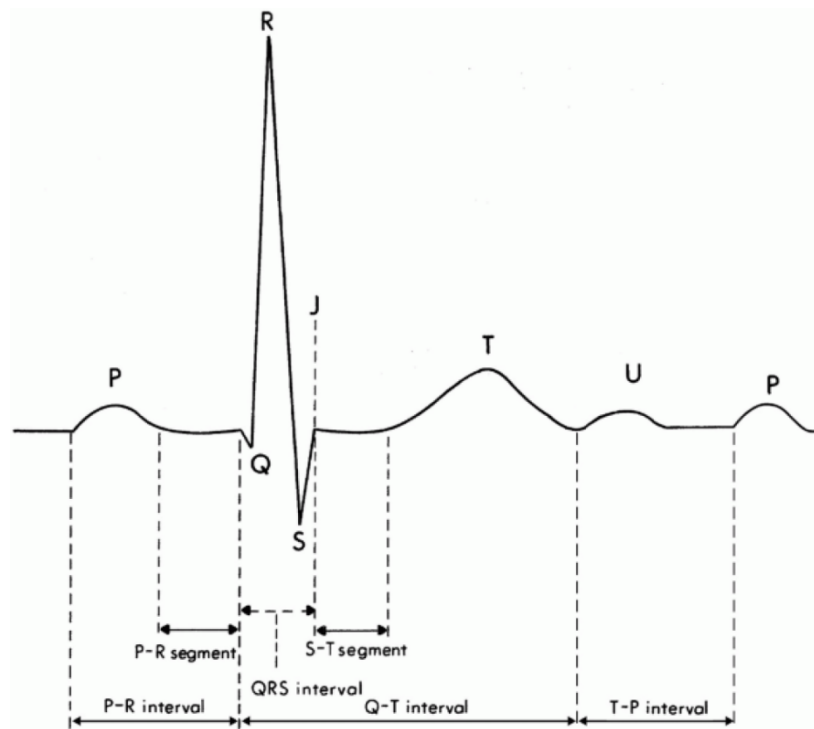


Figure 3.3. An example of each of the three parameters measured for each cardiac cycle from the animal EKG recordings. Reproduced with permission from Wagner, G., *Marriott's Practical Electrocardiography (Wagner) Series*. 11th edition 2007, Lippincott Williams & Wilkins [7].

3.2.3. Isolation of adult mouse cardiomyocytes

Two to three mice from the Sham/TAC experiment were used for isolation, and all solutions used for the procedure were sterile filtered. This protocol was adapted from the method used in Dr. Heinrich Taegtmeyer's lab at The University of Texas Health Science Center at Houston [228].

The animals were anesthetized with avertin. Once anesthetized, the mouse was rinsed with 70% ethanol followed by exposure of the abdominal cavity. The abdominal aorta was visualized and injected with 0.1mL of 1000U heparin. Immediately, the chest cavity was exposed and all organs in the chest cavity were removed quickly and placed in ice-cold PBS containing no calcium or magnesium. Excise the heart cleanly from other tissues but leaving the ascending aorta attached. The ascending aorta was cannulated using a flat-tipped 22 gauge catheter attached to a sterile syringe containing ice-cold perfusion buffer [120.4mM NaCl, 14.7mM KCl, 0.6mM KH_2PO_4 , 0.6mM Na_2HPO_4 , 1.2mM $\text{MgSO}_4 \cdot 7\text{H}_2\text{O}$, 10mM Na-HEPES, 4.6mM NaHCO_3 , 30mM taurine, 10mM BDM, 5.5mM glucose in ddH₂O and adjusted to pH 7.35 with HCl/NaOH] and fastened with a micro clip. Some perfusion buffer was injected through the catheter and into the aorta to ensure the success of the cannulation. Once cannulated, surgical knot was tied with a suture around the micro clip, micro clip was removed, and the catheter transferred to the primed Langendorff-style retrograde perfusion system containing calcium-free and collagenase-free perfusion buffer at 37⁰C. The heart was perfused at a flow rate of 4mL/minute throughout. Initially, the heart was perfused with the calcium-free and collagenase-free perfusion buffer for 3 minutes followed by 15mL calcium-free digestion buffer [perfusion buffer with 2.4mg/mL collagenase type II (Worthington)].

Finally, it is perfused with digestion buffer containing collagenase type II and 40 μ M CaCl₂ for an additional 6-8 minutes until the heart appears pale. This indicates a successful digestion of the extracellular matrix.

After completion of the digestion process, the heart was removed from the perfusion apparatus and transferred to a 60mm² dish containing 5mL stopping buffer [4.5mL perfusion buffer containing 100 μ M CaCl₂, and 0.5mL FBS]. The catheter was removed with the suture and heart was cut into small pieces in the stopping buffer. The pieces were further dispersed by mechanical trituration with a transfer pipette. The digested suspension was filtered through a 100 μ m-cell strainer into a 50mL conical, transferred to a 15mL conical, and centrifuged at 300rpm at 4°C for 5 minutes. The supernatant was immediately removed, and cell pellet was resuspended and fixed in 100% ice-cold ethanol. The fixed cells were kept in 100% ethanol and stored in -20°C until further processing.

3.2.4. Isolation of neonatal rat ventricular cardiomyocytes

1-2 days old neonatal Sprague-Dawley rats (Texas Animal Specialities, Humble, TX) were used to isolate neonatal rat ventricular cardiomyocytes. The isolation was performed under sterile conditions in the tissue culture hood and all solutions were sterile filtered in the hood. This protocol was adapted from the method used in Dr. Heinrich Taegtmeier and Dr. Diane Bick's lab at The University of Texas Health Science Center at Houston [228].

The neonatal rats were rinsed with 70% ethanol three times. They were decapitated, chest cavity exposed quickly and heart removed and placed in warmed 1x ADS buffer [6.8g NaCl, 0.4g KCl, 1.5g NaH₂PO₄, 1g glucose, 0.1g MgSO₄, 4.76g HEPES, pH to 7.38 with HCl/NaOH, and brought up to 1 L with ddH₂O]. Hearts were rinsed once more with fresh 1x ADS when all hearts have been collected, then cut into quarters with fine forceps to minimize tissue destruction. The cut tissues were transferred to a 25mm² culture flask containing 9mL of digestion buffer [0.6mg/mL pancreatin (Sigma P-3292-25g) and 73U/mL collagenase type II (Worthington) in 1x ADS] for a maximum of 15 hearts. Hearts were incubated in the flask for 20 minutes at 37⁰C while shaking at 140rpm. Supernatant from this first digestion was discarded and replaced with 9mL fresh digestion buffer for a total of four replacements. At the end of the final digestion, a transfer pipette was used to gently triturate the remaining undigested heart tissues in warm 1x ADS. Supernatant from all except for the first digestion was collected, centrifuged for 5 minutes at 300g at room temperature and the resultant supernatant discarded and pellet suspended in warmed 2mL fetal bovine serum (Gibco). The resuspensions were pooled together and kept in incubator at 37⁰C and 5% CO₂ until all digestion steps were completed.

The resuspensions were centrifuged for 5 minutes at 300g, supernatant discarded, and the pellet was resuspended in warm 1x ADS at 1mL/heart harvested. The resuspension were pre-plated in 6-well Nunc plates (Thermo Fisher Scientific) at 2mL per well and kept in incubator for 2-5 hours to decrease the number of fibroblasts in the final cardiomyocyte culture. The media from each well was collected without disturbing the bottom layer and centrifuged for 5 minutes at 300g. The resulting supernatant was

discarded and pellet was resuspended in complete media [500mL DMEM, 50mL BCS, 5mL of 100U/mL penicillin/streptomycin] at 1mL/heart harvested. Cells were counted with Trypan Blue solution and plated at 1 million cell/well in a 6-well Primaria plate (Fisher/Corning Life Sciences) or 1×10^5 cells per fibronectin-coated glass-bottom MatTek plate (MatTek Corporation).

3.2.5. Tissue and cell protein extraction and quantification

Two to three hearts from each treatment group outlined in **3.2** were snap frozen in liquid nitrogen. Protein was isolated from snap-frozen heart tissues using sucrose lysis buffer (1:4 weight to volume) containing 25mM sucrose, 1mM EDTA, 10mM Tris HCl, 1mM PMSF (a protease inhibitor), and phosphatase inhibitor cocktail. Tissues were pulverized in liquid-nitrogen chilled mortar and pestle then homogenized in a dounce homogenizer on ice. Lysates were centrifuged at 4°C for 13,000g for 15 minutes and supernatant recovered.

Cells were washed in ice-cold 1x PBS twice, then scraped and collected in the presence of ice-cold cell lysis buffer (5mM HEPES pH 7.4, 0.1mM EDTA pH 8.0, 0.1mM MgCl₂, 0.1mM DTT, 1% Triton-X, 150mM NaCl, 1 Mini-Tab protease inhibitor (Roche) per 10mL of lysis buffer, and 100µL of each phosphatase inhibitor cocktails 2 and 3 (Sigma) per 10mL of lysis buffer. Lysate was triturated 10-15 times on ice through a 1mL 27.5 gauge syringe, then underwent 3 rapid freeze/thaw cycles with dry ice in ethanol and 37°C water bath. The lysate was then sonicated on ice for 3 seconds then centrifuged at 13,000g for 10 minutes at 4°C, and the supernatant was recovered.

The protein concentration from each tissue/cell sample was quantified using colorimetric Bradford Protein Assay (BioRad). A series of known BSA protein concentrations were diluted to generate a standard curve (1-10 $\mu\text{g}/\mu\text{L}$). Protein samples were diluted 5- to 10-fold and each diluted sample at two distinct amounts (2 μL and 5 μL) were added to 200 μL of Bradford reagent in a 96-well plate. The absorbance was read on a microplate reader and each sample protein concentration was determined based on the standard curve.

3.2.6. Immunoblot assay

0.1mM DTT and 4x loading dye were added to equal quantities of protein lysates from **3.2.5** and heated at 70°C for 15 minutes. Protein lysates were then separated by SDS-PAGE and transferred onto a PVDF membrane (Bio-Rad) using XCell II Blot Module (Invitrogen). Membrane was washed with 1x TBST (0.1% tween-20) and blocked with 5% nonfat milk in 1x TBST for an hour at room temperature to block non-specific binding on the membrane. Membrane was incubated at 4°C in primary antibody solution (5% milk or BSA in TBST) overnight. Primary antibody was then washed off and incubated with horseradish peroxidase-conjugated secondary antibody for 1 hour at room temperature. Protein of interest was visualized using SuperSignal West Pico Chemiluminescent Substrate kit (Pierce). Primary antibodies used were: tuberin (1:500; Cell Signaling), phospho-S6 (1:500; Cell Signaling), S6 (1:500; Cell Signaling), pan-ankyrin-B [229], ankyrin-G [142], ankyrin-R (1:500; Aviva System Biology), NCX1 (1:500; Swant), and GAPDH (1:20,000; Fitzgerald).

3.2.7. Fluorescent immunocytochemistry

Cells isolated and cultured from **3.2.4** were washed twice with ice-cold 1x PBS and fixed in 2% paraformaldehyde for 15 minutes at room temperature and cells collected from **3.2.3** were washed in ice-cold phosphate-buffered saline (pH 7.4) 3 times. Cells were then blocked with 5% normal goat serum and 0.075% TritonX-100 for 30 minutes at room temperature then incubated in primary antibodies overnight at 4°C. The primary antibodies used were: tuberin (1:500; Cell Signaling), phospho-S6 (1:500; Cell Signaling), pan-ankyrin-B [229], ankyrin-G [142], ankyrin-R (1:500; Bethyl Laboratories), Myomesin (1:500; Developmental Studies Hybridoma Bank/University of Iowa), α -actinin (1:1000; Sigma). Secondary antibodies used were goat anti-rabbit conjugated to Alexa Fluor 488 and goat anti-mouse conjugated to Alexa Fluor 568 (1:500, LifeTechnologies). Hoechst 33258 (1:1000, LifeTechnologies) was used for nuclear staining after removal of the secondary antibody. ProLong® Gold Antifade reagent (LifeTechnologies) was used for mounting coverslips. Images were obtained with a Nikon A1 confocal microscope (Nikon, Melville, NY) equipped with 60X oil, numerical aperture 1.4 objective lens.

3.2.8. NRVM RNA interference experiments

The siRNA duplexes targeting rat TSC2 and non-targeting siRNA control (scramble) were purchased from Sigma. The siRNA was diluted in Tris-EDTA buffer [10mM Tris, 1mM EDTA, pH to 7.0 with HCl/NaOH] to a stock concentration of 25 μ M.

Prior to transfection, amount of siRNA calculated to have a final concentration of 100nM was mixed with Opti-MEM (Thermo Fisher Scientific). Separately, DharmaFECT® (Dharmacon GE) [4µL per 2mL of culture media] was mixed with Opti-MEM. After 5 minutes of incubation, the two are mixed together and allowed 15-20 minutes of incubation in room temperature prior to application to serum-free DMEM. The NRVMs were transfected for 6 hours with 100nM of each siRNA, then media was changed to fresh serum-free DMEM. Media change was the same for untransfected controls. Experiments with transfected NRVMs were performed 48 hours later for quantitative real-time PCR and 72 hours later for immunoblotting and cell contraction recordings. The sequence of siRNA is as follows:

TSC2 siRNA sequence 1 starts on target 1092

sense: 5'-GAGAUUGUUCUGUCCAUA[dT][dT]-3'

anti-sense: 5'-UUAUGGACAGAAACAUCUC[dT][dT]-3'

TSC2 siRNA sequence 2 starts on target 3271

sense: 5'-GAAUAAGCUGGUCACUGU[dT][dT]-3'

anti-sense: 5'-ACAGUGACCAGCUUAUUUC[dT][dT]-3'

Scramble siRNA sequence

sense: 5'-GCUCCCAGCUCGUCUAUGU[dT][dT]-3'

anti-sense: 5'-ACAUAGACGAGCUGGGAGC[dT][dT]-3'

3.2.9. Measurements of mRNA expression

Total RNA was extracted from NRVM with PerfectPure™ RNA Cell and Tissue kit (5 Prime). cDNA synthesis from 500µg of total RNA was performed using SuperScript III reverse transcriptase (LifeTechnologies) with random hexamers. Transcript expression levels of *TSC2* and *GAPDH* were measured in triplicate by quantitative real-time (qt)-PCR using SYBR Green Dye (Bio-Rad). Transcript levels of *TSC2* were adjusted to the expression of *GAPDH*. The sequence of PCR primer targeting junction of *TSC2* exons 23/24 is as follows; 5'-GACTAGACAG/CGTGAGATGG (slash indicates junction of exon 23 and 24)-3' and 3'-GCTAGCTGTAGCAGAGATGTG-5' for *TSC2*; targeting junction of *GAPDH* exons 6/7: 5'-CATCACTGCCACTCAGAAGAC-3' and 3'-CATACTTGGC/AGGTTTCTCC (slash indicates junction of exon 6 and 7) – 5'

3.2.10. NRVM syncytium contraction recording and analysis

A Mat-Tek plate with NRVMs was placed in a warm humidified chamber on a flat stage of a light microscope (Micromaster; Fisher) with 10X magnification eyepiece and 20X objective lens. A cell phone camera with 10 megapixel resolution (HTC One M8) was mounted on the microscope using Snapzoom Universal Digiscoping Adapter (Snapzoom). Once a NRVM syncytium was located visually, the contractions were recorded for 2 to 2.5 minutes. The same recording method was used for recording of the syncytia following stimulation with 1µM epinephrine.

Using Video Spot Tracker (VST) program (<http://cismm.cs.unc.edu/downloads>) and using the tracking method as described by Fassina *et. al.* [230], we placed a marker on the contracting syncytium for each video recording in the program. By starting the video, the program tracked the marker displacement frame by frame (30 frames per second) and registered the spatial-temporal coordinates x , y , (expressed in pixels), and t (expression in frame number that converts to second) of the marker. The coordinates are plotted in Excel (Microsoft) and each peak corresponds to an active syncytial contraction. We then assessed the rhythmicity of the syncytial contractions by randomly picking a consecutive 30-second interval then measuring the time between contractions. Figure 3.4 is an example of the spatial-temporal pattern of marker displacement. The time interval between contractions is plotted on GraphPad (GraphPad Software) as box-and-whisker plots.

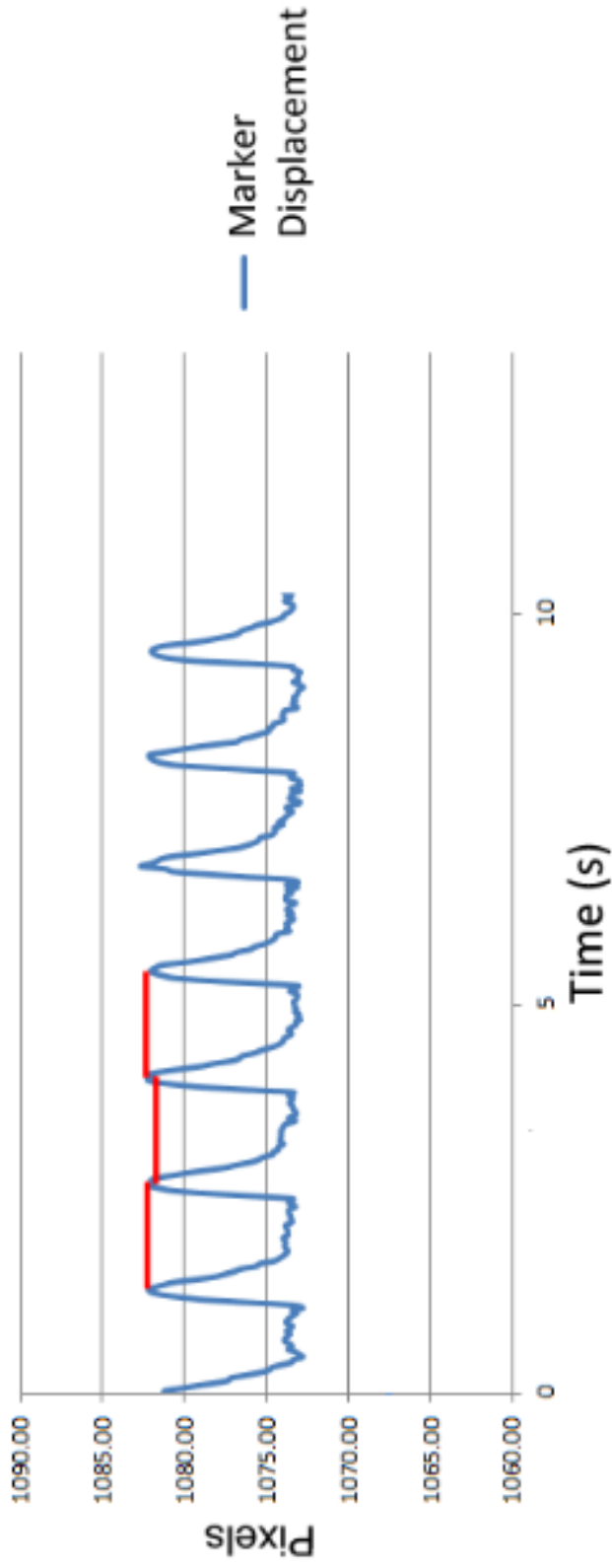


Figure 3.4. Example of marker displacement tracking. The peaks and troughs are identified as contractions and relaxations, respectively. The interval between peaks is used to measure the time between contractions. The 3 red double arrows in this figure are used as illustration for how the time between contractions are measured. X-axis, time (seconds); y-axis, location of the marker (pixels); blue line, marker displacement.

3.3 Results

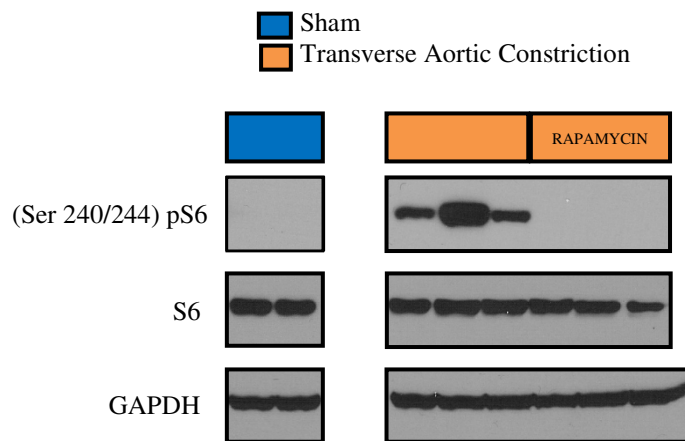
3.3.1. Electrical remodeling in response to chronic load-induced hemodynamic stress *in vivo*

We hemodynamically stressed the heart with increased load via transverse aortic constriction (TAC) to induce mTORC1 activation as evidenced by the increased phosphorylation of the ribosomal protein S6. Daily treatment with rapamycin, a known mTORC1 inhibitor, reduced the phosphorylation of S6 to baseline in the TAC group (Figure 3.5A).

To determine the effects of chronic mTORC1 activation on the electrical property in the heart, we obtained EKG for sham, TAC with vehicle treatment, and TAC with rapamycin treatment groups 1 week (recovery period with no drug administered) and 3 weeks (with drug treatment) post-surgery. We focused on three EKG parameters including P-R interval, Q-T interval, and QRS duration. P-R interval measures the conduction time of depolarization from sinus atrial (SA) node in the atria through the atrioventricular (AV) node to the ventricles. Q-T interval measures the time between ventricular depolarization and repolarization. QRS duration measures ventricular depolarization time. There was not a statistically significant change in P-R interval and Q-T interval between sham and TAC groups at 1 week post-surgery. However, we observed a slight yet statistically significant increase in the QRS duration in the TAC mice (Sham 15.90 ± 0.51 ms, TAC Vehicle 19.59 ± 1.44 ms, and TAC Rapa 18.55 ± 0.87 ms. * $p < 0.05$ between Sham and either TAC groups) (Figure 3.5B).

At 3 week post surgery, P-R interval increased to an average of 42ms in TAC treated with vehicle but normalized to 35ms with rapamycin treatment. The increased duration confirms the findings by *Zhang C et. al.*[75] and represents a significant first-degree heart block. Q-T interval decreased in both TAC groups treated with vehicle or daily administration of rapamycin at 2mg/kg/day. QRS duration was similar between all groups at the end of the experiment (Figure 3.5C). Thus, sustained mTORC1 activity partially affected the electrical property of the myocardium. Specifically, the conduction between the atria and the ventricle was delayed. Decreased Q-T interval in TAC with or without rapamycin demonstrated the contributions of mTORC1-independent pathways in electrical remodeling of the hemodynamically stressed heart.

A



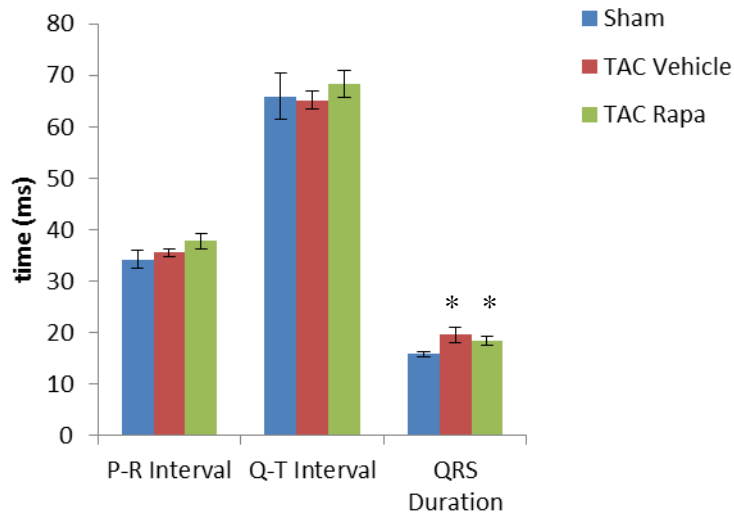
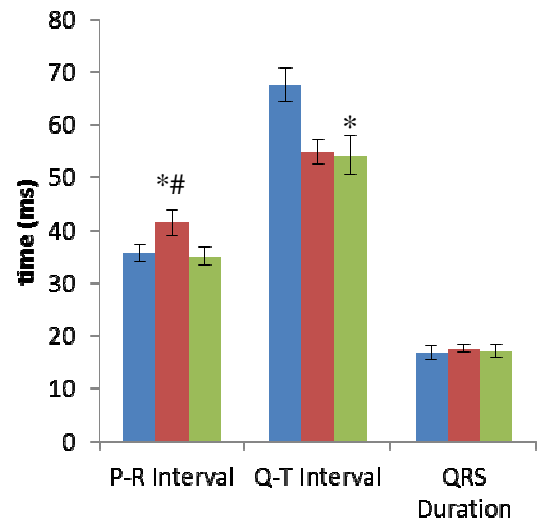
B**C**

Figure 3.5. mTORC1 activity and electrical remodeling in hearts subjected to high workload *in vivo*. Treatment with rapamycin rescues the conduction from atria to ventricles. A, Representative Western blots demonstrated an increase in S6 phosphorylation 3 week after TAC surgery and the phosphorylation returns to baseline with rapamycin treatment. B, Graph showing the three measured EKG parameters (P-R interval, Q-T interval, and QRS duration) at the end of 1 week recovery after TAC surgery. No drug treatment is yet administered at this time. No difference is seen in P-R interval and Q-T interval between groups. However, QRS duration increases slightly in the TAC groups (Sham 15.90 ± 0.51 ms, TAC Vehicle 19.59 ± 1.44 ms, and TAC Rapa 18.55 ± 0.87 ms). C, Graph showing the three measured EKG parameters 3 weeks after TAC surgery and with either vehicle or rapamycin treatment. P-R interval increases significantly in the TAC Vehicle group, but returns to baseline with rapamycin treatment (Sham, 35.68 ± 1.47 ms, TAC Vehicle 41.37 ± 2.5 ms, TAC Rapa 35.05 ± 1.76 ms). Q-T interval remains decreased in both TAC Vehicle and TAC Rapa groups suggests mTORC1-independent processes may play a role in electrical remodeling (Sham 67.46 ± 3.13 ms, TAC Vehicle 54.83 ± 2.40 ms, TAC Rapamycin 54.16 ± 3.65 ms). * $p < 0.05$ vs sham, # $p < 0.05$ vs TAC Rapa. $n = 6$ for each group. TAC, transverse aortic constriction; Rapa, rapamycin.

3.3.2. Ankyrin proteins expression changes in response to chronic load-induced hemodynamic stress and mTORC1 inhibition

Ankyrin proteins (ankyrin-B, -G, and -R) are adapter proteins pivotal in the regulation of normal cellular physiology. A wide spectrum of arrhythmias (e.g. sinus node disease, atrial fibrillation, and polymorphic ventricular tachycardia) have been directly linked with loss-of-function mutations in the adapter protein ankyrin-B (*ANK2*) [3, 5, 229]. Another specific type of arrhythmia characterized by S-T segment elevations, atrial fibrillation, and sudden cardiac death known as Brugada syndrome has been linked with disrupted interaction with ankyrin-G (*ANK3*) [142, 231]. Finally, although not yet linked to any arrhythmia phenotype, ankyrin-R (*ANK1*) has been shown to play an important role in calcium regulation - central to the integrity of the excitation-contraction coupling that establishes the normal rhythm and contraction of the myocardium - via establishment and maintenance of normal sarco-endoplasmic reticulum (SR) structure essential for normal functioning of sarco-endoplasmic reticulum calcium ATPase 2a (SERCA2a) [232-235]. To date, there is limited data in regulation of ankyrin-B [216], and no evidence yet exists for either ankyrin-G or ankyrin-R, expression in the stressed heart. Mechanisms that link structural and electrical remodeling in the stressed heart are also lacking.

mTORC1 signaling has been identified as a central regulator of cardiac hypertrophic growth [190, 192, 193] and modulates the expression of the calcium handling protein SERCA2a [236]. However, mTORC1 activity has not been shown to directly affect the function or the expression of sodium-calcium exchanger (NCX1) [237, 238], another essential calcium regulator, despite increased NCX1 expression in the stressed heart [239, 240]. Yet, it was reported that NCX1 current decreases in an animal model of pressure-overload cardiac hypertrophy [221].

NCX1 proper membrane localization and function requires direct interaction with adapter protein ankyrin-B [2, 133]. Reduced ankyrin-B expression reduces NCX1 function and localization to the transverse-tubule [4, 132]. Hence we assessed whether mTORC1 affects NCX1 function and localization via regulation of ankyrin-B.

Consistent with the published data, NCX1 expression increased in our hemodynamically stressed hearts and decreased when the hypertrophic process was attenuated [221, 239, 241]. Using the same set of heart samples, we evaluated the effects of mTORC1 activity on ankyrin-B expression. When mTORC1 activity was unopposed, in the TAC Vehicle group, ankyrin-B expression was significantly decreased compared with the sham control. However, attenuation of mTORC1 activity with rapamycin administration partially restored ankyrin-B expression (Figure 3.6A).

We also assessed the effects of mTORC1 activity on the subcellular localization of ankyrin-B using isolated cardiomyocytes from the stressed heart. In addition to overall generalized decreased expression, ankyrin-B localization also appeared to be slightly dispersed in the TAC Vehicle group compared to the sham control. Treatment with rapamycin (TAC Rapa group) not only restored ankyrin-B expression but also restricted the dispersion and the subcellular level (Figure 3.6B).

Other important factors in the regulation of calcium homeostasis are sarcoplasmic reticulum calcium ATPase (SERCA2a) expression and function and its proper localization at the sarcoplasmic reticulum (SR). Although alterations in SERCA2a function and expression may not be the initial cause of cardiomyopathy, the contributions to the consequent development of arrhythmia in the hypertrophic heart are

well-documented [219, 220, 242]. More recently, it has been shown that SERCA expression, proper localization, and function are regulated by the adapter protein ankyrin-R in striated muscle [232, 233]. Given that mTORC1 modulation alters levels of SERCA2a expression in the heart [23, 44, 236], we evaluated whether mTORC1 affects SERCA2a expression by regulating ankyrin-R expression.

When we mechanically triggered mTORC1 activation *in vivo* by pressure overloading the heart (TAC), our results showed that ankyrin-R expression clearly decreased similar to findings in SERCA2a. However, whereas mTORC1 inhibition with rapamycin in the stressed heart somewhat normalized SERCA2a expression, we did not observe any change between rapamycin or vehicle treated TAC mice. This pointed to the possibility of ankyrin-R regulation by mechanisms independent of mTORC1 signaling (Figure 3.6A).

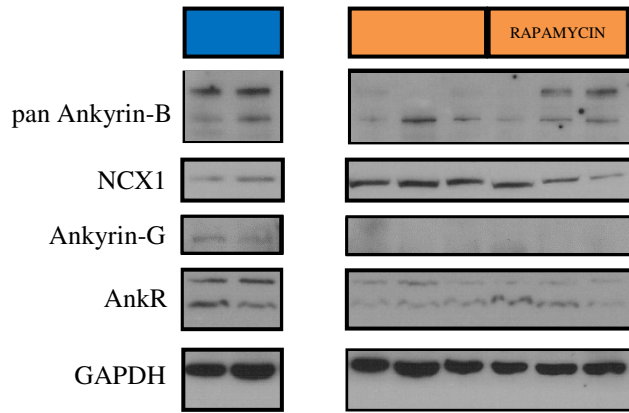
In addition to the calcium regulatory function of NCX1, intercellular electrical conduction to facilitate the transfer of current from one cardiomyocyte to another at the intercalated discs is another important mechanism in establishing normal cardiac rhythm. Key components of the intercalated disc include the gap junction protein connexin43 (Cx43), voltage-gated sodium channel ($\text{Na}_v1.5$), and desmosomal protein plakophilin-2 (PKP2), and all three exhibit decreased expressions in cardiomyopathies involving arrhythmias [23, 243, 244]. Central to this molecular complex involving these three proteins is ankyrin-G that interacts, targets, and maintains these proteins at the intercalated disc [142, 231, 245]. We asked how ankyrin-G expression changes in the hemodynamically stressed heart.

Using our TAC model, our results indicated that ankyrin-G expression is markedly decreased in pressure overloaded hearts. Regression of the cardiac hypertrophic process and inhibition of mTORC1 with rapamycin treatment did not attenuate the effects of pressure overload and normalize the expression of ankyrin-G (Fig 3.6A). Similar to ankyrin-R, this suggests the possibility of other mechanically-triggered pathways other than mTORC1 that is responsible for regulating the expression of ankyrin-G.

Collectively, our results suggest that mTORC1-responsive and mTORC1-independent factors contribute to arrhythmogenesis in the hypertrophied hearts. Among the three ankyrin proteins each with its unique set of interacting proteins, ankyrin-B appears to be the only one regulated by mTORC1 whereas ankyrin-R and ankyrin-G are mechano-sensitive but not mTORC1-specific. This idea is in line with our observations of the *EKG* changes in TAC Vehicle and TAC Rapa mice. We observed normalization of the P-R interval in the pressure-overload hearts with rapamycin treatment but it had no effect on the Q-T interval (Figure 3.5B and 5C).

A

■ Sham
■ Transverse Aortic Constriction



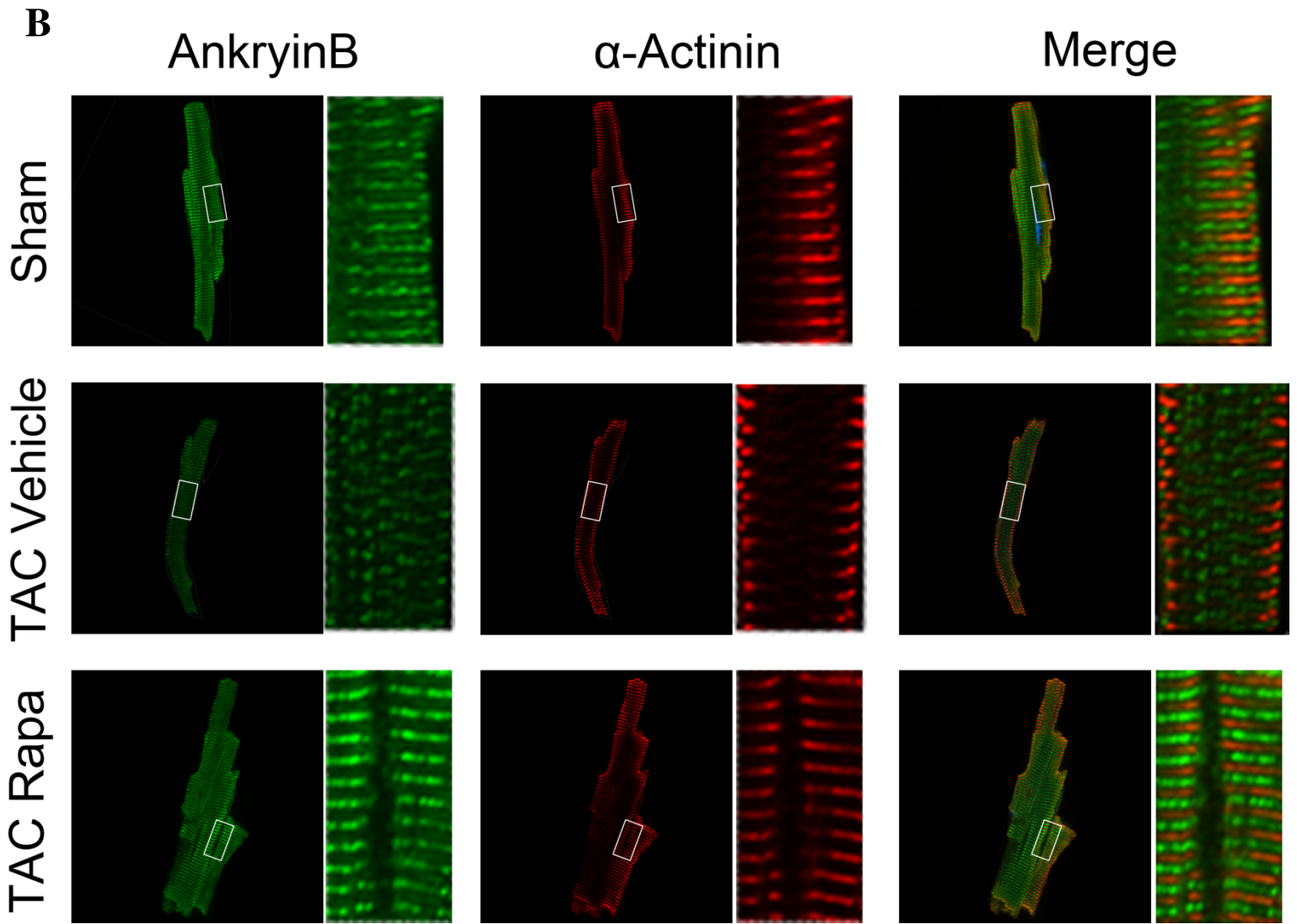


Figure 3.6. Effects of *in vivo* pressure overload on ankyrin-B, -G, and -R. A, Representative Western blots showing decreased ankyrin-B, -G, and -R expression in response to transverse aortic constriction. Treatment with rapamycin partially restored the level of ankyrin-B but had no effect on levels of ankyrin-G and -R. NCX1, one of the interacting partners of ankyrin-B, had increased expression in response to pressure overload and normalized with rapamycin treatment. B, Fluorescent immunocytochemistry of individually isolated adult mouse cardiomyocytes from sham control, TAC mice treated with DMSO vehicle, and TAC mice treated with rapamycin. In sham control, majority of the ankyrin-B population is concentrated at the M-line demonstrated by its localization in between the Z-line marker α -actinin whereas the minor population is localized at the Z-line. In contrast, the relative intensity of ankyrin-B decreases at the M-line and is not observed at the Z-line in TAC mice treated with DMSO vehicle. Furthermore, ankyrin-B population at the M-line shows some degree of dispersion. Rapamycin treatment reversed the expression and dispersion effects. Insets are shown to the right of the corresponding images. Green, ankyrin-B; red, α -actinin; blue, Hoechst. TAC, transverse aortic constriction; Rapa, rapamycin.

3.3.3 Effects of *in vitro* mTORC1 activation on ankyrin-B expression

The induced biomechanical stress with transverse aortic constriction directly activates numerous intracellular signaling pathways other than mTORC1 as well as paracrine and autocrine signaling. These include, but are not exclusive to, mitogen-activated protein kinase (MAPK) pathway, angiotensin II signaling, endothelin-I, and calcium/calmodulin-dependent kinase (CaMKII) [16, 82]. Hence, we wondered whether the findings observed *in vivo* with ankyrin-B and mTORC1 correlate with increased mTORC1 activity *in vitro*.

One strategy to elicit the regulatory mechanism between mTORC1 and ankyrin-B is by selectively activating mTORC1 without directly affecting other signaling pathways. mTORC1 becomes activated when its cellular negative regulator tuberous sclerosis complex (TSC) is disrupted [226, 246]. TSC is a heterodimer composed of the proteins hamartin (Tsc1) and tuberin (Tsc2), and deletion of tuberin has been demonstrated to lead to overt mTORC1 activation [73, 98, 99].

We used siRNA against Tsc2 to activate mTORC1 in primary neonatal rat ventricular myocyte cultures (NRVM) and studied the effects on ankyrin-B expression. NRVMs transfected with scramble siRNA served as controls. QT-PCR of extracts of NRVMs showed approximately 50% reduction in TSC2 transcripts with either TSC2 (1) or TSC2 (2) siRNA transfected compared to the untransfected or the scramble siRNA transfected (Figure 3.7A). Western blots showed a similar decrease in levels of tuberin for NRVMs transfected with TSC2 (1) or TSC2 (2) siRNA compared to either of the controls.

As expected, mTORC1 becomes more active when the TSC complex is disrupted by the knockdown of tuberlin as measured by levels of phosphorylated ribosomal protein S6 - a well-characterized downstream target of mTORC1 [69, 247]. And similar to the results we obtained from the TAC mouse hearts *in vivo*, selective mTORC1 activation *in vitro* reduced levels of ankyrin-B expression (Figure 3.7B). This further suggests that mTORC1 activity regulates ankyrin-B.

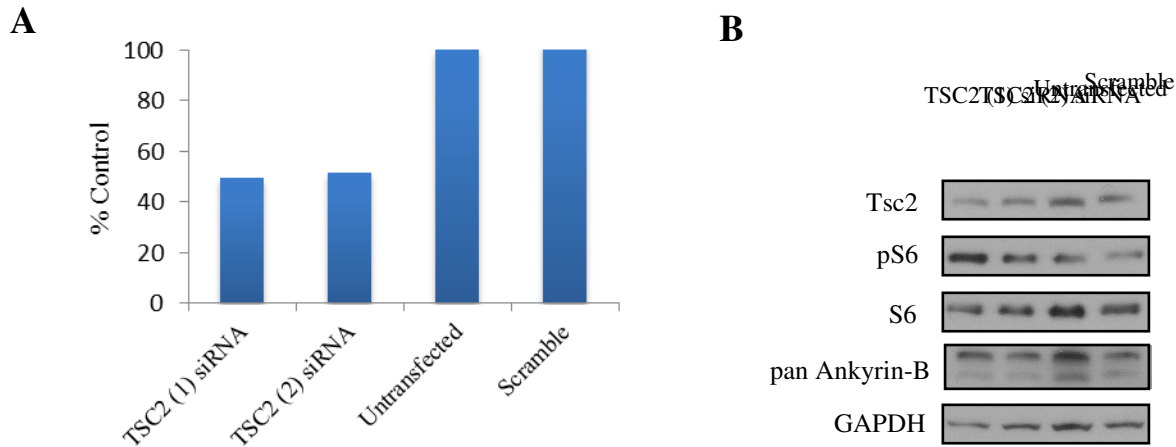


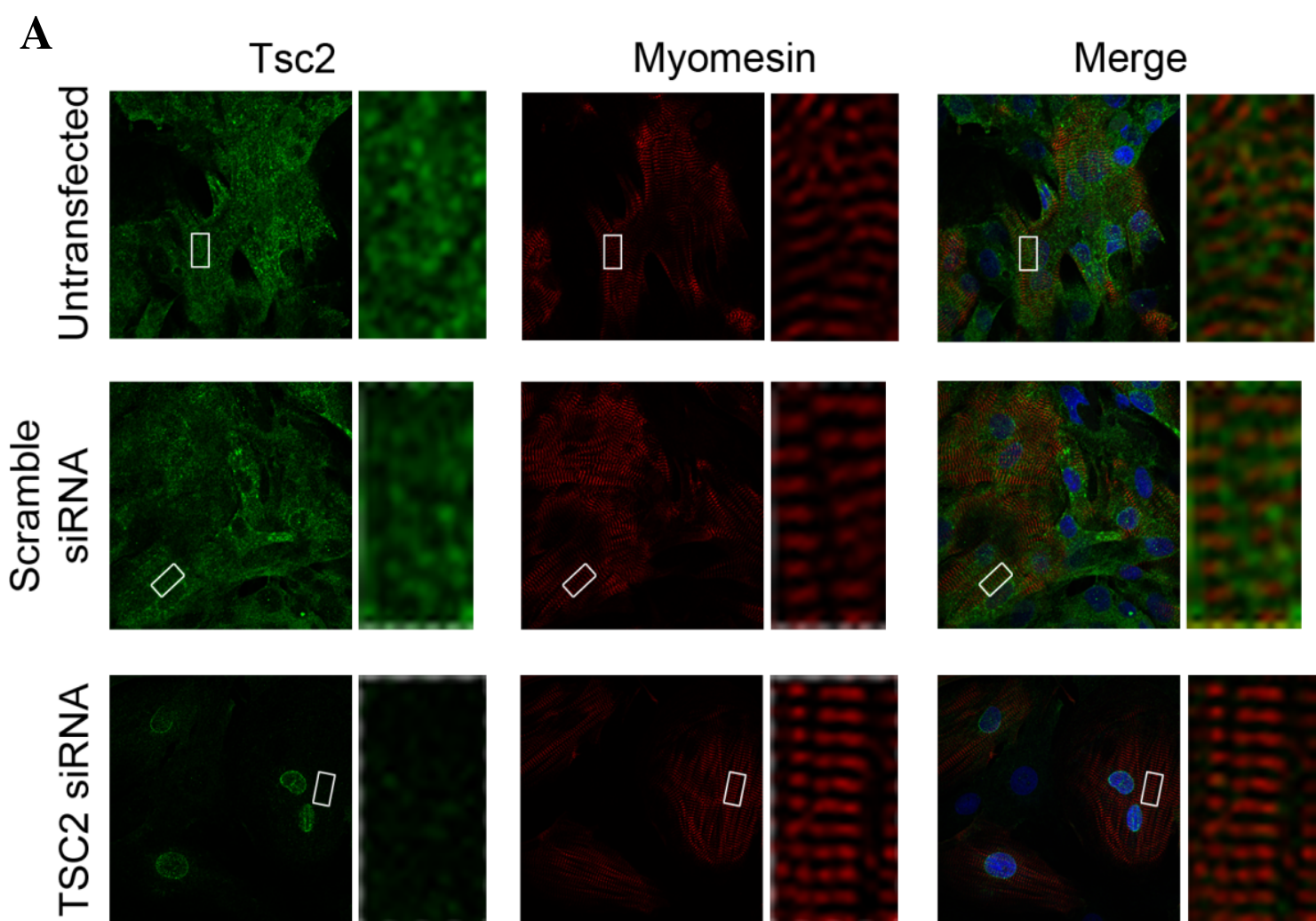
Figure 3.7. Selective mTORC1 activation reduces ankyrin-B expression *in vitro*. A, TSC2 transcripts are reduced in NRVM cultures transfected with either siRNA sequences against TSC2. TSC2 transcripts are not affected in either the untransfected or cultures transfected with scramble siRNA. B, Tuberlin protein is reduced in NRVM cultures transfected with either siRNA sequences targeting TSC2 and is not affected in the untransfected or scramble siRNA control transfected cultures. Ribosomal protein S6, a mTORC1 target, is phosphorylated demonstrating increased mTORC1 activity when tuberlin is knocked down. Ankyrin-B expression decreases when mTORC1 is active.

3.3.4 *In vitro* mTORC1 activation alters ankyrin-B subcellular expression

siRNA targeting TSC2 to activate mTORC1 *in vitro* obviated the use of mechanical force to activate mTORC1 as in the TAC hearts. Individually isolated cardiomyocytes from pressure-overloaded hearts showed decreased ankyrin-B expression and dispersion (Figure 3.6B). We now assessed whether similar changes can be recapitulated using the *in vitro* method.

Because the NRVM isolation procedure was not completely selective for cardiomyocytes as some cardiac fibroblasts continued to remain in culture, we performed fluorescent immunocytochemistry staining for Tsc2 to ensure that Tsc2 was removed from the cardiomyocytes. We observed that Tsc2 staining was either absent or significantly decreased in majority of the cardiomyocytes transfected with TSC2 siRNA (Figure 3.8A). This finding also corroborated our results in figure 3.7.

Using the same technique, we assayed for the subcellular localization of ankyrin-B. Similar to the cardiomyocytes from TAC hearts, ankyrin-B expression in the NRVMs transfected with TSC2 siRNA was decreased dramatically but displayed no dispersion at the M-line. Interestingly, while the TAC cardiomyocytes demonstrated an overall decrease in ankyrin-B expression at both the M-line and the transverse-tubule, the TSC2 siRNA treated NRVMs appeared to have an increase in ankyrin-B expression at the transverse-tubule (Figure 3.8B).



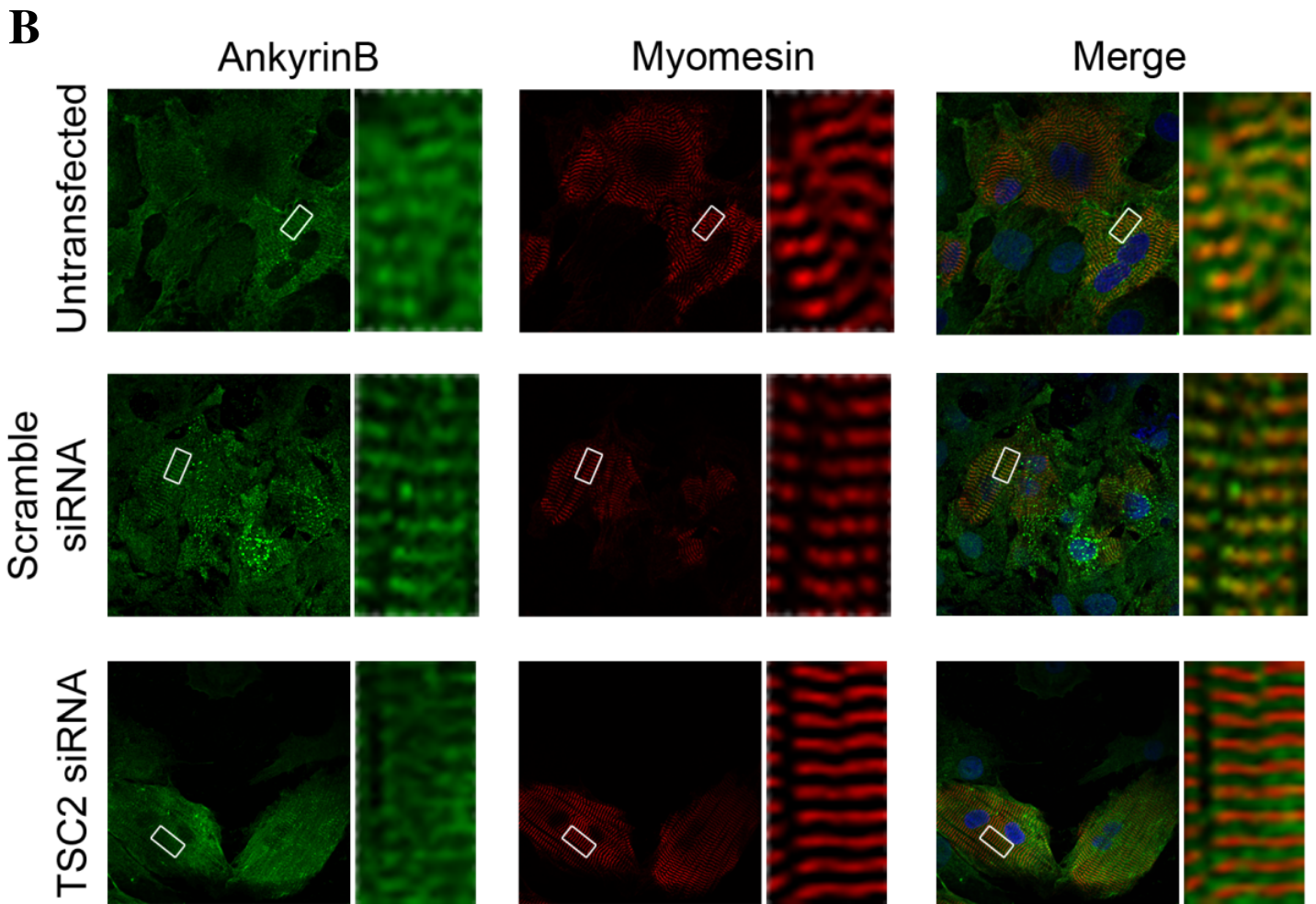


Figure 3.8. Selective mTORC1 activation changes ankyrin-B expression differently at different subcellular domains *in vitro*. Fluorescent immunocytochemistry of neonatal rat ventricular myocytes (NRVM) transfected with siRNA targeting *TSC2*, scramble siRNA control, or untransfected. Myomesin is used as a marker for the sarcomeric M-line and to differentiate NRVMs from fibroblasts in staining. A, *Tsc2* (tuberin) expression is either absent or dramatically decreased in the NRVMs transfected with *TSC2* siRNA compared to either of the control. Green, *Tsc2* (tuberin); red, myomesin (M-line marker); blue, Hoechst. B, Ankyrin-B expression at the M-line is decreased in the *TSC2* siRNA transfected NRVMs and no dispersion is observed. However, ankyrin-B intensity at the transverse-tubule (midway between two M-lines) is increased relative to the M-line population and the transverse-tubule population of either of the controls. Insets are shown to the right of the corresponding images. Green, ankyrin-B; red, myomesin; blue, Hoechst.

3.3.5 Physiologic consequences of *in vitro* mTORC1 activation

Our *in vivo* study with the hemodynamically stressed hearts demonstrated increased mTORC1 activity and abnormal EKG changes (Figure 3.5), we evaluated the functional consequences of mTORC1 activation on cardiomyocyte contraction rhythms. We tracked the contraction patterns of the NRVMs transfected with TSC2 siRNA and compared them against the untransfected and scramble siRNA transfected controls. In the absence of any exogenous stimulation, NRVM transfected with TSC2 siRNA in general contracted slower and had a higher variability in time interval between consecutive contractions. The box and whisker plot for TSC2 siRNA demonstrated an increased and a wider spread in the timing between contractions relative to the untransfected and scramble siRNA controls (Figure 3.9).

When stimulated with exogenous β -receptor agonist that increases the rate of contraction by increasing the cycling rate of intracellular calcium, we observed an overall increase in contraction rate as shown by the decrease in time between contractions for all three groups. However, administration of epinephrine to the TSC2 siRNA group further enhanced the contraction time variability. This suggests an underlying calcium handling dysfunction when mTORC1 is overactive and that it is further exacerbated by the pharmacologic stress with epinephrine application (Figure 3.9).

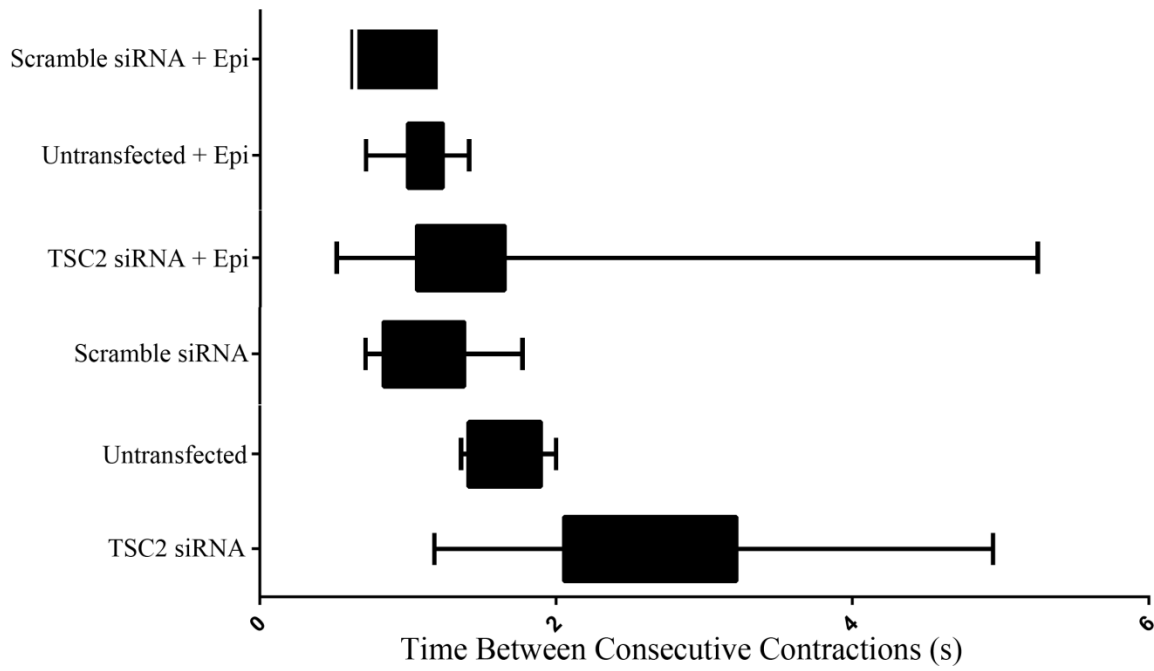


Figure 3.9. mTORC1 activation leads to arrhythmic contractions of NRVMs *in vitro*. Contractions of untransfected, scramble siRNA transfected control, and TSC2 siRNA transfected are recorded, and time between contractions was measured. Smaller time between consecutive contractions equates to faster contraction rate and vice versa. TSC2 siRNA transfected NRVMs tend to have a slower and a wider range of contraction rates compared with either of the controls. When pharmacologically stressed by epinephrine, all three groups tend to have similar contraction rates although TSC2 siRNA + Epi group displayed an even wider range of contraction rates. n = 5-7 NRVM syncytia per group and 30 seconds of recording was analyzed per n.

3.4 Discussion

A prominent mechanism of death in heart failure patients is arrhythmia leading to inadequate delivery of oxygen and nutrient to vital tissues. Mortality rate for patients with advanced heart failure is as high as 50% per year [14]. However, despite the advances in preserving cardiac function in heart failure, existing anti-arrhythmic therapeutics remain ineffective largely because the understanding of the mechanism linking structural heart disease and electrical abnormalities in the failing heart remains inadequate.

In the hypertrophic heart, expression and function changes in ion channels and transporters have been documented in an animal study conducted by *Zhang C et. al.*[75] They demonstrated electrical changes and inducible malignant arrhythmias at the tissue level secondary to pressure-overload cardiac hypertrophy. At the same time, when angiotensin II type 1 receptor was pharmacologically inhibited in the pressure-loaded hearts, many of the changes in the electrophysiology parameters were attenuated suggesting that underlying signaling changes associated with heart failure not only affects structural remodeling, but may also affect electrical remodeling [75]. However, the mechanism by which electrical properties of the heart is affected by pro-hypertrophic signaling pathways remains to be elucidated.

A well-characterized cellular hypertrophic signaling pathway that underlies the development of pressure-overload cardiac hypertrophy is the mammalian target of rapamycin complex 1 (mTORC1) signaling. Genetic studies and mechanically stressed hearts with activated mTORC1 recapitulated many signaling, structural, functional, and

electrical abnormalities observed in hypertrophic cardiomyopathy [23, 24, 193, 248]. Most importantly, calcium cycling, important for establishment of normal contractility and excitation-contraction coupling in cardiomyocytes, was dysregulated in these animal models. Conversely, when mTORC1 activity was inhibited with either rapamycin or metformin, many of the pathologic remodeling, especially abnormal calcium handling, were either attenuated or reversed [192, 236, 249].

Major calcium handling proteins in cardiomyocytes include sarcoplasmic-reticulum calcium ATPase (SERCA2a), SERCA2a-accessory protein phospholamban, and sodium-calcium exchanger (NCX1). SERCA2a actively transports cytosolic calcium ions into sarcoplasmic reticulum during the relaxation phase of a heartbeat allowing for repolarization and phospholamban modulates levels of SERCA2a activity. On the other hand, NCX1 extrudes the remaining cytosolic calcium to the extracellular space using sodium gradient as the driving force. In cardiomyopathy, changes in expression and activity of the calcium handling proteins results in altered calcium cycling - a pathologic hallmark of heart failure - that leads to defects in excitation-contraction coupling and reduced contractility [250]. Whereas SERCA2a and phospholamban have marked reduction in expression [23, 236], NCX1 shows increased expression that is likely an adaptive response to compensate for SERCA2a downregulation [251-253]. Interestingly, studies have shown that although NCX1 expression is increased in the stressed heart, the overall NCX1 current actually decreases, suggesting another level of regulation for NCX1 activity in the hypertrophic heart [221, 254].

Normal functioning of NCX1 requires precise localization and retention at the transverse-tubule [255, 256]. The molecular mechanism required for the targeting and maintenance of NCX1 at this specialized cardiomyocyte membrane domain was recently identified to be an adaptor protein, ankyrin-B. Ankyrin-B binds, coordinates, anchors, and is required for the post-translational stability of NCX1 at the transverse-tubule to the underlying cytoskeleton [2, 133, 257]. Cardiomyocytes deficient in ankyrin-B show decreased NCX1 expression and exhibit abnormal spontaneous contractions and calcium dynamics. Animal hearts deficient in ankyrin-B exhibit abnormal electrocardiogram recordings at baseline (increased P-R interval, QRS duration, QT interval, and intermittent R-R interval variability) and develop fatal polymorphic ventricular tachycardia with adrenergic stimulation by concomitant exercise and epinephrine stimulation [4, 5]. Lastly, expressions of ankyrin-B and its interacting partner are concurrently reduced in cardiomyopathy [216].

Even though ankyrin-B expression is decreased in heart failure and decreased ankyrin-B expression is clearly linked to various cardiac arrhythmias that are present in end-stage heart failure, pathway underlying ankyrin-B regulation in heart disease has not been explored. Coupling the increased mTORC1 activity commonly observed in hypertrophied hearts with changes in ankyrin-B expression, our findings provide data suggesting that ankyrin-B is regulated by mTORC1. Specifically, we demonstrate that TAC hearts have increased mTORC1 activity and significantly decreased overall ankyrin-B expression, but inhibition of mTORC1 returns ankyrin-B expression to baseline levels. Additionally, fluorescent immunocytochemistry demonstrates dispersion of the remaining ankyrin-B suggestive of an underlying cytoskeletal

organization in the pressure-overloaded cardiomyocytes. Furthermore, physiologic consequences of mTORC1 activity modulation is reflected by the electrocardiogram recordings and saw that P-R interval, a measure of conduction between the atria and the ventricles, increases in TAC hearts but returns to baseline with rapamycin treatment. However, it should be noted that Q-T interval, a measure of rate of ventricular repolarization, remains unchanged in TAC hearts with or without treatment, suggestive of mTORC1-independent factors that remodels the electrical properties of the heart.

The same observations in expression changes and physiology are observed in our *in vitro* system. The only exception in the NRVM is increased ankyrin-B expression at the transverse-tubule. This difference could be contributed to a lack of a mechanical force on the cultured cardiomyocytes that does not perturb the structural integrity of the transverse-tubule [235, 258-260]. On the other hand, the mechanical force applied to the intact heart likely contributes to the lack of expression changes for both ankyrin-G and ankyrin-R - localized at the intercalated disc and sarcoplasmic reticulum respectively – in TAC hearts treated with vehicle or rapamycin.

Even though the *in vitro* ankyrin-B fluorescent immunocytochemistry finding was different from cardiomyocytes isolated from TAC hearts, it is nevertheless interesting as one subpopulation decreases in expression while another increases with increased mTORC1 activity. This begs the possibility of whether there exists different isoforms of ankyrin-B that are differentially regulated. On closer observation, immunoblot from both TAC hearts and cultured cardiomyocytes shows ankyrin-B population with different molecular weights. This issue will be explored in greater detail in the following chapter.

This is the first demonstration of a hypertrophic cellular signaling pathway directly affecting the electrical remodeling of the myocardium by regulating the anchoring protein that targets and maintains the proteins that make up the excitable domains in the heart (Figure 3.10). But additional studies will be necessary to unravel the mechanisms that differentially regulate the ankyrin-B subpopulations. For instance, are there direct protein-protein interactions between the signaling proteins along the mTORC1 pathway and ankyrin-B? Is mTORC1-regulated autophagy the common mechanism that underlies decreased SERCA2a expression and ankyrin-B population at the M-line? Is there a transporting mechanism that shifts ankyrin-B localization from one subcellular domain to another? Is the change in ankyrin-B expression affecting functions of NCX1? All these questions will need to be adequately addressed to clearly define the role of ankyrin-B in cardiovascular health and disease. We will first start by addressing the different ankyrin-B populations and their interactions with NCX in the following chapter.

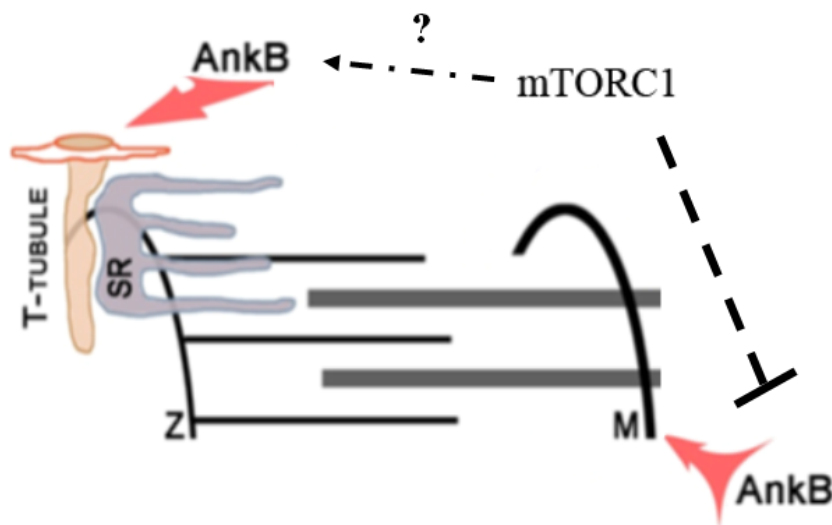


Figure 3.10. Proposed model for mTORC1 regulation of two subpopulations of ankyrin-B. Increased mTORC1 activities appears to decrease the ankyrin-B population at the M-line although there appears to be an increase expression of the ankyrin-B population at the SR/T-tubule.

**CHAPTER 4: IDENTIFICATION AND CHARACTERIZATION OF TWO
ANKYRIN-B ISOFORMS IN MAMMALIAN HEART**

Wu, H.C., G. Yamankurt, J. Luo, J. Subramaniam, S.S. Hashmi, H. Hu, and S.R. Cunha,
Identification and characterization of two ankyrin-B isoforms in mammalian heart.
Cardiovasc Res, 2015

Reprinted with permission to use in thesis/dissertation from Oxford University Press.
License numbers: 3671640981026 and 3671641193514

4.1 Introduction

Excitation-contraction coupling requires correct subcellular distribution of ion channels and transporters in cardiomyocytes. Ankyrin-B is an adaptor protein that facilitates recruitment and retention of membrane proteins to subcellular domains in cardiomyocytes such as the transverse tubule and M-line of the sarcomere. Mutations that disrupt interaction with ankyrin-B have been linked to a variety of cardiac arrhythmias including type 4 long QT syndrome, sick sinus syndrome, and atrial fibrillation [4, 229, 261].

In 1991, the cDNA for ankyrin-B 220kD was constructed by combining overlapping but partial cDNAs identified through an expression library screen using an antibody to ankyrin-R [147]. Since then, it has been assumed that this coding sequence represents the dominant ankyrin-B isoform in most tissues including the heart. Unfortunately, this assumption is not consistent with the common observation that tissues frequently express numerous alternative isoforms of ankyrin genes [1, 138-141, 262, 263].

Alternative splicing of ankyrin genes is an important process because it most likely confers specific functions to particular isoforms. In fact, the current paradigm that the heart only expresses ankyrin-B 220kD is confounded by the observation that ankyrin-B interacts with a variety of ion channels and transporters that lack similarity in function and subcellular distribution. We hypothesize that the heart expresses a diverse population of ankyrin-B isoforms that are tailored through alternative splicing to impart functional specificity and distinct subcellular distribution. We previously demonstrated

that the heart expresses over 25 unique iterations of *ANK2* transcripts, but a limitation of that study was that we only evaluated partial mRNA transcripts [1].

Here, we describe the identification and characterization of two ankyrin-B isoforms AnkB-188 and AnkB-212 that were isolated by long-range reverse transcriptase-PCR from human ventricular mRNA. Atrial and ventricular tissues from mouse, rat, and human hearts express *ANK2* transcripts corresponding to these isoforms as determined by quantitative real-time PCR. We demonstrate that both isoforms bind to the sodium calcium exchanger (NCX) in an *in vitro* binding assay, but only AnkB-188 increases NCX membrane expression and current. Furthermore, siRNA knockdown of AnkB-188 in neonatal cardiomyocytes decreases NCX expression and localization at transverse-tubules. We generated an isoform-specific antibody to AnkB-212 and demonstrate that this isoform is selectively expressed in heart and skeletal muscle. Moreover, endogenous AnkB-212 localizes to the M-line in adult and neonatal cardiomyocytes. Only AnkB-212 binds to obscurin, a large scaffolding protein implicated in M-line formation and maintenance, and this interaction regulates AnkB-212 targeting to the M-line. Moreover, siRNA treatment to AnkB-212 significantly reduces the expression of endogenous ankyrin-B at the M-line, but has no effect on NCX localization at the T-tubules. In summary, our data provide the first description of two ankyrin-B isoforms that display unique functions and subcellular distributions in cardiomyocytes.

4.2 Materials and Methods

4.2.1 Animals

Mice used in these studies include adult and neonatal wild-type (C57BL/6) and ankyrin-B (C57BL/6) heterozygous and homozygous null animals. Neonatal Sprague-Dawley rats used in these studies were ordered from Texas Animal Specialties (Humble, TX). Studies were conducted in accordance with the *Guide for the Care and Use of Laboratory Animals* published by the National Institute of Health following protocols that were reviewed and approved by the University of Texas Health Science Center at Houston Animal Welfare Committee.

4.2.2 Human tissue samples

Ventricular and atrial tissues from healthy donor hearts not suitable for transplantation were obtained through the Iowa Donors Network and the National Disease Research Interchange. Age and sex were the only identifying information acquired from tissue providers and the Iowa Human Subjects Committee determined that informed consent was not required. This investigation conforms to the principles outlined in the Declaration of Helsinki.

4.2.3 Isolation and cloning of full-length ANK2 transcripts from human ventricular mRNAs

RNA was isolated from ventricular tissue using a Qiagen RNeasy mini-kit and 500 ng of RNA was reverse-transcribed with a poly dT primer using SuperScript III reverse transcriptase (LifeTechnologies). cDNAs corresponding to AnkB-188 and AnkB-212 were PCR-amplified using the primer sets (atgaccaccatgttgcaaaag, ctttaattattgatccatcctc) and (atgaccaccatgttgcaaaag, ctttcaaagctgcatcttc). PCR products were subcloned into pcDH1-MCS lenti-viral expression plasmid (System Biosciences). The complete amino acid sequences for each isoform are shown here:

AnkB-188 kD:

1 10 20 30 40 50 60 70 80 90 100
MTTMLQKSDSNASFLRAARAGNLDKVVVEYLKGGIDINTCNQNGLNALHLAAKEGHVGLVQELLGRGSSVDSATKKNGTALHIASLAGQAEEVVKVLVKEGANINA
110 120 130 140 150 160 170 180 190 200
QSONGFTPLYMAAQENHIDVVKYLLENGANQSTATEDGFTPLAVALQQGHNAVAIILENDTKGKVRLLPALHIAARKDDTKSAALLQNDHNADVQSKSGFTPL
210 220 230 240 250 260 270 280 290 300 310
HIAAHYGNVNVAATLLNRRGAADVFTARNGITPLHVASKRGNNTMVKLLDRGGQIDAKTRDGLTPLHCAARSGHDQVVELLERGAPLLARTKNGLSPLHMAAQ
320 330 340 350 360 370 380 390 400 410
GDHVECVKHLQLQHKAPVDDVLDYLTALHVAACHGHYRVTKLLLDKRANPNARALNGFTPLHIAACKNRIKVMELLVKYGASIQAITESGLTPIHVAAFMGHLN
420 430 440 450 460 470 480 490 500 510 520
IVLLLLQNGASPDVTNIRGETALHMAARAGQEVVRCLLRNGALVDARAREEQTPHIAARLQKTEIVQLLQHMHAHPDAAATNGYTPLHISAREGQVDVASVL
530 540 550 560 570 580 590 600 610 620
LEAGAAHSLATKKGFTPLHVAAKYGSGLDVAKLLQRRRAADSAGKNGLTPLHVAAHYDNQKVALLLLEKGAHPHATAKNGYTPLHIAAKKNQMQUIASTLLNYGA
630 640 650 660 670 680 690 700 710 720
ETNIVTKQGVTPHLHLSAQEGHTDMVTLLLDKGANIHMSTKSGLTSLHLAAQEDKVNVAADILTKHGADQDAHTKLGYPPLIVACHYGNVKMNVNLLKQGANVNAK
730 740 750 760 770 780 790 800 810 820 830
TKNGYTPLHQAAQQGHTHINVLQHGAKPNATTANGNTALAIKRLGYISVVDTLKVVTVEEVTTTTTITTEKHKLNVPETMTEVLVDVDEEGDDTMTGDDGGEY
840 850 860 870 880 890 900 910 920 930
LRPEDLKELGDDSLPSSQFLDGMNLYRYSLEGGRSDSLRSFSSDRSHTLSHASYLRDSAVMDDSVVIPS HQVSTLAKAEARNNSYRLSWGTELDNVALSSSPIH
940 950 960 970 980 990 1,000 1,010 1,020 1,030 1,040
SGFLVSFVMDARGGAMRCRHNGLRIIPPRCKTAPTRVTCRLVKRRHLATMPMVEGEGELASRLIEVGPSSGAQFLGVPVIVEIPHFAALRGKERELVVLRSNG
1,050 1,060 1,070 1,080 1,090 1,100 1,110 1,120 1,130 1,140
DSWKEHFCDYTEDELNEILNGMDEVLDSPEDLEKKRICRIITRDFPQYFVAVSRIKQDSNLIGPEGGVLSSVVPPQVQAVFPEGALTKRIRVGLQAOQPMHSELV
1,150 1,160 1,170 1,180 1,190 1,200 1,210 1,220 1,230 1,240
KKILGNKATFSPIVTLEPRRRKFKPIITMTIPVPKASSDVMLNGFGGDAPTLRLLCSITGGTTPAQWEDITGTTPLTFVNECVSFTTNVSARFWLIDCRQIQES
1,250 1,260 1,270 1,280 1,290 1,300 1,310 1,320 1,330 1,340 1,350
VTFASQVYREIICVPYMAKFVVFVAKSHDPIEARLRCFCMTDDKVDKTTLEQQENFAEVARSRDVEVLEGGKPIYVDFGNLVPPLTKSGQHHIFSFFAFKENRLLPLF
1,360 1,370 1,380 1,390 1,400 1,410 1,420 1,430 1,440 1,450
VKVRDTTQEPCCGRLSFMKEPKSTRGLVHQAINLNIITLPIYTKIDMTSEKNPQDEQERIEERLAYIADHLGFSWTELARELDFTEEQIHQIRIENPNLSLQDQSH
1,460 1,470 1,480 1,490 1,500 1,510 1,520 1,530 1,540 1,550 1,560
ALLKYWLERDGKHATDNLVECLTKINRMDIVHLMETNTEPLQERISHSYAIEQITITLDHSEFGSVLQEELECTAQHKQKEEQAVSKESETCDHPPPIVSEEDIS
1,570 1,580 1,590 1,600 1,610 1,620 1,630 1,640 1,650 1,660
VGYSTFQDGVPKTEGSSATALFPQTHKEQVQDFSGKMQDLPPESSLEYQQEYFVTTTPGTSETQKAMIVPSSPKTPPEEVSPTPAEEEEKLYLQTPPTSSEERG
1,670 1,680 1,690 1,700 1,710 1,716
SPIIQEPEEPSEHREESSPRKTSLVIVESADNQPETCERLDEDAAFEKDNNE

AnkB-212 kd:

1 10 20 30 40 50 60 70 80 90 100 110
MTTMLQSDSNASF LRAARAGNLDKVV EYLKGGIDINTCNQNGLNALHLAAKEGHVGLVQELLGRSSVDSATKKGN TALHIASLAGOAEVVKVLVKEGANINAQSQNGFTPLY
120 130 140 150 160 170 180 190 200 210 220
MAAQENHIDVVKYLLLENGANOSTATEDGFTPLAVALQOGHNQAVAILLENDTKGKVR L PALHIAARKDDTKSAALLQNDHNADVQSKSGFTPLHIAAHYGNVNVATLLLN RGA
230 240 250 260 270 280 290 300 310 320 330 340
AVDFTARNGITPLHVASKRGNMVKLLLD RGGQIDAKTRDGLTPLHCAARS GHDQVVELL ERGAPLLARTKNGLSPLHMAAQGDHVEC VKHLLQHKAPVDDVTL DYL TALHV
350 360 370 380 390 400 410 420 430 440 450
AAHCGHYRVTKLLLDK RANPNARALRGETALHMAARAGQVEVVRCLLRNGALVDARAREEQTP LHIASRLGKTEIVQLLLQHMAHPDAATNGYTP LHIASAREGQVDVASV LLE
460 470 480 490 500 510 520 530 540 550 560 570
AGAAHSLATKKGFTPLHVAAYGSLDVAKLLQRRAAADSAGKNGYTPLHIAAKKNQMQUIASTLLNYGAETNIVTKQGV TPLHLASQEGHTDMVTLLLDKGANIHMSTKSGLTS
580 590
LHLAAQEDKVNVAIDLTKHGADQDAHTKLG YTPLIVACHYGNVKMVFLLKQGANVNAKTKNGYTPLHQAAQOGHHTHIINVL LQHGAKNP NATANGNTALAI AKRLGYISVVD T
690 700 710 720 730 740 750 760 770 780 790
LKVVTEEYTTTTITTEKHKLNVPETMTEVLDVSD EALKQFGDHFIDG EALSDSGDDTMTGDCGEYLRPEDLKELGDDSLPSSQFLDGMNYLRY SLEGGRSLSRFSFSDRSR H
800 810 820 830 840 850 860 870 880 890 900 910
TLSHASYLRDSAVMDDSVV IPSHQVSTLAKEAERN SYRLSWG TENLDNVALSSSPIHSGRAS PCLERD NSSFLVSEFVMDARGGAMRGCRHNGLR IIPPRKCTAPT RVTCLRVK
920 930 940 950 960 970 980 990 1,000 1,010 1,020
RHRLATMP PMVEGEGLASRLIEVGP SGAQFLGPVIVEIPHF AALRGKERELVLRSENGDSWKHFCDYTEDELNEILNGMDEVLDSPEDLEKKR ICRIITRDFPQYFAVV SRI
1,030 1,040 1,050 1,060 1,070 1,080 1,090 1,100 1,110 1,120 1,130 1,140
KQDSNLIGPEGGVL SSTVVPQVQAVFPEGALTKRIRVGLQAQPMHSELVKKILGNKATFSPIVLEPRRRKFKPI TMTIPVPKASSDVM LNGFGGDAPT LRL LICSITGGTTPA
1,150 1,160 1,170 1,180 1,190 1,200 1,210 1,220 1,230 1,240 1,250
QWEDITG TPLTFVNECVS FTTNV SARFWLIDCRQIQESVT FASQVYREIICVPYMAKFVFAKSHDP IEARLRCFCMTDDKVDK TLEQQENFAEVARSRDVEVLE GKPIYVDC
1,260 1,270 1,280 1,290 1,300 1,310 1,320 1,330 1,340 1,350 1,360
FGNLVPLTKSGQHHIF SFFAFKENRLPLFVKVRDTQ EPCGRLSFMKEPKSTRGLVHQAINLNLITLP IYTKES ESDQEQE E E I DMTSEKNPQDEQERIEERLAIADHLGFSW
1,370 1,380 1,390 1,400 1,410 1,420 1,430 1,440 1,450 1,460 1,470 1,480
TELARELDFTEEQI HQIRI ENPNS LQDQSHALLKYLWLERD GKHA DTNLV ECLTKINRMDIVHLMETNTEPLQERISHS YAEIEQTITLDHSEGF SVLQEE LCTAQHKQKEQA
1,490 1,500 1,510 1,520 1,530 1,540 1,550 1,560 1,570 1,580 1,590
VSKESETCDHPPIVSEEDI SVGYS TFQDGV PKTEGDS SATALFPQTHKEQVQDFSGKMODLPEESSLEYQEQEYFVTPGTETSETQKAMIVPSSPSKTPPEEVSTPAEE EKLYL
1,600 1,610 1,620 1,630 1,640 1,650 1,660 1,670 1,680 1,690 1,700 1,710
QTP TSSERGGSP I IQEPEEPSHREESSPRKTSLVIVESADNQPETCERLDEDAAFEKELTEBELGELEASSDEEAMVTRVRRRRI IQGDDMPEIPPETVTEEY IDEHGHTV
1,720 1,730 1,740 1,750 1,760 1,770 1,780 1,790 1,800 1,810 1,820
VKKVTRKI RRYVS SEGTEKEEIMVQMPQEPVNI BEGDGY SKVIKRVVLKSDTEQSEVTLCEPSILS STSQFAEPVEGRRVSKVVTIVVLGERMEKHLG DSSSLATDLP SAK
1,830 1,840 1,850 1,860 1,870 1,880 1,890 1,900 1,910 1,922
DDFEALS YTGSHMKVHLP SLVENEILKASEDGS I IKRRTMSKAITQKRAVVKDQHGKRIDL EHL E DVPEALDQDDLQRDLQQLLRHFCKEDLKQEK

4.2.4 Quantitative real-time (qt)-PCR analysis of ANK2 transcripts

Exon-exon boundary spanning primers were designed to the unique splice junctions encoding the C-terminal domains of AnkB-188 kD (exon junction 45 to 51) and AnkB-212 kD (exon junction 50 to 51). Primers were optimized based on nucleotide sequence and annealing temperatures such that primer efficiencies were between 90 – 110%. cDNAs were generated from ventricular and atrial mRNA that was isolated from three human and three mouse hearts. Relative expression of ANK2 transcripts was measured in triplicate by qt-PCR using SYBR Green dye (Bio-Rad) and experiments were replicated three times. Individual C_t values were normalized to the average of the C_t values of ANK2 transcripts with exon junction 31 to 32 (which encodes the minimal spectrin-binding domain).

The following table **4.1** contains the ANK2 qt-PCR primer sequences:

Primer set	5' primer	3' primer	Size (bp)	T _m (C°)	Primer eff. (%)
Hu-E31/32	GCATGGATGAAG/tactggatag	ctgctcagtacacctcttc	151	64	91
Hu-E45/51	CAGCTTTTGAAAAG/gacaac aatgag	caagtcctccttgagaaa tg	180	62.5	90
Hu-E50/51	GGATCAATAATTAAGAG/g acaacaatgag	caagtcctccttgagaaa tg	183	57	94
Mu-E31/32	CATGGATGAAG/tgctggacag	cactgtgctgctcagtact c	158	67	90
Mu-E45/51	CGCTTTTCAAAG/gacaacaat gcg	gaaggagttgctggagat ctc	157	59	97
Mu-E50/51	GATCAATAATTAAGAG/gac aacaatgag	gaaggagttgctggagat ctc	160	62	90

Ra-E12/13	GGTTTTACTCCACTGCACA TTG	GTTAGTGACAT CTGGAGAGGC	192	64.5	107
Ra-E31/32	CATGGATGAAG/tgctggacag	gacagcttcacctgtgat ac	178	64.5	101
Ra-E50/51	GATCAATAATTAAGAG/gac aacaatgag	gaaggagttgctggagat ctc	159	57	101

Hu: human; Mu: mouse; Ra: rat; T_m: optimal annealing temperature

4.2.5 AnkB-212 antibody generation

93 amino acids encoded by *ANK2* exons 50 and 51 and unique to AnkB-212 were subcloned in triplicate into pET-15b (Novagen), over-expressed in BL21(DE3)pLysS competent cells (Promega), and purified over a nickel column. Polyclonal antibody production was contracted to Pocono Rabbit Farm and Laboratory (Canadensis, PA).

4.2.6 Tissue immunoblot assay

Heart, skeletal muscle, brain, lung, and liver lysates were isolated from neonatal wild-type and ankyrin-B null mice. Human atrial and ventricular heart lysates were obtained from donor hearts. Protein lysates were separated by SDS-PAGE, transferred to nitrocellulose membrane (Whatman), incubated with primary antibody at 4°C overnight, and visualized using SuperSignal West Pico Chemiluminescent Substrate (Pierce). Primary antibodies used were: pan-ankyrin-B [229], AnkB-212 specific antibody (1:3000), and pan-actin-5 (1:10,000; Thermo Scientific).

4.2.7 Cellular fractionation immunoblot assay

HeLa-T7 cells stably expressing NCX lentivirally transduced with GFP, AnkB-188-GFP, or AnkB-212-GFP were washed with cold PBS, lysed in 200 μ L of homogenization buffer (10mM Tris pH 7.5, 5mM MgCl₂, 1mM EGTA, 0.003mg aprotinin, 0.1mM Na₃VO₄, 0.033mg leupeptin, and 1mM DTT), and homogenized with 1mL-syringe and 23G1 $\frac{1}{4}$ needle with repeated strokes. The homogenate was centrifuged 1500 x g for 10 minutes at 4°C and the supernatant was removed for ultracentrifugation at 100,000 x g for 40 minutes at 4°C. The resulting supernatant (cytosolic fraction) was placed in a new tube, and the pellet (membrane fraction) was washed and resuspended in homogenization buffer by sonication for 1 min at 4°C. Protein contents for both fractions were measured and same protein quantities were separated by SDS-PAGE and immunoblotted with the following primary antibodies: NCX (1:250, Swant, Switzerland), GFP (1:500, Santa Cruz), and pan-actin-5 (1:10,000; Thermo Scientific).

4.2.8 Isolation of neonatal mouse hearts and cultures of neonatal rat ventricular cardiomyocytes

Neonatal mouse cardiomyocytes were isolated from newborn mouse pups (P0) and NRVM were isolated from 1-2 day old Sprague-Dawley rat hearts as previously described with a minor modification [228]. In accordance with the animal protocol approved by the Animal Welfare Committee at University of Texas Health Science Center at Houston, neonatal rat pups were euthanized by decapitation. Briefly, hearts were exposed, excised, minced, and digested through a series of agitations in buffer

containing collagenase type II (Worthington, Collagenase type II 305U/mg) and pancreatin (Sigma). Cells from each digestion were collected and pooled, and pre-plated on Nunc plates (Thermo Fisher Scientific) to reduce fibroblasts and enrich for cardiomyocytes. Cells were then collected and plated on either Primaria plates (Corning) or fibronectin-coated glass-bottom MatTek plates (MatTek Corporation). Media was changed 24-hours after plating and experiments started 2 days after plating to ensure homogenous cultures. Following 3 days in culture, cardiomyocytes were transfected with either siRNA or lenti-viral constructs of GFP-tagged full-length AnkB-188 or AnkB-212. Cells were harvested for RNA or protein lysates or were and imaged 4 days later by confocal microscopy.

4.2.9 siRNA construct and NRVM transfections

NRVMs were transfected with siRNAs at a final concentration of 50 nM with DharmaFECT (Dharmacon GE) targeting rat AnkB-188, AnkB-212, and non-targeting siRNA control (scramble). The NRVMs were transfected for 6 hours, then media was changed to serum-free DMEM. Experiments were performed 48 hours later for quantitative real-time PCR and 72 hours later for immunoblot analysis and cell contraction recordings. The following table 4.2 contains the siRNA sequences targeting rat Ank2:

Target	Oligo Name	Sequence (5'-3')
E12	B188-siRNA sequence #2 sense	CUGCCUUCAUGGGCCACUU[dT][dT]
	B188-siRNA sequence #2 anti-	AAGUGGCCCAUGAAGGCAG[dT][dT]

	sense	
E17	B188-siRNA sequence #1 sense	CCAUGUUGCUGCUCUCAUUAU[dT][dT]
	B188-siRNA sequence #1 anti-sense	AUAAUGAGCAGCAACAUGG[dT][dT]
E48	B212-siRNA sequence #1 sense	CAGCUAUUCCAAAGUGAUA[dT][dT]
	B212-siRNA sequence #1 anti-sense	UAUCACUUUGGAAUAGCUG[dT][dT]
E49	B212-siRNA sequence #2 sense	GUUUCAGGCGGAACCAGUA[dT][dT]
	B212-siRNA sequence #2 anti-sense	UACUGGUUCCGCCUGAAAC[dT][dT]-
	Scramble sense	GCUCCCAGCUCGUCUAUGU[dT][dT]
	Scramble anti-sense	ACAUAGACGAGCUGGGAGC[dT][dT]

4.2.10 Isolation of individual adult mouse cardiomyocytes

Adult mouse cardiomyocytes were isolated as described previously (Baskin KK and Taegtmeier H. *Circ Res* 2011). In accordance with the animal protocol approved by the Animal Welfare Committee at University of Texas Health Science Center at Houston, 3 month-old mice were anesthetized with intraperitoneal injection of tribromoethanol-Avertin (Sigma T48402) at 250 mg/kg in 1X PBS and euthanized by removing the heart. Hearts from wild type or ankyrin-B^{+/-} mice were placed in ice-cold saline and the aorta was cannulated. Hearts were first perfused with warm perfusion buffer for a few

minutes, followed by perfusion with digestion buffer containing collagenase (Worthington, Collagenase type II 305U/mg). Once digested, hearts were minced and triturated, then centrifuged at 300 rpm x 5 minutes at 4°C. Supernatant was removed and cells were immediately fixed in ice-cold 100% ethanol, and kept in -20°C until use.

4.2.11 Fluorescent immunocytochemistry and image quantification

Cells were washed in ice-cold phosphate-buffered saline (PBS, pH 7.4) 3x. Cells were then blocked with 5% normal goat serum and 0.075% TritonX-100 for 30 minutes at room temperature then incubated in primary antibodies overnight at 4°C. Primary antibodies used were: ankyrin-B [229], ankyrinB-212 (1:300), α -actinin (1:1000, Sigma), myomesin (1:500, Developmental Studies Hybridoma Bank, University of Iowa), MyBPC3 (1:250, Santa Cruz), GFP (1:250, UC Davis/NIH NeuroMab Facility). Secondary antibodies used were goat anti-rabbit conjugated to Alexa Fluor 488 and goat anti-mouse conjugated to Alexa Fluor 568 (1:500, LifeTechnologies). Hoechst 33258 (1:1000, LifeTechnologies) was used for nuclear staining after removal of the secondary antibody. Images were obtained with a Nikon A1 confocal microscope (Nikon, Melville, NY) equipped with 100X oil, numerical aperture 1.4 objective. Fluorescence intensities for ankyrin-B populations and sarcomeric markers were analyzed with ImageJ (version 1.47, NIH, Bethesda, MD) and Excel (Microsoft, Bellevue, WA). Intensities were obtained by the mean pixel intensity of the magnified image.

4.2.12 Binding studies

AnkB-188-GFP and AnkB-212-GFP were expressed in HeLa-T7 cells and purified using an affinity-purified GFP Ig coupled to protein A-agarose beads as previously described [133] and incubated with *in-vitro* translated ³⁵S-radiolabeled fragments of the sodium-calcium exchanger (Asp-253 to Lys-615, NM_021097) or the C-terminal domain of human obscurin (Leu-6148 to Asn-6460, NM_052843) (TnT T7-Coupled Reticulate Lysate System, Promega). Binding reactions occurred in 500µL binding buffer (50mM Tris pH 7.4, 1mM EDTA, 1mM EGTA, 150mM NaCl, 0.1% TritonX-100) at 4°C overnight. Reactions were washed in wash buffer (binding buffer with 500 mM NaCl and 1% TritonX-100), pelleted, re-suspended in SDS-sample buffer, separated by SDS-PAGE, and visualized with autoradiography film (HyBlot CL, Denville Scientific).

4.2.13 Patch-clamp recording

Whole-cell patch-clamp recordings were performed using an Axopatch 200B amplifier (Molecular Devices, CA) at room temperature (22–24 °C) on the stage of an inverted phase-contrast microscope equipped with an appropriate filter set for green fluorescence protein visualization. Pipettes pulled from borosilicate glass (BF 150-86-10; Sutter Instrument Company, Novato, CA) with a Sutter P-97 pipette puller had resistances of 2–4 MΩ when filled with pipette solution containing (mM) 120 CsCl, 20 NaCl, 5 Na₂ATP, 3 CaCl₂, 1 MgCl₂, 10 HEPES, and 10 EGTA with pH 7.3 and 315 mOsm l⁻¹ in osmolarity. The extracellular solution for whole-cell recording contains (mM) 140 NaCl, 5 CsCl, 2 CaCl₂, 1 MgCl₂, 10 mM glucose, and 5 mM

HEPES (the pH was adjusted to 7.4 with NaOH, and the osmolarity was adjusted to 340 mOsm l⁻¹ with sucrose). The whole-cell membrane currents were recorded using a voltage ramp (from +80 to -100 mV at 100 mV/s) following 100-ms step depolarization to +80 mV from a holding potential of -40 mV. Data were acquired and analyzed using pClamp 10 software (Molecular Devices, CA). Currents were filtered at 2 kHz and digitized at 10 kHz with Digidata 1440A acquisition system (Molecular Devices, CA). Membrane capacitance was directly read from the membrane test function of pClamp 10. Current density was obtained by dividing the current amplitude by cell capacitance.

4.2.14 Recording and analysis of NRVM contraction rates

Contracting NRVM syncytium was located on light microscope (Micromaster; Fisher) with 10X magnification eyepiece and 20X objective lens. A camera with 10 megapixel resolution (HTC One M8) was mounted on the microscope using Snapzoom Universal Digiscoping Adapter (Snapzoom). Contractions were recorded for 2 to 2.5 minutes. The same recording method was used following stimulation with 1 μM epinephrine.

Using Video Spot Tracker (VST) program (<http://cismm.cs.unc.edu/downloads>) and the tracking method described by Fassina L *et. al.* [230], we placed a marker on the contracting syncytium and the program tracked the marker displacement frame by frame (30 frames per second) registering the spatial-temporal coordinates x, y, (expressed in pixels), and t (expression in frame number that converts to second). Coordinates were

plotted in Excel (Microsoft) with each peak corresponding to an active syncytial contraction. We assessed rhythmicity of the syncytial contractions by randomly picking a consecutive 30-second interval and measuring the time between contractions. The average contraction time for each video was calculated and the time difference between each contraction and the average was plotted on GraphPad Prism 6 (GraphPad Software) using box-and-whisker plots.

4.2.15 Statistical analysis

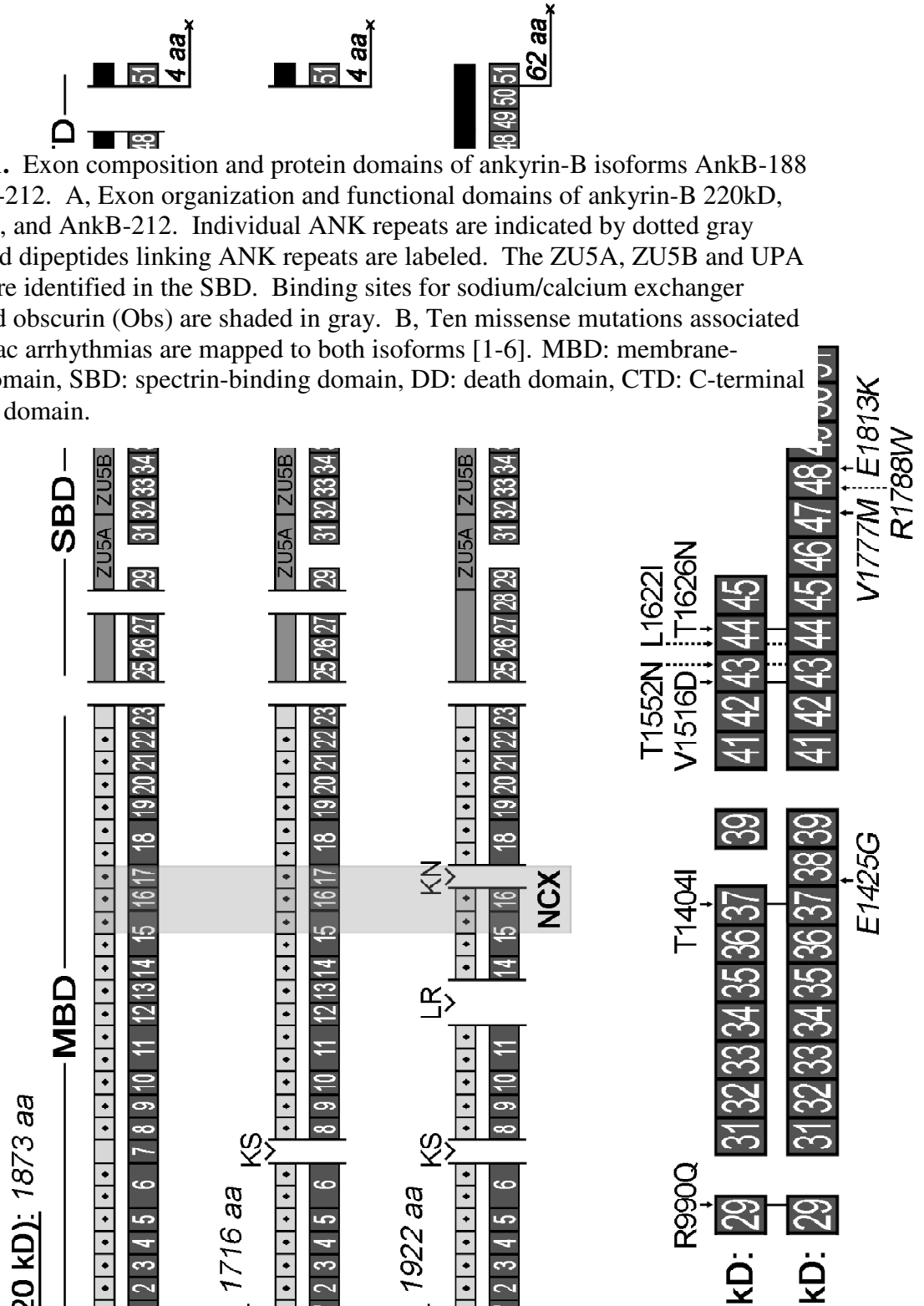
P-values were determined for single comparisons using unpaired Student's *t*-test (two-tailed). The NRVM contraction data was assessed for normality and processed to calculate the mean and the standard deviation separately for each syncytial recording. To standardize the dispersion of the time difference between each contraction and the average contraction time for each respective syncytium, the coefficient of variation for each recording was calculated. The coefficients of variation across the groups were compared using the Kruskal-Wallis test with post-hoc Wilcoxon rank-sum test. A *P*-value of less than 0.05 was considered statistically significant. Values are expressed as means \pm SE except for the box-and-whisker plot for contractile rhythm variability where the box contains interquartile range covering 25-75% of the readings and the whiskers contains 90% of the readings.

4.3 Results

4.3.1 Identification and cardiac expression of ankyrin-B isoforms

The biggest challenge to isolating tissue-specific ankyrin cDNAs is that ankyrin genes are long and complex containing over 50 exons that are alternatively spliced resulting in mRNA transcripts over 5000 bases in length. To identify full-length *ANK2* cDNAs encoding ankyrin-B isoforms expressed in human heart, we performed long-range PCR on reverse transcribed mRNA isolated from human hearts. We identified two novel ankyrin-B isoforms AnkB-188 and AnkB-212, which are labeled based on their predicted molecular weights (Figure 4.1A). In contrast to ankyrin-B 220kD, which starts with exon 1, both isoforms start with exon 1' [1]. Both isoforms display similar alternative splicing patterns including excision of exons 7, 30, and 40. Unique alternative splicing to AnkB-188 includes excision of exons 24, 28, 38, and 46-50. Remarkably, exons 46-50 encode the majority of the C-terminal regulatory domain including the binding site for the large scaffolding protein obscurin [136]. Unique alternative splicing to AnkB-212 includes excision of exons 12-13 and 17. Previously, we have mapped the NCX binding site to the three ANK repeats encoded by exons 15-17 [133] suggesting that AnkB-212 does not interact with NCX. In addition, the cDNA for AnkB-212 includes exon 50 that shifts the open reading frame by plus one such that exon 51 encodes a unique stretch of 62 amino acids terminating with the residues QEAK. In contrast, the amino acid sequences for both ankyrin-B 220kD and AnkB-188 terminate with residues DNNE (see materials and methods 4.2.3 for the complete sequences). Missense mutations associated with ankyrin-B dysfunction and cardiac arrhythmias have been mapped to the spectrin-binding and C-terminal regulatory

domains of both isoforms (Figure 4.1B). Interestingly, the mutation E1425G resides in exon 38 and this exon is not present in the AnkB-188 isoform. E1425G has been well studied and linked to a variety of arrhythmias including type 4 long QT syndrome, sick sinus syndrome, and atrial fibrillation [2-5, 261].



To validate and measure the expression of these isoforms in heart mRNA, we designed exon-exon boundary spanning primers that specifically amplify partial transcripts based on unique exon junctions in each isoform. For example, to detect partial mRNAs encoding AnkB-188 we designed a primer set to the unique exon junction of exons 45 to 51. This exon-exon boundary spanning primer anneals to the terminal 14 nucleotides of exon 45 (CAGCTTTTGAAAAG) and the initial 12 nucleotides of exon 51 (GACAACAATGAG). We validated that a PCR product is only amplified using a full-length exon-exon boundary spanning primer (Figure 4.2A, lane 3). In contrast, no PCR products are amplified using half the exon-exon boundary spanning primer (Figure 4.2A, lanes 1 & 2). To amplify partial transcripts of AnkB-212, we designed a primer set to amplify the junction of exons 50 to 51. All primer sets were optimized based on nucleotide sequences and annealing temperatures such that primer efficiencies are within 90 – 110% (see materials and methods **4.2.4**).

Using these exon-exon boundary spanning primers, we performed qt-PCR to measure the relative mRNA expression of AnkB-188 and AnkB-212 in ventricular and atrial tissues isolated from both human and mouse hearts (Figure 4.2B and C). Relative expression of each isoform was normalized to expression of exon junction 31/32. These exons encode the minimal spectrin-binding domain and presumably this domain is expressed in the majority of ankyrin-B isoforms. Both isoforms are expressed in atrial and ventricular tissues. Interestingly, each primer set demonstrated a similar expression pattern between human and mouse. Both human and mouse hearts express less mRNA for AnkB-188 (45/51) than AnkB-212 (50/51). While the trends are the same in human and mouse hearts, the magnitude of difference between the paired junctions (45/51 vs.

50/51) is not the same. For example, junction 50/51 is ~3-fold greater than junction 45/51 in mouse, but only ~1.5-fold greater in human. We speculate that variations in tissue extraction and preservation most likely account for these differences. Taken together, these findings demonstrate that mouse and human hearts express *ANK2* transcripts with unique exon junctions present in AnkB-188 and AnkB-212.

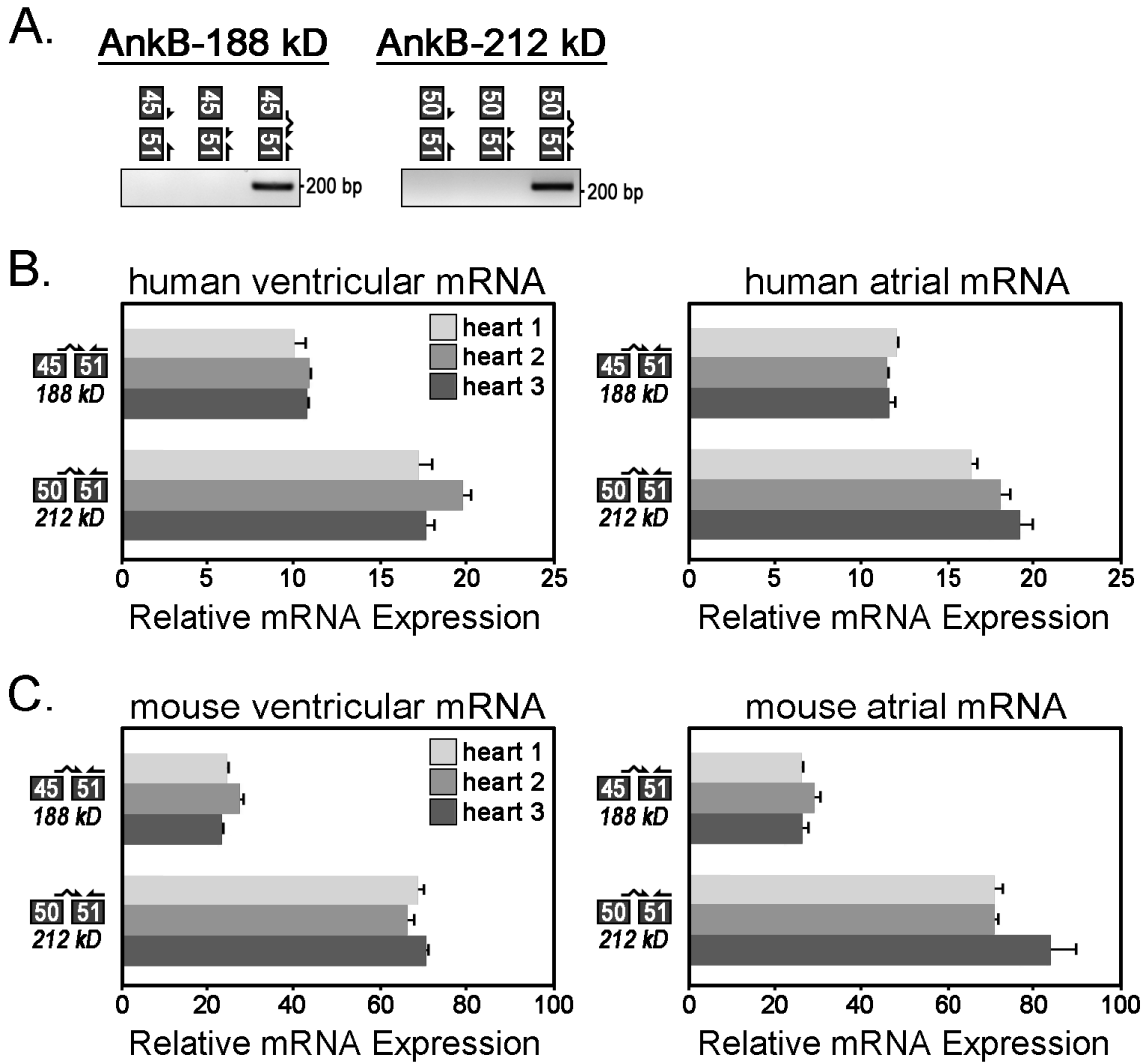


Figure 4.2. Relative mRNA expression of AnkB-188 and AnkB-212 in human and mouse cardiac tissues. A, Exon-exon boundary spanning primers were used to PCR amplify alternative splice junctions unique to each isoform (AnkB-188: junction 45/51, AnkB-212: junction 50/51). B, Relative mRNA expression of alternative splice junctions in AnkB-188 and AnkB-212 was measured in cardiac tissues from three

human hearts. Expression of each splice junction was normalized to the expression of exon junction 31/32 (presumably expressed in all *ANK2* transcripts and set to 100%). C, Relative mRNA expression of alternative splice junctions in AnkB-188 and AnkB-212 was measured in cardiac tissues from three mouse hearts. For B & C, samples were repeated in triplicate (n=3) and experiments were repeated three times

4.3.2 AnkB-188 and AnkB-212 binding to NCX

In the heart, many different functions have been ascribed to ankyrin-B including the recruitment and retention of various membrane proteins including dystrophin [264], sodium potassium ATPase (NKA) [2, 4], IP₃ receptor [2, 4, 265], and NCX [4, 133]. We previously demonstrated that ANK repeats 16-18 in the membrane-binding domain of ankyrin-B encodes the binding site for NCX [133]. Considering AnkB-212 lacks exon 17 that encodes ANK repeat 18, we anticipated that NCX would not bind to this isoform (Figure 4.3A).

To assess whether the AnkB isoforms display different NCX binding, we performed an *in vitro* binding assay with radiolabelled NCX fragment and full-length AnkB-188 or AnkB-212 (Figure 4.3B). GFP-tagged AnkB isoforms were transiently expressed in HeLa-T7 cells and immunoprecipitated from lysate using a GFP antibody. Interestingly, both isoforms equally bound NCX suggesting that the absence of ANK repeat 18 had no effect on NCX binding in this *in vitro* paradigm.

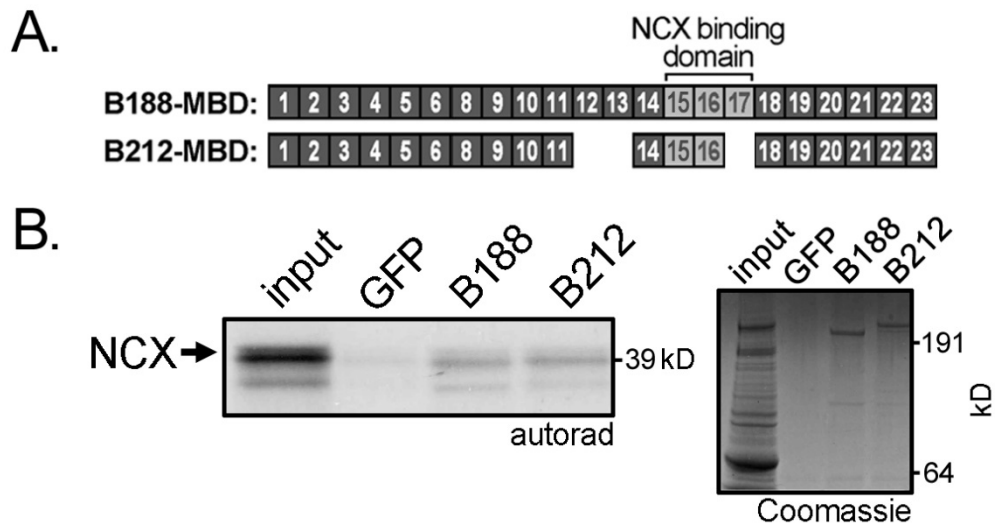


Figure 4.3. Both AnkB-188 and AnkB-212 bind NCX. A, Exons encoding the membrane-binding domains of AnkB-188 and AnkB-212. The NCX binding site maps to *ANK2* exons 15-17. (B) ^{35}S -labelled, *in vitro* translated NCX fragment binds to both AnkB isoforms. Experiments were repeated three times. Coomassie Blue Stain demonstrates equal expression of both isoforms.

4.3.3 AnkB-188 increases NCX membrane expression and current

To examine the effect of each isoform on NCX function, we measured the NCX current in HeLa-T7 cells stably expressing NCX and transiently expressing either GFP-tagged AnkB isoform. Similar expression of each isoform was demonstrated by immunoblot analysis of the GFP-tag, and individual GFP-positive cells were measured for NCX current (Figure 4.4A). While a basal NCX current was also detected in the stable cell lines, only the transient expression of AnkB-188 enhanced this current compared to cells expressing GFP alone or AnkB-212 (Figure 4.4B). HeLa-T7 cells express an endogenous isoform of ankyrin-B as detected by immunoblot (data not shown), which most likely accounts for the basal NCX current in the stable cell lines. Qrt-PCR analysis demonstrated that NCX mRNA expression was equivalent in all

transfection conditions, indicating that neither ankyrin isoform increases NCX mRNA expression (Figure 4.4E).

To investigate the molecular basis for increased NCX current mediated by AnkB-188, we measured the expression of NCX in cytosolic and membrane fractions of cells transiently expressing GFP alone, AnkB-188, or AnkB-212 by immunoblot analysis (Figure 4.4C). We found that membrane expression of NCX was 2-fold greater in cells expressing AnkB-188 compared to cells expressing GFP alone or AnkB-212 as determined by densitometry analysis of immunoblots from three independent experiments (Figure 4.4D). Taken together, these data suggest that cells expressing AnkB-188 display enhanced NCX current because this isoform increases NCX expression in the plasma membrane.

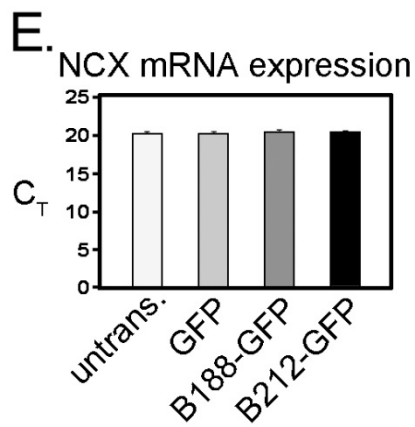
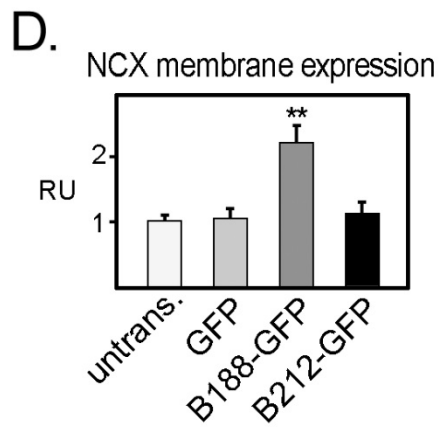
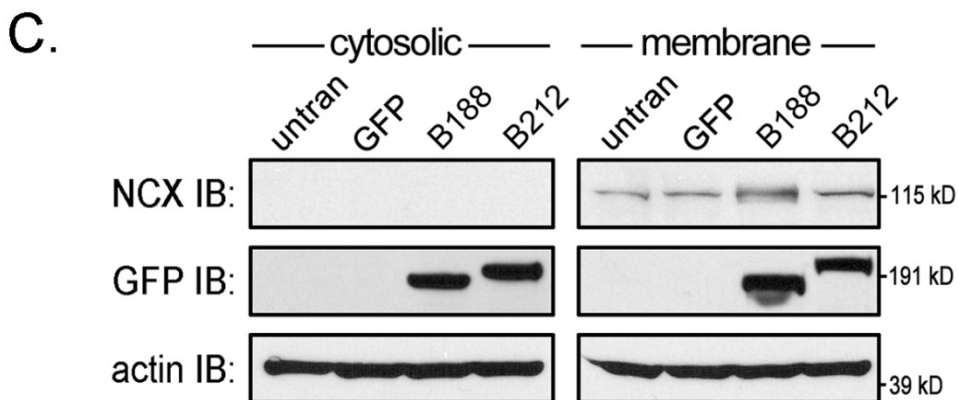
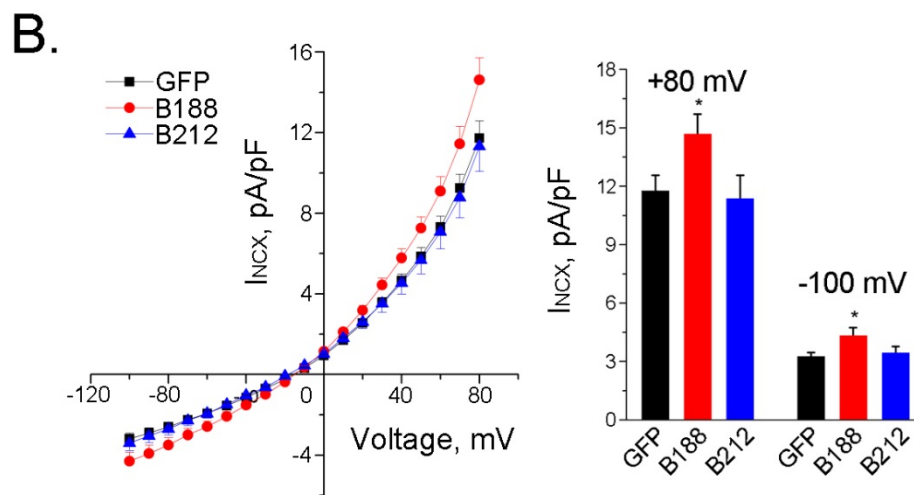
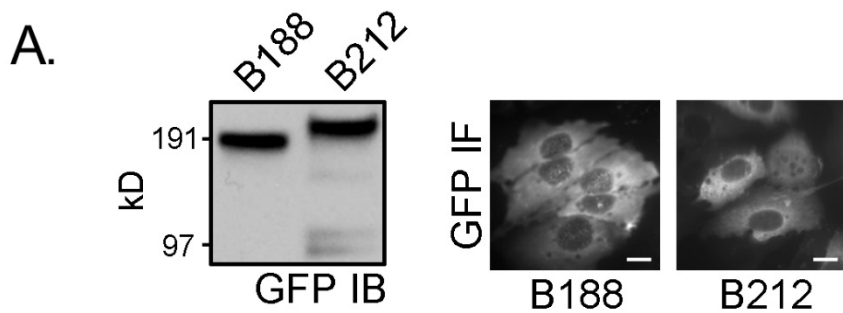


Figure 4.4. AnkB-188, but not AnkB-212, increases NCX current and membrane expression. A, Detection of the GFP-tag on isoforms by immunoblot and immunofluorescence in HeLa-T7 cells that stably express NCX. Scale bar is 5 μ m. B, NCX voltage-current curves of HeLa-T7 cells transiently expressing GFP, AnkB-188, or AnkB-212 (n=29 for GFP and AnkB-188, n=27 for AnkB-212, * P <0.05). C, NCX expression is increased in the membrane fraction of HeLa-T7 cells expressing AnkB-188. Equal protein loading was demonstrated by immunoblot to pan-actin, while membrane enrichment was demonstrated by immunoblot to caveolin-1. Experiments were replicated three times. D, Densitometry of NCX membrane expression from C. E, Qrt-PCR of NCX mRNA expression in untransfected HeLa cells and HeLa cells transiently expressing GFP, B188-GFP, or B212-GFP.

4.3.4 AnkB-212 is selectively expressed in heart and skeletal muscle

In the initial characterization of ankyrin-B, a polyclonal antibody was generated against the death and C-terminal domains (Figure 4.5A). We have previously demonstrated that the C-terminal regulatory domain is subject to complex alternative splicing presumably resulting in numerous alternative ankyrin-B isoforms [1]. Using this pan-AnkB antibody, we demonstrate that multiple AnkB isoforms are expressed in adult mouse heart and in mouse neonatal tissue including heart, skeletal muscle, brain, lung, and liver (Figure 4.5A). In contrast, no isoforms are detected in the same tissues isolated from neonatal AnkB null (-/-) mice. Using the same antibody, multiple ankyrin-B isoforms are also detected in atrial and ventricular tissues isolated from adult human heart.

One of the challenges in characterizing alternative isoforms is identifying a unique stretch of amino acids that could be used to generate an isoform-specific antibody. Fortunately, the coding sequence for AnkB-212 includes exon 50, which shifts the open reading frame plus one such that exon 51 encodes a unique stretch of 62 amino acids (Figure 4.5B). Numerous expressed sequence tags (>10) from human cDNAs contain

this unique coding sequence including DB499390.1, DA768553.1, and DA364599.1. To generate an isoform-specific antibody to AnkB-212, we made a bacterially expressed and purified His-tag fusion protein of the 93 amino acids encoded by exons 50 and 51. Rabbit anti-serum was used to detect AnkB-212 expression in AnkB wild-type (+/+) and null (-/-) tissues including heart, skeletal muscle, brain, lung, and liver (Figure 4.5B). Interestingly, AnkB-212 is expressed in wild-type adult and neonatal mouse heart as well as skeletal muscle. However, it is *not* expressed in brain, lung, or liver from wild-type neonates. AnkB-212 was also detected in human atrial and ventricular tissues. These findings suggest that expression of AnkB-212 is restricted to striated muscle.

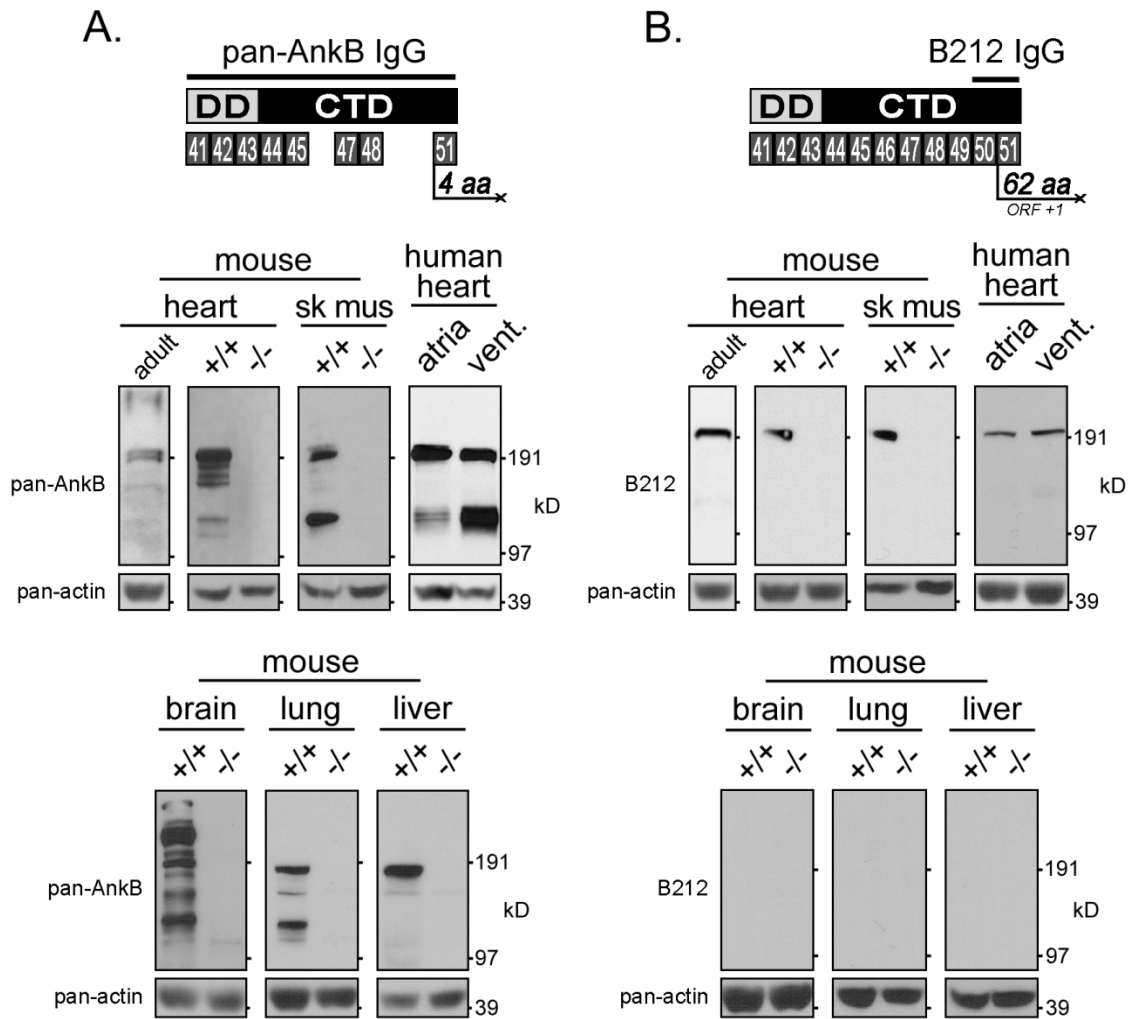


Figure 4.5. Expression of pan-AnkB and AnkB-212 in various tissues. A, The antibody to pan-AnkB was generated against the death and C-terminal domains encoded by exons 41-45, 47-48 and 51. Expression of multiple AnkB isoforms was detected in neonatal mouse heart, skeletal muscle, brain, lung, and liver of wild-type (+/+) and adult mouse heart. B, The antibody to AnkB-212 was generated against amino acids encoded by exons 50 and 51. Only one isoform of AnkB-212 was detected in heart and skeletal muscle of wild-type neonates and adult mouse heart. Pan-actin immunoblot demonstrates equal protein loading. For A & B, experiments were replicated three times.

4.3.5 Endogenous AnkB-212 is expressed at the cardiomyocyte M-line

Within cardiomyocytes, ankyrin-B is expressed at the sarcomeric M-line and the sarcoplasmic reticulum/transverse-tubule junctions, which generally co-localize with components of the sarcomeric Z-line. Using the pan-AnkB antibody, we demonstrate

the expression of these two ankyrin-B subpopulations at the Z- and M-lines in isolated adult cardiomyocytes (Figure 4.6A and C). We measured the relative fluorescence intensity of this signal and found that the less abundant ankyrin-B population co-localizes with the resident Z-line marker protein α -actinin, while the more abundant population co-localizes with myomesin, a M-line resident protein. Interestingly, AnkB-212 is only detected at the M-line of adult cardiomyocytes (Figure 4.6B and D). Specifically, AnkB-212 co-localizes with myomesin, but not with α -actinin. Similar results were found in experiments using cardiomyocytes isolated from ankyrin-B heterozygous hearts (Figure 4.7). These findings suggest that the M-line population of ankyrin-B is partially comprised of the AnkB-212 isoform.

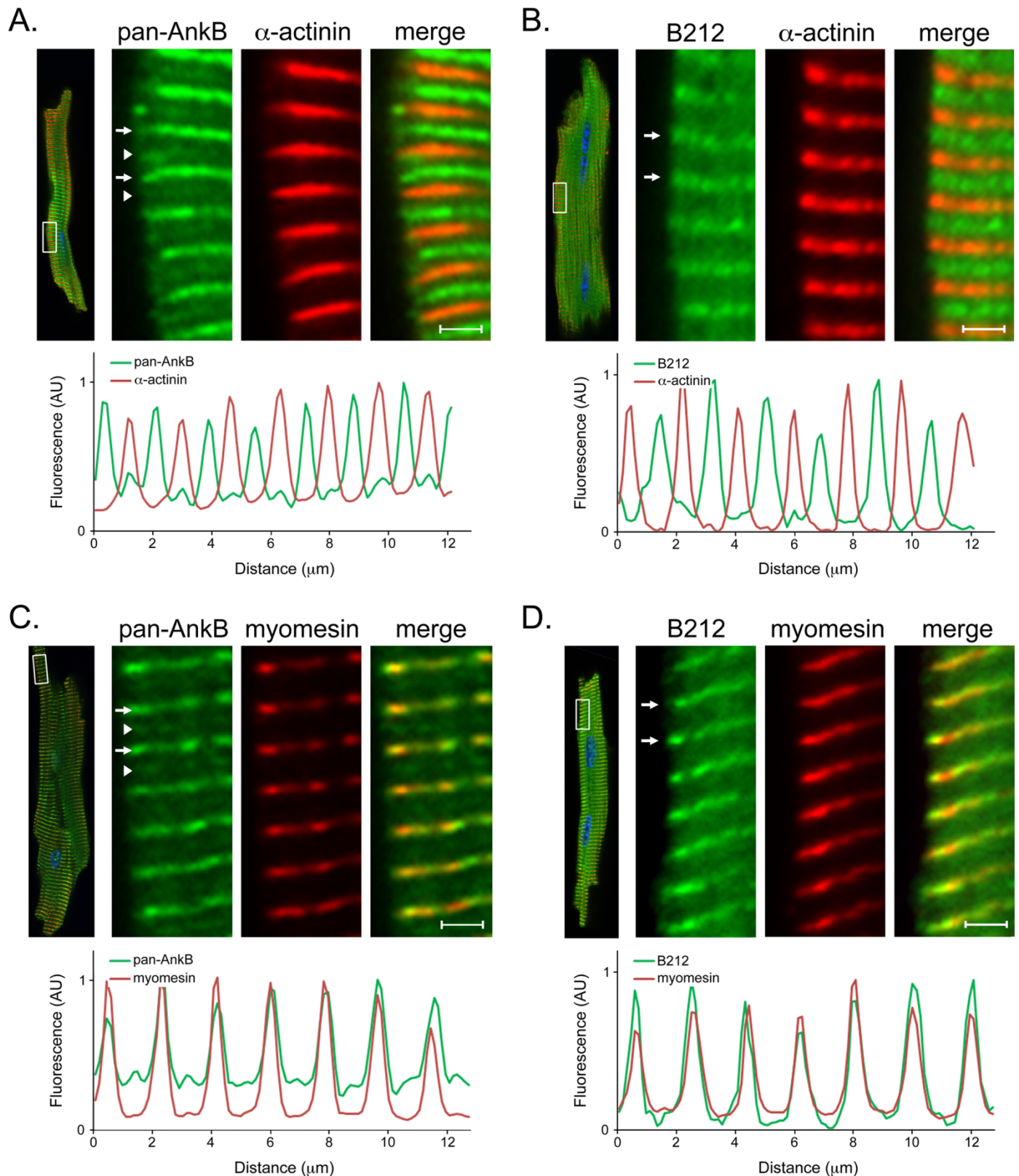


Figure 4.6. AnkB and AnkB-212kD endogenous localizations in adult cardiomyocytes. A and C, Two subpopulations of ankyrin-B are detected using the pan-AnkB antibody. The less abundant population (white arrow heads) co-localizes with the Z-line marker α -actinin while the more abundant population (white arrows) co-localizes with the M-line marker myomesin. Relative fluorescence intensities of the insets were measured and graphed. B and D, Only one population of AnkB-212kD (white arrows) is detected and co-localizes with the M-line marker myomesin and not the Z-line marker α -actinin. For all antibody conditions, 6-8 myocytes per condition were imaged. Scale bar = 2 μm

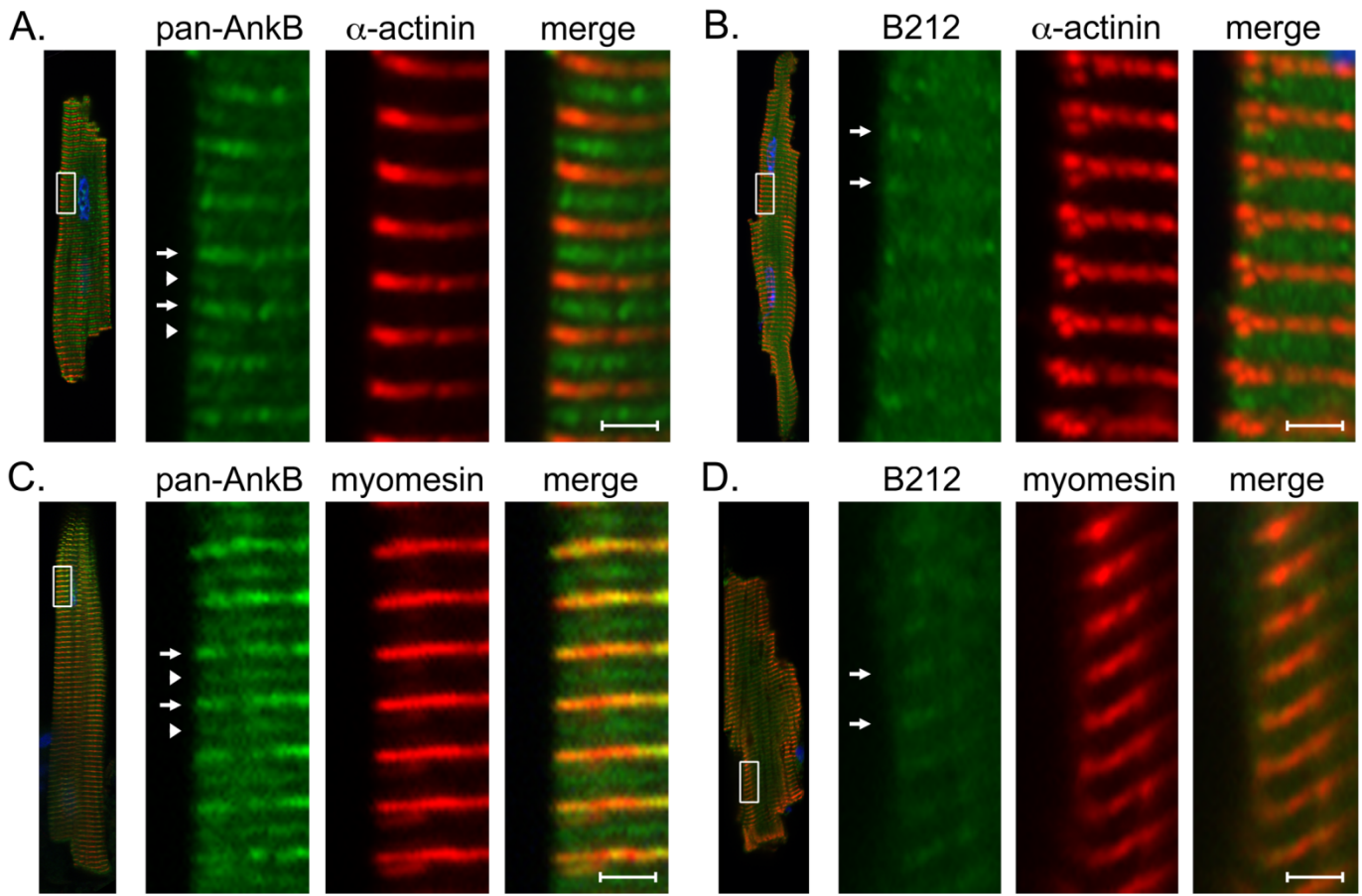


Figure 4.7. Expression of pan-AnkB and AnkB-212 in isolated AnkB^{+/-} adult cardiomyocytes. A and C, Two subpopulations of ankyrin-B are expressed in AnkB^{+/-} cardiomyocytes. The less abundant population (white arrowheads) co-localizes with α -actinin at the Z-line while the more abundant population (white arrows) co-localizes with myomesin at the M-line. B and D, There is one population of AnkB-212 (white arrows) that co-localizes with myomesin, but not with α -actinin. For all antibody conditions, 6-8 myocytes per condition were imaged. Scale bar = 2 μ m

4.3.6 Exogenous AnkB-212 is targeted to the M-line via an interaction with obscurin

To investigate the molecular basis of AnkB-212 targeting and retention at the sarcomeric M-line, we evaluated the isoforms for binding to obscurin, an 800kD structural protein that has been implicated in M-line formation and alignment [234, 266, 267]. Two ankyrin-binding sites reside in the C-terminal domain (CTD) of obscurin

[268]. We previously demonstrated that the ankyrin-B C-terminal domain contains two obscurin-binding sites encoded by *ANK2* exons 46 and 47 [136]. Interestingly, the C-terminal domain of AnkB-188 lacks exons 46 through 50, while the same domain in AnkB-212 contains these exons (Figure 4.8A). We performed an *in vitro* binding assay in which the obscurin CTD was *in vitro* translated and radiolabelled with ^{35}S methionine, then incubated with GFP-tagged AnkB-188 or AnkB-212, which was over-expressed and purified from HeLa-T7 cells. Obscurin only bound to AnkB-212, and not to AnkB-188 (Figure 4.8B).

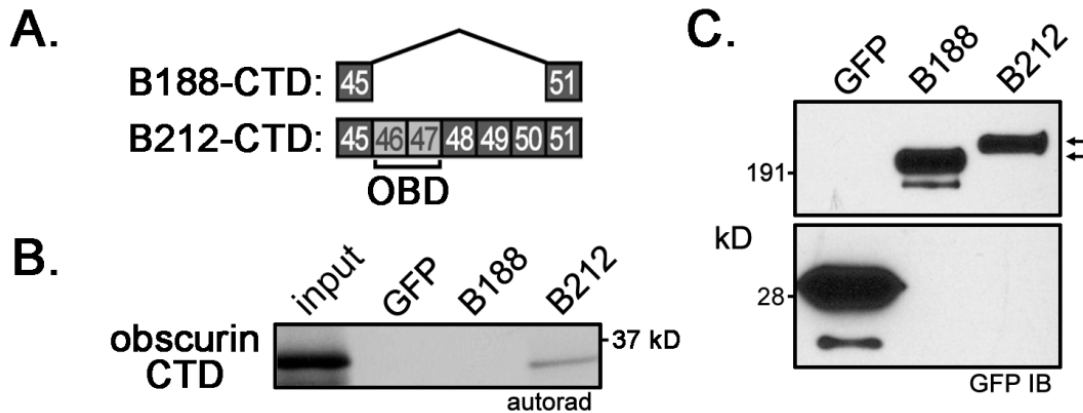


Figure 4.8. AnkB-212, but not AnkB-188, binds to obscurin. A, Exons coding the C-terminal regulatory domains of AnkB-188 and AnkB-212. *ANK2* exons 46 and 47 encode two obscurin binding domains. B, *In vitro* translated obscurin CTD binds GFP-tagged AnkB-212. C, GFP immunoblot demonstrates similar expression of ankyrin isoforms. Experiments were replicated twice. OBD, obscurin binding domains.

Because we lack an antibody specific to AnkB-188, we evaluated the co-localization of each isoform to three sarcomeric proteins: α -actinin (Z-line), myosin-binding protein C (A-band), and myomesin (M-line) to assess whether AnkB-188 and AnkB-212 display differential subcellular localization in cardiomyocytes. GFP-tagged ankyrin isoforms were expressed in rat neonatal cardiomyocytes by lenti-virus and images were acquired by confocal microscopy. AnkB-188 expression was diffusely cytosolic and lacked sarcomeric localization (Figure 4.9A). In contrast, AnkB-212 distinctly co-localizes with myomesin and is flanked by myosin-binding protein C suggesting that its localization does not extend beyond the M-line (Figure 4.9B). Removal of exon 46, which encodes the first obscurin-binding site, from the CTD of AnkB-212 disrupts AnkB-212's interaction with obscurin and abrogates the M-line localization (Figure 4.10). Taken together, these data suggest that AnkB-212 is targeted to the M-line via its interaction with obscurin.

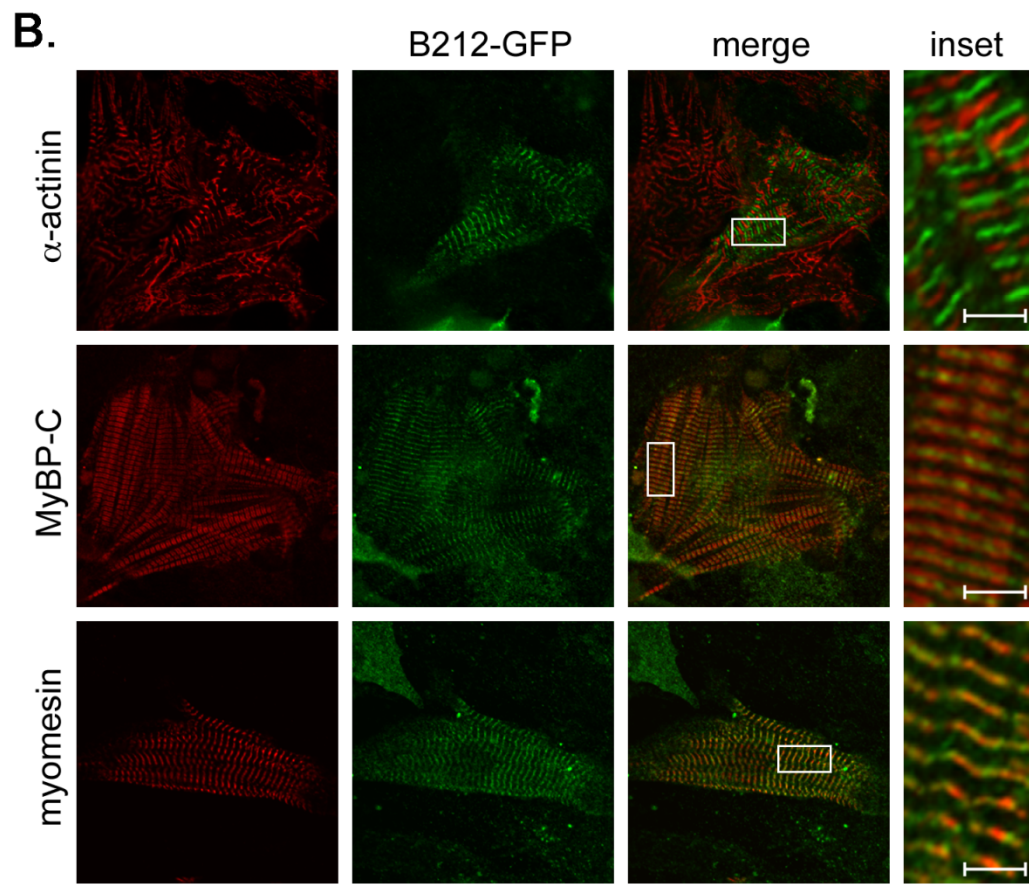
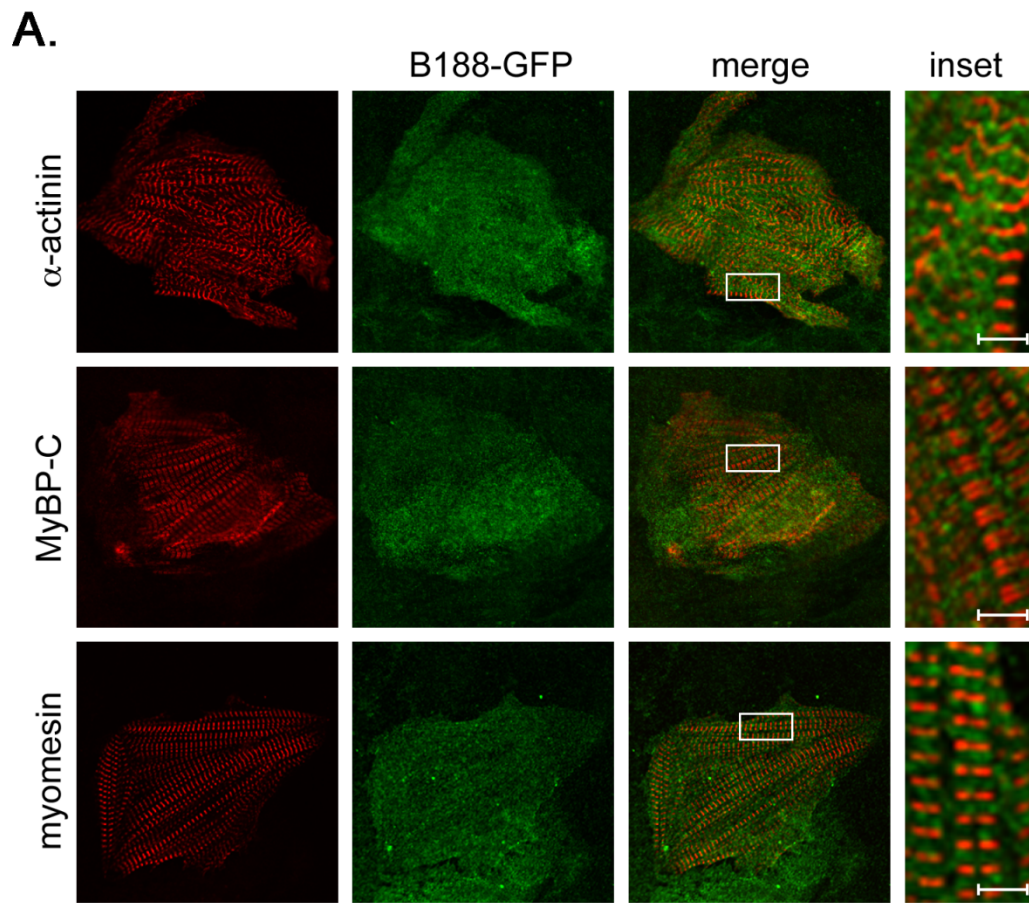


Figure 4.9. AnkB-212 is targeted to the M-line of cardiomyocytes. Double labeling of A, GFP-tagged AnkB-188 or B, GFP-tagged AnkB-212 with Z-line marker α -actinin, A-band marker MyBP-C, and M-line marker myomesin in neonatal rat cardiomyocytes. AnkB-212, but not AnkB-188, colocalizes with myomesin at the M-line. For all antibody conditions, 6-8 myocytes were imaged. MyBP-C, myosin binding protein C. Scale bar = 2 μ m.

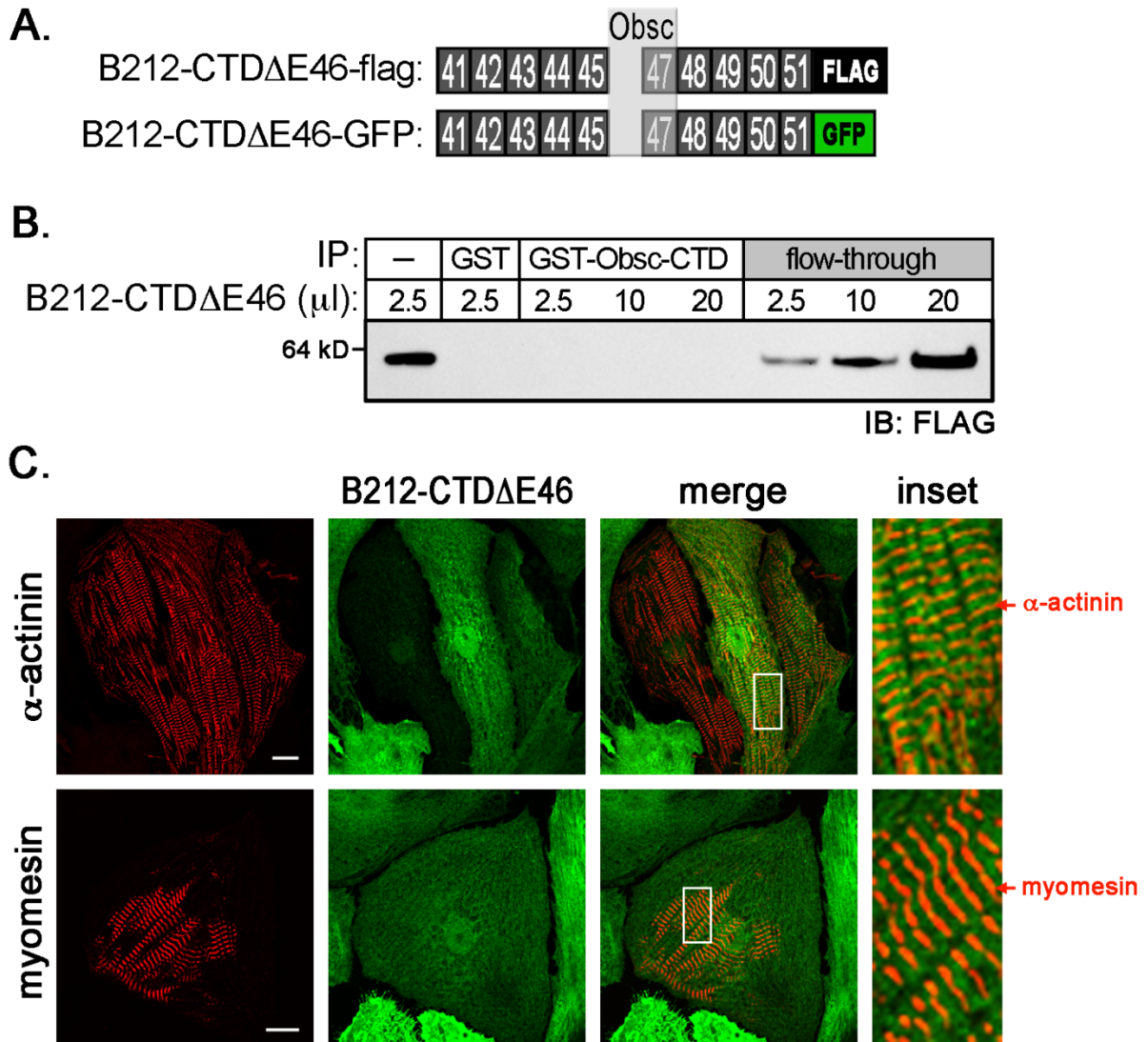


Figure 4.10. _AnkB-212 CTD Δ E46 lacks obscurin-binding and M-line targeting. A, Diagram of two tagged (flag and GFP) constructs of AnkB-212 CTD that lack exon 46, the first obscurin binding site in *ANK2*. B, A GST-fusion protein of obscurin CTD (containing the ankyrin-binding sites) does not precipitate AnkB-212 CTD Δ E46. C, GFP-tagged AnkB-212 CTD Δ E46 does not co-localize with myomesin in virally transduced cardiomyocytes. Scale bar = 2 μ M.

4.3.7 AnkB-188 knockdown decreases the expression and proper subcellular localization of NCX

To identify potential functions associated with either ankyrin-B isoform in rat neonatal cardiomyocytes, we used siRNAs to selectively knockdown each isoform. SiRNAs were designed to unique exons in each isoform (Figure 4.11A). We used qPCR transcript analysis to evaluate the efficacy and specificity of the siRNAs against its intended isoform (Figure 11B, gray bars) versus the other isoform (Figure 4.11B, black bars). SiRNAs that displayed preferential knockdown of each isoform were used in subsequent assays. Immunoblot analysis was performed to confirm siRNA-mediated knockdown of each isoform. Using the pan-AnkB antibody, two high molecular weight isoforms are clearly resolved and siRNAs to AnkB-188 reduce the expression of the smaller isoform although expression of the larger isoform also decreases but to lesser extent (Figure 4.11C). The isoform-specific antibody to AnkB-212 demonstrates a marked reduction in the expression of this isoform following siRNA treatment (Figure 4.11C).

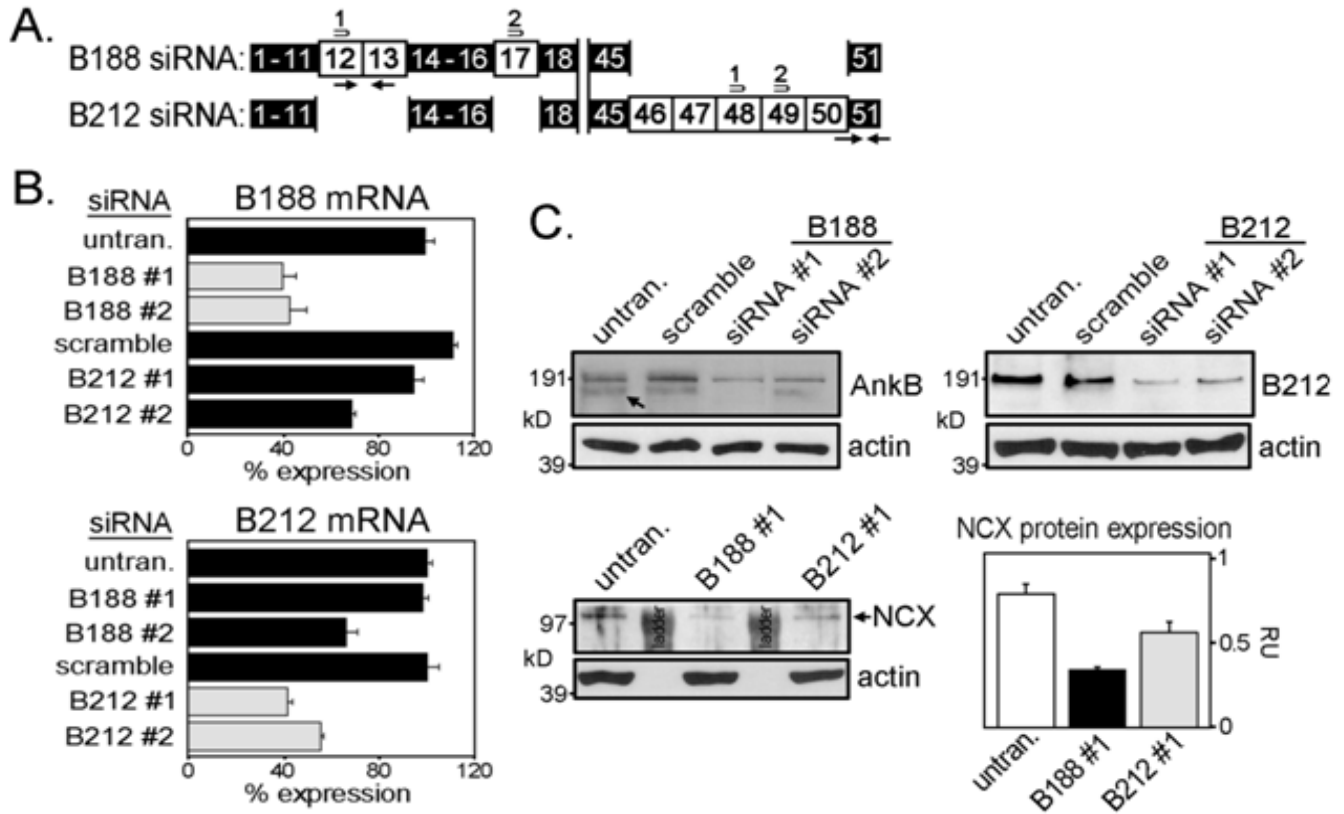
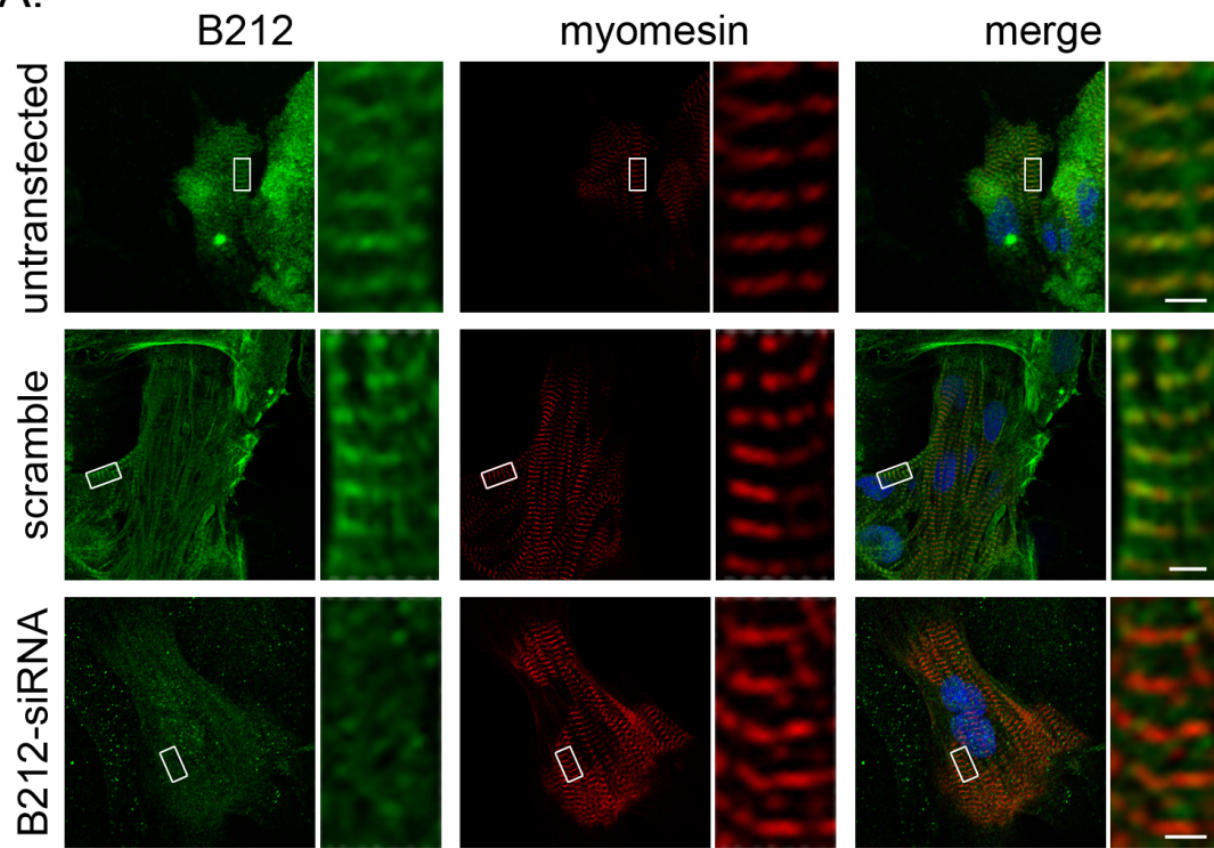


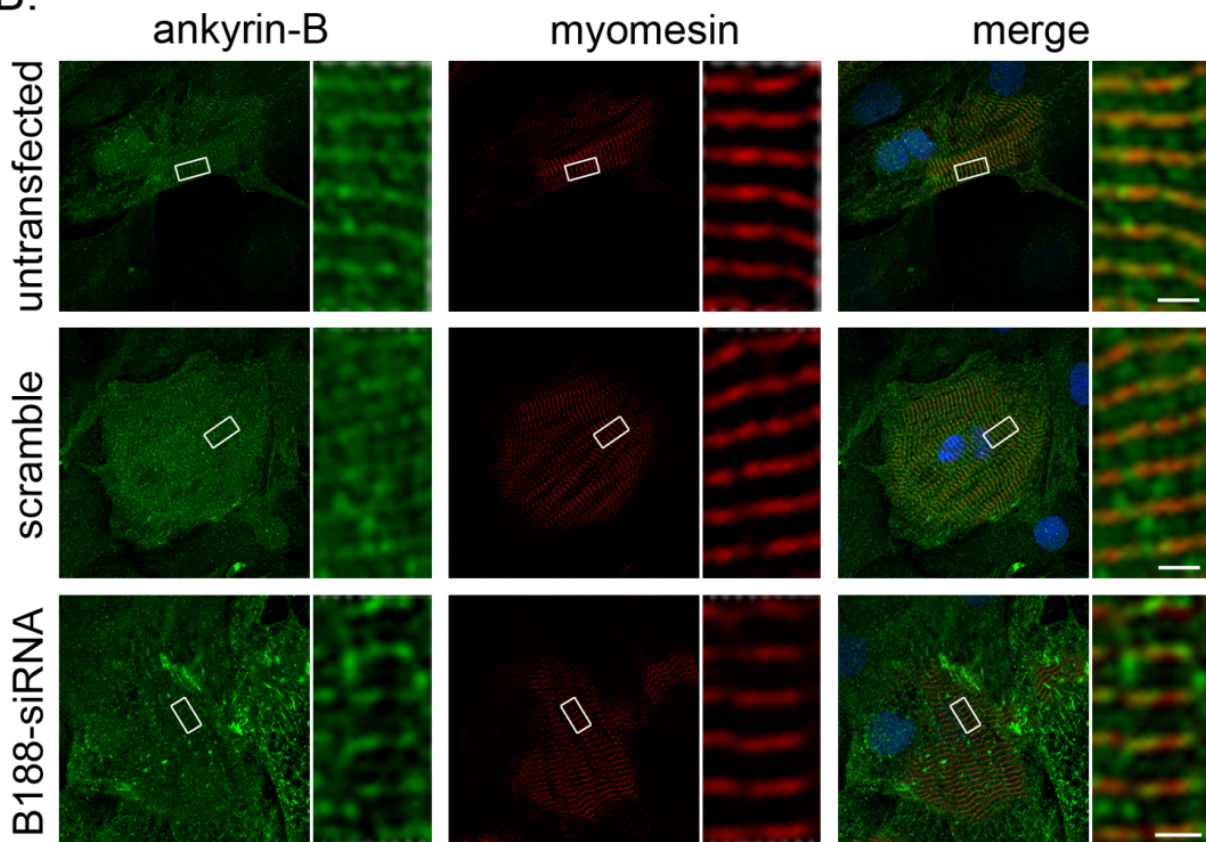
Figure 4.11. AnkB-188 knockdown decreases the expression of NCX. A, Isoform-specific siRNAs were designed to exons unique to AnkB-188 and AnkB-212. B, Knockdown of isoform mRNA was assessed by qt-PCR using primer sets unique to each isoform (black arrows). Qt-PCR values were normalized to GAPDH mRNA expression and expressed as a percentage of isoform expression in untransfected cardiomyocytes, which was set to 100%. Gray bars represent isoform mRNA expression targeted by the siRNAs. Black bars represent mRNA expression of controls and the other isoform. C, Immunoblot analysis of AnkB-188, AnkB-212, and NCX in control and siRNA-treated cardiomyocytes. Pan-actin immunoblot demonstrates equal protein loading.

Previous studies have demonstrated that ankyrin-B is important for the expression and proper subcellular targeting of NCX [2, 4, 133]. Considering AnkB-188 increases NCX membrane expression and current in HeLa-T7 cells (Figure 4.4 B, C, and D), we evaluated siRNA-mediated knockdown of each isoform on the expression and localization of NCX in neonatal rat cardiomyocytes. While NCX protein expression is slightly reduced following AnkB-212 knockdown, AnkB-188 knockdown results in a more significant reduction in NCX protein expression (Figure 4.11C). In untransfected cardiomyocytes, NCX predominantly co-localizes with α -actinin at the Z-line (Figure 4.12D) while two populations of ankyrin-B are detected at the M- and Z-lines (Figure 4.12A and B). AnkB-212 knockdown dramatically reduces ankyrin-B expression in cardiomyocytes, but interestingly NCX maintains its striated patterning over the Z-lines (Figure 4.12A and D). In contrast, the Z-line striated patterning of NCX is markedly reduced in cardiomyocytes following AnkB-188 knockdown (Figure 4.12C and D) suggesting that this isoform is important for NCX subcellular localization in cardiomyocytes.

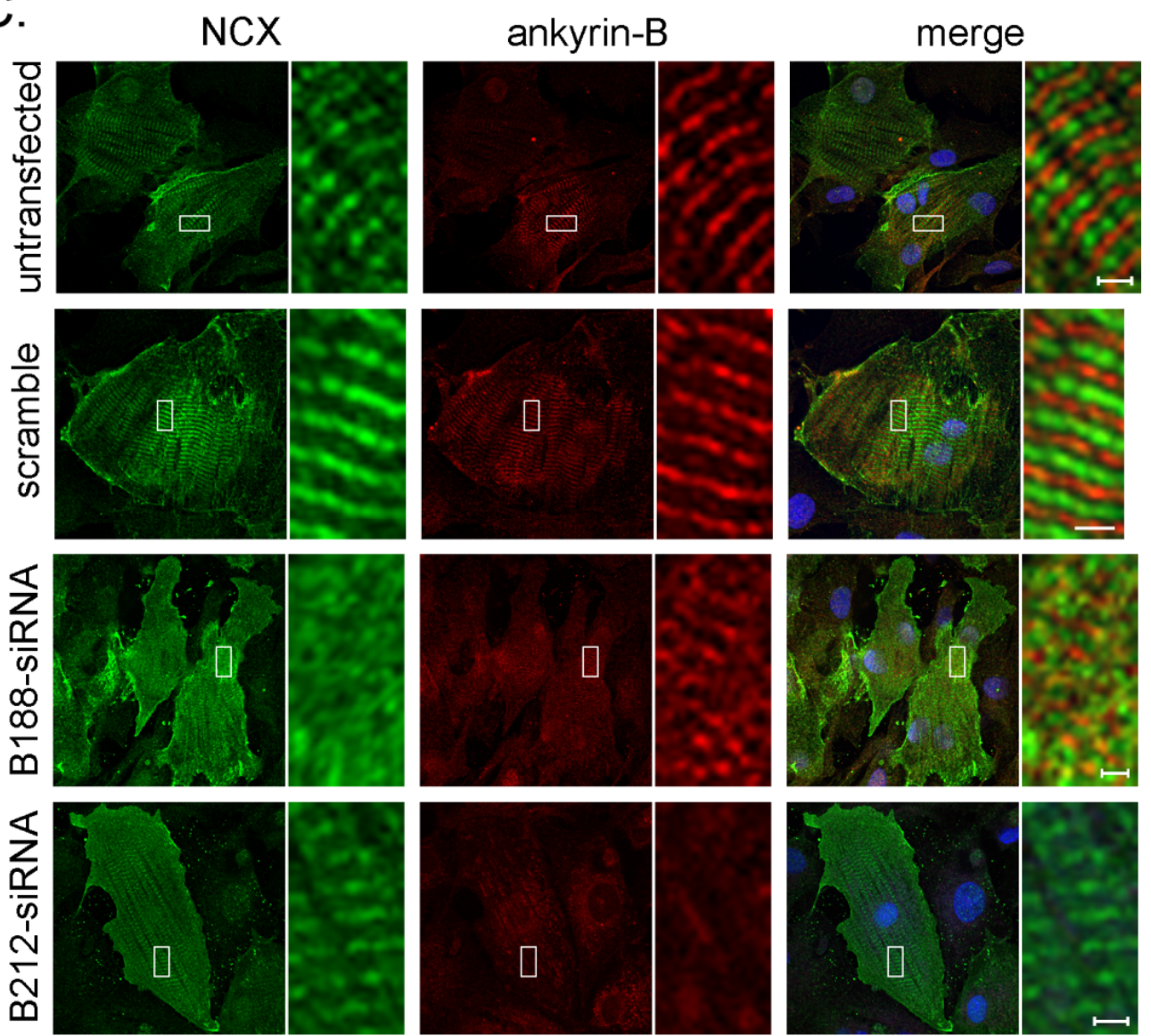
A.



B.



C.



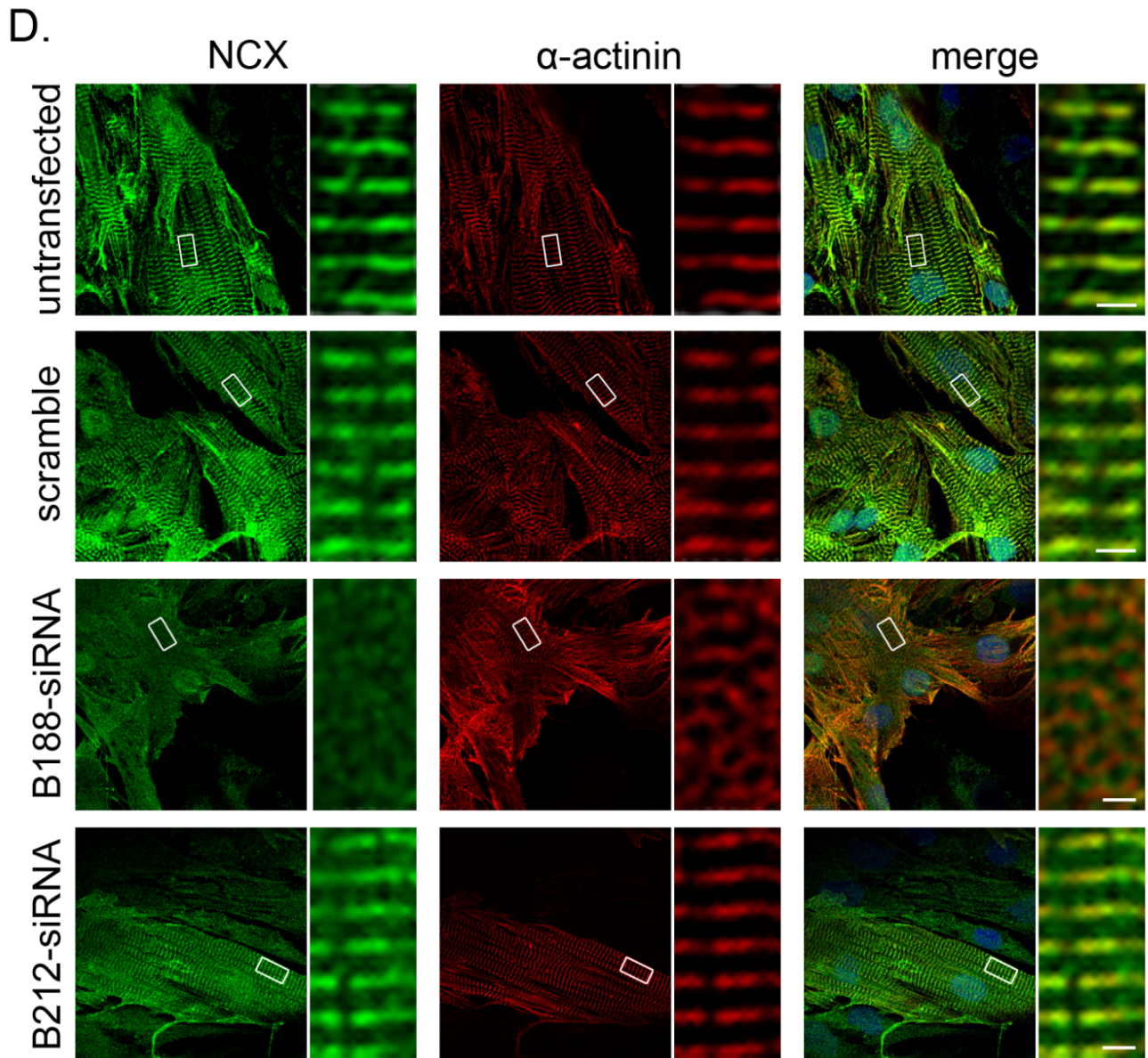


Figure 4.12. AnkB-188 knockdown decreases NCX Z-line localization. A, Endogenous AnkB-212 co-localizes with the M-line marker myomesin. AnkB-212 siRNA treatment reduces AnkB-212 expression at the M-line. B, Both the M-line and Z-line populations of ankyrin-B are visualized in the untransfected and scramble controls. AnkB-188 siRNA treatment diminishes the AnkB subpopulation at the Z-line. C, NCX localization is diminished by AnkB-188 siRNA. (D) NCX expression at the Z-line (α -actinin) is not affected by either scramble or AnkB-212 siRNA treatment. In contrast, AnkB-188 siRNA treatment dramatically reduces the expression and striated patterning of NCX.

4.3.8 AnkB-188 and AnkB-212 knockdown causes different arrhythmic contraction patterns

Ankyrin-B haploinsufficiency results in decreased NCX membrane expression, altered calcium dynamics, and decreased contractions in ventricular cardiomyocytes [3, 4, 133]. Considering the numerous cardiac arrhythmias associated with ankyrin-B dysfunction, we evaluated the effect of isoform-specific knockdown on cardiomyocyte contractile rhythms. Both untransfected and scramble siRNA-treated cardiomyocytes display a pattern of uniformly timed contractions (Figure 4.13A). In contrast, cardiomyocytes with knockdown of AnkB-188 display patterns of arrhythmic contractions. Surprisingly, cardiomyocytes with knockdown of AnkB-212, which has no effect on NCX membrane expression or localization, also exhibits patterns of arrhythmic contractions (Figure 4.13A). The same patterns are observed following epinephrine treatment (Figure 4.13B).

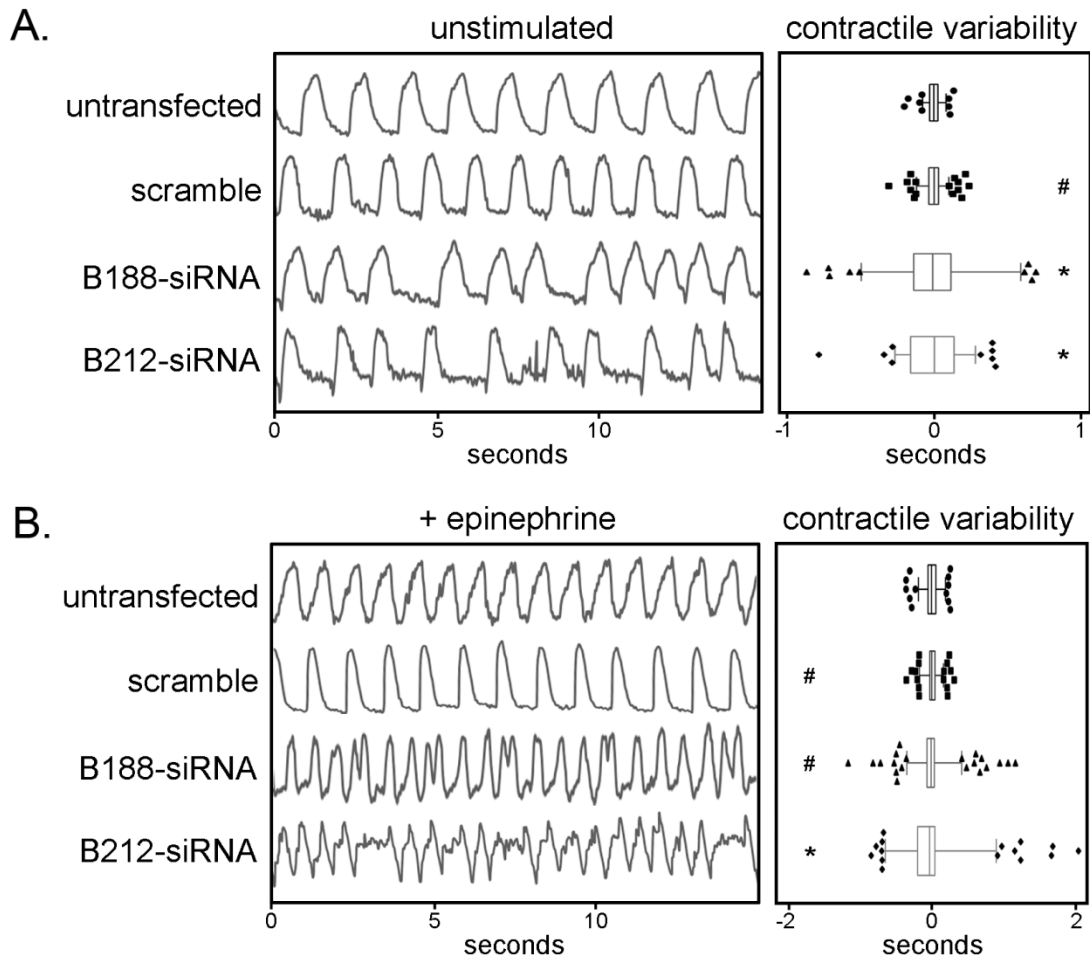


Figure 4.13. AnkB-188 and AnkB-212 knockdown precipitates different contraction irregularities. A, The left panel presents representative contraction rhythms of untransfected and transfected cardiomyocytes. The right panel presents the summary data. Box-and-whisker plots represent the difference in time between individual contractions and the average contraction time over a 30-second interval. B, The left panel presents representative contraction rhythms in control and transfected (scramble, B188-siRNA, B212-siRNA) cardiomyocytes following epinephrine stimulation (1 μ M). The right panel presents the summary data for each condition. Box-and-whisker plots represent the difference in time between individual contractions and the average contraction time over a 30-second interval. Sample size for unstimulated NRVM is untransfected: 6, scramble: 7, B188-siRNA: 7, and B212-siRNA: 5. Sample size for NRVM stimulated with epinephrine is untransfected: 5, scramble: 5, B188-siRNA: 7, B212-siRNA: 5. # $p > 0.05$ and * $p < 0.05$ when compared to the untransfected control.

4.4 Discussion

Normal heart function requires the proper functioning of proteins at unique membrane and sarcomeric domains in cardiomyocytes such as the costamere, intercalated disc, and T-tubules. As an adaptor protein, ankyrin targets and maintains distinctive networks of membrane and signaling proteins at these domains by tethering them to the underlying cytoskeletal network. The alternative splicing of an ankyrin gene regulates the modular nature of ankyrin isoforms such that they can serve as a common interface between β -spectrin and unique cohorts of proteins that define functionally distinct subcellular domains.

In earlier studies that initially described ankyrin genes, there were many references to alternative isoforms. Some of these isoforms displayed tissue specific expression, while other isoforms demonstrated unique subcellular distribution. For example, while ankyrin-G expression is relatively ubiquitous throughout tissues, a brain-specific isoform is targeted to the neuronal axon initial segment by a ~6000 bp exon [137, 138]. Likewise, an alternative start site in the ankyrin-R gene gives rise to a truncated muscle-specific isoform with a novel transmembrane domain that sequesters it to the membrane of the sarcoplasmic reticulum [262, 269, 270].

In the initial characterization of the ankyrin-B gene, two isoforms (440kD and 220kD) were detected in the brain [146, 147]. The cDNA for the 220kD isoform was synthesized by combining seven partial, but overlapping cDNA clones that were identified in an expression library screen [147]. The only difference between these cDNAs is that a ~6000 bp exon is included in the cDNA of the brain-specific 440kD

isoform. With time, it became tacitly assumed that the 220kD isoform represented the predominant isoform expressed in other tissues.

This study is the first to describe two novel ankyrin-B isoforms identified by long-range PCR of reverse transcribed mRNA isolated from human ventricular tissue. We demonstrate the expression of mRNA and protein of these isoforms in human, rat, and mouse hearts. In addition, we can discriminate between the two isoforms based on their function and subcellular distribution in cardiomyocytes. Specifically, over-expression of AnkB-188 in HeLa-T7 cells increases NCX membrane expression and current, while siRNA-mediated knockdown of this isoform decreases NCX expression and subcellular localization at Z-lines in neonatal cardiomyocytes. Using an isoform-specific antibody, we demonstrate that expression of AnkB-212 is restricted to striated muscle and distinctly expressed at the M-line in cardiomyocytes. Moreover, the M-line targeting of AnkB-212 is regulated by its interaction with the large scaffolding protein obscurin. In contrast to AnkB-188, the preferential knockdown of AnkB-212 in neonatal cardiomyocytes does not alter the Z-line striated patterning of NCX. Interestingly, knockdown of either isoform results in arrhythmic contractions. The function of AnkB-212 at the M-line and whether these isoforms share areas of functional overlap remain unanswered questions but are important lines of inquiry for future experiments. The summary of the experiments and results is shown below (Table 4.3).

Experiments	Ankyrin-B 188	Ankyrin-B 212
mRNA Expression	atria and ventricles	atria and ventricles
Immunoblot and Immunofluorescence	Indiscernible	one isoform, M-line expression
Obscurin Binding	No	Yes
NCX Binding	Yes	Yes
NCX Membrane Expression	Increases	No effect
NCX Expression in Cardiomyocytes	Dramatic reduction	Slight reduction
NCX Localization in Cardiomyocytes	Decreased SR/T-tubule localization	No effect

Table 4.3. Summary of the experiments and findings. The last two rows are experiments involving the use of isoform specific siRNA.

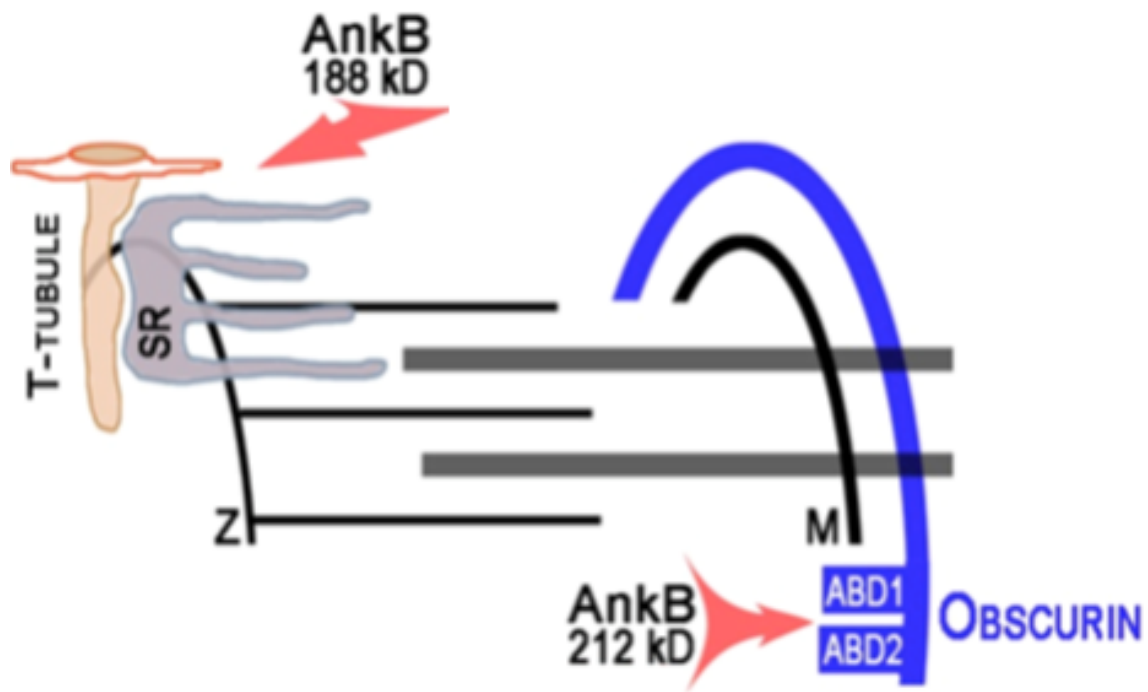


Figure 4.14. Summary model of the subcellular domain localizations of the two full-length ankyrin-B isoforms. AnkB-188 localizes to the transverse tubule with NCX. AnkB-212 localizes to the sarcomeric M-line by interacting with ankyrin-binding domains (ABD) of obscurin.

One unresolved question in the ankyrin field is what regulates ankyrin specificity for particular membrane proteins. Ankyrin-B 220kD has been shown to interact with a diverse array of proteins including the sodium calcium exchanger (NCX), sodium potassium ATPase (NKA), inositol 1,4,5-triphosphate receptor (IP₃R), ATP-sensitive inward-rectifying potassium channel subunit (Kir6.2), dystrophin, and obscurin [2, 133, 136, 264, 265, 271-273]. Our data supports the hypothesis that alternative splicing tailors ankyrin proteins such that they are specific for particular membrane or scaffolding proteins. We anticipate that the heart expresses additional ankyrin-B isoforms that have yet to be identified.

The expression of different function-specific ankyrin-B isoforms in heart would provide a fitting explanation for the diversity of arrhythmias associated with ankyrin-B dysfunction. In fact, the designation of ankyrin-B syndrome has been adopted to incorporate the various arrhythmias associated with ankyrin-B dysfunction, which partially include bradycardia, idiopathic ventricular fibrillation, catecholaminergic polymorphic ventricular tachycardia, and atrial fibrillation [3-5, 229]. Past efforts to understand the molecular basis of dysfunction stemming from these mutations have been performed in the context of ankyrin-B 220kD. While these studies have provided insight into ankyrin-B function, it is important to re-evaluate ankyrin-B syndrome in the context of the newly identified ankyrin-B isoforms. For example, previous studies have

demonstrated that the arrhythmia-associated AnkB missense mutation E1425G decreases NCX membrane expression in ventricular cardiomyocytes. Our data demonstrates that NCX membrane expression is regulated by AnkB-188, which lacks exon 38 and would not express the E1425G missense mutation. We anticipate future experiments characterizing these isoforms will provide a more complete picture of ankyrin-B function in normal hearts and how missense mutations in different ankyrin-B isoforms result in various atrial, nodal, and ventricular arrhythmias.

CHAPTER 5: CONCLUDING CHAPTER

5.1 Summary of results and perspectives

On the surface, it may appear that the heart simply beats. In reality, it is an extremely dynamic organ subjected to complex signaling and metabolic regulations. In establishing and maintaining a normal beat-to-beat rhythm in response to various stressors, the heart remodels functionally, electrically, and metabolically. Central to all these changes is the immediate and prolonged intracellular signaling modifications: the mammalian/mechanistic target of rapamycin.

Like the heart, another organ subjected to such complex signaling and metabolic regulation is the brain. Although the brain does not perform mechanical work, its main function is to communicate via excitation and conduction. Instead of beat-to-beat contractions, the brain utilizes and dedicates most of its energy to the active transport of ions to restore membrane potentials for its unceasing activities [274]. However, when the normal excitation-conduction becomes dysregulated, the abnormal neuronal firings manifests physically as seizures. A classic seizure disorder is the neurodevelopmental disease tuberous sclerosis complex where up to 95% of the patients exhibit medically refractory epilepsy [275, 276].

A well-characterized brain-specific mouse model of TSC, the $Tsc2^{lox/ko};hGFAP-Cre$ [98], exhibits intractable seizures that result in death at around weaning age (median survival at postnatal day 23). Additionally, many aspects of the TSC neuropathology were recapitulated including defects in neuronal migration, cortical lamination, subcortical organization, myelination, and maturation [98, 99]. Interestingly, the seizure disorder and the histologic pathologies observed in this mouse model were alleviated

with the treatment of rapamycin, an allosteric inhibitor of mTORC1 [277, 278]. Furthermore, as long as the animal is maintained on a regular treatment with rapamycin, no seizure activity is observed. This is in stark contrast to the cessation of rapamycin treatment where 100% of the animals have seizures that result in death. Taken altogether, this suggests the high degree of mTORC1 involvement in maintaining the ionic homeostasis of the neurons and its role in general seizure disorders.

Unlike the brain where abnormal electrical activities result in seizures, the abnormal electrical activities in the heart - whose primary function is to beat regularly – is manifested as arrhythmia, or irregular contractions. Whereas there is a readily available genetic model of brain-specific dysregulated mTORC1, no such model yet exists for the heart. Instead, it was discovered that increased hemodynamic load by constricting the transverse or the descending abdominal aorta can trigger increased mTORC1 activity in addition to other cellular growth pathways such as the MAP-kinase and angiotensin pathways in the heart [16, 75, 192, 193, 279]. Prolonged exposure to hemodynamic stress in the animals results in abnormal electrical activities in the heart at baseline that appears to have slowed conduction – increased P-wave duration and PR interval as measured by electrocardiogram. The labile electrical nature of the stressed heart is made evident when frank ventricular fibrillation can easily be induced by fast external pacing [75].

In the preceding chapters I demonstrated changes in electrical conductance in the heart in as early as 1-week of aortic constriction. But the heart, being a dynamic organ, remodels itself continuously such that the electrical changes observed acutely are different from the chronically stressed heart. As expected, overactivity of mTORC1 in

the stressed heart is abated by rapamycin administration that also attenuates the hypertrophic and fibrotic (structural), functional, and metabolic remodeling secondary to pressure overload [190, 192, 193].

Like the neurons, the heart must repolarize after every depolarization in order to initiate the next depolarization wave. The time between depolarization and repolarization is termed Q-T interval. Calcium removal processes are paramount during the repolarization period, and the two major players involved are the sarco/endoplasmic reticulum calcium ATPase (SERCA2a) and sodium-calcium exchanger (NCX1). SERCA2a is responsible for sequestering approximately 90% of the cytosolic calcium ions and NCX1 contributes around 7% in small animals and 70% and 25% in humans, respectively [280]. SERCA2a expression decreases in the stressed heart but is normalized with rapamycin treatment [23, 192, 219, 281]. In contrast, NCX1 expression is increased in the stressed heart and rapamycin does not alter its expression, surface localization, or transporter activity [221, 237]. Contrary to the expected, NCX1 current is decreased in the stressed heart despite the increased expression and surface localization [221]. The heart may adapt to the decreased NCX1 activity by reducing L-type calcium current and shortening action potential to further limit calcium similar to the NCX knockout mouse model [282-284]. This may in part explain our finding that despite the regression of structural, functional, metabolic, and most of the electrical changes in the hemodynamically stressed heart with mTORC1 inhibition, the Q-T interval remains shortened and seems unresponsive to rapamycin treatment.

Even though NCX1 seemingly only contributes to a small percentage of the calcium removal process during repolarization, it has a profound impact on the

maintenance of a normal cardiac rhythm. In animal models where NCX1 stability is affected by a loss-of-function mutation in the adaptor protein ankyrin-B, the main targeting and interacting partner of NCX1 in the heart, high degree of heart rate variability, rhythm variability, and lethal arrhythmias with adrenergic stimulation have been reported. At the cellular level, calcium transients are irregular and both slow and fast pacing induced unsolicited action potentials [2, 4, 5, 133]. Thus, when we interrogate ankyrin-B expression in the stressed heart, we observe a change in ankyrin-B expression that could account for the decreased NCX1 current despite the increased NCX1 expression and secondarily lead to arrhythmias. Similar findings are found in our *in vitro* system when we genetically activated mTORC1 by knocking down Tsc2. This also marks the first study where the adaptor protein ankyrin-B is shown to be regulated by the mTORC1 pathway.

Although ankyrin-B expression was altered with dysregulated mTORC1 activity both *in vivo* by hemodynamic stress and *in vitro* by genetic ablation, it should be noted that ankyrin-B expression was reduced ubiquitously in the stressed heart whereas the mTORC1-specific activation *in vitro* saw a reduction in expression at the cardiac M-line and a dramatic upregulation at the SR/T-tubule, the subcellular domain where NCX1 resides. The discrepancy between the *in vivo* and *in vitro* systems brings up several interesting issues: 1.) what other cell signaling pathway(s) is/are able to regulate ankyrin-B expression, 2.) what mechanism is responsible for the degradation of ankyrin-B at the M-line secondary to mTORC1 activity, and 3.) what specific regulatory mechanisms govern which ankyrin-B isoform expression.

Increased mTORC1 activity generally increases protein synthesis, but the reduction of protein expressions has also been observed. For example, SERCA2a and α -myosin heavy chain both have documented reduced expressions in the hemodynamically stressed heart that are reversible with rapamycin, but the reductions are at least in part associated with transcriptional changes [23, 192, 219, 281]. On the other hand, ankyrin-B mRNA transcript level remains the same in the stressed heart suggesting that mTORC1-regulation of ankyrin-B (at least the M-line population) is a post-translational event. It was reported recently that chronic mTORC1 activation leads to endoplasmic reticulum stress in the heart [190], and given the relationship between endoplasmic reticulum stress and mechanisms of autophagy, it is possible that ankyrin-B is degraded via autophagic processes [285, 286]. In addition to autophagy, it is also possible that the calpain system contributes to the ankyrin-B degradation [216] although the specificity for the M-line versus the SR/T-tubule population remains to be elucidated.

In the preceding chapters, we present compelling evidence for the existence of multiple ankyrin-B isoforms and the different subcellular localizations of two full-length ankyrin-B isoforms – AnkB-188 and AnkB-212. Given that AnkB-188 interacts with the SR/T-tubule resident protein NCX1 and that knockdown of AnkB-188 decreases NCX1 expression, AnkB-188 likely accounts for the changes in NCX1 function in the stressed heart although this is yet to be determined because of the absence of transcriptional changes and the lack of an AnkB-188-specific antibody. What is more surprising to us is that ankyrin-B population at the M-line, of which AnkB-212 is a part of, is important, and perhaps even more so than AnkB-188, for maintaining regular cardiac rhythm. In both the *in vitro* models where either Tsc2 or AnkB-212 is targeted

by siRNA knockdown, the expression of the ankyrin-B population at the SR/T-tubule either increases or remains the same. However, both demonstrate a dramatic decrease in ankyrin-B expression at the cardiac M-line and significant irregular contraction patterns. Although AnkB-212 interacts with the M-line organizer obscurin, the molecular function(s) of AnkB-212 remains to be determined and represents an interesting and imperative direction for future investigation of the mechanisms of cardiac hypertrophic changes and arrhythmias. Finally, there are many other ankyrin-B isoforms that have yet to be identified and characterized. It will be interesting to see how each functions and contributes to maintenance of normal cardiac rhythm.

While this thesis explores the relationship between mTORC1 signaling, ankyrins, and electrical properties of the heart, it brings forth another interesting area for further investigation: seizure disorders associated with TSC. In the nervous system, multiple isoforms of all three ankyrin genes have been identified and characterized and their proper localization and function are critical to the formation and maintenance of excitable subcellular domains in neurons. It was recently identified that seizure activities affects the expressions of the adaptor protein ankyrin-G at the axon initial segment, the site where information is integrated and the action potential is generated, and its interacting partner voltage-gated sodium channel (Nav 1.6) [128]. We showed that dysregulated mTORC1 causes electrical remodeling in the heart and that the M-line ankyrin-B population expression is subjected to regulation by mTORC1. The *Tsc2^{fllox/ko};hGFAP-Cre* has a pronounced dysregulated mTORC1 activity, cortical disorganization, and severe myelination defect in addition to a lethal tonic-clonic seizure phenotype. It will be intriguing to see how the expression and localization of different

ankyrin proteins are affected in *Tsc2^{lox/ko};hGFAP-Cre* mice (Tsc2-hGFAP) which may potentially shed light on the mechanistic relationship between cell signaling and aberrant electrical activities in the central nervous system of the TSC patients.

While there are still many questions and interesting areas of investigation, it is evident that mTORC1 activity is at least in part responsible for structural, functional, metabolic, and electrical remodeling processes in the heart and that proper ankyrin function and localizations are central for maintaining the normal electrical properties of the heart. This thesis provides evidence that supports the idea that mTORC1 regulation of ankyrin-B serves as the link between the hypertrophic response and arrhythmogenesis in the stressed heart. The results I present in this thesis have wide-ranging implications for heart diseases and central nervous system disorders, and uncovering the relationship between mTORC1 activity and ankyrin regulation could potentially lead to novel therapeutics.

5.2 Future experiments

There remain many questions to be addressed. First, how is the trafficking of AnkB-188 handled and how does NCX1 get transported to the SR/T-tubule to be anchored by AnkB-188? A related question is what are the interacting partners of AnkB-212 such that its knockdown mediates arrhythmias? Second, what mechanism directs mTORC1 downregulation/upregulation of ankyrin-B expression in the heart? Third, how do the expressions of different ankyrin proteins change in the *Tsc2*-deficient neurons and do different ankyrin proteins play a role in the neuropathology of TSC?

The first two inquiries can be addressed by exogenously expressing GFP-tagged full-length AnkB-188 and RFP-tagged NCX in the neonatal rat ventricular cardiomyocytes starting immediately after isolation. The timepoint is important as the sarcomeric structures are disturbed during the isolation procedure and will start to re-organize right after plating. At this time, we can perform live cell imaging on the transfected NRVMs to monitor trafficking of AnkB-188 and NCX to the developing transverse tubules. The results of this study will differentiate whether AnkB-188 interacts with NCX first and then is co-transported to the SR/T-tubule. Alternatively, separate intracellular transport machinery may exist for both AnkB-188 and NCX1 and they may subsequently interact at the SR/T-tubule. Also, rate of protein turnover must be balanced by the rate of protein synthesis. Previously NCX half-life has been determined to be around 27.2 hours in wild type cardiomyocytes [133], so future experiments should determine mechanisms of transport and retention at the SR/T-tubule for both AnkB-188 and NCX1. Similarly, to address the molecular transport of AnkB-212, we will use GFP-tagged AnkB-212 and assess its transport from the Golgi network to the M-line where it interacts with the M-line organizer protein obscurin.

Separately, to identify the unique interacting partners of each isoform, we will precipitate macromolecular complexes associated with each of the two ankyrin-B isoforms for mass spectrometry analysis. One of the most interesting and challenging questions from our study in Chapter 4 is identifying the mechanism(s) responsible for the abnormal contractions rhythms of the cardiomyocytes with decreased levels of AnkB-212. We may begin addressing this question by identifying the interacting partners of AnkB-212.

Although it has previously been demonstrated that calpain may be a mechanism for ankyrin-B degradation in the heart [216], given our findings with decreased ankyrin-B expression at the M-line following induced mTORC1 activation, we cannot discount the fact that prolonged mTORC1 activation may induce autophagy from imbalance between protein synthesis and degradation [285]. To address this issue, we will investigate the role of autophagy in ankyrin-B regulation by inhibiting autophagy with bafilomycin or chloroquine in models of mTORC1 overactivity. If inhibition of autophagy restores ankyrin-B expression at the M-line, it would highly suggest mTORC1 regulates ankyrin-B expression at the M-line by increasing autophagic flux. Alternatively, another key degradation pathway in the heart is the ubiquitin-proteasome pathway [228].

Finally, virtually nothing is known regarding mTORC1-mediated regulation of ankyrin proteins in the central nervous system. Fortunately, there is a well-characterized TSC mouse model with overactive mTORC1 [98, 99]. Preliminary experiment will assess expression of all three different ankyrin proteins, voltage-gated sodium and potassium channels (known interacting partners of ankyrin-G) in brain lysates of the Tsc2-hGFAP at embryonic day 15.5 (3 days after genetic mTORC1 activation), at birth, and at postnatal day 21 (weaning age when the mice are nearing 50% mortality). The results will be compared side-by-side with the mice treated with the combined rapamycin protocol.

Ankyrin proteins, especially ankyrin-G, have been shown to be important for establishing axo-dendritic polarity and axon initial segment (AIS) [287, 288]. Tsc2-hGFAP mice have increased dendritic sprouting, neuronal migration and cortical

lamination defects. Therefore, another experiment will assess the establishment of neuronal polarity from the neurite stage, dendritic arborization, axon initial segment (AIS), and nodes of Ranvier formations in primary cortical neurons from Tsc2-hGFAP mice by immunocytochemistry at different timepoints. It will be important to note the clustering of the ankyrin proteins such as ankyrin-G at the AIS and nodes of Ranvier and ankyrin-B clustering at the developing axon and at the dendrites as migration and cortical lamination defects may be secondary to a loss or delayed axo-dendritic specification.

Lastly, since all Tsc2-hGFAP mice exhibit seizures and if mTORC1-mediated dysregulated ankyrin protein expression mediates abnormal action potential conductance, the necessary experiments are 1.) exogenously express the decreased or knockdown the increased ankyrin in the Tsc2-hGFAP primary neurons, 2.) re-assess the expression and localization of the respective interacting partners such as voltage-gated ion channels at the appropriate subcellular domains by immunocytochemistry, and 3.) record the intrinsic electrical activities in the neurons and assess the synaptic strength. Coupling these findings with mTORC1 inhibition with rapamycin or torin1 (a potent *in vitro* mTOR inhibitor) will establish mTORC1-mediated ankyrin expression/localization changes as a mechanism for the abnormal electrical activities and neuropathologies in TSC.

References

1. Cunha, S.R., S. Le Scouarnec, J.J. Schott, and P.J. Mohler, *Exon organization and novel alternative splicing of the human ANK2 gene: implications for cardiac function and human cardiac disease*. *J Mol Cell Cardiol*, 2008. **45**(6): p. 724-34.
2. Mohler, P.J., J.Q. Davis, and V. Bennett, *Ankyrin-B coordinates the Na/K ATPase, Na/Ca exchanger, and InsP3 receptor in a cardiac T-tubule/SR microdomain*. *PLoS Biol*, 2005. **3**(12): p. e423.
3. Mohler, P.J., S. Le Scouarnec, I. Denjoy, J.S. Lowe, P. Guicheney, L. Caron, I.M. Driskell, J.J. Schott, K. Norris, A. Leenhardt, R.B. Kim, D. Escande, and D.M. Roden, *Defining the cellular phenotype of "ankyrin-B syndrome" variants: human ANK2 variants associated with clinical phenotypes display a spectrum of activities in cardiomyocytes*. *Circulation*, 2007. **115**(4): p. 432-41.
4. Mohler, P.J., J.J. Schott, A.O. Gramolini, K.W. Dilly, S. Guatimosim, W.H. duBell, L.S. Song, K. Haurogne, F. Kyndt, M.E. Ali, T.B. Rogers, W.J. Lederer, D. Escande, H. Le Marec, and V. Bennett, *Ankyrin-B mutation causes type 4 long-QT cardiac arrhythmia and sudden cardiac death*. *Nature*, 2003. **421**(6923): p. 634-9.
5. Mohler, P.J., I. Splawski, C. Napolitano, G. Bottelli, L. Sharpe, K. Timothy, S.G. Priori, M.T. Keating, and V. Bennett, *A cardiac arrhythmia syndrome caused by loss of ankyrin-B function*. *Proc Natl Acad Sci U S A*, 2004. **101**(24): p. 9137-42.
6. Smith, S.A., A.C. Sturm, J. Curran, C.F. Kline, S.C. Little, I.M. Bonilla, V.P. Long, M. Makara, I. Polina, L.D. Hughes, T.R. Webb, Z. Wei, P. Wright, N. Voigt, D. Bhakta, K.G. Spoonamore, C. Zhang, R. Weiss, P.F. Binkley, P.M. Janssen, A. Kilic, R.S. Higgins, M. Sun, J. Ma, D. Dobrev, M. Zhang, C.A. Carnes, M. Vatta, M.N. Rasband, T.J. Hund, and P.J. Mohler, *Dysfunction in the betaII spectrin-dependent cytoskeleton underlies human arrhythmia*. *Circulation*, 2015. **131**(8): p. 695-708.
7. Wagner, G., in *Marriott's Practical Electrocardiography (Wagner) Series*. 2007, Lippincott Williams & Wilkins.
8. Cunha, S.R. and P.J. Mohler, *Cardiac ankyrins: Essential components for development and maintenance of excitable membrane domains in heart*. *Cardiovasc Res*, 2006. **71**(1): p. 22-9.
9. Guertin, D.A. and D.M. Sabatini, *Defining the role of mTOR in cancer*. *Cancer Cell*, 2007. **12**(1): p. 9-22.
10. Go, A.S., D. Mozaffarian, V.L. Roger, E.J. Benjamin, J.D. Berry, M.J. Blaha, S. Dai, E.S. Ford, C.S. Fox, S. Franco, H.J. Fullerton, C. Gillespie, S.M. Hailpern, J.A. Heit, V.J. Howard, M.D. Huffman, S.E. Judd, B.M. Kissela, S.J. Kittner, D.T. Lackland, J.H. Lichtman, L.D. Lisabeth, R.H. Mackey, D.J. Magid, G.M. Marcus, A. Marelli, D.B. Matchar, D.K. McGuire, E.R. Mohler, 3rd, C.S. Moy, M.E. Mussolino, R.W. Neumar, G. Nichol, D.K. Pandey, N.P. Paynter, M.J. Reeves, P.D. Sorlie, J. Stein, A. Towfighi, T.N. Turan, S.S. Virani, N.D. Wong, D. Woo, M.B. Turner, C. American Heart Association Statistics, and S. Stroke Statistics, *Heart disease and stroke statistics--2014 update: a report from the American Heart Association*. *Circulation*, 2014. **129**(3): p. e28-e292.

11. Ghali, J.K., S. Kadakia, R.S. Cooper, and Y.L. Liao, *Impact of left ventricular hypertrophy on ventricular arrhythmias in the absence of coronary artery disease*. J Am Coll Cardiol, 1991. **17**(6): p. 1277-82.
12. Levy, D., K.M. Anderson, D.D. Savage, S.A. Balkus, W.B. Kannel, and W.P. Castelli, *Risk of ventricular arrhythmias in left ventricular hypertrophy: the Framingham Heart Study*. Am J Cardiol, 1987. **60**(7): p. 560-5.
13. Wolk, R., *Arrhythmogenic mechanisms in left ventricular hypertrophy*. Europace, 2000. **2**(3): p. 216-23.
14. Mozaffarian, D., E.J. Benjamin, A.S. Go, D.K. Arnett, M.J. Blaha, M. Cushman, S. de Ferranti, J.P. Despres, H.J. Fullerton, V.J. Howard, M.D. Huffman, S.E. Judd, B.M. Kissela, D.T. Lackland, J.H. Lichtman, L.D. Lisabeth, S. Liu, R.H. Mackey, D.B. Matchar, D.K. McGuire, E.R. Mohler, 3rd, C.S. Moy, P. Muntner, M.E. Mussolino, K. Nasir, R.W. Neumar, G. Nichol, L. Palaniappan, D.K. Pandey, M.J. Reeves, C.J. Rodriguez, P.D. Sorlie, J. Stein, A. Towfighi, T.N. Turan, S.S. Virani, J.Z. Willey, D. Woo, R.W. Yeh, M.B. Turner, C. American Heart Association Statistics, and S. Stroke Statistics, *Heart disease and stroke statistics--2015 update: a report from the American Heart Association*. Circulation, 2015. **131**(4): p. e29-322.
15. Yancy, C.W., M. Jessup, B. Bozkurt, J. Butler, D.E. Casey, Jr., M.H. Drazner, G.C. Fonarow, S.A. Geraci, T. Horwich, J.L. Januzzi, M.R. Johnson, E.K. Kasper, W.C. Levy, F.A. Masoudi, P.E. McBride, J.J. McMurray, J.E. Mitchell, P.N. Peterson, B. Riegel, F. Sam, L.W. Stevenson, W.H. Tang, E.J. Tsai, and B.L. Wilkoff, *2013 ACCF/AHA guideline for the management of heart failure: executive summary: a report of the American College of Cardiology Foundation/American Heart Association Task Force on practice guidelines*. Circulation, 2013. **128**(16): p. 1810-52.
16. Hill, J.A. and E.N. Olson, *Cardiac plasticity*. N Engl J Med, 2008. **358**(13): p. 1370-80.
17. Asakura, M. and M. Kitakaze, *Global gene expression profiling in the failing myocardium*. Circ J, 2009. **73**(9): p. 1568-76.
18. Steenman, M., Y.W. Chen, M. Le Cunff, G. Lamirault, A. Varro, E. Hoffman, and J.J. Leger, *Transcriptomal analysis of failing and nonfailing human hearts*. Physiol Genomics, 2003. **12**(2): p. 97-112.
19. Mann, D.L., *Mechanisms and models in heart failure: A combinatorial approach*. Circulation, 1999. **100**(9): p. 999-1008.
20. Sandler, H. and H.T. Dodge, *Left Ventricular Tension and Stress in Man*. Circ Res, 1963. **13**: p. 91-104.
21. Gao, X., Y. Zhang, P. Arrazola, O. Hino, T. Kobayashi, R.S. Yeung, B. Ru, and D. Pan, *Tsc tumour suppressor proteins antagonize amino-acid-TOR signalling*. Nat Cell Biol, 2002. **4**(9): p. 699-704.
22. Smith, E.M., S.G. Finn, A.R. Tee, G.J. Browne, and C.G. Proud, *The tuberous sclerosis protein TSC2 is not required for the regulation of the mammalian target of rapamycin by amino acids and certain cellular stresses*. J Biol Chem, 2005. **280**(19): p. 18717-27.

23. Ikeda, Y., K. Sato, D.R. Pimentel, F. Sam, R.J. Shaw, J.R. Dyck, and K. Walsh, *Cardiac-specific deletion of LKB1 leads to hypertrophy and dysfunction*. J Biol Chem, 2009. **284**(51): p. 35839-49.
24. Kim, M., R.W. Hunter, L. Garcia-Menendez, G. Gong, Y.Y. Yang, S.C. Kolwicz, Jr., J. Xu, K. Sakamoto, W. Wang, and R. Tian, *Mutation in the gamma2-subunit of AMP-activated protein kinase stimulates cardiomyocyte proliferation and hypertrophy independent of glycogen storage*. Circ Res, 2014. **114**(6): p. 966-75.
25. Dorn, G.W., 2nd, J. Robbins, and P.H. Sugden, *Phenotyping hypertrophy: eschew obfuscation*. Circ Res, 2003. **92**(11): p. 1171-5.
26. Lorell, B.H. and B.A. Carabello, *Left ventricular hypertrophy: pathogenesis, detection, and prognosis*. Circulation, 2000. **102**(4): p. 470-9.
27. Elster, S.K., H. Horn, and L.R. Tuchman, *Cardiac hypertrophy and insufficiency of unknown etiology; a clinical and pathologic study of ten cases*. Am J Med, 1955. **18**(6): p. 900-22.
28. Gunther, S. and W. Grossman, *Determinants of ventricular function in pressure-overload hypertrophy in man*. Circulation, 1979. **59**(4): p. 679-88.
29. Huber, D., J. Grimm, R. Koch, and H.P. Krayenbuehl, *Determinants of ejection performance in aortic stenosis*. Circulation, 1981. **64**(1): p. 126-34.
30. Krayenbuehl, H.P., O.M. Hess, M. Ritter, E.S. Monrad, and H. Hoppeler, *Left ventricular systolic function in aortic stenosis*. Eur Heart J, 1988. **9 Suppl E**: p. 19-23.
31. Hood, W.P., Jr., C.E. Rackley, and E.L. Rolett, *Wall stress in the normal and hypertrophied human left ventricle*. Am J Cardiol, 1968. **22**(4): p. 550-8.
32. Koren, M.J., R.B. Devereux, P.N. Casale, D.D. Savage, and J.H. Laragh, *Relation of left ventricular mass and geometry to morbidity and mortality in uncomplicated essential hypertension*. Ann Intern Med, 1991. **114**(5): p. 345-52.
33. Levy, D., R.J. Garrison, D.D. Savage, W.B. Kannel, and W.P. Castelli, *Prognostic implications of echocardiographically determined left ventricular mass in the Framingham Heart Study*. N Engl J Med, 1990. **322**(22): p. 1561-6.
34. Frank, D., C. Kuhn, B. Brors, C. Hanselmann, M. Ludde, H.A. Katus, and N. Frey, *Gene expression pattern in biomechanically stretched cardiomyocytes: evidence for a stretch-specific gene program*. Hypertension, 2008. **51**(2): p. 309-18.
35. Molkenin, J.D. and G.W. Dorn, 2nd, *Cytoplasmic signaling pathways that regulate cardiac hypertrophy*. Annu Rev Physiol, 2001. **63**: p. 391-426.
36. Zou, Y., H. Akazawa, Y. Qin, M. Sano, H. Takano, T. Minamino, N. Makita, K. Iwanaga, W. Zhu, S. Kudoh, H. Toko, K. Tamura, M. Kihara, T. Nagai, A. Fukamizu, S. Umemura, T. Iiri, T. Fujita, and I. Komuro, *Mechanical stress activates angiotensin II type 1 receptor without the involvement of angiotensin II*. Nat Cell Biol, 2004. **6**(6): p. 499-506.
37. Feldman, A.M., E.O. Weinberg, P.E. Ray, and B.H. Lorell, *Selective changes in cardiac gene expression during compensated hypertrophy and the transition to cardiac decompensation in rats with chronic aortic banding*. Circ Res, 1993. **73**(1): p. 184-92.
38. Hill, J.A., M. Karimi, W. Kutschke, R.L. Davisson, K. Zimmerman, Z. Wang, R.E. Kerber, and R.M. Weiss, *Cardiac hypertrophy is not a required*

- compensatory response to short-term pressure overload.* Circulation, 2000. **101**(24): p. 2863-9.
39. Molkentin, J.D., J.R. Lu, C.L. Antos, B. Markham, J. Richardson, J. Robbins, S.R. Grant, and E.N. Olson, *A calcineurin-dependent transcriptional pathway for cardiac hypertrophy.* Cell, 1998. **93**(2): p. 215-28.
 40. Sussman, M.A., H.W. Lim, N. Gude, T. Taigen, E.N. Olson, J. Robbins, M.C. Colbert, A. Gualberto, D.F. Wiczorek, and J.D. Molkentin, *Prevention of cardiac hypertrophy in mice by calcineurin inhibition.* Science, 1998. **281**(5383): p. 1690-3.
 41. Backs, J., T. Backs, S. Neef, M.M. Kreusser, L.H. Lehmann, D.M. Patrick, C.E. Grueter, X. Qi, J.A. Richardson, J.A. Hill, H.A. Katus, R. Bassel-Duby, L.S. Maier, and E.N. Olson, *The delta isoform of CaM kinase II is required for pathological cardiac hypertrophy and remodeling after pressure overload.* Proc Natl Acad Sci U S A, 2009. **106**(7): p. 2342-7.
 42. Zhang, R., M.S. Khoo, Y. Wu, Y. Yang, C.E. Grueter, G. Ni, E.E. Price, Jr., W. Thiel, S. Guatimosim, L.S. Song, E.C. Madu, A.N. Shah, T.A. Vishnivetskaya, J.B. Atkinson, V.V. Gurevich, G. Salama, W.J. Lederer, R.J. Colbran, and M.E. Anderson, *Calmodulin kinase II inhibition protects against structural heart disease.* Nat Med, 2005. **11**(4): p. 409-17.
 43. Khoo, M.S., J. Li, M.V. Singh, Y. Yang, P. Kannankeril, Y. Wu, C.E. Grueter, X. Guan, C.V. Oddis, R. Zhang, L. Mendes, G. Ni, E.C. Madu, J. Yang, M. Bass, R.J. Gomez, B.E. Wadzinski, E.N. Olson, R.J. Colbran, and M.E. Anderson, *Death, cardiac dysfunction, and arrhythmias are increased by calmodulin kinase II in calcineurin cardiomyopathy.* Circulation, 2006. **114**(13): p. 1352-9.
 44. Kim, E., P. Goraksha-Hicks, L. Li, T.P. Neufeld, and K.L. Guan, *Regulation of TORC1 by Rag GTPases in nutrient response.* Nat Cell Biol, 2008. **10**(8): p. 935-45.
 45. Sancak, Y., L. Bar-Peled, R. Zoncu, A.L. Markhard, S. Nada, and D.M. Sabatini, *Ragulator-Rag complex targets mTORC1 to the lysosomal surface and is necessary for its activation by amino acids.* Cell, 2010. **141**(2): p. 290-303.
 46. Sancak, Y., T.R. Peterson, Y.D. Shaul, R.A. Lindquist, C.C. Thoreen, L. Bar-Peled, and D.M. Sabatini, *The Rag GTPases bind raptor and mediate amino acid signaling to mTORC1.* Science, 2008. **320**(5882): p. 1496-501.
 47. Crespo, J.L. and M.N. Hall, *Elucidating TOR signaling and rapamycin action: lessons from Saccharomyces cerevisiae.* Microbiol Mol Biol Rev, 2002. **66**(4): p. 579-91, table of contents.
 48. Chang, J.Y., S.N. Sehgal, and C.C. Bansbach, *FK506 and rapamycin: novel pharmacological probes of the immune response.* Trends Pharmacol Sci, 1991. **12**(6): p. 218-23.
 49. Garza, L., Y.W. Aude, and J.F. Saucedo, *Can we prevent in-stent restenosis?* Curr Opin Cardiol, 2002. **17**(5): p. 518-25.
 50. Huang, S. and P.J. Houghton, *Targeting mTOR signaling for cancer therapy.* Curr Opin Pharmacol, 2003. **3**(4): p. 371-7.
 51. Bayle, J.H., J.S. Grimley, K. Stankunas, J.E. Gestwicki, T.J. Wandless, and G.R. Crabtree, *Rapamycin analogs with differential binding specificity permit orthogonal control of protein activity.* Chem Biol, 2006. **13**(1): p. 99-107.

52. Shiota, C., J.T. Woo, J. Lindner, K.D. Shelton, and M.A. Magnuson, *Multiallelic disruption of the rictor gene in mice reveals that mTOR complex 2 is essential for fetal growth and viability*. Dev Cell, 2006. **11**(4): p. 583-9.
53. Cardenas, M.E., N.S. Cutler, M.C. Lorenz, C.J. Di Como, and J. Heitman, *The TOR signaling cascade regulates gene expression in response to nutrients*. Genes Dev, 1999. **13**(24): p. 3271-9.
54. Kunz, J., R. Henriquez, U. Schneider, M. Deuter-Reinhard, N.R. Movva, and M.N. Hall, *Target of rapamycin in yeast, TOR2, is an essential phosphatidylinositol kinase homolog required for G1 progression*. Cell, 1993. **73**(3): p. 585-96.
55. Chen, J., X.F. Zheng, E.J. Brown, and S.L. Schreiber, *Identification of an 11-kDa FKBP12-rapamycin-binding domain within the 289-kDa FKBP12-rapamycin-associated protein and characterization of a critical serine residue*. Proc Natl Acad Sci U S A, 1995. **92**(11): p. 4947-51.
56. Sabatini, D.M., H. Erdjument-Bromage, M. Lui, P. Tempst, and S.H. Snyder, *RAFT1: a mammalian protein that binds to FKBP12 in a rapamycin-dependent fashion and is homologous to yeast TORs*. Cell, 1994. **78**(1): p. 35-43.
57. Sarbassov, D.D., S.M. Ali, and D.M. Sabatini, *Growing roles for the mTOR pathway*. Curr Opin Cell Biol, 2005. **17**(6): p. 596-603.
58. Wang, L., C.J. Rhodes, and J.C. Lawrence, Jr., *Activation of mammalian target of rapamycin (mTOR) by insulin is associated with stimulation of 4EBP1 binding to dimeric mTOR complex 1*. J Biol Chem, 2006. **281**(34): p. 24293-303.
59. Holz, M.K., B.A. Ballif, S.P. Gygi, and J. Blenis, *mTOR and S6K1 mediate assembly of the translation preinitiation complex through dynamic protein interchange and ordered phosphorylation events*. Cell, 2005. **123**(4): p. 569-80.
60. Raught, B., F. Peiretti, A.C. Gingras, M. Livingstone, D. Shahbazian, G.L. Mayeur, R.D. Polakiewicz, N. Sonenberg, and J.W. Hershey, *Phosphorylation of eucaryotic translation initiation factor 4B Ser422 is modulated by S6 kinases*. EMBO J, 2004. **23**(8): p. 1761-9.
61. Shaw, R.J. and L.C. Cantley, *Ras, PI(3)K and mTOR signalling controls tumour cell growth*. Nature, 2006. **441**(7092): p. 424-30.
62. Schmelzle, T. and M.N. Hall, *TOR, a central controller of cell growth*. Cell, 2000. **103**(2): p. 253-62.
63. Garcia-Martinez, J.M. and D.R. Alessi, *mTOR complex 2 (mTORC2) controls hydrophobic motif phosphorylation and activation of serum- and glucocorticoid-induced protein kinase 1 (SGK1)*. Biochem J, 2008. **416**(3): p. 375-85.
64. Laplante, M. and D.M. Sabatini, *mTOR signaling at a glance*. J Cell Sci, 2009. **122**(Pt 20): p. 3589-94.
65. Jacinto, E., R. Loewith, A. Schmidt, S. Lin, M.A. Ruegg, A. Hall, and M.N. Hall, *Mammalian TOR complex 2 controls the actin cytoskeleton and is rapamycin insensitive*. Nat Cell Biol, 2004. **6**(11): p. 1122-8.
66. Sarbassov, D.D., S.M. Ali, S. Sengupta, J.H. Sheen, P.P. Hsu, A.F. Bagley, A.L. Markhard, and D.M. Sabatini, *Prolonged rapamycin treatment inhibits mTORC2 assembly and Akt/PKB*. Mol Cell, 2006. **22**(2): p. 159-68.
67. Inoki, K., M.N. Corradetti, and K.L. Guan, *Dysregulation of the TSC-mTOR pathway in human disease*. Nat Genet, 2005. **37**(1): p. 19-24.

68. Chong-Kopera, H., K. Inoki, Y. Li, T. Zhu, F.R. Garcia-Gonzalo, J.L. Rosa, and K.L. Guan, *TSC1 stabilizes TSC2 by inhibiting the interaction between TSC2 and the HERC1 ubiquitin ligase*. J Biol Chem, 2006. **281**(13): p. 8313-6.
69. Tee, A.R., B.D. Manning, P.P. Roux, L.C. Cantley, and J. Blenis, *Tuberous sclerosis complex gene products, Tuberin and Hamartin, control mTOR signaling by acting as a GTPase-activating protein complex toward Rheb*. Curr Biol, 2003. **13**(15): p. 1259-68.
70. van Slegtenhorst, M., M. Nellist, B. Nagelkerken, J. Cheadle, R. Snell, A. van den Ouweland, A. Reuser, J. Sampson, D. Halley, and P. van der Sluijs, *Interaction between hamartin and tuberin, the TSC1 and TSC2 gene products*. Hum Mol Genet, 1998. **7**(6): p. 1053-7.
71. Tee, A.R., R. Anjum, and J. Blenis, *Inactivation of the tuberous sclerosis complex-1 and -2 gene products occurs by phosphoinositide 3-kinase/Akt-dependent and -independent phosphorylation of tuberin*. J Biol Chem, 2003. **278**(39): p. 37288-96.
72. Bai, X., D. Ma, A. Liu, X. Shen, Q.J. Wang, Y. Liu, and Y. Jiang, *Rheb activates mTOR by antagonizing its endogenous inhibitor, FKBP38*. Science, 2007. **318**(5852): p. 977-80.
73. Inoki, K., Y. Li, T. Xu, and K.L. Guan, *Rheb GTPase is a direct target of TSC2 GAP activity and regulates mTOR signaling*. Genes Dev, 2003. **17**(15): p. 1829-34.
74. Wullschleger, S., R. Loewith, and M.N. Hall, *TOR signaling in growth and metabolism*. Cell, 2006. **124**(3): p. 471-84.
75. Zhang, C., S. Yasuno, K. Kuwahara, D.P. Zankov, A. Kobori, T. Makiyama, and M. Horie, *Blockade of angiotensin II type 1 receptor improves the arrhythmia morbidity in mice with left ventricular hypertrophy*. Circ J, 2006. **70**(3): p. 335-41.
76. Frey, N. and E.N. Olson, *Cardiac hypertrophy: the good, the bad, and the ugly*. Annu Rev Physiol, 2003. **65**: p. 45-79.
77. Heineke, J. and J.D. Molkentin, *Regulation of cardiac hypertrophy by intracellular signalling pathways*. Nat Rev Mol Cell Biol, 2006. **7**(8): p. 589-600.
78. Hilfiker-Kleiner, D., U. Landmesser, and H. Drexler, *Molecular Mechanisms in Heart Failure Focus on Cardiac Hypertrophy, Inflammation, Angiogenesis, and Apoptosis*. Journal of the American College of Cardiology, 2006. **48**(9s1): p. A56-A66.
79. Passier, R., H. Zeng, N. Frey, F.J. Naya, R.L. Nicol, T.A. McKinsey, P. Overbeek, J.A. Richardson, S.R. Grant, and E.N. Olson, *CaM kinase signaling induces cardiac hypertrophy and activates the MEF2 transcription factor in vivo*. J Clin Invest, 2000. **105**(10): p. 1395-406.
80. Ramirez, M.T., X.L. Zhao, H. Schulman, and J.H. Brown, *The nuclear deltaB isoform of Ca²⁺/calmodulin-dependent protein kinase II regulates atrial natriuretic factor gene expression in ventricular myocytes*. J Biol Chem, 1997. **272**(49): p. 31203-8.
81. Shiojima, I. and K. Walsh, *Regulation of cardiac growth and coronary angiogenesis by the Akt/PKB signaling pathway*. Genes Dev, 2006. **20**(24): p. 3347-65.

82. Sugden, P.H., *Signalling pathways in cardiac myocyte hypertrophy*. *Ann Med*, 2001. **33**(9): p. 611-22.
83. Goldberg, E.M. and D.A. Coulter, *Mechanisms of epileptogenesis: a convergence on neural circuit dysfunction*. *Nat Rev Neurosci*, 2013. **14**(5): p. 337-49.
84. Crino, P.B., *Focal brain malformations: seizures, signaling, sequencing*. *Epilepsia*, 2009. **50 Suppl 9**: p. 3-8.
85. Crino, P.B., *mTOR: A pathogenic signaling pathway in developmental brain malformations*. *Trends Mol Med*, 2011. **17**(12): p. 734-42.
86. McDaniel, S.S. and M. Wong, *Therapeutic role of mammalian target of rapamycin (mTOR) inhibition in preventing epileptogenesis*. *Neurosci Lett*, 2011. **497**(3): p. 231-9.
87. Striano, P. and F. Zara, *Genetics: mutations in mTOR pathway linked to megalencephaly syndromes*. *Nat Rev Neurol*, 2012. **8**(10): p. 542-4.
88. Wong, M., *Mammalian target of rapamycin (mTOR) inhibition as a potential antiepileptogenic therapy: From tuberous sclerosis to common acquired epilepsies*. *Epilepsia*, 2010. **51**(1): p. 27-36.
89. Chen, S., C.M. Atkins, C.L. Liu, O.F. Alonso, W.D. Dietrich, and B.R. Hu, *Alterations in mammalian target of rapamycin signaling pathways after traumatic brain injury*. *J Cereb Blood Flow Metab*, 2007. **27**(5): p. 939-49.
90. Erlich, S., A. Alexandrovich, E. Shohami, and R. Pinkas-Kramarski, *Rapamycin is a neuroprotective treatment for traumatic brain injury*. *Neurobiol Dis*, 2007. **26**(1): p. 86-93.
91. Huang, X., H. Zhang, J. Yang, J. Wu, J. McMahon, Y. Lin, Z. Cao, M. Gruenthal, and Y. Huang, *Pharmacological inhibition of the mammalian target of rapamycin pathway suppresses acquired epilepsy*. *Neurobiol Dis*, 2010. **40**(1): p. 193-9.
92. van Vliet, E.A., G. Forte, L. Holtman, J.C. den Burger, A. Sinjewel, H.E. de Vries, E. Aronica, and J.A. Gorter, *Inhibition of mammalian target of rapamycin reduces epileptogenesis and blood-brain barrier leakage but not microglia activation*. *Epilepsia*, 2012. **53**(7): p. 1254-63.
93. Zeng, L.H., N.R. Rensing, and M. Wong, *The mammalian target of rapamycin signaling pathway mediates epileptogenesis in a model of temporal lobe epilepsy*. *J Neurosci*, 2009. **29**(21): p. 6964-72.
94. Ostendorf, A.P. and M. Wong, *mTOR inhibition in epilepsy: rationale and clinical perspectives*. *CNS Drugs*, 2015. **29**(2): p. 91-9.
95. Ehninger, D., S. Han, C. Shilyansky, Y. Zhou, W. Li, D.J. Kwiatkowski, V. Ramesh, and A.J. Silva, *Reversal of learning deficits in a Tsc2+/- mouse model of tuberous sclerosis*. *Nat Med*, 2008. **14**(8): p. 843-8.
96. Meikle, L., K. Pollizzi, A. Egnor, I. Kramvis, H. Lane, M. Sahin, and D.J. Kwiatkowski, *Response of a neuronal model of tuberous sclerosis to mammalian target of rapamycin (mTOR) inhibitors: effects on mTORC1 and Akt signaling lead to improved survival and function*. *J Neurosci*, 2008. **28**(21): p. 5422-32.
97. Zeng, L.H., L. Xu, D.H. Gutmann, and M. Wong, *Rapamycin prevents epilepsy in a mouse model of tuberous sclerosis complex*. *Ann Neurol*, 2008. **63**(4): p. 444-53.

98. Way, S.W., J. McKenna, 3rd, U. Mietzsch, R.M. Reith, H.C. Wu, and M.J. Gambello, *Loss of Tsc2 in radial glia models the brain pathology of tuberous sclerosis complex in the mouse*. Hum Mol Genet, 2009. **18**(7): p. 1252-65.
99. Way, S.W., N.S. Rozas, H.C. Wu, J. McKenna, 3rd, R.M. Reith, S.S. Hashmi, P.K. Dash, and M.J. Gambello, *The differential effects of prenatal and/or postnatal rapamycin on neurodevelopmental defects and cognition in a neuroglial mouse model of tuberous sclerosis complex*. Hum Mol Genet, 2012. **21**(14): p. 3226-36.
100. Holmes, G.L., C.E. Stafstrom, and G. Tuberous Sclerosis Study, *Tuberous sclerosis complex and epilepsy: recent developments and future challenges*. Epilepsia, 2007. **48**(4): p. 617-30.
101. Stafstrom, C.E. and G.L. Holmes, *Can preventative antiepileptic therapy alter outcome in infants with tuberous sclerosis complex?* Epilepsia, 2007. **48**(8): p. 1632-4.
102. Crino, P.B., A.C. Duhaime, G. Baltuch, and R. White, *Differential expression of glutamate and GABA-A receptor subunit mRNA in cortical dysplasia*. Neurology, 2001. **56**(7): p. 906-13.
103. Kossoff, E.H., *Infantile spasms*. Neurologist, 2010. **16**(2): p. 69-75.
104. Moddel, G., B. Jacobson, Z. Ying, D. Janigro, W. Bingaman, J. Gonzalez-Martinez, C. Kellinghaus, R.A. Prayson, and I.M. Najm, *The NMDA receptor NR2B subunit contributes to epileptogenesis in human cortical dysplasia*. Brain Res, 2005. **1046**(1-2): p. 10-23.
105. Najm, I.M., Z. Ying, T. Babb, A. Mohamed, J. Hadam, E. LaPresto, E. Wyllie, P. Kotagal, W. Bingaman, N. Foldvary, H. Morris, and H.O. Luders, *Epileptogenicity correlated with increased N-methyl-D-aspartate receptor subunit NR2A/B in human focal cortical dysplasia*. Epilepsia, 2000. **41**(8): p. 971-6.
106. Feliciano, D.M., T. Su, J. Lopez, J.C. Platel, and A. Bordey, *Single-cell Tsc1 knockout during corticogenesis generates tuber-like lesions and reduces seizure threshold in mice*. J Clin Invest, 2011. **121**(4): p. 1596-607.
107. Meikle, L., D.M. Talos, H. Onda, K. Pollizzi, A. Rotenberg, M. Sahin, F.E. Jensen, and D.J. Kwiatkowski, *A mouse model of tuberous sclerosis: neuronal loss of Tsc1 causes dysplastic and ectopic neurons, reduced myelination, seizure activity, and limited survival*. J Neurosci, 2007. **27**(21): p. 5546-58.
108. Uhlmann, E.J., M. Wong, R.L. Baldwin, M.L. Bajenaru, H. Onda, D.J. Kwiatkowski, K. Yamada, and D.H. Gutmann, *Astrocyte-specific TSC1 conditional knockout mice exhibit abnormal neuronal organization and seizures*. Ann Neurol, 2002. **52**(3): p. 285-96.
109. Jansen, L.A., E.J. Uhlmann, P.B. Crino, D.H. Gutmann, and M. Wong, *Epileptogenesis and reduced inward rectifier potassium current in tuberous sclerosis complex-1-deficient astrocytes*. Epilepsia, 2005. **46**(12): p. 1871-80.
110. Raab-Graham, K.F., P.C. Haddick, Y.N. Jan, and L.Y. Jan, *Activity- and mTOR-dependent suppression of Kv1.1 channel mRNA translation in dendrites*. Science, 2006. **314**(5796): p. 144-8.

111. Weston, M.C., H. Chen, and J.W. Swann, *Multiple roles for mammalian target of rapamycin signaling in both glutamatergic and GABAergic synaptic transmission*. J Neurosci, 2012. **32**(33): p. 11441-52.
112. Lozovaya, N., S. Gataullina, T. Tsintsadze, V. Tsintsadze, E. Pallesi-Pocachard, M. Minlebaev, N.A. Goriounova, E. Buhler, F. Watrin, S. Shityakov, A.J. Becker, A. Bordey, M. Milh, D. Scavarda, C. Bulteau, G. Dorfmueller, O. Delalande, A. Represa, C. Cardoso, O. Dulac, Y. Ben-Ari, and N. Burnashev, *Selective suppression of excessive GluN2C expression rescues early epilepsy in a tuberous sclerosis murine model*. Nat Commun, 2014. **5**: p. 4563.
113. Kizhatil, K., W. Yoon, P.J. Mohler, L.H. Davis, J.A. Hoffman, and V. Bennett, *Ankyrin-G and beta2-spectrin collaborate in biogenesis of lateral membrane of human bronchial epithelial cells*. J Biol Chem, 2007. **282**(3): p. 2029-37.
114. Bennett, V. and A.J. Baines, *Spectrin and ankyrin-based pathways: metazoan inventions for integrating cells into tissues*. Physiol Rev, 2001. **81**(3): p. 1353-92.
115. Bennett, V. and L. Chen, *Ankyrins and cellular targeting of diverse membrane proteins to physiological sites*. Curr Opin Cell Biol, 2001. **13**(1): p. 61-7.
116. Mohler, P.J., A.O. Gramolini, and V. Bennett, *Ankyrins*. J Cell Sci, 2002. **115**(Pt 8): p. 1565-6.
117. Dzhashiashvili, Y., Y. Zhang, J. Galinska, I. Lam, M. Grumet, and J.L. Salzer, *Nodes of Ranvier and axon initial segments are ankyrin G-dependent domains that assemble by distinct mechanisms*. J Cell Biol, 2007. **177**(5): p. 857-70.
118. Jenkins, S.M. and V. Bennett, *Ankyrin-G coordinates assembly of the spectrin-based membrane skeleton, voltage-gated sodium channels, and LI CAMs at Purkinje neuron initial segments*. J Cell Biol, 2001. **155**(5): p. 739-46.
119. Mohler, P.J. and V. Bennett, *Defects in ankyrin-based cellular pathways in metazoan physiology*. Front Biosci, 2005. **10**: p. 2832-40.
120. Mohler, P.J. and V. Bennett, *Ankyrin-based cardiac arrhythmias: a new class of channelopathies due to loss of cellular targeting*. Curr Opin Cardiol, 2005. **20**(3): p. 189-93.
121. Chang, K.J., D.R. Zollinger, K. Susuki, D.L. Sherman, M.A. Makara, P.J. Brophy, E.C. Cooper, V. Bennett, P.J. Mohler, and M.N. Rasband, *Glial ankyrins facilitate paranodal axoglial junction assembly*. Nat Neurosci, 2014. **17**(12): p. 1673-81.
122. Hedstrom, K.L. and M.N. Rasband, *Intrinsic and extrinsic determinants of ion channel localization in neurons*. J Neurochem, 2006. **98**(5): p. 1345-52.
123. Rasband, M.N., *The axon initial segment and the maintenance of neuronal polarity*. Nat Rev Neurosci, 2010. **11**(8): p. 552-62.
124. Rasmussen, H.B., C. Frokjaer-Jensen, C.S. Jensen, H.S. Jensen, N.K. Jorgensen, H. Misonou, J.S. Trimmer, S.P. Olesen, and N. Schmitt, *Requirement of subunit co-assembly and ankyrin-G for M-channel localization at the axon initial segment*. J Cell Sci, 2007. **120**(Pt 6): p. 953-63.
125. Pan, Z., T. Kao, Z. Horvath, J. Lemos, J.Y. Sul, S.D. Cranstoun, V. Bennett, S.S. Scherer, and E.C. Cooper, *A common ankyrin-G-based mechanism retains KCNQ and NaV channels at electrically active domains of the axon*. J Neurosci, 2006. **26**(10): p. 2599-613.

126. Xu, M. and E.C. Cooper, *An Ankyrin-G N-terminal Gate and Protein Kinase CK2 Dually Regulate Binding of Voltage-gated Sodium and KCNQ2/3 Potassium Channels*. J Biol Chem, 2015. **290**(27): p. 16619-32.
127. Zhou, D., S. Lambert, P.L. Malen, S. Carpenter, L.M. Boland, and V. Bennett, *AnkyrinG is required for clustering of voltage-gated Na channels at axon initial segments and for normal action potential firing*. J Cell Biol, 1998. **143**(5): p. 1295-304.
128. Feng, L., A.P. Li, M.P. Wang, D.N. Sun, Y.L. Wang, L.L. Long, and B. Xiao, *Plasticity at axon initial segment of hippocampal CA3 neurons in rat after status epilepticus induced by lithium-pilocarpine*. Acta Neurochir (Wien), 2013. **155**(12): p. 2373-80; discussion 2380.
129. Araya, R., J.L. Liberona, J.C. Cardenas, N. Riveros, M. Estrada, J.A. Powell, M.A. Carrasco, and E. Jaimovich, *Dihydropyridine receptors as voltage sensors for a depolarization-evoked, IP3R-mediated, slow calcium signal in skeletal muscle cells*. J Gen Physiol, 2003. **121**(1): p. 3-16.
130. Reichel, H. and A. Bleichert, *Excitation-contraction coupling in heart muscle*. Nature, 1959. **183**(4664): p. 826-7.
131. Winegrad, S., *The possible role of calcium in excitation-contraction coupling of heart muscle*. Circulation, 1961. **24**: p. 523-9.
132. Camors, E., P.J. Mohler, D.M. Bers, and S. Despa, *Ankyrin-B reduction enhances Ca spark-mediated SR Ca release promoting cardiac myocyte arrhythmic activity*. J Mol Cell Cardiol, 2012. **52**(6): p. 1240-8.
133. Cunha, S.R., N. Bhasin, and P.J. Mohler, *Targeting and stability of Na/Ca exchanger 1 in cardiomyocytes requires direct interaction with the membrane adaptor ankyrin-B*. J Biol Chem, 2007. **282**(7): p. 4875-83.
134. Chiang, C.E. and D.M. Roden, *The long QT syndromes: genetic basis and clinical implications*. J Am Coll Cardiol, 2000. **36**(1): p. 1-12.
135. Schott, J.J., F. Charpentier, S. Peltier, P. Foley, E. Drouin, J.B. Bouhour, P. Donnelly, G. Vergnaud, L. Bachner, J.P. Moisan, and et al., *Mapping of a gene for long QT syndrome to chromosome 4q25-27*. Am J Hum Genet, 1995. **57**(5): p. 1114-22.
136. Cunha, S.R. and P.J. Mohler, *Obscurin targets ankyrin-B and protein phosphatase 2A to the cardiac M-line*. J Biol Chem, 2008. **283**(46): p. 31968-80.
137. Kordeli, E., S. Lambert, and V. Bennett, *AnkyrinG. A new ankyrin gene with neural-specific isoforms localized at the axonal initial segment and node of Ranvier*. J Biol Chem, 1995. **270**(5): p. 2352-9.
138. Zhang, X. and V. Bennett, *Restriction of 480/270-kD ankyrin G to axon proximal segments requires multiple ankyrin G-specific domains*. J Cell Biol, 1998. **142**(6): p. 1571-81.
139. Devarajan, P., P.R. Stabach, A.S. Mann, T. Ardito, M. Kashgarian, and J.S. Morrow, *Identification of a small cytoplasmic ankyrin (AnkG119) in the kidney and muscle that binds beta I sigma spectrin and associates with the Golgi apparatus*. J Cell Biol, 1996. **133**(4): p. 819-30.
140. Gagelin, C., B. Constantin, C. Deprette, M.A. Ludosky, M. Recouvreur, J. Cartaud, C. Cognard, G. Raymond, and E. Kordeli, *Identification of Ank(G107), a muscle-specific ankyrin-G isoform*. J Biol Chem, 2002. **277**(15): p. 12978-87.

141. Hopitzan, A.A., A.J. Baines, M.A. Ludosky, M. Recouvreur, and E. Kordeli, *Ankyrin-G in skeletal muscle: tissue-specific alternative splicing contributes to the complexity of the sarcolemmal cytoskeleton*. *Exp Cell Res*, 2005. **309**(1): p. 86-98.
142. Mohler, P.J., I. Rivolta, C. Napolitano, G. LeMaillet, S. Lambert, S.G. Priori, and V. Bennett, *Nav1.5 E1053K mutation causing Brugada syndrome blocks binding to ankyrin-G and expression of Nav1.5 on the surface of cardiomyocytes*. *Proc Natl Acad Sci U S A*, 2004. **101**(50): p. 17533-8.
143. Thevananther, S., A.H. Kolli, and P. Devarajan, *Identification of a novel ankyrin isoform (AnkG190) in kidney and lung that associates with the plasma membrane and binds alpha-Na, K-ATPase*. *J Biol Chem*, 1998. **273**(37): p. 23952-8.
144. Yamankurt, G., H.C. Wu, M. McCarthy, and S.R. Cunha, *Exon organization and novel alternative splicing of ank3 in mouse heart*. *PLoS One*, 2015. **10**(5): p. e0128177.
145. Kunimoto, M., *A neuron-specific isoform of brain ankyrin, 440-kD ankyrinB, is targeted to the axons of rat cerebellar neurons*. *J Cell Biol*, 1995. **131**(6 Pt 2): p. 1821-9.
146. Kunimoto, M., E. Otto, and V. Bennett, *A new 440-kD isoform is the major ankyrin in neonatal rat brain*. *J Cell Biol*, 1991. **115**(5): p. 1319-31.
147. Otto, E., M. Kunimoto, T. McLaughlin, and V. Bennett, *Isolation and characterization of cDNAs encoding human brain ankyrins reveal a family of alternatively spliced genes*. *J Cell Biol*, 1991. **114**(2): p. 241-53.
148. Ooashi, N. and H. Kamiguchi, *The cell adhesion molecule L1 controls growth cone navigation via ankyrin(B)-dependent modulation of cyclic AMP*. *Neurosci Res*, 2009. **63**(3): p. 224-6.
149. Whittard, J.D., T. Sakurai, M.R. Cassella, M. Gazdoiu, and D.P. Felsenfeld, *MAP kinase pathway-dependent phosphorylation of the L1-CAM ankyrin binding site regulates neuronal growth*. *Mol Biol Cell*, 2006. **17**(6): p. 2696-706.
150. European Chromosome 16 Tuberous Sclerosis, C., *Identification and characterization of the tuberous sclerosis gene on chromosome 16*. *Cell*, 1993. **75**(7): p. 1305-15.
151. van Slegtenhorst, M., R. de Hoogt, C. Hermans, M. Nellist, B. Janssen, S. Verhoef, D. Lindhout, A. van den Ouweland, D. Halley, J. Young, M. Burley, S. Jeremiah, K. Woodward, J. Nahmias, M. Fox, R. Ekong, J. Osborne, J. Wolfe, S. Povey, R.G. Snell, J.P. Cheadle, A.C. Jones, M. Tachataki, D. Ravine, J.R. Sampson, M.P. Reeve, P. Richardson, F. Wilmer, C. Munro, T.L. Hawkins, T. Sepp, J.B. Ali, S. Ward, A.J. Green, J.R. Yates, J. Kwiatkowska, E.P. Henske, M.P. Short, J.H. Haines, S. Jozwiak, and D.J. Kwiatkowski, *Identification of the tuberous sclerosis gene TSC1 on chromosome 9q34*. *Science*, 1997. **277**(5327): p. 805-8.
152. Chan, J.A., H. Zhang, P.S. Roberts, S. Jozwiak, G. Wieslawa, J. Lewin-Kowalik, K. Kotulska, and D.J. Kwiatkowski, *Pathogenesis of tuberous sclerosis subependymal giant cell astrocytomas: biallelic inactivation of TSC1 or TSC2 leads to mTOR activation*. *J Neuropathol Exp Neurol*, 2004. **63**(12): p. 1236-42.
153. Crino, P.B., E. Aronica, G. Baltuch, and K.L. Nathanson, *Biallelic TSC gene inactivation in tuberous sclerosis complex*. *Neurology*, 2010. **74**(21): p. 1716-23.

154. Crino, P.B., *Molecular pathogenesis of tuber formation in tuberous sclerosis complex*. J Child Neurol, 2004. **19**(9): p. 716-25.
155. Crino, P.B., K.L. Nathanson, and E.P. Henske, *The tuberous sclerosis complex*. N Engl J Med, 2006. **355**(13): p. 1345-56.
156. DiMario, F.J., Jr., *Brain abnormalities in tuberous sclerosis complex*. J Child Neurol, 2004. **19**(9): p. 650-7.
157. Gao, X. and D. Pan, *TSC1 and TSC2 tumor suppressors antagonize insulin signaling in cell growth*. Genes Dev, 2001. **15**(11): p. 1383-92.
158. Tapon, N., N. Ito, B.J. Dickson, J.E. Treisman, and I.K. Hariharan, *The Drosophila tuberous sclerosis complex gene homologs restrict cell growth and cell proliferation*. Cell, 2001. **105**(3): p. 345-55.
159. Anderl, S., M. Freeland, D.J. Kwiatkowski, and J. Goto, *Therapeutic value of prenatal rapamycin treatment in a mouse brain model of tuberous sclerosis complex*. Hum Mol Genet, 2011. **20**(23): p. 4597-604.
160. Goto, J., D.M. Talos, P. Klein, W. Qin, Y.I. Chekaluk, S. Anderl, I.A. Malinowska, A. Di Nardo, R.T. Bronson, J.A. Chan, H.V. Vinters, S.G. Kernie, F.E. Jensen, M. Sahin, and D.J. Kwiatkowski, *Regulable neural progenitor-specific Tsc1 loss yields giant cells with organellar dysfunction in a model of tuberous sclerosis complex*. Proc Natl Acad Sci U S A, 2011. **108**(45): p. E1070-9.
161. Campen, C.J. and B.E. Porter, *Subependymal Giant Cell Astrocytoma (SEGA) Treatment Update*. Curr Treat Options Neurol, 2011. **13**(4): p. 380-5.
162. Krueger, D.A., M.M. Care, K. Holland, K. Agricola, C. Tudor, P. Mangeshkar, K.A. Wilson, A. Byars, T. Sahmoud, and D.N. Franz, *Everolimus for subependymal giant-cell astrocytomas in tuberous sclerosis*. N Engl J Med, 2010. **363**(19): p. 1801-11.
163. Kwon, C.H., X. Zhu, J. Zhang, and S.J. Baker, *mTor is required for hypertrophy of Pten-deficient neuronal soma in vivo*. Proc Natl Acad Sci U S A, 2003. **100**(22): p. 12923-8.
164. Magri, L., M. Cambiagli, M. Cominelli, C. Alfaro-Cervello, M. Corsi, M. Pala, A. Bulfone, J.M. Garcia-Verdugo, L. Leocani, F. Minicucci, P.L. Poliani, and R. Galli, *Sustained activation of mTOR pathway in embryonic neural stem cells leads to development of tuberous sclerosis complex-associated lesions*. Cell Stem Cell, 2011. **9**(5): p. 447-62.
165. Jaworski, J. and M. Sheng, *The growing role of mTOR in neuronal development and plasticity*. Mol Neurobiol, 2006. **34**(3): p. 205-19.
166. Urbanska, M., A. Gozdz, L.J. Swiech, and J. Jaworski, *Mammalian target of rapamycin complex 1 (mTORC1) and 2 (mTORC2) control the dendritic arbor morphology of hippocampal neurons*. J Biol Chem, 2012. **287**(36): p. 30240-56.
167. Rivera, V.M., X. Ye, N.L. Courage, J. Sachar, F. Cerasoli, Jr., J.M. Wilson, and M. Gilman, *Long-term regulated expression of growth hormone in mice after intramuscular gene transfer*. Proc Natl Acad Sci U S A, 1999. **96**(15): p. 8657-62.
168. Guzowski, J.F. and J.L. McGaugh, *Antisense oligodeoxynucleotide-mediated disruption of hippocampal cAMP response element binding protein levels impairs consolidation of memory for water maze training*. Proc Natl Acad Sci U S A, 1997. **94**(6): p. 2693-8.

169. Morris, R., *Developments of a water-maze procedure for studying spatial learning in the rat.* J Neurosci Methods, 1984. **11**(1): p. 47-60.
170. Morris, R.G., P. Garrud, J.N. Rawlins, and J. O'Keefe, *Place navigation impaired in rats with hippocampal lesions.* Nature, 1982. **297**(5868): p. 681-3.
171. Schenk, F. and R.G. Morris, *Dissociation between components of spatial memory in rats after recovery from the effects of retrohippocampal lesions.* Exp Brain Res, 1985. **58**(1): p. 11-28.
172. Frankland, P.W., V. Cestari, R.K. Filipkowski, R.J. McDonald, and A.J. Silva, *The dorsal hippocampus is essential for context discrimination but not for contextual conditioning.* Behav Neurosci, 1998. **112**(4): p. 863-74.
173. Danglot, L., A. Triller, and S. Marty, *The development of hippocampal interneurons in rodents.* Hippocampus, 2006. **16**(12): p. 1032-60.
174. Nieto, M., E.S. Monuki, H. Tang, J. Imitola, N. Haubst, S.J. Khoury, J. Cunningham, M. Gotz, and C.A. Walsh, *Expression of Cux-1 and Cux-2 in the subventricular zone and upper layers II-IV of the cerebral cortex.* J Comp Neurol, 2004. **479**(2): p. 168-80.
175. Rowitch, D.H. and A.R. Kriegstein, *Developmental genetics of vertebrate glial-cell specification.* Nature, 2010. **468**(7321): p. 214-22.
176. Goorden, S.M., G.M. van Woerden, L. van der Weerd, J.P. Cheadle, and Y. Elgersma, *Cognitive deficits in Tsc1+/- mice in the absence of cerebral lesions and seizures.* Ann Neurol, 2007. **62**(6): p. 648-55.
177. Young, D.M., A.K. Schenk, S.B. Yang, Y.N. Jan, and L.Y. Jan, *Altered ultrasonic vocalizations in a tuberous sclerosis mouse model of autism.* Proc Natl Acad Sci U S A, 2010. **107**(24): p. 11074-9.
178. Muta, K., D.A. Morgan, and K. Rahmouni, *The role of hypothalamic mTORC1 signaling in insulin regulation of food intake, body weight, and sympathetic nerve activity in male mice.* Endocrinology, 2015. **156**(4): p. 1398-407.
179. Dash, P.K., S.A. Orsi, and A.N. Moore, *Spatial memory formation and memory-enhancing effect of glucose involves activation of the tuberous sclerosis complex-Mammalian target of rapamycin pathway.* J Neurosci, 2006. **26**(31): p. 8048-56.
180. Sosunov, A.A., X. Wu, H.L. Weiner, C.B. Mikell, R.R. Goodman, P.D. Crino, and G.M. McKhann, 2nd, *Tuberous sclerosis: a primary pathology of astrocytes?* Epilepsia, 2008. **49 Suppl 2**: p. 53-62.
181. Choi, Y.J., A. Di Nardo, I. Kramvis, L. Meikle, D.J. Kwiatkowski, M. Sahin, and X. He, *Tuberous sclerosis complex proteins control axon formation.* Genes Dev, 2008. **22**(18): p. 2485-95.
182. Nie, D., A. Di Nardo, J.M. Han, H. Baharanyi, I. Kramvis, T. Huynh, S. Dabora, S. Codeluppi, P.P. Pandolfi, E.B. Pasquale, and M. Sahin, *Tsc2-Rheb signaling regulates EphA-mediated axon guidance.* Nat Neurosci, 2010. **13**(2): p. 163-72.
183. Tavazoie, S.F., V.A. Alvarez, D.A. Ridenour, D.J. Kwiatkowski, and B.L. Sabatini, *Regulation of neuronal morphology and function by the tumor suppressors Tsc1 and Tsc2.* Nat Neurosci, 2005. **8**(12): p. 1727-34.
184. Tsai, P. and M. Sahin, *Mechanisms of neurocognitive dysfunction and therapeutic considerations in tuberous sclerosis complex.* Curr Opin Neurol, 2011. **24**(2): p. 106-13.

185. Berry, R.J., Z. Li, J.D. Erickson, S. Li, C.A. Moore, H. Wang, J. Mulinare, P. Zhao, L.Y. Wong, J. Gindler, S.X. Hong, and A. Correa, *Prevention of neural-tube defects with folic acid in China. China-U.S. Collaborative Project for Neural Tube Defect Prevention*. N Engl J Med, 1999. **341**(20): p. 1485-90.
186. Briggs G., F.R., Yaffe S., *Drugs in Pregnancy and Lactation*, in *A Reference Guide to Fetal and Neonatal Risk*. 2011, Lippincott Williams and Wilkins: Philadelphia. p. 1336-37.
187. Pun, R.Y., I.J. Rolle, C.L. Lasarge, B.E. Hosford, J.M. Rosen, J.D. Uhl, S.N. Schmeltzer, C. Faulkner, S.L. Bronson, B.L. Murphy, D.A. Richards, K.D. Holland, and S.C. Danzer, *Excessive activation of mTOR in postnatally generated granule cells is sufficient to cause epilepsy*. Neuron, 2012. **75**(6): p. 1022-34.
188. Noga, A.A., C.L. Soltys, A.J. Barr, S. Kovacic, G.D. Lopaschuk, and J.R. Dyck, *Expression of an active LKB1 complex in cardiac myocytes results in decreased protein synthesis associated with phenylephrine-induced hypertrophy*. Am J Physiol Heart Circ Physiol, 2007. **292**(3): p. H1460-9.
189. Pereira, R.O., A.R. Wende, A. Crum, D. Hunter, C.D. Olsen, T. Rawlings, C. Riehle, W.F. Ward, and E.D. Abel, *Maintaining PGC-1alpha expression following pressure overload-induced cardiac hypertrophy preserves angiogenesis but not contractile or mitochondrial function*. FASEB J, 2014. **28**(8): p. 3691-702.
190. Sen, S., B.K. Kundu, H.C. Wu, S.S. Hashmi, P. Guthrie, L.W. Locke, R.J. Roy, G.P. Matherne, S.S. Berr, M. Terwelp, B. Scott, S. Carranza, O.H. Frazier, D.K. Glover, W.H. Dillmann, M.J. Gambello, M.L. Entman, and H. Taegtmeier, *Glucose regulation of load-induced mTOR signaling and ER stress in mammalian heart*. J Am Heart Assoc, 2013. **2**(3): p. e004796.
191. Fassett, J.T., X. Hu, X. Xu, Z. Lu, P. Zhang, Y. Chen, and R.J. Bache, *Adenosine kinase regulation of cardiomyocyte hypertrophy*. Am J Physiol Heart Circ Physiol, 2011. **300**(5): p. H1722-32.
192. McMullen, J.R., M.C. Sherwood, O. Tarnavski, L. Zhang, A.L. Dorfman, T. Shioi, and S. Izumo, *Inhibition of mTOR signaling with rapamycin regresses established cardiac hypertrophy induced by pressure overload*. Circulation, 2004. **109**(24): p. 3050-5.
193. Shioi, T., J.R. McMullen, O. Tarnavski, K. Converso, M.C. Sherwood, W.J. Manning, and S. Izumo, *Rapamycin attenuates load-induced cardiac hypertrophy in mice*. Circulation, 2003. **107**(12): p. 1664-70.
194. Boyden, P.A. and C.D. Jeck, *Ion channel function in disease*. Cardiovasc Res, 1995. **29**(3): p. 312-8.
195. Clarke, J.D., J.L. Caldwell, M.A. Horn, E.F. Bode, M.A. Richards, M.C. Hall, H.K. Graham, S.J. Briston, D.J. Greensmith, D.A. Eisner, K.M. Dibb, and A.W. Trafford, *Perturbed atrial calcium handling in an ovine model of heart failure: potential roles for reductions in the L-type calcium current*. J Mol Cell Cardiol, 2015. **79**: p. 169-79.
196. Pye, M.P. and S.M. Cobbe, *Mechanisms of ventricular arrhythmias in cardiac failure and hypertrophy*. Cardiovasc Res, 1992. **26**(8): p. 740-50.

197. Antzelevitch, C. and S. Sicouri, *Clinical relevance of cardiac arrhythmias generated by afterdepolarizations. Role of M cells in the generation of U waves, triggered activity and torsade de pointes*. J Am Coll Cardiol, 1994. **23**(1): p. 259-77.
198. Fozzard, H.A., *Afterdepolarizations and triggered activity*. Basic Res Cardiol, 1992. **87 Suppl 2**: p. 105-13.
199. Surawicz, B., *Electrophysiologic substrate of torsade de pointes: dispersion of repolarization or early afterdepolarizations?* J Am Coll Cardiol, 1989. **14**(1): p. 172-84.
200. Bryant, S.M., S.J. Shipsey, and G. Hart, *Regional differences in electrical and mechanical properties of myocytes from guinea-pig hearts with mild left ventricular hypertrophy*. Cardiovasc Res, 1997. **35**(2): p. 315-23.
201. Shipsey, S.J., S.M. Bryant, and G. Hart, *Effects of hypertrophy on regional action potential characteristics in the rat left ventricle: a cellular basis for T-wave inversion?* Circulation, 1997. **96**(6): p. 2061-8.
202. Burghardt, R.C., R. Barhoumi, T.C. Sewall, and J.A. Bowen, *Cyclic AMP induces rapid increases in gap junction permeability and changes in the cellular distribution of connexin43*. J Membr Biol, 1995. **148**(3): p. 243-53.
203. Cooper, C.D. and P.D. Lampe, *Casein kinase 1 regulates connexin-43 gap junction assembly*. J Biol Chem, 2002. **277**(47): p. 44962-8.
204. Cottrell, G.T., R. Lin, B.J. Warn-Cramer, A.F. Lau, and J.M. Burt, *Mechanism of v-Src- and mitogen-activated protein kinase-induced reduction of gap junction communication*. Am J Physiol Cell Physiol, 2003. **284**(2): p. C511-20.
205. Lampe, P.D., E.M. TenBroek, J.M. Burt, W.E. Kurata, R.G. Johnson, and A.F. Lau, *Phosphorylation of connexin43 on serine368 by protein kinase C regulates gap junctional communication*. J Cell Biol, 2000. **149**(7): p. 1503-12.
206. Saez, J.C., A.C. Nairn, A.J. Czernik, G.I. Fishman, D.C. Spray, and E.L. Hertzberg, *Phosphorylation of connexin43 and the regulation of neonatal rat cardiac myocyte gap junctions*. J Mol Cell Cardiol, 1997. **29**(8): p. 2131-45.
207. Shah, M.M., A.M. Martinez, and W.H. Fletcher, *The connexin43 gap junction protein is phosphorylated by protein kinase A and protein kinase C: in vivo and in vitro studies*. Mol Cell Biochem, 2002. **238**(1-2): p. 57-68.
208. Warn-Cramer, B.J., P.D. Lampe, W.E. Kurata, M.Y. Kanemitsu, L.W. Loo, W. Eckhart, and A.F. Lau, *Characterization of the mitogen-activated protein kinase phosphorylation sites on the connexin-43 gap junction protein*. J Biol Chem, 1996. **271**(7): p. 3779-86.
209. Bastide, B., L. Neyses, D. Ganten, M. Paul, K. Willecke, and O. Traub, *Gap junction protein connexin40 is preferentially expressed in vascular endothelium and conductive bundles of rat myocardium and is increased under hypertensive conditions*. Circ Res, 1993. **73**(6): p. 1138-49.
210. Peters, N.S., C.R. Green, P.A. Poole-Wilson, and N.J. Severs, *Reduced content of connexin43 gap junctions in ventricular myocardium from hypertrophied and ischemic human hearts*. Circulation, 1993. **88**(3): p. 864-75.
211. Bierhuizen, M.F., M. Boulaksil, L. van Stuijvenberg, R. van der Nagel, A.T. Jansen, N.A. Mutsaers, C. Yildirim, T.A. van Veen, L.J. de Windt, M.A. Vos, and H.V. van Rijen, *In calcineurin-induced cardiac hypertrophy expression of*

- Nav1.5, Cx40 and Cx43 is reduced by different mechanisms.* J Mol Cell Cardiol, 2008. **45**(3): p. 373-84.
212. Sasano, C., H. Honjo, Y. Takagishi, M. Uzzaman, L. Emdad, A. Shimizu, Y. Murata, K. Kamiya, and I. Kodama, *Internalization and dephosphorylation of connexin43 in hypertrophied right ventricles of rats with pulmonary hypertension.* Circ J, 2007. **71**(3): p. 382-9.
213. Kowey, P.R., T.D. Friechling, J. Sewter, Y. Wu, A. Sokil, J. Paul, and J. Nocella, *Electrophysiological effects of left ventricular hypertrophy. Effect of calcium and potassium channel blockade.* Circulation, 1991. **83**(6): p. 2067-75.
214. Kowey, P.R., R. O'Brien, Y. Wu, J. Sewter, A. Sokil, J. Nocella, and S.J. Rials, *Effect of gallopamil on electrophysiologic abnormalities and ventricular arrhythmias associated with left ventricular hypertrophy in the feline heart.* Am Heart J, 1992. **124**(4): p. 898-905.
215. Rials, S.J., Y. Wu, N. Ford, F.J. Pauletto, S.V. Abramson, A.M. Rubin, R.A. Marinchak, and P.R. Kowey, *Effect of left ventricular hypertrophy and its regression on ventricular electrophysiology and vulnerability to inducible arrhythmia in the feline heart.* Circulation, 1995. **91**(2): p. 426-30.
216. Kashef, F., J. Li, P. Wright, J. Snyder, F. Suliman, A. Kilic, R.S. Higgins, M.E. Anderson, P.F. Binkley, T.J. Hund, and P.J. Mohler, *Ankyrin-B protein in heart failure: identification of a new component of metazoan cardioprotection.* J Biol Chem, 2012. **287**(36): p. 30268-81.
217. Richard, S., F. Leclercq, S. Lemaire, C. Piot, and J. Nargeot, *Ca²⁺ currents in compensated hypertrophy and heart failure.* Cardiovasc Res, 1998. **37**(2): p. 300-11.
218. Wickenden, A.D., R. Kaprielian, Z. Kassiri, J.N. Tsoporis, R. Tsushima, G.I. Fishman, and P.H. Backx, *The role of action potential prolongation and altered intracellular calcium handling in the pathogenesis of heart failure.* Cardiovasc Res, 1998. **37**(2): p. 312-23.
219. Arai, M., H. Matsui, and M. Periasamy, *Sarcoplasmic reticulum gene expression in cardiac hypertrophy and heart failure.* Circ Res, 1994. **74**(4): p. 555-64.
220. de la Bastie, D., D. Levitsky, L. Rappaport, J.J. Mercadier, F. Marotte, C. Wisnewsky, V. Brovkovich, K. Schwartz, and A.M. Lompre, *Function of the sarcoplasmic reticulum and expression of its Ca²⁺(+)-ATPase gene in pressure overload-induced cardiac hypertrophy in the rat.* Circ Res, 1990. **66**(2): p. 554-64.
221. Wang, Z., B. Nolan, W. Kutschke, and J.A. Hill, *Na⁺-Ca²⁺ exchanger remodeling in pressure overload cardiac hypertrophy.* J Biol Chem, 2001. **276**(21): p. 17706-11.
222. Philipson, K.D. and D.A. Nicoll, *Sodium-calcium exchange: a molecular perspective.* Annu Rev Physiol, 2000. **62**: p. 111-33.
223. Volkers, M., H. Toko, S. Doroudgar, S. Din, P. Quijada, A.Y. Joyo, L. Ornelas, E. Joyo, D.J. Thuerauf, M.H. Konstandin, N. Gude, C.C. Glembotski, and M.A. Sussman, *Pathological hypertrophy amelioration by PRAS40-mediated inhibition of mTORC1.* Proc Natl Acad Sci U S A, 2013. **110**(31): p. 12661-6.

224. Bauer, S., S.K. Maier, L. Neyses, and A.H. Maass, *Optimization of gene transfer into neonatal rat cardiomyocytes and unmasking of cytomegalovirus promoter silencing*. DNA Cell Biol, 2005. **24**(6): p. 381-7.
225. Perissel, B., F. Charbonne, J.M. Moalic, and P. Malet, *Initial stages of trypsinized cell culture of cardiac myoblasts: ultrastructural data*. J Mol Cell Cardiol, 1980. **12**(1): p. 63-75.
226. Inoki, K., Y. Li, T. Zhu, J. Wu, and K.L. Guan, *TSC2 is phosphorylated and inhibited by Akt and suppresses mTOR signalling*. Nat Cell Biol, 2002. **4**(9): p. 648-57.
227. Nobukuni, T., M. Joaquin, M. Rocco, S.G. Dann, S.Y. Kim, P. Gulati, M.P. Byfield, J.M. Backer, F. Natt, J.L. Bos, F.J. Zwartkruis, and G. Thomas, *Amino acids mediate mTOR/raptor signaling through activation of class 3 phosphatidylinositol 3OH-kinase*. Proc Natl Acad Sci U S A, 2005. **102**(40): p. 14238-43.
228. Baskin, K.K. and H. Taegtmeyer, *AMP-activated protein kinase regulates E3 ligases in rodent heart*. Circ Res, 2011. **109**(10): p. 1153-61.
229. Cunha, S.R., T.J. Hund, S. Hashemi, N. Voigt, N. Li, P. Wright, O. Koval, J. Li, H. Gudmundsson, R.J. Gumina, M. Karck, J.J. Schott, V. Probst, H. Le Marec, M.E. Anderson, D. Dobrev, X.H. Wehrens, and P.J. Mohler, *Defects in ankyrin-based membrane protein targeting pathways underlie atrial fibrillation*. Circulation, 2011. **124**(11): p. 1212-22.
230. Fassina, L., A. Di Grazia, F. Naro, L. Monaco, M.G. De Angelis, and G. Magenes, *Video evaluation of the kinematics and dynamics of the beating cardiac syncytium: an alternative to the Langendorff method*. Int J Artif Organs, 2011. **34**(7): p. 546-58.
231. Lowe, J.S., O. Palygin, N. Bhasin, T.J. Hund, P.A. Boyden, E. Shibata, M.E. Anderson, and P.J. Mohler, *Voltage-gated Nav channel targeting in the heart requires an ankyrin-G dependent cellular pathway*. J Cell Biol, 2008. **180**(1): p. 173-86.
232. Ackermann, M.A., A.P. Ziman, J. Strong, Y. Zhang, A.K. Hartford, C.W. Ward, W.R. Randall, A. Kontrogianni-Konstantopoulos, and R.J. Bloch, *Integrity of the network sarcoplasmic reticulum in skeletal muscle requires small ankyrin I*. J Cell Sci, 2011. **124**(Pt 21): p. 3619-30.
233. Cusimano, V., F. Pampinella, E. Giacomello, and V. Sorrentino, *Assembly and dynamics of proteins of the longitudinal and junctional sarcoplasmic reticulum in skeletal muscle cells*. Proc Natl Acad Sci U S A, 2009. **106**(12): p. 4695-700.
234. Lange, S., K. Ouyang, G. Meyer, L. Cui, H. Cheng, R.L. Lieber, and J. Chen, *Obscurin determines the architecture of the longitudinal sarcoplasmic reticulum*. J Cell Sci, 2009. **122**(Pt 15): p. 2640-50.
235. Pinali, C., H. Bennett, J.B. Davenport, A.W. Trafford, and A. Kitmitto, *Three-dimensional reconstruction of cardiac sarcoplasmic reticulum reveals a continuous network linking transverse-tubules: this organization is perturbed in heart failure*. Circ Res, 2013. **113**(11): p. 1219-30.
236. Gao, X.M., G. Wong, B. Wang, H. Kiriazis, X.L. Moore, Y.D. Su, A. Dart, and X.J. Du, *Inhibition of mTOR reduces chronic pressure-overload cardiac hypertrophy and fibrosis*. J Hypertens, 2006. **24**(8): p. 1663-70.

237. Kimchi-Sarfaty, C., J. Kasir, S.V. Ambudkar, and H. Rahamimoff, *Transport activity and surface expression of the Na⁺-Ca²⁺ exchanger NCX1 are inhibited by the immunosuppressive agent cyclosporin A and by the nonimmunosuppressive agent PSC833*. J Biol Chem, 2002. **277**(4): p. 2505-10.
238. Rahamimoff, H., B. Elbaz, M. Valitsky, M. Khatib, M. Eskin-Schwartz, and D. Elmaz, *Immunosuppressive drugs, immunophilins, and functional expression of NCX isoforms*. Adv Exp Med Biol, 2013. **961**: p. 275-87.
239. Kent, R.L., J.D. Rozich, P.L. McCollam, D.E. McDermott, U.F. Thacker, D.R. Menick, P.J. McDermott, and G.t. Cooper, *Rapid expression of the Na(+)-Ca²⁺ exchanger in response to cardiac pressure overload*. Am J Physiol, 1993. **265**(3 Pt 2): p. H1024-9.
240. Pogwizd, S.M., M. Qi, W. Yuan, A.M. Samarel, and D.M. Bers, *Upregulation of Na(+)/Ca(2+) exchanger expression and function in an arrhythmogenic rabbit model of heart failure*. Circ Res, 1999. **85**(11): p. 1009-19.
241. Schillinger, W., J.W. Fiolet, K. Schlotthauer, and G. Hasenfuss, *Relevance of Na⁺-Ca²⁺ exchange in heart failure*. Cardiovasc Res, 2003. **57**(4): p. 921-33.
242. Lamers, J.M. and J.T. Stinis, *Defective calcium pump in the sarcoplasmic reticulum of the hypertrophied rabbit heart*. Life Sci, 1979. **24**(25): p. 2313-9.
243. Fontes, M.S., A.J. Raaijmakers, T. van Doorn, B. Kok, S. Nieuwenhuis, R. van der Nagel, M.A. Vos, T.P. de Boer, H.V. van Rijen, and M.F. Bierhuizen, *Changes in Cx43 and NaV1.5 expression precede the occurrence of substantial fibrosis in calcineurin-induced murine cardiac hypertrophy*. PLoS One, 2014. **9**(1): p. e87226.
244. Oxford, E.M., H. Musa, K. Maass, W. Coombs, S.M. Taffet, and M. Delmar, *Connexin43 remodeling caused by inhibition of plakophilin-2 expression in cardiac cells*. Circ Res, 2007. **101**(7): p. 703-11.
245. Sato, P.Y., W. Coombs, X. Lin, O. Nekrasova, K.J. Green, L.L. Isom, S.M. Taffet, and M. Delmar, *Interactions between ankyrin-G, Plakophilin-2, and Connexin43 at the cardiac intercalated disc*. Circ Res, 2011. **109**(2): p. 193-201.
246. Manning, B.D., A.R. Tee, M.N. Logsdon, J. Blenis, and L.C. Cantley, *Identification of the tuberous sclerosis complex-2 tumor suppressor gene product tuberin as a target of the phosphoinositide 3-kinase/akt pathway*. Mol Cell, 2002. **10**(1): p. 151-62.
247. Tee, A.R., D.C. Fingar, B.D. Manning, D.J. Kwiatkowski, L.C. Cantley, and J. Blenis, *Tuberous sclerosis complex-1 and -2 gene products function together to inhibit mammalian target of rapamycin (mTOR)-mediated downstream signaling*. Proc Natl Acad Sci U S A, 2002. **99**(21): p. 13571-6.
248. Kemi, O.J., M. Ceci, U. Wisloff, S. Grimaldi, P. Gallo, G.L. Smith, G. Condorelli, and O. Ellingsen, *Activation or inactivation of cardiac Akt/mTOR signaling diverges physiological from pathological hypertrophy*. J Cell Physiol, 2008. **214**(2): p. 316-21.
249. Song, X., Y. Kusakari, C.Y. Xiao, S.D. Kinsella, M.A. Rosenberg, M. Scherrer-Crosbie, K. Hara, A. Rosenzweig, and T. Matsui, *mTOR attenuates the inflammatory response in cardiomyocytes and prevents cardiac dysfunction in pathological hypertrophy*. Am J Physiol Cell Physiol, 2010. **299**(6): p. C1256-66.

250. Gorski, P.A., D.K. Ceholski, and R.J. Hajjar, *Altered myocardial calcium cycling and energetics in heart failure-a rational approach for disease treatment*. Cell Metab, 2015. **21**(2): p. 183-94.
251. Flesch, M., R.H. Schwinger, F. Schiffer, K. Frank, M. Sudkamp, F. Kuhn-Regnier, G. Arnold, and M. Bohm, *Evidence for functional relevance of an enhanced expression of the Na(+)-Ca²⁺ exchanger in failing human myocardium*. Circulation, 1996. **94**(5): p. 992-1002.
252. O'Rourke, B., D.A. Kass, G.F. Tomaselli, S. Kaab, R. Tunin, and E. Marban, *Mechanisms of altered excitation-contraction coupling in canine tachycardia-induced heart failure, I: experimental studies*. Circ Res, 1999. **84**(5): p. 562-70.
253. Studer, R., H. Reinecke, J. Bilger, T. Eschenhagen, M. Bohm, G. Hasenfuss, H. Just, J. Holtz, and H. Drexler, *Gene expression of the cardiac Na(+)-Ca²⁺ exchanger in end-stage human heart failure*. Circ Res, 1994. **75**(3): p. 443-53.
254. Mitarai, S., T.D. Reed, and A. Yatani, *Changes in ionic currents and beta-adrenergic receptor signaling in hypertrophied myocytes overexpressing G alpha(q)*. Am J Physiol Heart Circ Physiol, 2000. **279**(1): p. H139-48.
255. Chen, F., G. Mottino, V.Y. Shin, and J.S. Frank, *Subcellular distribution of ankyrin in developing rabbit heart--relationship to the Na⁺-Ca²⁺ exchanger*. J Mol Cell Cardiol, 1997. **29**(10): p. 2621-9.
256. Scriven, D.R., P. Dan, and E.D. Moore, *Distribution of proteins implicated in excitation-contraction coupling in rat ventricular myocytes*. Biophys J, 2000. **79**(5): p. 2682-91.
257. Wu, H.C., G. Yamankurt, J. Luo, J. Subramaniam, S.S. Hashmi, H. Hu, and S.R. Cunha, *Identification and characterization of two ankyrin-B isoforms in mammalian heart*. Cardiovasc Res, 2015.
258. Crossman, D.J., P.N. Ruygrok, C. Soeller, and M.B. Cannell, *Changes in the organization of excitation-contraction coupling structures in failing human heart*. PLoS One, 2011. **6**(3): p. e17901.
259. Guo, A., C. Zhang, S. Wei, B. Chen, and L.S. Song, *Emerging mechanisms of T-tubule remodelling in heart failure*. Cardiovasc Res, 2013. **98**(2): p. 204-15.
260. Shah, S.J., G.L. Aistrup, D.K. Gupta, M.J. O'Toole, A.F. Nahhas, D. Schuster, N. Chirayil, N. Bassi, S. Ramakrishna, L. Beussink, S. Misener, B. Kane, D. Wang, B. Randolph, A. Ito, M. Wu, L. Akintilo, T. Mongkolrattanothai, M. Reddy, M. Kumar, R. Arora, J. Ng, and J.A. Wasserstrom, *Ultrastructural and cellular basis for the development of abnormal myocardial mechanics during the transition from hypertension to heart failure*. Am J Physiol Heart Circ Physiol, 2014. **306**(1): p. H88-100.
261. Le Scouarnec, S., N. Bhasin, C. Vieyres, T.J. Hund, S.R. Cunha, O. Koval, C. Marionneau, B. Chen, Y. Wu, S. Demolombe, L.S. Song, H. Le Marec, V. Probst, J.J. Schott, M.E. Anderson, and P.J. Mohler, *Dysfunction in ankyrin-B-dependent ion channel and transporter targeting causes human sinus node disease*. Proc Natl Acad Sci U S A, 2008. **105**(40): p. 15617-22.
262. Birkenmeier, C.S., J.J. Sharp, E.J. Gifford, S.A. Deveau, and J.E. Barker, *An alternative first exon in the distal end of the erythroid ankyrin gene leads to production of a small isoform containing an NH₂-terminal membrane anchor*. Genomics, 1998. **50**(1): p. 79-88.

263. Birkenmeier, C.S., R.A. White, L.L. Peters, E.J. Hall, S.E. Lux, and J.E. Barker, *Complex patterns of sequence variation and multiple 5' and 3' ends are found among transcripts of the erythroid ankyrin gene*. J Biol Chem, 1993. **268**(13): p. 9533-40.
264. Randazzo, D., E. Giacomello, S. Lorenzini, D. Rossi, E. Pierantozzi, B. Blaauw, C. Reggiani, S. Lange, A.K. Peter, J. Chen, and V. Sorrentino, *Obscurin is required for ankyrinB-dependent dystrophin localization and sarcolemma integrity*. J Cell Biol, 2013. **200**(4): p. 523-36.
265. Mohler, P.J., J.Q. Davis, L.H. Davis, J.A. Hoffman, P. Michaely, and V. Bennett, *Inositol 1,4,5-trisphosphate receptor localization and stability in neonatal cardiomyocytes requires interaction with ankyrin-B*. J Biol Chem, 2004. **279**(13): p. 12980-7.
266. Ackermann, M.A., L.Y. Hu, A.L. Bowman, R.J. Bloch, and A. Kontrogianni-Konstantopoulos, *Obscurin interacts with a novel isoform of MyBP-C slow at the periphery of the sarcomeric M-band and regulates thick filament assembly*. Mol Biol Cell, 2009. **20**(12): p. 2963-78.
267. Kontrogianni-Konstantopoulos, A., D.H. Catino, J.C. Strong, W.R. Randall, and R.J. Bloch, *Obscurin regulates the organization of myosin into A bands*. Am J Physiol Cell Physiol, 2004. **287**(1): p. C209-17.
268. Busby, B., C.D. Willis, M.A. Ackermann, A. Kontrogianni-Konstantopoulos, and R.J. Bloch, *Characterization and comparison of two binding sites on obscurin for small ankyrin I*. Biochemistry, 2010. **49**(46): p. 9948-56.
269. Gallagher, P.G. and B.G. Forget, *An alternate promoter directs expression of a truncated, muscle-specific isoform of the human ankyrin 1 gene*. J Biol Chem, 1998. **273**(3): p. 1339-48.
270. Zhou, D., C.S. Birkenmeier, M.W. Williams, J.J. Sharp, J.E. Barker, and R.J. Bloch, *Small, membrane-bound, alternatively spliced forms of ankyrin 1 associated with the sarcoplasmic reticulum of mammalian skeletal muscle*. J Cell Biol, 1997. **136**(3): p. 621-31.
271. Ayalon, G., J.Q. Davis, P.B. Scotland, and V. Bennett, *An ankyrin-based mechanism for functional organization of dystrophin and dystroglycan*. Cell, 2008. **135**(7): p. 1189-200.
272. Kline, C.F., H.T. Kurata, T.J. Hund, S.R. Cunha, O.M. Koval, P.J. Wright, M. Christensen, M.E. Anderson, C.G. Nichols, and P.J. Mohler, *Dual role of K ATP channel C-terminal motif in membrane targeting and metabolic regulation*. Proc Natl Acad Sci U S A, 2009. **106**(39): p. 16669-74.
273. Li, J., C.F. Kline, T.J. Hund, M.E. Anderson, and P.J. Mohler, *Ankyrin-B regulates Kir6.2 membrane expression and function in heart*. J Biol Chem, 2010. **285**(37): p. 28723-30.
274. WA., H.B.a.C., *Electrical Excitability and Ion Channels*, in *Basic Neurochemistry*, A.B. Siegel GJ, Albers W, Fisher SK, Uhler MD., Editor. 1999, Lippincott-Raven: Philadelphia.
275. Asato, M.R. and A.Y. Hardan, *Neuropsychiatric problems in tuberous sclerosis complex*. J Child Neurol, 2004. **19**(4): p. 241-9.
276. Ess, K.C., *Tuberous sclerosis complex: everything old is new again*. J Neurodev Disord, 2009. **1**(2): p. 141-9.

277. Brown, E.J., M.W. Albers, T.B. Shin, K. Ichikawa, C.T. Keith, W.S. Lane, and S.L. Schreiber, *A mammalian protein targeted by G1-arresting rapamycin-receptor complex*. Nature, 1994. **369**(6483): p. 756-8.
278. Chiu, M.I., H. Katz, and V. Berlin, *RAPT1, a mammalian homolog of yeast Tor, interacts with the FKBP12/rapamycin complex*. Proc Natl Acad Sci U S A, 1994. **91**(26): p. 12574-8.
279. Yamazaki, T., I. Komuro, S. Kudoh, Y. Zou, I. Shiojima, T. Mizuno, H. Takano, Y. Hiroi, K. Ueki, K. Tobe, and et al., *Mechanical stress activates protein kinase cascade of phosphorylation in neonatal rat cardiac myocytes*. J Clin Invest, 1995. **96**(1): p. 438-46.
280. O'Rourke, B., *The ins and outs of calcium in heart failure*. Circ Res, 2008. **102**(11): p. 1301-3.
281. Miyamoto, M.I., F. del Monte, U. Schmidt, T.S. DiSalvo, Z.B. Kang, T. Matsui, J.L. Guerrero, J.K. Gwathmey, A. Rosenzweig, and R.J. Hajjar, *Adenoviral gene transfer of SERCA2a improves left-ventricular function in aortic-banded rats in transition to heart failure*. Proc Natl Acad Sci U S A, 2000. **97**(2): p. 793-8.
282. Pott, C., S.A. Henderson, J.I. Goldhaber, and K.D. Philipson, *Na⁺/Ca²⁺ exchanger knockout mice: plasticity of cardiac excitation-contraction coupling*. Ann N Y Acad Sci, 2007. **1099**: p. 270-5.
283. Pott, C., X. Ren, D.X. Tran, M.J. Yang, S. Henderson, M.C. Jordan, K.P. Roos, A. Garfinkel, K.D. Philipson, and J.I. Goldhaber, *Mechanism of shortened action potential duration in Na⁺-Ca²⁺ exchanger knockout mice*. Am J Physiol Cell Physiol, 2007. **292**(2): p. C968-73.
284. Pott, C., M. Yip, J.I. Goldhaber, and K.D. Philipson, *Regulation of cardiac L-type Ca²⁺ current in Na⁺-Ca²⁺ exchanger knockout mice: functional coupling of the Ca²⁺ channel and the Na⁺-Ca²⁺ exchanger*. Biophys J, 2007. **92**(4): p. 1431-7.
285. Yorimitsu, T., U. Nair, Z. Yang, and D.J. Klionsky, *Endoplasmic reticulum stress triggers autophagy*. J Biol Chem, 2006. **281**(40): p. 30299-304.
286. Yu, X. and Y.C. Long, *Autophagy modulates amino acid signaling network in myotubes: differential effects on mTORC1 pathway and the integrated stress response*. FASEB J, 2015. **29**(2): p. 394-407.
287. Buttermore, E.D., C. Piochon, M.L. Wallace, B.D. Philpot, C. Hansel, and M.A. Bhat, *Pinceau organization in the cerebellum requires distinct functions of neurofascin in Purkinje and basket neurons during postnatal development*. J Neurosci, 2012. **32**(14): p. 4724-42.
288. Sobotzik, J.M., J.M. Sie, C. Politi, D. Del Turco, V. Bennett, T. Deller, and C. Schultz, *AnkyrinG is required to maintain axo-dendritic polarity in vivo*. Proc Natl Acad Sci U S A, 2009. **106**(41): p. 17564-9.

**Appendix : GLUCOSE REGULATION OF LOAD-INDUCED mTOR
SIGNALING**

J Am Heart Assoc. 2013 May 17;2(3):e004796. Doi: 10. 1161/JAHA 113.004796

PMID: 23686371

PMCID: PMC3698799

Acknowledgement: The study presented in this chapter was written collaboratively with the first author Dr. Shiraj Sen, who also contributed significantly to acquisition of the data presented in this chapter.

Sen, S., B.K. Kundu, H.C. Wu, S.S. Hashmi, P. Guthrie, L.W. Locke, R.J. Roy, G.P. Matherne, S.S. Berr, M. Terwelp, B. Scott, S. Carranza, O.H. Frazier, D.K. Glover, W.H. Dillmann, M.J. Gambello, M.L. Entman, and H. Taegtmeyer, *Glucose regulation of load-induced mTOR signaling and ER stress in mammalian heart*. J Am Heart Assoc, 2013. 2(3): p. e004796

Journal of American Heart Association articles are published under the terms of the Creative Commons Attribution Non-Commercial License, and copyright is retained by the author(s). The Creative Commons Attribution Non-Commercial License permits use, distribution, and reproduction in any medium, provided the original is properly cited and is not used for commercial purposes.

A.1 Introduction

Increases in the rates of energy substrate metabolism are the first responders to hemodynamic stress in the heart (Goodwin GW, Taylor CS, Taegtmeyer H. JBC 1998). When subjected to a sustained increase in pressure, hearts remodel both metabolically and structurally. Metabolically, hearts increase their reliance on carbohydrates for energy provision (Goodwin GW, Taylor CS, Taegtmeyer H. JBC 1998; Bishop S and Altschuld R. Am J Physiol 1970). Structurally, hearts hypertrophy (Dorn GW II, Force T. JCI 2005). In independent studies we have previously demonstrated that the footprints of metabolic remodeling precede structural remodeling of the heart in hypertension and that activation of the insulin signaling pathway downstream of Akt requires hexose-6-phosphate (Taegtmeyer H and Overturf ML. Hypertension 1988; Sharma S et. al. Cardiovasc Res 2007). We now asked: Could the metabolic remodeling process also regulate signaling pathways of structural remodeling in the heart?

Remodeling is to some extent driven by the mammalian target of rapamycin (mTOR), a regulator of myocardial protein synthesis that is downstream of Akt in the insulin signaling pathway. mTOR kinase nucleates 2 major protein complexes – mTOR complex 1 (mTORC1) and mTOR complex 2 (mTORC2). Under stressed conditions, mTORC1 activity in the heart is inhibited by the tuberous sclerosis complex (TSC), composed of hamartin (TSC1) and tuberin (TSC2). Phosphorylation of a number of serine and threonine residues on TSC2 relieves TSC's inhibition on mTORC1 (Huang J and Manning BD. Biochem J 2008; Inoki K et. al. Nat Cell Biol 2002). Activated mTORC1 triggers protein synthesis and cardiac growth by phosphorylating p70S6

kinase (p70S6K) and eIF-4E binding protein 1 (4E-BP1) to promote ribosomal biogenesis and CAP-dependent protein translation, respectively.

It is already known that mTORC1 plays a critical role in promoting cardiac growth in response to increased workload (Shioi T et. al. Circ 2003) and that mTORC1 is activated by nutrients and growth factors (Proud CG. Eur J Biochem 2002). Whether inotropic mTORC1 activation is regulated by changes in energy substrate metabolism that occur in response to increased workload is unknown, however. We therefore investigated the functional and structural consequences of glucose-mediated mTOR signaling in the stressed heart and discovered that it is both deleterious and preventable.

A.2 Materials and Methods

To determine whether enhanced glucose uptake regulates mTOR activation at increased workload, we first tested the hypothesis *ex vivo*. The hearts were obtained from 4 groups of animals: (1) rats pretreated with vehicle for 7 days before *ex vivo* perfusion with noncarbohydrate substrates; (2) rats pretreated with vehicle for 7 days before *ex vivo* perfusion with glucose; (3) rats pretreated with mTOR inhibitor rapamycin for 7 days before *ex vivo* perfusion with NCS; (4) rats pretreated with the mTOR inhibitor rapamycin for 7 days before *ex vivo* perfusion with glucose. **TABLE A.1** lists the perfusion protocols. Each of the experimental groups was then evaluated in normal workload conditions for 60 minutes or for 30 minutes at normal workload followed by increased workload conditions for another 30 minutes. Hearts were freeze-clamped at the end of the protocol.

Group	Workload	Time (min)	Additions to Krebs Buffer
1	Normal	0-60	Propionate (2mM) + Acetoacetate (5mM)
	Normal	0-15	Substrate-free (Glycogen Depletion)
	High	15-60 30-60	Propionate (2mM) + Acetoacetate (5mM) Epinephrine (1uM)
2	Normal	0-60	Glucose (5mM)
	Normal High	0-30 30-60	*Glucose (5mM) Epinephrine (1uM)
3	Normal	0-60	2 Deoxy-D-glucose (5mM) + Propionate (2mM) + Acetoacetate (5mM)
	Normal High	0-30 30-60	2 Deoxy-D-glucose (5mM) + Propionate (2mM) + Acetoacetate (5mM) Epinephrine (1uM)
	Normal	0-60	3-O-methylglucose (5mM) + Propionate (2mM) + Acetoacetate (5mM)
4	Normal	0-30 30-60	2 Deoxy-D-glucose (5mM) + Propionate (2mM) + Acetoacetate (5mM) Epinephrine (1uM)
	Mixed	0-60	Glucose (5mM) + Oleate (0.4mM) + Propionate (2mM) + Acetoacetate (5mM)

Table A.1. *Ex vivo* perfusion protocols containing four different sets of rats used to study glucose regulated mTOR activation at high workload. 1) untreated prior to perfusion; 2) received mTOR inhibitor rapamycin (PO, 4 mg/kg/day) for 7 days prior to perfusion (or vehicle control); 3) received metformin (IP, 250 mg/kg/day or 500 mg/kg/day) for 7 days prior to perfusion (or vehicle control). 4) hearts was perfused with metformin (10 mM, 7.5 mM, 5 mM) added directly to the buffer. No significant differences in cardiac power were found between all perfusion groups under normal workload. *Animals were pretreated with rapamycin.

A.2.1. Rationale for animal models used and overall strategy

The structural and functional response to increased workload has been extensively studied in the murine transverse aortic constriction (TAC) model (Rockman et. al. PNAS 1991). How the metabolic response to increased workload regulates these changes has yet to be investigated. To systematically answer this question, we used 3 models. First, we used the isolated working rat heart *ex vivo* to elucidate the mechanisms for the observed *in vivo* phenomena. The isolated working rat heart permitted a dynamic minute-by-minute assessment of metabolism and function and allowed for assessment of intracellular metabolites and activation of relevant signaling pathways at the end of the perfusion. The *ex vivo* isolated working heart model was also chosen because it gave us complete control over workload, substrate concentration, and hormone supply. Second, we optimized *in vivo* 2-deoxy, 2-[¹⁸F]fluorodeoxy-glucose positron emission tomography (FDG-PET) and magnetic resonance imaging (MRI) to simultaneously image changes in metabolism, function, and structure in mice subjected to TAC for up to 4 weeks. In this model we established that metabolic remodeling (enhanced glucose uptake) and contractile dysfunction precede structural remodeling (growth and dilation of the left ventricle). In addition, a set of mice underwent *in vivo* aortic banding for molecular and metabolite analyses. Third, we analyzed left ventricular tissue from failing human heart muscle before and after mechanical unloading with a left ventricular assist device to correlate our findings to the failing human heart.

A.2.2. Experimental groups

The experimental groups and conditions are listed in **TABLE A.1**. The animals received standard laboratory chow and water *ad libitum*. A subset of rats received either rapamycin (4 mg/kg per day) or vehicle control (propylene glycol) by oral gavage for 7 days before experimentation. A second subset received either metformin (250 or 500 mg/kg per day) or vehicle control (saline) intraperitoneally for 7 days before experimentation. On day 7, animals were anesthetized with chloral hydrate (300 mg/kg) and anticoagulated with heparin (200 U) immediately before their hearts were isolated and perfused in the working mode as described previously (Taegtmeyer, Hems, Krebs. Biochem J 1980). A third subset of untreated rats hearts were isolated and perfused with metformin (10, 5, 1 mmol/L) added directly to the perfusion buffer.

A.2.3. Isolated working rat heart perfusions

To assess rates of myocardial glucose metabolism in response to increased workload, male Sprague-Dawley rats (387±11 g) were obtained from Harlan Laboratories (Indianapolis, IN) and housed in the Animal Care Center of the University of Texas Medical School at Houston under controlled conditions (23±1°C; 12-hour light/12-hour dark cycle).

Briefly, hearts were perfused as working hearts (Taegtmeyer, Hems, Krebs. Biochem J 1980) in the presence or absence of glucose (5 mmol/L) plus 0.05 µCi/L [2-³H]-glucose to measure rates of glucose uptake and 20 µCi/L [U-¹⁴C]-glucose to measure rates of glucose oxidation. In the absence of glucose, sodium propionate (2

mmol/L) plus lithium acetoacetate (5 mmol/L) were used as a noncarbohydrate substrate (NCS) control. Together these substrates fuel the Krebs cycle without generating any upstream metabolites (Russell, Mommessin, Taegtmeyer. *Am J Physiol* 1995) and sustain cardiac work in the absence of glucose and in the presence of nonmetabolizable glucose analogues (Doenst, Taegtmeyer. *J Nucl Med* 2000). Hearts perfused with NCS were first perfused substrate-free for 15 minutes to deplete endogenous glycogen stores (Goodwin, Taegtmeyer *JBC* 1998). Under steady-state conditions, hearts were perfused at a normal (physiological) workload (afterload set to 100 cm H₂O) for 60 minutes (protocol A). Hearts subjected to a high workload were perfused for 30 minutes at normal workload followed by 30 minutes of perfusion at increased workload (afterload raised to 140 cm H₂O plus 1 μmol/L epinephrine bitartrate added to the perfusate; protocol B). Left atrial pressure was 15 cm H₂O in each perfusion protocol. At 60 minutes the beating hearts were freeze-clamped with aluminum tongs cooled in liquid nitrogen. A portion of frozen heart tissue was weighed and dried to constant weight. The remainder was stored at -80°C for further analyses.

A.2.4 Cardiac power, oxygen consumption, metabolic rates, metabolite concentrations

In *ex vivo* isolated working hearts, coronary and aortic flows were recorded every 5 minutes, and aortic pressures were recorded continuously with a 3F Millar pressure transducer (Millar Instruments, Houston, TX) in sidearm to the aortic cannula linked to a physiologic recorder (Gould Model 2400S, Gould Instruments, Cleveland, OH). Cardiac

power (in milliwatts) was calculated as the product of cardiac output (coronary plus aortic flow, m³/s) and mean aortic pressure (in pascals).

Myocardial oxygen consumption and rates of glucose uptake and oxidation were determined as previously described (Goodwin, Taegtmeyer. JBC 1998; Katz, Dunn. Biochemistry 1967). ATP, ADP, and AMP levels were quantified in freeze-clamped hearts as described previously (Taegtmeyer. JMCC 1985). Glucose 6-phosphate levels were measured by spectrophotometric enzymatic analysis using glucose 6-phosphate dehydrogenase coupled to NADPH production with extinction at 340 nm (Bergmeyer HU. Methods of Enzymatic Analysis 1974).

A.2.5. PET and MRI imaging

Male C57BL/6 mice (8 to 9 weeks of age) obtained from Charles River Laboratories (Raleigh, NC) were subjected to sham operation or transverse aortic constriction to induce pressure-overload hypertrophy by methods previously described (Liao, Takashima. Circ Res 2003). All mice were housed in a 12-hour light/12-hour dark cycle and given standard laboratory chow and water *ad libitum*. Prior to imaging, animals were fasted overnight with access to water. All experiments were performed in compliance with the Guide for the Care and Use of Laboratory Animals, published by the National Institutes of Health, and were conducted under protocols approved by the Animal Care and Use Committee at the University of Virginia.

Left ventricular pressure measurements were performed using a Mikro-tip Catheter Transducer (Model SPR-671, size 1.4F; Millar Instruments Inc, Houston, TX)

connected to Millar and PowerLab hardware and ADI Software (AD Instruments Inc, Colorado Springs, CO). Animals were anesthetized with 3% isoflurane and maintained at 1% to 2% while the catheter was placed in the right carotid artery under stereomagnification and advanced through the aorta so that the tip was positioned in the left ventricle. Heart rate and cardiac pressure were continuously monitored throughout. Body temperature was maintained at 37°C with a warming blanket.

FDG-PET and MRI were sequentially performed in anesthetized animals. PET imaging was performed in a Focus 120 micro PET scanner (Siemens Molecular Imaging Inc, Knoxville, TN) to assess changes in metabolism. The protocol was initiated by injecting 150 to 200 μL of 18.5-37 MBq FDG solution intravenously over a period of 1 minute. Myocardial glucose uptake was assessed using FDG (IBA Molecular, Sterling, VA) at baseline, 1 day, 2 weeks, and 4 weeks after surgery. The net FDG influx constant, K_i (mL/min per gram), was measured over a period of 4 weeks (Locke, Berr, Kundu. *Mol Imaging Biol* 2011). Determination of K_i is considered a robust index of glucose transport and phosphorylation (Nguyen, Mossberg, Taegtmeier. *Am J Physiol* 1990). Therefore, our present work focused on determination of K_i with partial volume and attenuation corrections in vivo. Throughout the procedure, heart rate, respiration, and body temperature were recorded with a physiological recorder (model 1025L; SA Instruments, Inc, Stony Brook, NY), and the ECG was monitored (Blue Sensor, Ambu Inc, Glen Burnie, MD). All the signals were sent to a single SA Instruments software interface, which was configured to trigger data acquisition based on the ECG. The SAI 1025L was also used to maintain the animal's core body temperature at 37°C.

Mice were also imaged using a 7T Bruker-Siemens Clinscan MRI system for structural and functional analyses of the heart. After once again being anesthetized, each mouse was placed prone inside the radiofrequency coil, and the ECG leads were connected to an ECG monitoring module (SA Instruments, Inc, Stony Brook, NY). An ECG-triggered 2-dimensional cine gradient echo pulse sequence was used (Berr, Roy, French. *Magn Reson Med* 2005), with a slice thickness of 1 mm and a zero-filled, in-plane resolution of $100 \times 100 \mu\text{m}^2$. During each session, the entire left ventricle (LV) was imaged with 6 to 7 contiguous short-axis slices. The MR images were analyzed using the ARGUS software package (Siemens Medical Systems, Erlangen, Germany) for left ventricular end-systolic volume, left ventricular end-diastolic volume, and left ventricular ejection fraction was computed from the traced borders. Epicardial contours were also traced at the end-diastolic and end-systolic phases to compute LV mass (Vinnakota, Bassingthwaighe. *Am J Physiol Heart Circ Physiol* 2004). This was divided by the body weight to obtain the heart weight to body weight (HW/BW) ratios.

A.2.6. Transgenic mice overexpressing cardiac-specific isoform of SERCA2a

Transgenic mice overexpressing rat SERCA2a (TG) in heart were produced as described before (He, Giordano, Dillmann. *JCI* 1997). Ascending aortic constriction was performed in both TG and age-matched wild-type mice to induce pressure-overload left ventricular hypertrophy (Pinz, Tian, Ingwall. *JBC* 2011). Mice were studied 8 weeks after surgery. Cardiac function was assessed by M-mode echocardiography.

Subsequently, hearts were freeze-clamped and stored at the temperature of liquid N₂ before extraction at a later time. Sham-operated mice were used as controls.

A.2.7. Tissues from failing human hearts

Cardiac tissue samples were obtained from 11 nondiabetic patients with idiopathic dilated cardiomyopathy (10 were male) referred to the Texas Heart Institute for heart transplantation and placed on left ventricular assist device (LVAD) support for a mean duration of 254±63 days. Tissue from the left ventricular apex was obtained during LVAD implantation and again during LVAD explantation (each patient went on to transplantation). Tissue samples were immediately frozen in liquid nitrogen and stored at -80°C for metabolic and molecular analyses at a later time. **TABLE A.2** provides further detail on the patients assessed in this study. The protocol was approved by the Committee for the Protection of Human Subjects of St. Luke's Episcopal Hospital in Houston, Texas, and of the University of Texas Medical School at Houston.

Gender	10 males, 1 female
Ethnicity	
Mean age	5 Caucasian, 5 African-American, 1 Hispanic
Mean LVEDD before LVAD	48±4 years (range, 19-67)
LVAD	75.33±4.40 mm
Mean LVEDD after LVAD	55.67±3.22 mm
Mean EF before LVAD	21±3%

Table A.2. Clinical Data: Samples from Failing Human Hearts. LVEDD, left ventricular end-diastolic dimension; LVAD, left-ventricular assist device; EF, ejection fraction

A.2.8. Western Blot Analyses

Protein was extracted from frozen heart tissue after homogenization (Polytron, Brinkman Instruments), and Western blot analyses were performed as previously described (Razeghi, Sharma, Taegtmeier. Circ 2003). Antibodies for PI3K, Akt 1/2, TSC2, mTOR, RAPTOR, p70S6K1, 4EBP1, AMP kinase (AMPK), acetyl CoA carboxylase (ACC), phospho-PI3K p85 (Tyr458), phospho-Akt1/2 (Ser473), phospho-TSC2 (Ser939), phospho-TSC2 (Ser1387), phospho-mTOR (Ser2448), phospho-p70S6K (Thr389), phospho-4EBP1 (Thr70), phospho-AMPKinase (Thr172), phospho-ACC (Ser79), and phospho-RAPTOR (Ser792) were obtained from Cell Signaling (Beverly, MA). GAPDH was used to normalize for protein loading (Research Diagnostics, Flanders, NJ). Densitometry was performed with ImageJ program provided by the NIH. For clarity, densitometry values (mean±SEM) are presented for all blots collectively following the figures.

A.2.9. RNA Extraction and qRT-PCR

For transcriptional analysis, total RNA was extracted with TRI Reagent (Molecular Research Center, Cincinnati, OH) and treated for genomic DNA contamination with DNA-*free* (Applied Biosystems/Ambion, Austin, TX). RNA concentration was measured with a NanoDrop 1000 Spectrophotometer (Thermo Scientific, Wilmington DE). Absolute quantification of transcripts was based on known amounts of synthetic DNA standard (Integrated DNA Technologies, Coralville, IA).

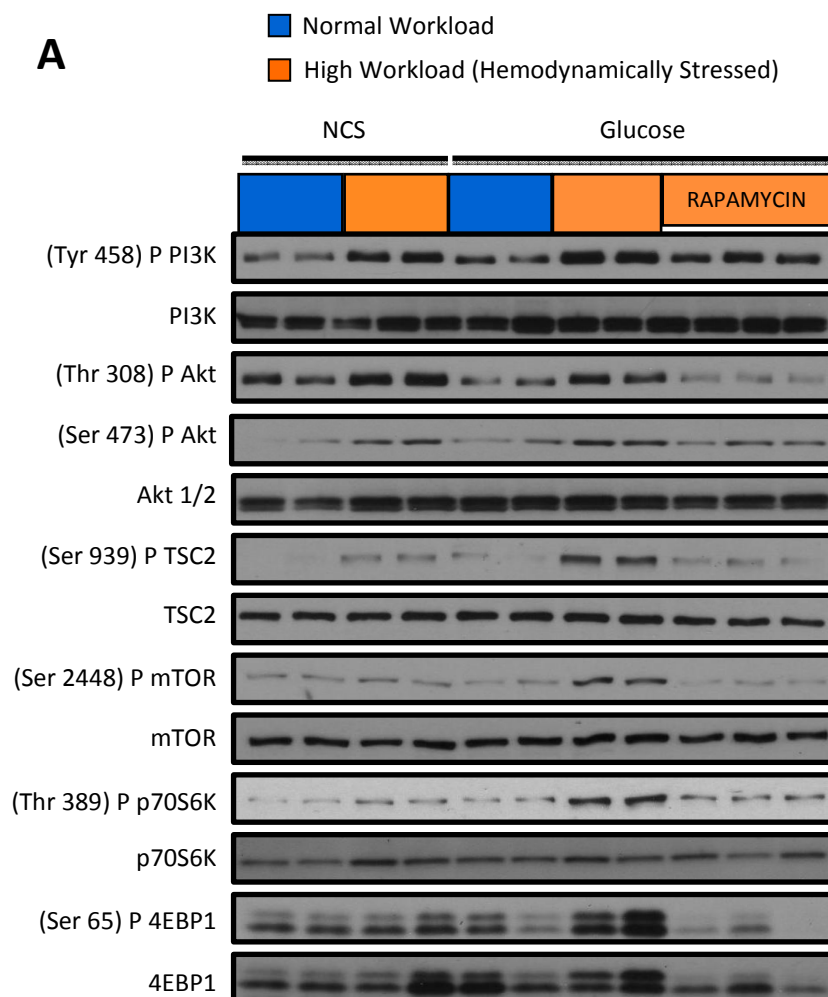
A.3 Results

A.3.1. mTORC1 Activation and Impaired Cardiac Power With Increased Workload

Irrespective of the substrate present in the perfusate, increased workload alone induced phosphorylation of PI3K, and Akt at both Thr308 and Ser473 (Figure A.1A). However, strong phosphorylation of TSC2, mTOR, p70S6K, and 4EBP1 was observed only in the presence of glucose at high workload. Rapamycin pretreatment of the rats for 1 week inhibited phosphorylation of Akt at both Thr308 and Ser473, TSC2, mTORC1, p70S6K, and 4EBP1. mTORC1 signaling was not activated in hearts perfused either at normal workload with glucose or at increased workload in the absence of glucose.

To determine the functional consequence of mTORC1 activation, we measured cardiac power in hearts from vehicle-treated and rapamycin-treated rats perfused with

glucose or non-carbohydrate substrate (NCS) (Figure 1B). At normal workload, there was no significant difference in mean cardiac power between the experimental groups. When subjected to increased workload, all perfused hearts demonstrated an increase in cardiac power relative to their normal workload values. However, in the vehicle-pretreated group, hearts perfused with glucose as the only substrate did not increase their cardiac power to the same extent as the other 2 groups. Because this differential effect of glucose on cardiac power was mitigated by pretreatment with rapamycin, the difference is most likely mTORC1 dependent.



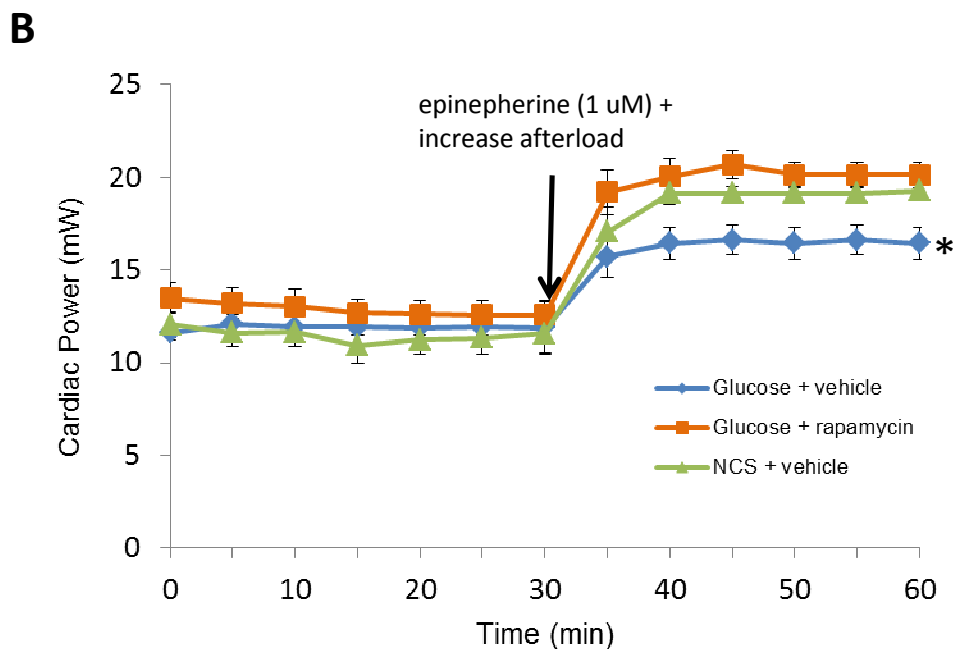


Figure A.1. At high workload, glucose activates mTORC1 and impairs cardiac power in perfused rat hearts. Pretreatment of animals with rapamycin inhibits mTORC1 and rescues contractile function. A, Representative Western blots of the mTORC1 signaling pathway in hearts freeze-clamped at the end of perfusion. High workload resulted in phosphorylation of PI3K and Akt in all hearts. However, phosphorylation of TSC2, mTOR, and p70S6K at high workload occurred only in the presence of glucose. Pretreating rats for 7 days with rapamycin (4 mg/kg per day) before perfusion of the heart resulted in decreased phosphorylation of Akt, TSC2, mTOR, and its downstream targets. B, At normal workload there was no difference in cardiac power among the 3 groups. At high workload the presence of the glucose substrate decreased cardiac power in hearts from vehicle-treated rats. Pretreatment of rats with rapamycin for 7 days rescued cardiac performance in glucose-perfused hearts. Data shown are mean \pm SEM; n=5 to 7 for each group. * p <0.05 (Mann–Whitney rank sum test) for hearts from vehicle-treated rats perfused with glucose in comparison with hearts from vehicle-treated rats perfused with NCS and those from rats pretreated with rapamycin and perfused with glucose at high workload. mTOR indicates mammalian target of rapamycin; TSC2, tuberlin; NCS, noncarbohydrate substrate.

A.3.2. Oxygen Utilization and Mitochondrial Efficiency Were Not Affected By Increased Workload or Rapamycin Treatment

To evaluate whether the differences in cardiac power were the result of changes in efficiency, we also measured oxygen consumption in groups at comparable workloads. There was no difference in oxygen consumption (Figure A.2A) or efficiency (Figure A.2B) between groups at comparable workloads.

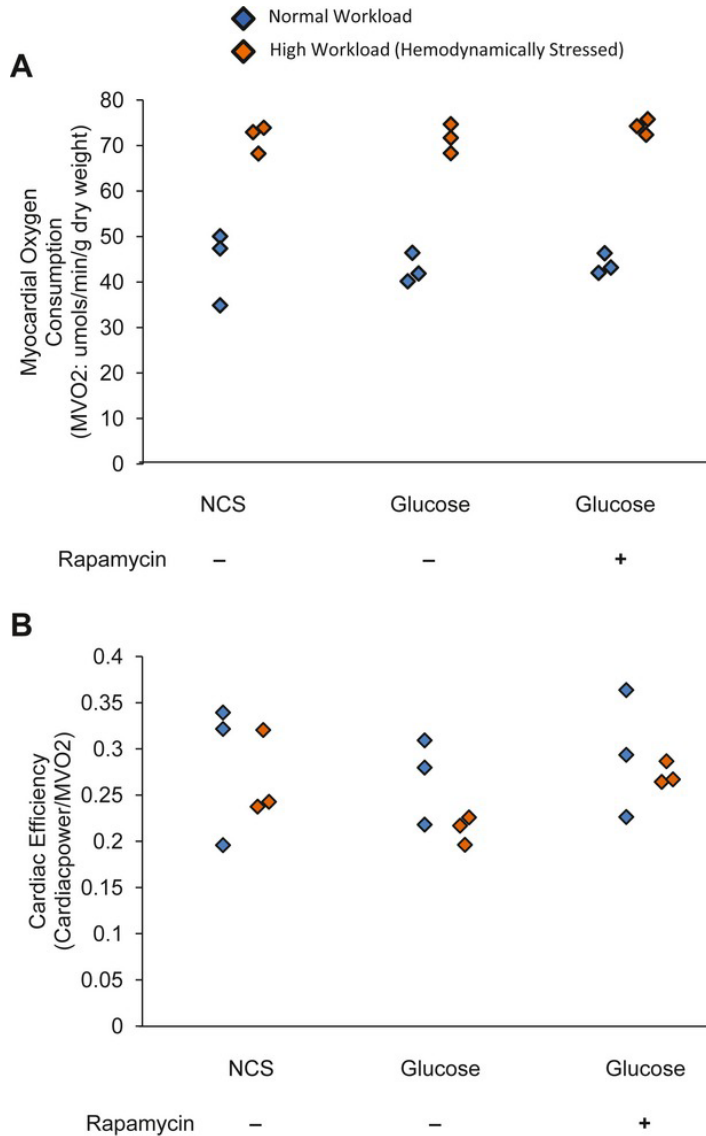


Figure A.2. Pretreatment with rapamycin has no effect on cardiac efficiency in rat hearts perfused with glucose at high workload. A, Myocardial oxygen consumption (MVO₂) at low and high workloads did not differ in hearts perfused with noncarbohydrate substrate (NCS) and in hearts from rats pretreated with vehicle or with rapamycin and perfused with glucose. B, Cardiac efficiency, as calculated by dividing cardiac power by MVO₂, was also unchanged. The dot plots show individual measurements for each heart at 2 different workloads. Comparison within each group and between groups showed no significant difference ($p>0.05$).

We also measured UCP3. Both mRNA (Figure A.3A) and protein (Figure A.3B) levels of UCP3 were unchanged with rapamycin treatment or increased workload, suggesting that mitochondrial efficiency was also unchanged with rapamycin pretreatment (2 to 3 repeated measures for each animal). We also noted that under all experimental conditions the adenine nucleotide levels (ATP, ADP, and AMP) did not differ significantly despite differences in mTORC1 activity and contractile function (data not presented). This is in keeping with our earlier observation that the levels of ATP, ADP, and AMP as well as total adenine nucleotides do not change with increased workload of the perfused heart (Taegtmeyer. JMCC 1985).

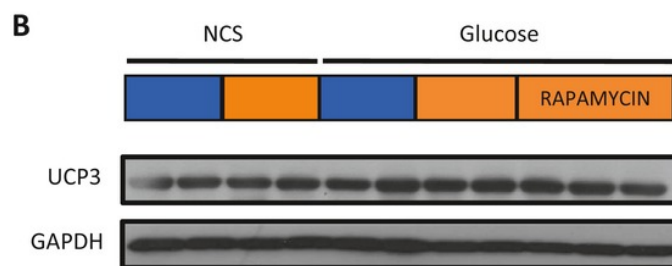
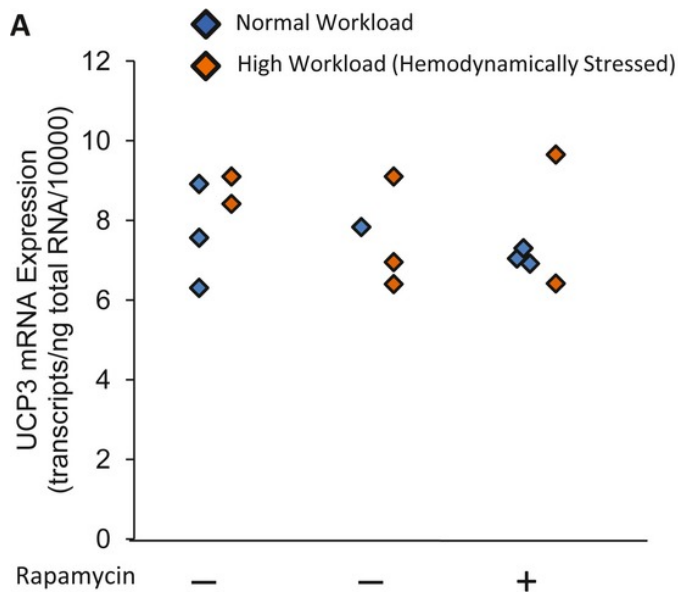


Figure A.3. Uncoupling protein 3 (UCP3) mRNA and protein levels are not associated with G6P-mediated mammalian target of rapamycin (mTOR) activation. A, Transcript analysis of *UCP3* gene expression in isolated working rat hearts. The dot plots show median values for n=2 to 3 rat hearts with 2 to 3 repeats per animal. $P>0.05$ for all comparisons based on Friedman test on repeated measurements of all hearts in each group compared with hearts perfused with noncarbohydrate substrate (NCS) at a normal workload. Neither workload nor glucose in the perfusate nor pretreatment of mice with rapamycin changed UCP3 mRNA expression at the end of perfusion. B, Compared with hearts perfused with NCS at a normal workload, neither workload, glucose, nor rapamycin pretreatment changed UCP3 protein levels

A.3.3. Glucose 6-Phosphate (G6P) and mTOR Activation

To elucidate possible mechanisms of glucose-mediated mTORC1 activation, rates of glucose uptake and oxidation were simultaneously quantitated in *ex vivo* hearts.

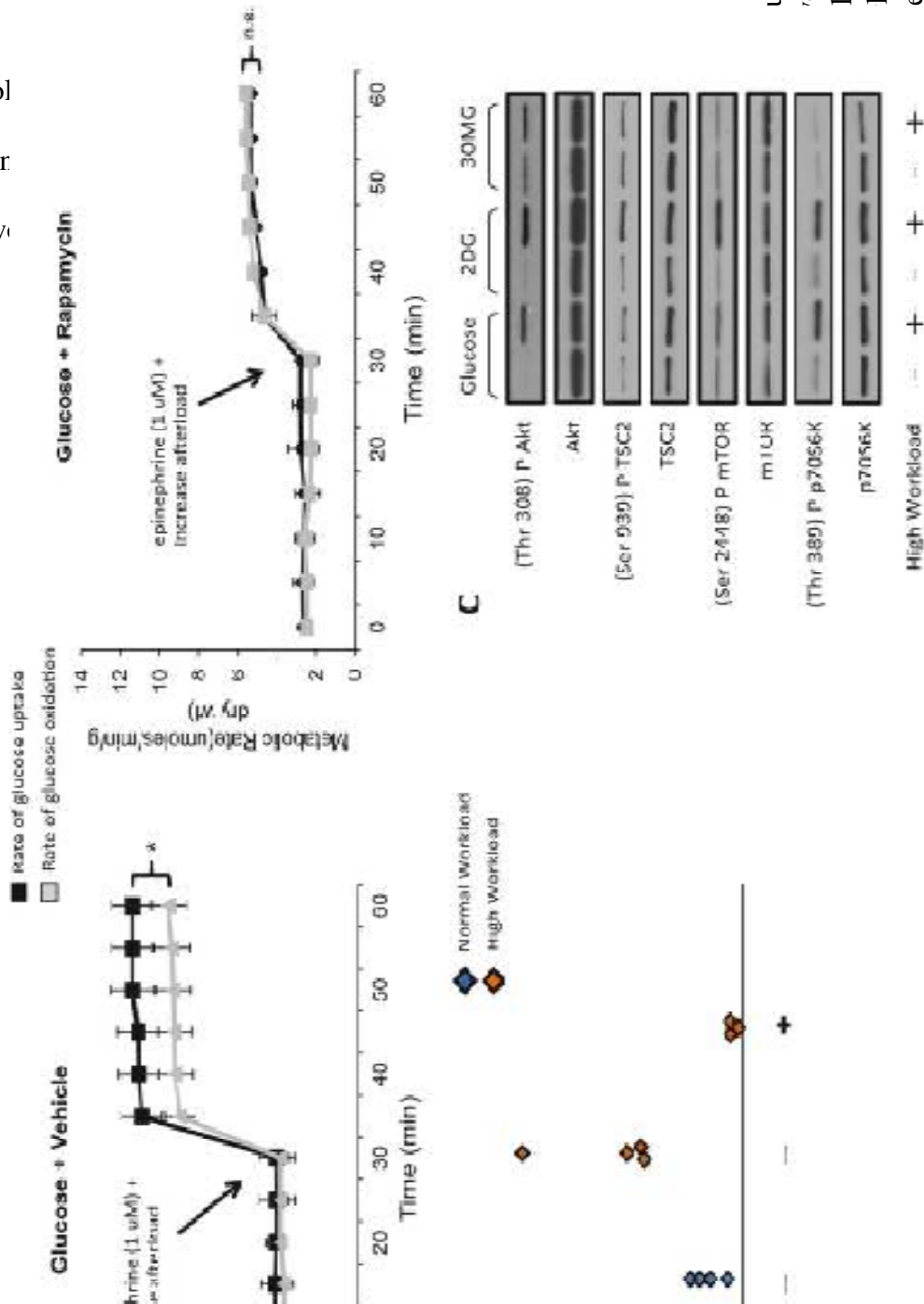
At normal workload, rates of glucose uptake (4.2 ± 0.7 $\mu\text{mol}/\text{min}$ per gram dry weight) matched rates of glucose oxidation (3.9 ± 0.7 $\mu\text{mol}/\text{min}$ per gram dry weight). However, when the workload was increased, rates of glucose uptake (11.5 ± 0.8 $\mu\text{mol}/\text{min}$ per gram dry weight) exceeded rates of glucose oxidation (9.5 ± 0.6 $\mu\text{mol}/\text{min}$ per gram dry weight) by $>10\%$. Rapamycin pretreatment reduced rates of glucose uptake and rates of glucose, correcting the mismatch between glucose uptake and oxidation (Figure A.4A). Lactate production, an indirect measure of glycolytic activity, was unchanged in both groups (data not shown).

Because mTORC1 activation was associated with a suggested mismatch between glucose uptake and oxidation, we investigated whether the accumulation of glucose or one of its metabolites was associated with mTORC1 activation. G6P levels were 4-fold higher on average in hearts subjected to an acute increase in workload (4.8 ± 1.0 nmol/mg protein) compared with hearts perfused at normal workload (1.3 ± 0.2 nmol/mg protein). Rapamycin pretreatment severely reduced the tissue content of G6P (0.36 ± 0.1 nmol/mg protein) in hearts perfused with glucose at increased workload (Figure A.4B). In contrast, levels of other glycolytic intermediates were unchanged at high workload (data not shown).

To assess whether hexose-6-phosphate accumulation leads to load-induced mTORC1 activation, we next perfused 2 groups of hearts with either of the 2 glucose analogues: 3-O-methylglucose (which is transported in and out of the cardiomyocyte, but not metabolized), or 2-deoxyglucose (which is taken up by the cardiomyocyte, phosphorylated, and trapped as a G6P analogue and not further degraded) (Doenst and Taegtmeyer. *J Nucl Med* 2000). 2-Deoxyglucose, but not 3-O-methylglucose, increased

phosphorylation of TSC2, mTOR, and its downstream targets in hearts perfused at high workload (Figure A.4C). mTOR and its downstream targets were not phosphorylated in hearts perfused with either glucose analogue at normal workload. These experiments provided strong evidence that hexose phosphate levels are associated with mTORC1 activation in hearts subjected to increased workload.

physiol
 combir
 high w



ulates,
 vehicle
 glucose
 glucose
 e G6P

observed when rats were pretreated with rapamycin. Dot plots show G6P levels for each heart. Kruskal–Wallis test
 .. C. To test the hypothesis that hexose-6-phosphate (and no other glucose metabolite) activates mTOR, we also
 CS plus 2-deoxyglucose or 3-O-methylglucose. Representative Western blots of Akt, TSC2, mTOR and p70S6K
 earts perfused with glucose (5 mmol/L) or NCS plus the glucose analogues 2-deoxyglucose (2DG; 5 mmol/L), or
 DMG; 5 mmol/L) at either normal or high workload are shown. Glucose or 2DG, but not 30MG, increased
 2, mTOR, and p70S6K at high workload. mTOR indicates mammalian target of rapamycin; TSC2, tuberlin; NCS,
 ate

although not quite statistically significant, hearts perfused with this “physiological” mix of substrate at high workload displayed a 2.5-fold increase on average in G6P levels (Figure A.5A) and increased phosphorylation of both downstream targets of mTORC1, p70S6K and 4EBP1 (Figure A.5B) compared with hearts perfused with NCS. Phosphorylation of the mTORC1 targets are similar between hearts perfused with physiologic substrates and glucose alone.

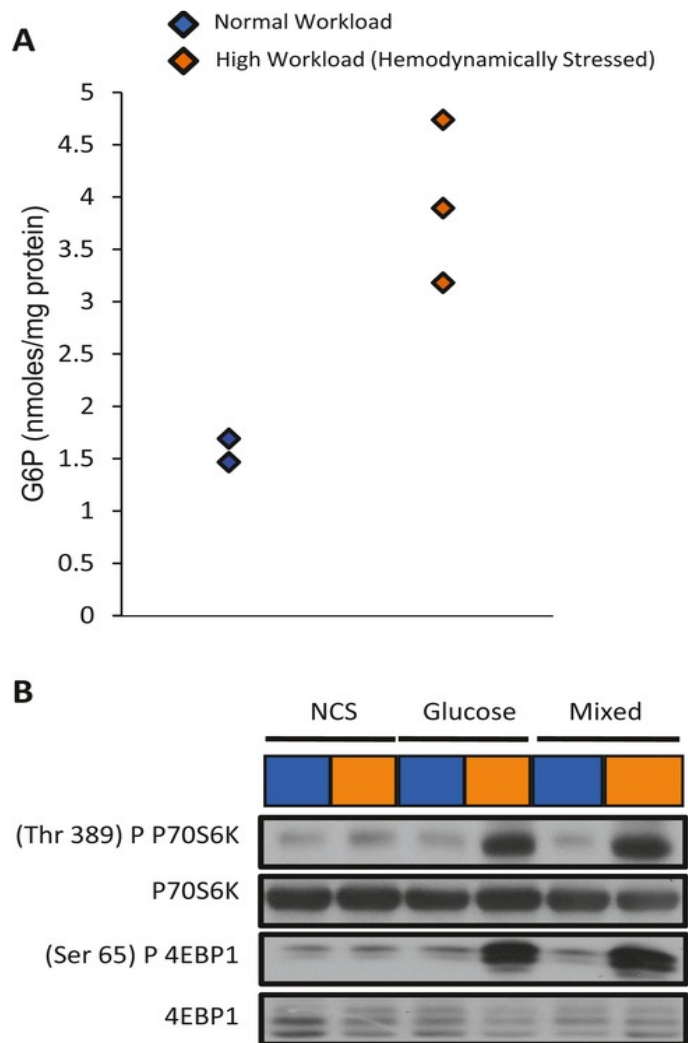


Figure A.5. In the presence of mixed substrates (glucose, NCS, and oleate), G6P levels are increased and mTORC1 signaling is activated at high workload. A, G6P accumulates in hearts perfused with glucose, oleate, and NCS. Dot plot shows G6P levels for each heart at the end of perfusion at low or high workload; $p=0.083$ using Mann–Whitney test.

B, Representative Western blots showing phosphorylation of mTORC1 targets p70S6K and 4EBP1 in *ex vivo* working rat. Both glucose and mixed substrates in the perfusate increased p70S6K and 4EBP1 phosphorylation. NCS indicates noncarbohydrate substrate; mTOR, mammalian target of rapamycin; G6P, glucose 6-phosphate.

A.3.4. G6P-Dependent mTOR Activation and AMPK Downregulation

Next we investigated the effect of enzyme 5'-AMP activated protein kinase (AMPK), an enzyme with a dual role in signaling and metabolic regulation. AMPK is upstream of TSC2 and mTORC1 and regulates fuel supply and substrate metabolism in the heart. When phosphorylated at Thr172, AMPK phosphorylates and inhibits acetyl-CoA carboxylase (ACC), which is also used as a marker of AMPK activation. AMPK also phosphorylates TSC2 (Ser1387) and RAPTOR (Ser792) to inhibit mTORC1. Neither increased workload nor glucose alone was associated with a change in AMPK phosphorylation (Figure 6A). However, perfusion at increased workload with glucose resulted in downregulation of phospho-AMPK (Thr172), phospho-ACC (Ser79), and phospho-TSC2 (Ser1387). Pretreating animals with rapamycin prevented the downregulation of AMPK, ACC, and TSC2 phosphorylation with increased workload and glucose as the only substrate. RAPTOR (Ser792) phosphorylation was unchanged with workload or rapamycin treatment (Figure A.6A).

To determine the functional consequences of AMPK activation, hearts from rats pretreated with metformin (500 mg/kg per day for 7 days IP) to pharmacologically activate AMPK underwent *ex vivo* working heart perfusions. Metformin restored cardiac power by 26% in hearts perfused with glucose substrate at increased workload (Figure A.6B); 2 time points were statistically significant (denoted by asterisks in the figure).

To examine whether changes in glucose metabolism secondary to AMPK activation were associated with the restoration of cardiac power, rates of glucose uptake and oxidation were quantitated. Systemic metformin pretreatment did not change rates of glucose uptake (11.7 ± 1.1 $\mu\text{mol}/\text{min}$ per gram dry weight) in perfused hearts subjected to high workload, but it improved rates of glucose oxidation (11.0 ± 0.7 $\mu\text{mol}/\text{min}$ per gram dry weight) (Figure A.6C) and blunted G6P accumulation (2.1 ± 0.1 nmol/mg protein) compared with vehicle-pretreated animals (Figure A.6D). To further determine whether AMPK mediates glucose-dependent mTORC1 activation, animals were treated with the AMPK activator metformin for 7 days (500 or 250 mg/kg per day IP) before perfusion with glucose at high workload. Systemic treatment with metformin prevented AMPK downregulation and inhibited mTOR activation in hearts perfused with glucose at high workload (Figure A.6E). Metformin treatment had no effect on mTOR phosphorylation or on cardiac power in hearts perfused at physiologic workload (data not shown). To circumvent systemic or off-target effects of metformin, we also perfused hearts of untreated animals with buffer containing metformin. The perfusion of hearts with buffer containing metformin demonstrated that metformin prevented AMPK downregulation and inhibited mTORC1 activation in a dose-dependent manner (Figure A.6E).

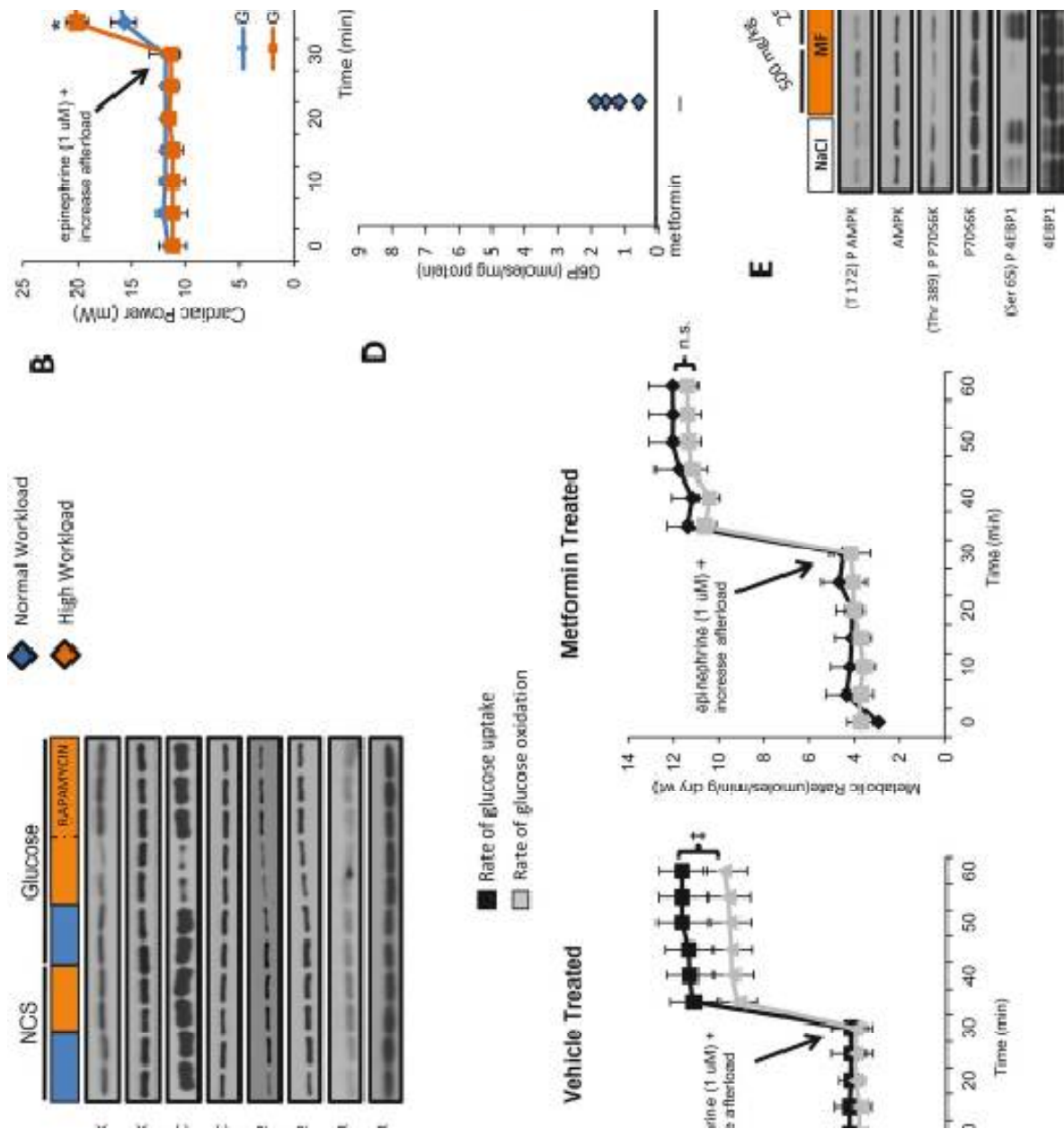


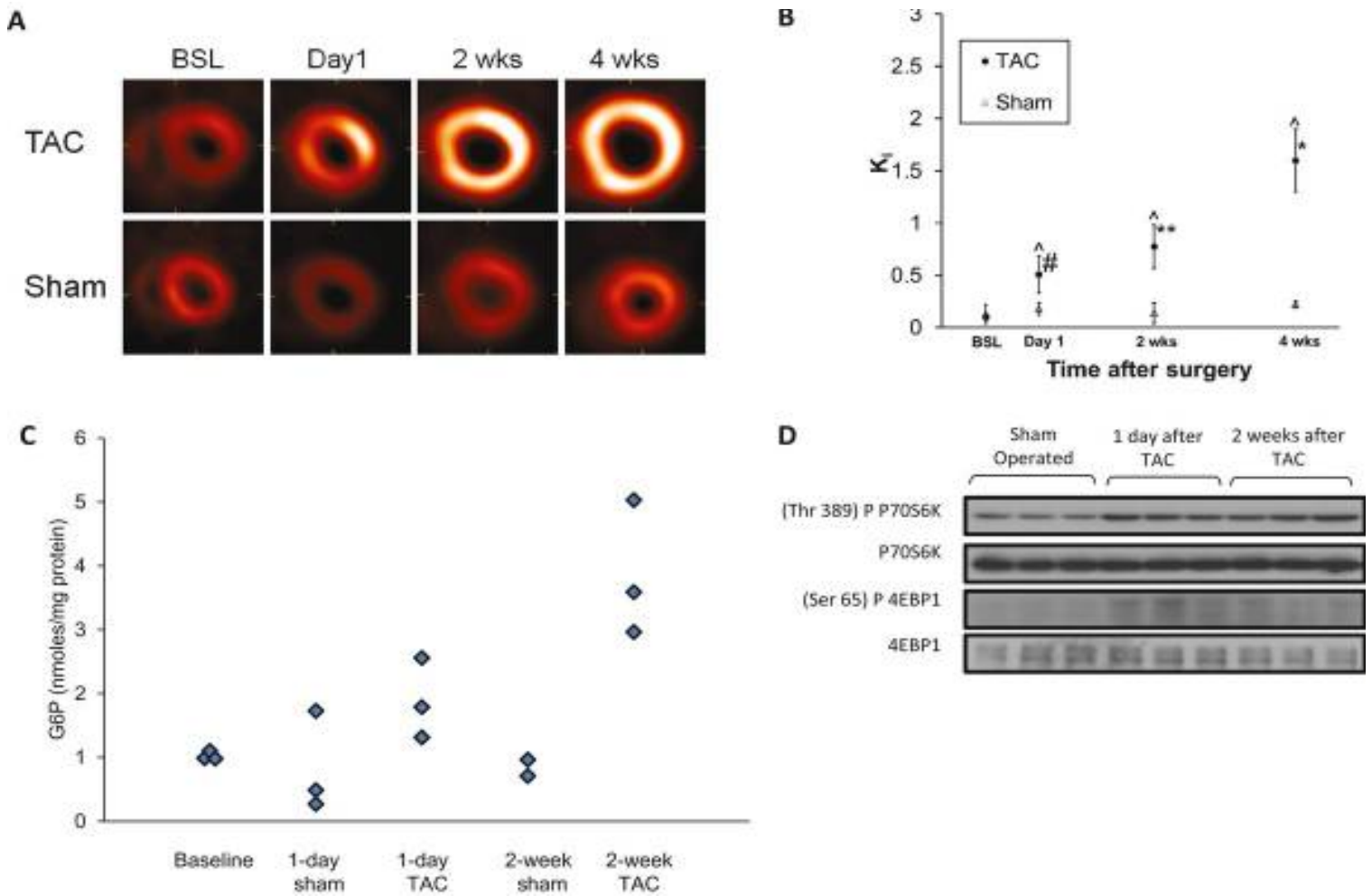
Figure A.6. G6P-dependent mTOR activation is associated with downregulation of AMPK. A, Representative Western blots demonstrate reduction in phosphorylation of AMPK (T172) and ACC (S79), its downstream target, in hearts perfused with glucose at high workload. B, Contractile performance in the working heart perfused with glucose in the presence and absence of metformin. Data shown are mean±SEM; n=5 to 7 for each group. Metformin improves cardiac power at high workload. * $P<0.05$, # $p=0.08$, using Mann–Whitney rank sum test. C, Rates of glucose uptake and oxidation by hearts from animals receiving vehicle or metformin pretreatment for 7 days (vehicle treated, metformin treated). Data shown are mean±SEM; n=5 to 6 per group. Metformin treatment did not change rates of glucose uptake and oxidation at normal workload. At high workload, pretreating animals with metformin corrected the mismatch between rates of glucose uptake and oxidation. ‡ $p=0.021$ using Mann–Whitney rank sum test. D, G6P levels in hearts from rats receiving either vehicle or metformin for 7 days before

perfusion of their hearts with glucose as the only substrate. Dot plots of G6P show individual measurements for each heart at normal and high workloads. G6P accumulation was reduced in stressed hearts perfused with glucose in hearts of animals pretreated with metformin. Kruskal–Wallis test yielded an overall $p=0.012$. E, Representative Western blots demonstrating increased AMPK phosphorylation and decreased p70S6K as well as 4EBP1 phosphorylation in hearts from animals pretreated for 7 days with metformin (500 or 250 mg/kg) and perfused with glucose at high workload or in hearts from untreated animals perfused with glucose plus metformin at high workload. The concentrations of metformin in the perfusate were (a) 10 mmol/L, (b) 7.5 mmol/L, or (c) 5 mmol/L. mTOR indicates mammalian target of rapamycin; AMPK, AMP kinase; ACC, acetyl-CoA carboxylase; G6P, glucose 6-phosphate; MF, metformin.

A.3.5. Metabolic, Structural, and Signaling Remodeling in Response to Increased Workload *In Vivo*

We wondered whether the findings observed *ex vivo* correlate with hearts subjected to pressure overload *in vivo*. In mice subjected to aortic constrictions (TAC), transverse end-diastolic mid-ventricular positron emission tomography (PET) images indicated an increase in 2-deoxy,2-fluoro-d-glucose (FDG) uptake beginning 1 day after transverse aortic constriction (TAC), which increased further and was sustained over 4 weeks (Figure A.7A). Sham-operated animals showed no change in FDG uptake over the same period. Quantitatively, a 5-fold increase in the rate of myocardial FDG uptake, K_i (mL/min per gram), a specific measurement of metabolic remodeling, was observed 1 day after TAC using a 3-compartment model (Figure A.7B). The rate of FDG uptake continued to increase (1.5- to 3.2-fold) over time from 1 day to 4 weeks. Calculated K_i at baseline (0.11 ± 0.03) agreed well with the measured K_i (0.14 ± 0.06) obtained from arterial blood samples used for input function estimation. No significant difference in K_i values was observed over 4 weeks in shams. In addition, we assessed G6P levels in

these hearts 1 day and 2 weeks after TAC to corroborate the metabolic remodeling observed with PET imaging. We observed a slight increase in G6P levels 1 day after TAC, and the increase was more pronounced 2 weeks after TAC (Figure A.7C). To determine the association between the increased G6P levels and mTORC1 activation *in vivo*, we assessed G6P levels and mTORC1 signaling 1 day and 2 weeks after TAC. Representative Western blots demonstrated an apparent increase in p70S6K and 4EBP1



phosphorylation at both time points (Figure A.7D).

Figure A.7. Metabolic remodeling and mTOR activation precede structural remodeling in hearts subjected to high workload *in vivo*. A, Representative serial transverse, end-diastolic PET slices for TAC and sham-operated mice 1 day, 2 weeks, and 4 weeks

after surgery. One day after TAC, there was an increase in FDG uptake that increased further over 4 weeks. B, Quantification of the rate of cardiac FDG uptake (K_i) of PET images from all TAC (n=8) and sham-operated (n=5) mice. Data shown are mean \pm SEM. K_i in TAC mice demonstrated a 5-fold increase in FDG uptake on day 1 and a 1.5- to 3.2-fold increase from day 1 to 4 weeks. Sham-operated mice showed no significant change in FDG uptake over 4 weeks. Comparisons at different times within TAC group: day 1 vs baseline (BSL), # p <0.05; 2 weeks vs BSL or day 1, ** p <0.05; 4 weeks vs BSL, day 1, or 2 weeks, * P <0.001. Comparisons between TAC and sham groups at the same points, ^ p <0.05. C, Tissue G6P levels in hearts after TAC or sham operation at baseline and after 1 day and 2 weeks. Dot plots of G6P levels for each group; n=6 for TAC and n=5 for sham. G6P levels were 2.3- and 4.6-fold higher compared with sham-operated animals 1 day and 2 weeks after TAC, respectively. Kruskal–Wallis test yielded overall p =0.0356. D, Representative Western blots demonstrated an increase in p70S6K and 4EBP1 phosphorylation 1 day and 2 weeks after TAC. mTOR indicates mammalian target of rapamycin; PET, positron emission tomography; TAC, transverse aortic constriction; FDG, 2-deoxy, 2[¹⁸F]fluorodeoxy-glucose.

A.3.6. Structural and Functional Remodeling in Response to Increased Workload

In Vivo

Although significant change in metabolic remodeling was observed starting 1 day after TAC, there was no appreciable change at this early time in the heart weight to body weight ratio (HW/BW; Figure 8A). On day 1 there was a small increase in wall thickness. However, the increase in left ventricular pressure was accompanied by a much greater increase in the rate of glucose uptake (Figure 7A) and a decrease in the ejection fraction (Figure 8E). Thus, profound changes in cardiac metabolism were accompanied by functional changes (decreased ejection fraction), whereas the structural changes were small in the acute period. **TABLE A.3** summarizes additional metabolic, functional, and structural parameters measured 1 day after TAC.

Parameter	Baseline	Day 1	Change (%)	n	P Value
K _i	0.10	0.51	407.67	8	0.011
Ejection fraction, %	53.77	42.5	-20.9	8	0.011
HW/BW	3.54	3.89	9.89	5	NS
Wall thickness, mm	0.9	1.0	11.1	5	0.043
Heart rate, bpm	406.8	470.8	15.7	5	NS
LV systolic pressure, mm Hg	83.95	119	41.8	3	NS

TABLE A.3. Comparison of baseline and day 1 values for different parameters among TAC mice. P-values were obtained using the Wilcoxon signed rank test. Change (%) indicates average change from baseline to day 1 in each of the measured corresponding parameters; “n” indicates number of animals used in each of the measured corresponding parameters; TAC, transverse aortic constriction; HW/BW, heart weight to body weight ratio; LV, left ventricle.

To see whether functional and structural changes accompany metabolic and cell signaling changes after TAC, end-diastolic wall thickness, end-diastolic volume (EDV), end-systolic volume (ESV), and ejection fraction (EF) were followed for a period up to 4 weeks. 2 and 4 weeks after TAC, the HW/BW had increased by 1.4- and 1.7-fold, respectively (Figure A.8A). Similarly, end-diastolic wall thickness increased significantly (Figure A.8B). Increases in the ESV (Figure A.8C) and EDV (Figure A.8D) and significant decreases in the EF (Figure A.8E) followed the metabolic changes seen 1 day after TAC. Both the ESV and EDV (Figure A.8C and D) progressively increased 2 and 4 weeks after TAC. Subsequently, the EF continued to decrease 1.4- and 1.6-fold 2 and 4 weeks after TAC, respectively. No significant changes in HW/BW, wall thickness, EDV, ESV, or EF were observed in sham-operated animals over 4 weeks.

Taken together, the in vivo imaging experiments support the hypothesis that metabolic, signaling, and functional changes precede or accompany structural changes in pressure overload-induced left ventricular hypertrophy (LVH).

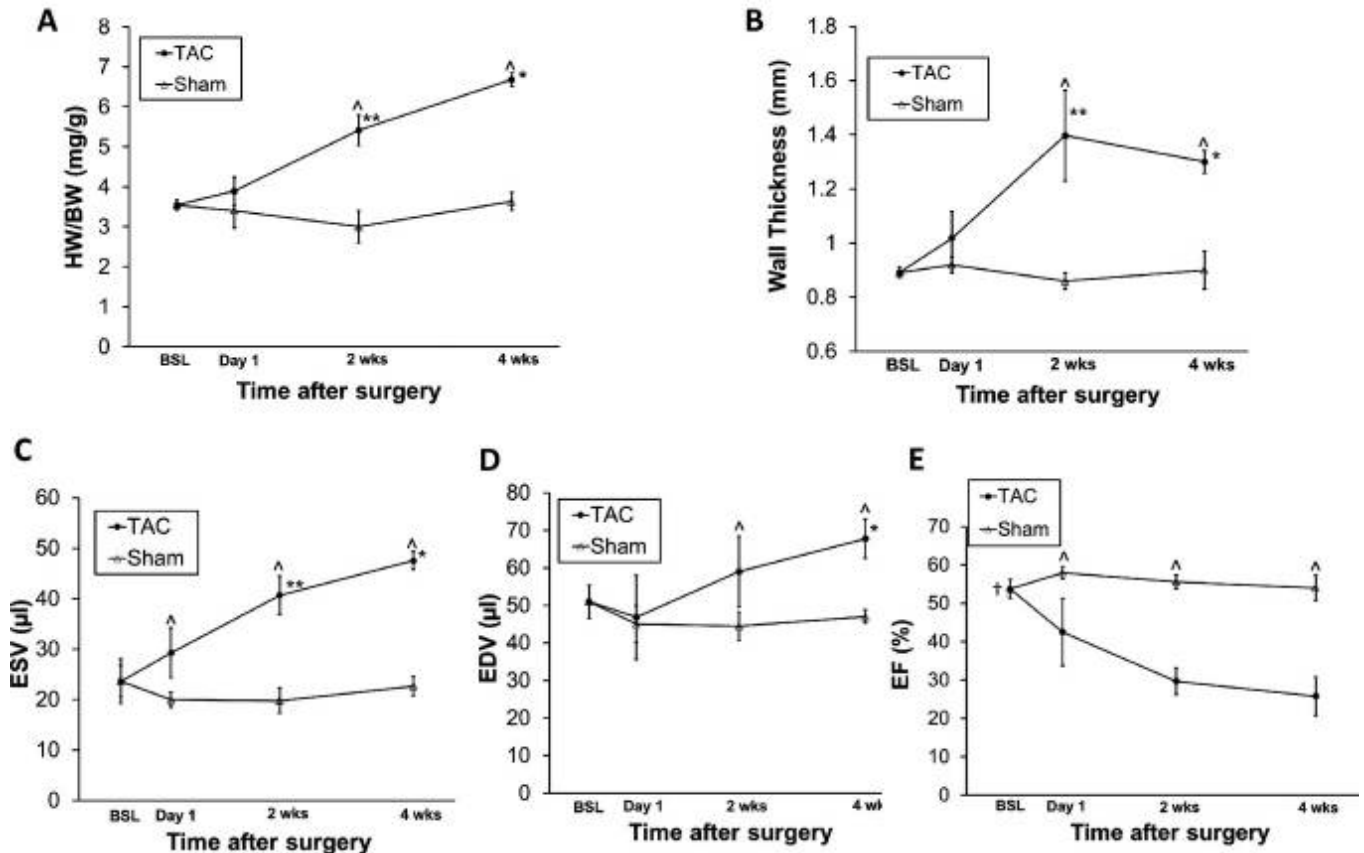


Figure A.8. *In vivo* structural and functional changes accompany metabolic changes in response to pressure overload. Data shown are mean±SEM; n=8 for TAC and n=5 for shams. A, Ratio of heart weight (HW) measured using MRI and body weight (BW). HW/BW ratio remained unchanged 1 day after TAC, but increased by 1.4- and 1.7-fold between day 1 and 4 weeks, respectively. HW/BW showed no significant change over 4 weeks in sham-operated mice. B, End-diastolic wall thickness measured *in vivo* using MRI. Wall thickness was unchanged 1 day after TAC, but increased about 1.4-fold between day 1 and 4 weeks. Wall thickness showed no significant change over 4 weeks in sham-operated mice. End-systolic volume (ESV; C), end-diastolic volume (EDV; D), and resultant ejection fraction (EF; E) assessed *in vivo* using MRI imaging. An increase in ESV and decline in EF occurred 1 day after TAC. Sham-operated mice exhibited no significant change in EDV, ESV, and EF over 4 weeks. Comparisons at different times in the TAC group: day 1 vs baseline (BSL), # $P<0.05$; 2 weeks vs BSL or day 1, ** $P<0.05$; 4 weeks vs BSL or day 1, * $P<0.01$; BSL vs day 1, 2 weeks, and 4 weeks, † $P<0.05$. Comparisons between TAC and sham groups at the same points, ^ $P<0.05$. Two-way repeated-measures ANOVA analyzed, and Holm-Sidak post hoc test performed to obtain individual significance factors. TAC indicates transverse aortic constriction.

A.3.7. Failing Human Hearts Before and After Unloading With a Left Ventricular Assist Device (LVAD)

Finally, we assessed whether the findings in rodent heart had any relevance in the failing human hearts of patients with nonischemic idiopathic dilated cardiomyopathy receiving a left ventricular assist device to unload the heart as bridge to transplant. Changes in energy substrate metabolism have been observed in failing human hearts (Razeghi, Taegtmeier. *Circ* 2001; Razeghi, Taegtmeier. *Cardiology* 2002). We noted that G6P levels dramatically decreased after mechanical unloading (Figure A.9A), and to investigate whether changes in cardiac glucose metabolism accompanied changes in mTORC1 activation in the human hearts, we assessed the downstream targets of mTORC1 activity by the phosphorylation status of p70S6K and 4EBP1. Phosphorylation of p70S6K and 4EBP1 (Figure A.9B) decreased after mechanical unloading with an LVAD, suggesting that tight coupling of glucose uptake and oxidation with mechanical unloading led to decreased mTORC1 activity.

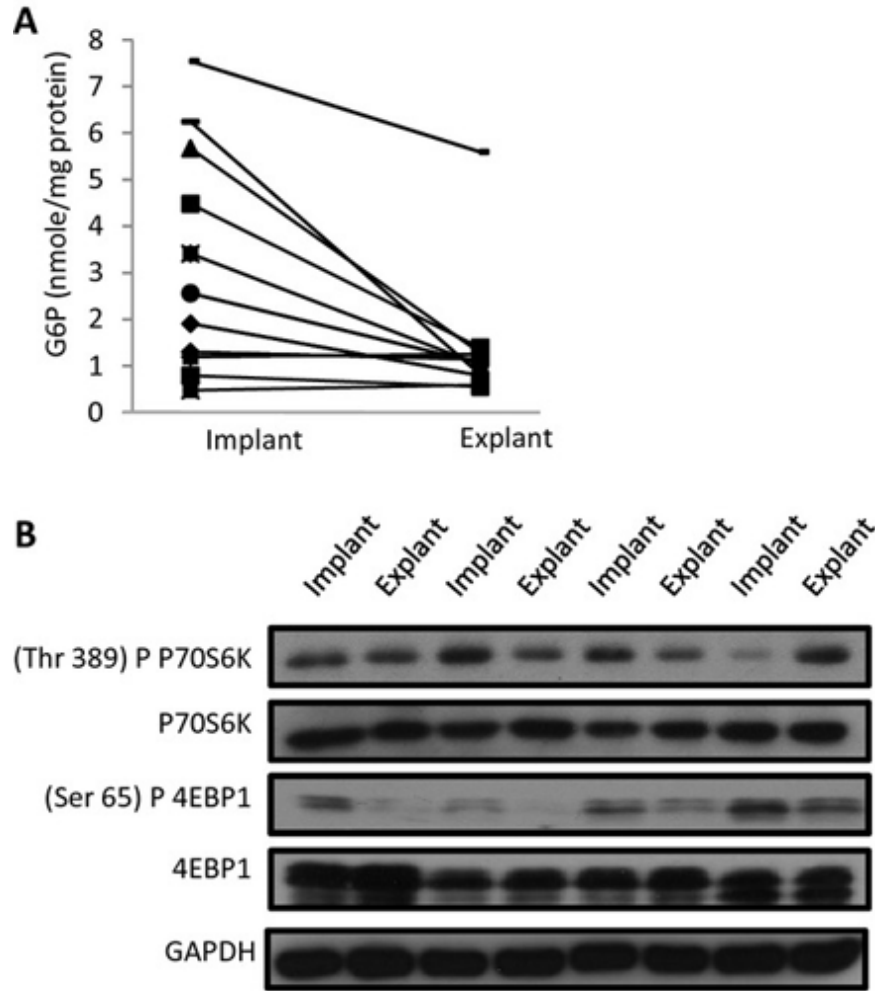
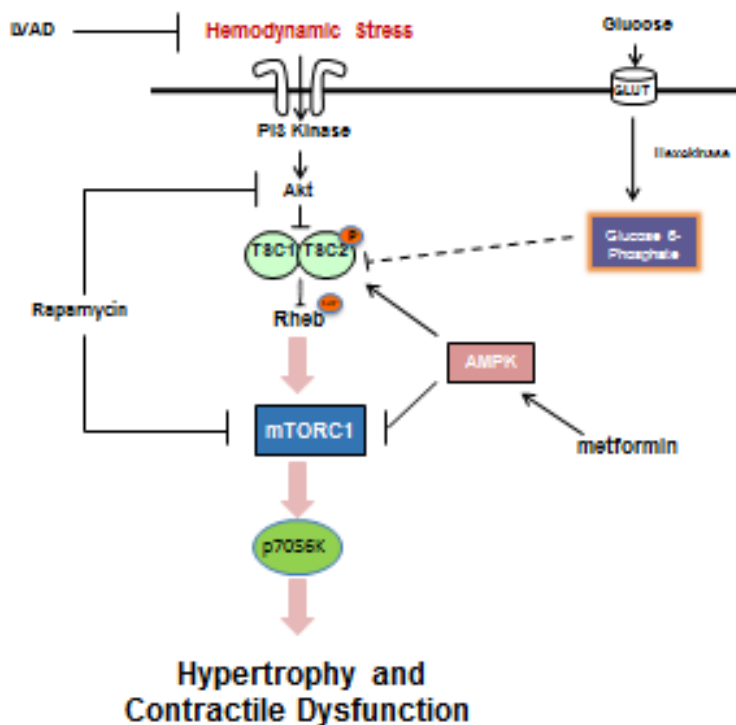


Figure A.9. Mechanical unloading of failing human hearts results in reduced G6P accumulation and reduced mTORC1 activation. A, Tissue G6P levels for individual patients with idiopathic dilated cardiomyopathy before and after mechanical unloading; $n=11$ paired samples, $p<0.05$ using paired t test. B, Representative Western blots of p70S6K and 4EBP1 before and after mechanical unloading. Each “implant” refers to time of LVAD implantation and “explant” refers to removal of post-LVAD heart at the time of transplantation. Each adjacent “implant” and “explant” constitute 1 patient's heart—4 total patients. G6P indicates glucose 6-phosphate.

A.4 Discussion

We set out to test the hypothesis that a metabolic signal links hemodynamic stress with activation of the mTOR pathway. Our main findings are summarized in Figure A.10 and include the following points. (1) Doubling the workload of rat hearts perfused *ex vivo* with glucose as the only substrate increases rates of myocardial glucose uptake beyond the hearts' oxidative capacity, resulting in G6P accumulation, which mediates load-induced mTOR activation. (2) Load-induced mTOR activation impairs cardiac power and induces ER stress response in a glucose-dependent manner. Administration of rapamycin or metformin *in vivo* rescues cardiac power. (3) Correcting the mismatch between glucose uptake and oxidation in the stressed heart prevents G6P accumulation and rescues contractile function in hearts subjected to pressure overload. (4) In hearts subjected to increased workload, metabolic remodeling precedes structural remodeling of the heart and accompanies load-induced contractile dysfunction. (5) In the failing human heart, mechanical unloading decreases levels of G6P and reduces mTORC1 activation.

Interventions Along mTORC1 Signaling



Sen et. al. JAMA 2013

Figure A.10. Proposed mechanism by which G6P accumulation regulates load-induced mTORC1 activation. The intersections of the metabolic pathway of glucose transport and phosphorylation with the molecular signaling pathways addressed in the study are shown. We propose that rapamycin (mTORC1 inhibitor), metformin (AMPK activator), or LVAD (mechanical unloading) protect the heart from metabolic stress at high workload. G6P indicates glucose-6-phosphate; mTORC1, mammalian target of rapamycin complex 1; AMPK, AMP kinase; LVAD, left ventricular assist device; HK, hexokinase; TSC, or tuberous sclerosis complex, is composed of TSC1 (hamartin) and TSC2 (tuberin).

These findings deserve consideration in a broader context. Although the normal heart preferentially oxidizes fatty acids, the increased energy requirements of hearts subjected to high workload are met by the oxidation of carbohydrates (Goodwin GW, Taylor CS, Taegtmeyer H. JBC 1998). The classic explanation for this phenomenon is

based on the hypothesis that the heart oxidizes the most efficient substrate for a given environment (Taegtmeyer H, Hems R, Krebs HA. *Biochem J* 1980). Aside from merely providing energy for cell function, however, glucose metabolites also regulate gene expressions in the liver, pancreatic β -cells (Girard J, Ferre P, Foufelle F. *Annu Rev Nutr* 1997; Schuit FC et. al. *Diabetes* 2001), and heart (Young ME et. al. *Gene Regul Syst Bio* 2007). More recently, we have suggested that the glucose metabolite G6P mediates activation of the transcription factor carbohydrate responsive binding protein (ChrebP) (Li MV et. al. *Biochem Biophys Res Commun* 2010) and that G6P activates insulin-dependent mTOR signaling in the unstressed heart (Sharma S. et. al. *Cardiovasc Res* 2007). We now provide evidence in 3 models (mouse, rat, and human heart) to suggest that load-induced mTOR activation and the ensuing ER stress are mediated by G6P, as well.

Until now, no study has addressed whether cardiac substrate metabolism can regulate “load-induced” hypertrophy via the mTOR signaling pathway (Shioi T et. al. *Circ* 2003; McMullen JR et. al. *Circ* 2004; Zhang D et. al. *JCI* 2010). Our findings in the working heart *ex vivo* demonstrate that acute increases in workload require glucose metabolism to activate mTOR, suggesting that “load-induced” hypertrophic signaling through mTORC1 is substrate specific. More to the point, we propose that mTORC1 is activated by the metabolic signal G6P, which accumulates at increased workload when rates of glucose uptake exceed the heart's oxidative capacity for glucose. The G6P hypothesis is confirmed by the glucose analogue 2-deoxyglucose, which is phosphorylated to 2-deoxyglucose 6-phosphate and not metabolized further, resulting in strong activation of mTOR (Figure A.4C). In contrast, the glucose analogue

3-O-methylglucose, which is transported into the cell and not phosphorylated, exhibited no effect on mTOR activation (Figure A.4C). We consider this evidence compelling and in support of our hypothesis.

The metabolic findings require a discussion of mTOR activation by a metabolic signal. In the unstimulated state, mTORC1 is inhibited by the heterodimer tuberous sclerosis complex (TSC), composed of hamartin (TSC1) and tuberin (TSC2). Differential phosphorylation states of TSC2 are necessary to dissociate the complex to release its inhibition on mTORC1. We dissected the load- and substrate dependence of mTORC1 signaling in the heart and determined that increased workload alone triggers PI3K, Akt, and minimal Akt-dependent phosphorylation of TSC2 at Ser939, regardless of glucose. However, complete load-induced mTORC1 activation requires downregulation of AMPK-dependent phosphorylation of TSC2 at Ser1387, which occurs with G6P accumulation. Indeed, AMPK activation with metformin, both *in vivo* and *ex vivo*, prevents G6P-mediated mTOR activation at increased workload. In skeletal muscle, high levels of glucose activate mTOR in an AMPK-dependent manner by modulating the redox state (Saha AK et. al. Diabetes 2010). In heart, the redox state does not change with workload (Taegtmeyer H. JMCC 1985). However, like in skeletal muscle, AMPK downregulation by glucose in the heart occurs independently of the energy state, which is consistent with previous work both *ex vivo* (Taegtmeyer H. JMCC 1985) and *in vivo* (Balaban RS, Kontor HL, Katz LA, Briggs RW. Science 1986). In the genetically modified ACSL1^{-/-} mouse, in which cardiac glucose metabolism is upregulated (like a heart subjected to increased workload), mTOR activation correlates with G6P accumulation and AMPK downregulation independent of change in the

AMP/ATP ratio (Ellis JM et. al. Mol Cell Biol 2011). Taken together, our study reveals that load-induced mTOR activation is mediated by changes in glucose metabolism.

Excessive glucose uptake by the heart has been associated with contractile dysfunction and deemed glucotoxic by increasing flux through the hexosamine biosynthetic pathway, dysregulating protein glycosylation, and producing reactive oxygen species (Modesti A et. al. Diabetes 2005; Ren J and Davidoff AJ. Am J Physiol 1997). Genetically modified mice that take up excess glucose but also demonstrate enhanced glycolytic flux are, however, protected from glucotoxicity (Taegtmeyer H, McNulty P, and Young ME. Circ 2002; Liao R et. al. Circ 2002). We now propose that intermediary glucose metabolite (G6P) accumulation itself may impose metabolic stress on the heart and contribute to contractile dysfunction by activating mTORC1.

Rapamycin pretreatment also rescues G6P-mediated ER stress and cardiac dysfunction at increased workload. Rapamycin binds and disrupts the mTOR complexes. We now discover that its indirect metabolic effects may mediate via its inhibition of mTOR complexes. Prolonged rapamycin treatment inhibits mTORC2 assembly, which prevents phosphorylation of Akt (Sarboassov DD et. al. Mol Cell 2006), a known regulator of glucose uptake in the heart (Gong LN et. al. Mol Endocrinol 1997). Therefore, not surprisingly, we observed that rapamycin administration blunts Akt phosphorylation and rates of glucose uptake at increased workload. In doing so, rapamycin prevents the mismatch between glucose uptake and oxidation, depletes intracardiac G6P, and inhibits mTOR complexes.

Despite lowering rates of myocardial glucose uptake and oxidation to “unstressed” levels, rapamycin treatment also improves cardiac power (Figures A.1 and A.4). From an energetic perspective, this suggests that the increased energy requirements of hearts subjected to high workload, which are met by the oxidation of carbohydrates, may largely be responsible for fueling protein turnover and protein quality control (“internal work”). Protein turnover utilizes roughly 15% to 20% of a cell's energy in the resting state (Waterlow JC. *Q J Exp Physiol* 1984) and at least 3 times more energy during times of growth (Laurent GJ and Millward DJ. *Fed Proc* 1980; Lane N and Martin W. *Nature* 2010). It is, therefore, tempting to speculate that the energy conserved by rapamycin's inhibition of protein synthesis and the resulting ER stress improves cardiac efficiency and contributes to its ability to reverse load-induced cardiac dysfunction (Shioi T et. al. *Circ* 2003; McMullen JR et. al. *Circ* 2004; Martin TM et. al. *JCI* 2011). Furthermore, the improvement in cardiac power observed in rapamycin-treated rats gives credence to the hypothesis that the hypertrophic process may not be necessary to maintain systolic function in hearts subjected to increased workload (Hill JA et. al. *Circ* 2000). Our results offer a new perspective on the energy cost of protein synthesis and protein quality control.

Metformin is known to improve cardiac function in murine models of heart failure (Yin M et. al. *Am J Physiol Heart Circ Physiol* 2011; Gundewar S et. al. *Circ Res* 2009). When administered systemically, metformin also improves the oxidative capacity of the heart, blunts G6P accumulation, and improves cardiac function. Therefore, we propose that, like rapamycin, metformin metabolically protects hearts

subjected to increased workload and, in doing so, may account for improving survival in diabetic patients with heart failure (Aguilar D et. al. Circ Heart Fail 2011).

We now report that in hearts from a cohort of 11 nondiabetic patients with idiopathic dilated cardiomyopathy and heart failure, mechanical unloading with an LVAD reduces intracardiac G6P levels and decreases mTORC1 activation. We observed a significant decrease in G6P accumulation after LVAD support. We have previously observed decreased myocardial glycogen content in failing human hearts after mechanical unloading (Razeghi P and Taegtmeier H. Cardiovasc Res 2004), and more recently, proteomic analysis has revealed upregulation of proteins involved in glycolysis, energy, and oxidative metabolism in LVAD-supported patients (de Weger RA et. al. J Heart Lung Transplant 2011). Taken together, these studies support our findings and suggest that mechanical unloading promotes recoupling of glucose uptake and oxidation, and prevents intermediary metabolite accumulation. However, we wish to emphasize that we relied on metabolic and/or pharmacologic interventions in our experimental work. The results are therefore largely descriptive, and off-target effects cannot be discounted.

Finally, previous studies performed in rat models of progressive hypertrophy used the tracer FDG analogue and semiquantitative measurements of myocardial FDG standardized uptake value with partial volume corrections (Handa N et. al. Ann Nucl Med 2007). We have shown quantitatively *in vivo* that enhanced glucose uptake in the heart accompanies load-induced contractile dysfunction before an increase in left ventricular mass. When increased, workload was sustained for up to 4 weeks, and increased wall thickness and HW/BW ratio directly correlated with increased FDG

retention, suggesting that metabolic remodeling precedes and sustains structural remodeling of the heart.

In summary, we have provided evidence in support of the concept that metabolic remodeling precedes, triggers, and sustains structural remodeling of the heart. Specifically, we propose that dysregulated glucose metabolism and subsequent G6P accumulation mediate load-induced mTOR activation and contractile dysfunction. Our study highlights the general notion that intermediary metabolism is a rich source of signals for cardiac growth and demonstrates the potential to reduce internal work and improve cardiac efficiency by targeting the metabolic axis in load-induced heart disease.

A.5 References

1. Goodwin GW, Taylor CS, Taegtmeyer H. Regulation of energy metabolism of the heart during acute increase in heart work. *J Biol Chem.* 1998; 273:29530-29539
2. Bishop S, Altschuld R. Increased glycolytic metabolism in cardiac hypertrophy and congestive heart failure. *Am J Physiol.* 1970; 218:153-159
3. Dorn GW, II, Force T. Protein kinase cascades in the regulation of cardiac hypertrophy. *J Clin Invest.* 2005; 115:527-537
4. Taegtmeyer H, Overturf ML. Effects of moderate hypertension on cardiac function and metabolism in the rabbit. *Hypertension.* 1988; 11:416-426
5. Sharma S, Guthrie PH, Chan SS, Haq S, Taegtmeyer H. Glucose phosphorylation is required for insulin-dependent mTOR signalling in the heart. *Cardiovasc Res.* 2007; 76:71-80
6. Huang J, Manning BD. The TSC1-TSC2 complex: a molecular switchboard controlling cell growth. *Biochem J.* 2008; 412:179-190
7. Inoki K, Li Y, Zhu T, Wu J, Guan KL. TSC2 is phosphorylated and inhibited by AKT and suppresses mTOR signalling. *Nat Cell Biol.* 2002; 4:648-657
8. Shioi T, McMullen JR, Tarnavski O, Converso K, Sherwood MC, Manning WJ, Izumo S. Rapamycin attenuates load-induced cardiac hypertrophy in mice. *Circulation.* 2003; 107:1664-1670
9. Proud CG. Regulation of mammalian translation factors by nutrients. *Eur J Biochem.* 2002; 269:5338-5349
10. Ozcan U, Ozcan L, Yilmaz E, Duvel K, Sahin M, Manning BD, Hotamisligil GS. Loss of the tuberous sclerosis complex tumor suppressors triggers the unfolded protein response to regulate insulin signaling and apoptosis. *Mol Cell.* 2008; 29:541-551
11. Okada K, Minamino T, Tsukamoto Y, Liao Y, Tsukamoto O, Takashima S, Hirata A, Fujita M, Nagamachi Y, Nakatani T, Yutani C, Ozawa K, Ogawa S, Tomoike H, Hori M, Kitakaze M. Prolonged endoplasmic reticulum stress in hypertrophic and failing heart after aortic constriction: possible contribution of endoplasmic reticulum stress to cardiac myocyte apoptosis. *Circulation.* 2004; 110:705-712
12. Rockman H, Ross R, Harris A, Knowlton K, Steinhilber M, Field L, Ross J, Chien K. Segregation of atrial-specific and inducible expression of an atrial natriuretic factor transgene in an in vivo murine model of cardiac hypertrophy. *Proc Natl Acad Sci USA.* 1991; 88:8277-8281
13. Taegtmeyer H, Hems R, Krebs HA. Utilization of energy-providing substrates in the isolated working rat heart. *Biochem J.* 1980; 186:701-711

14. Russell RR, Mommessin JI, Taegtmeier H. Propionyl-l-carnitine-mediated improvement in contractile function of rat hearts oxidizing acetoacetate. *Am J Physiol.* 1995; 268:H441-H447
15. Doenst T, Taegtmeier H. Kinetic differences and similarities among 3 tracers of myocardial glucose uptake. *J Nucl Med.* 2000; 41:488-492
16. Katz J, Dunn A. Glucose-2-*t* as a tracer for glucose metabolism. *Biochemistry.* 1967; 6:1-5
17. Taegtmeier H. On the role of the purine nucleotide cycle in the isolated working rat heart. *J Mol Cell Cardiol.* 1985; 17:1013-1018
18. Bergmeyer HU. *Methods of Enzymatic Analysis.* 1974Deerfield Beach, FL: Verlag-Chemie International
19. Liao Y, Takashima S, Asano Y, Asakura M, Ogai A, Shintani Y, Minamino T, Asanuma H, Sanada S, Kim J, Ogita H, Tomoike H, Hori M, Kitakaze M. Activation of adenosine a1 receptor attenuates cardiac hypertrophy and prevents heart failure in murine left ventricular pressure-overload model. *Circ Res.* 2003;93:759-766
20. Locke LW, Berr SS, Kundu BK. Image-derived input function from cardiac gated maximum a posteriori reconstructed PET images in mice. *Mol Imaging Biol.* 2011; 13:342-347
21. Nguyễn VTB, Mossberg KA, Tewson TJ, Wong WH, Rowe RW, Coleman GC, Taegtmeier H. Temporal analysis of myocardial glucose metabolism by 18F-2-deoxy-2-fluoro-d-glucose. *Am J Physiol.* 1990; 259:H1022-H1031
22. Berr SS, Roy RJ, French BA, Yang Z, Gilson W, Kramer CM, Epstein FH. Black blood gradient echo cine magnetic resonance imaging of the mouse heart. *Magn Reson Med.* 2005; 53:1074-1079
23. Vinnakota KC, Bassingthwaighte JB. Myocardial density and composition: a basis for calculating intracellular metabolite concentrations. *Am J Physiol Heart Circ Physiol.* 2004; 286:H1742-H1749
24. He H, Giordano FJ, Hilal-Dandan R, Choi DJ, Rockman HA, McDonough PM, Bluhm WF, Meyer M, Sayen MR, Swanson E, Dillmann WH. Overexpression of the rat sarcoplasmic reticulum Ca²⁺ ATPase gene in the heart of transgenic mice accelerates calcium transients and cardiac relaxation. *J Clin Invest.* 1997;100:380-389
25. Pinz I, Tian R, Belke D, Swanson E, Dillmann W, Ingwall JS. Compromised myocardial energetics in hypertrophied mouse hearts diminish the beneficial effect of overexpressing SERCA2a. *J Biol Chem.* 2011;286:10163-10168
26. Razeghi P, Sharma S, Ying J, Li YP, Stepkowski S, Reid MB, Taegtmeier H. Atrophic remodeling of the heart in vivo simultaneously activates pathways of protein synthesis and degradation. *Circulation.* 2003;108:2536-2541

27. Harmancey R, Wilson CR, Wright NR, Taegtmeier H. Western diet changes cardiac acyl-CoA composition in obese rats: a potential role for hepatic lipogenesis. *J Lipid Res.* 2010; 51:1380-1393
28. Glembotski CC. The role of the unfolded protein response in the heart. *J Mol Cell Cardiol.* 2008; 44:453-459
29. Belke DD, Swanson E, Suarez J, Scott BT, Stenbit AE, Dillmann WH. Increased expression of SERCA in the hearts of transgenic mice results in increased oxidation of glucose. *Am J Physiol Heart Circ Physiol.* 2007; 292:H1755-H1763
30. Razeghi P, Young ME, Alcorn JL, Moravec CS, Frazier OH, Taegtmeier H. Metabolic gene expression in fetal and failing human heart. *Circulation.* 2001; 104:2923-2931
31. Girard J, Ferre P, Foufelle F. Mechanisms by which carbohydrates regulate expression of genes for glycolytic and lipogenic enzymes. *Annu Rev Nutr.* 1997; 17:325-352
32. Schuit FC, Huypens P, Heimberg H, Pipeleers DG. Glucose sensing in pancreatic beta-cells: a model for the study of other glucose-regulated cells in gut, pancreas, and hypothalamus. *Diabetes.* 2001; 50:1-11
33. Young ME, Yan J, Razeghi P, Cooksey RC, Guthrie PH, Stepkowski SM, McClain DA, Tian R, Taegtmeier H. Proposed regulation of gene expression by glucose in rodent heart. *Gene Regul Syst Bio.* 2007; 1:251-262
34. Li MV, Chen W, Harmancey RN, Nuotio-Antar AM, Imamura M, Saha P, Taegtmeier H, Chan L. Glucose-6-phosphate mediates activation of the carbohydrate responsive binding protein (ChREBP). *Biochem Biophys Res Commun.* 2010; 395:395-400
35. McMullen JR, Sherwood MC, Tarnavski O, Zhang L, Dorfman AL, Shioi T, Izumo S. Inhibition of mTOR signaling with rapamycin regresses established cardiac hypertrophy induced by pressure overload. *Circulation.* 2004; 109:3050-3055
36. Zhang D, Contu R, Latronico MV, Zhang J, Rizzi R, Catalucci D, Miyamoto S, Huang K, Ceci M, Gu Y, Dalton ND, Peterson KL, Guan KL, Brown JH, Chen J, Sonenberg N, Condorelli G. mTORC1 regulates cardiac function and myocyte survival through 4e-bp1 inhibition in mice. *J Clin Invest.* 2010; 120:2805-2816
37. Saha AK, Xu XJ, Lawson E, Deoliveira R, Brandon AE, Kraegen EW, Ruderman NB. Downregulation of AMPK accompanies leucine- and glucose-induced increases in protein synthesis and insulin resistance in rat skeletal muscle. *Diabetes.* 2010; 59:2426-2434
38. Balaban RS, Kontor HL, Katz LA, Briggs RW. Relation between work and phosphate metabolite in the in vivo paced mammalian heart. *Science.* 1986; 232:1121-1123

39. Ellis JM, Mentock SM, Depetrillo MA, Koves TR, Sen S, Watkins SM, Muoio DM, Cline GW, Taegtmeyer H, Shulman GI, Willis MS, Coleman RA. Mouse cardiac acyl coenzyme a synthetase 1 deficiency impairs fatty acid oxidation and induces cardiac hypertrophy. *Mol Cell Biol.* 2011; 31:1252-1262
40. Modesti A, Bertolozzi I, Gamberi T, Marchetta M, Lumachi C, Coppo M, Moroni F, Toscano T, Lucchese G, Gensini GF, Modesti PA. Hyperglycemia activates JAK2 signaling pathway in human failing myocytes via angiotensin II-mediated oxidative stress. *Diabetes.* 2005; 54:394-401
41. Ren J, Davidoff AJ. Diabetes rapidly induces contractile dysfunctions in isolated ventricular myocytes. *Am J Physiol.* 1997; 272:H148-H158
42. Taegtmeyer H, McNulty P, Young ME. Adaptation and maladaptation of the heart in diabetes: part I: general concepts. *Circulation.* 2002; 105:1727-1733
43. Liao R, Mohit J, Lei C, D'Agostino J, Aiello F, Luptak I, Ngoy S, Mortensen R, Tian R. Cardiac-specific overexpression of GLUT1 prevents the development of heart failure due to pressure-overload in mice. *Circulation.* 2002; 106:2125-2131
44. Tang WH, Cheng WT, Kravtsov GM, Tong XY, Hou XY, Chung SK, Chung SS. Cardiac contractile dysfunction during acute hyperglycemia due to impairment of SERCA by polyol pathway-mediated oxidative stress. *Am J Physiol Cell Physiol.* 2010; 299:C643-C653
45. Dudek J, Benedix J, Cappel S, Greiner M, Jalal C, Muller L, Zimmermann R. Functions and pathologies of BiP and its interaction partners. *Cell Mol Life Sci.* 2009; 66:1556-1569
46. Rubenstein RC, Zeitlin PL. A pilot clinical trial of oral sodium 4-phenylbutyrate (Buphenyl) in deltaF508-homozygous cystic fibrosis patients: partial restoration of nasal epithelial CFTR function. *Am J Respir Crit Care Med.* 1998; 157:484-490
47. Sarbassov DD, Ali SM, Sengupta S, Sheen JH, Hsu PP, Bagley AF, Markhard AL, Sabatini DM. Prolonged rapamycin treatment inhibits mTORC2 assembly and AKT/PKB. *Mol Cell.* 2006; 22:159-168
48. Cong LN, Chen H, Li Y, Zhou L, McGibbon MA, Taylor SI, Quon MJ. Physiological role of AKT in insulin-stimulated translocation of GLUT4 in transfected rat adipose cells. *Mol Endocrinol.* 1997; 11:1881-1890
49. Waterlow JC. Protein turnover with special reference to man. *Q J Exp Physiol.* 1984; 69:409-438
50. Laurent GJ, Millward DJ. Protein turnover during skeletal muscle hypertrophy. *Fed Proc.* 1980; 39:42-47
51. Lane N, Martin W. The energetics of genome complexity. *Nature.* 2010; 467:929-934
52. Marin TM, Keith K, Davies B, Conner DA, Guha P, Kalaitzidis D, Wu X, Lauriol J, Wang B, Bauer M, Bronson R, Franchini KG, Neel BG, Kontaridis MI. Rapamycin

reverses hypertrophic cardiomyopathy in a mouse model of leopard syndrome-associated PTPN11 mutation. *J Clin Invest.* 2011; 121:1026-1043

53. Hill JA, Karimi M, Kutschke W, Davisson RL, Zimmerman K, Wang Z, Kerber RE, Weiss RM. Cardiac hypertrophy is not a required compensatory response to short-term pressure overload. *Circulation.* 2000; 101:2863-2869

54. Dong Y, Zhang M, Wang S, Liang B, Zhao Z, Liu C, Wu M, Choi HC, Lyons TJ, Zou MH. Activation of AMP-activated protein kinase inhibits oxidized LDL-triggered endoplasmic reticulum stress in vivo. *Diabetes.* 2010; 59:1386-1396

55. Yeh CH, Chen TP, Wang YC, Lin YM, Fang SW. AMP-activated protein kinase activation during cardioplegia-induced hypoxia/reoxygenation injury attenuates cardiomyocytic apoptosis via reduction of endoplasmic reticulum stress. *Mediators Inflamm.* 2010; 2010:130636

56. Yin M, van der Horst IC, van Melle JP, Qian C, van Gilst WH, Sillje HH, de Boer RA. Metformin improves cardiac function in a non-diabetic rat model of post-MI heart failure. *Am J Physiol Heart Circ Physiol.* 2011; 301:H459-H468

57. Gundewar S, Calvert JW, Jha S, Toedt-Pingel I, Ji SY, Nunez D, Ramachandran A, Anaya-Cisneros M, Tian R, Lefer DJ. Activation of AMP-activated protein kinase by metformin improves left ventricular function and survival in heart failure. *Circ Res.* 2009; 104:403-411

58. Aguilar D, Chan W, Bozkurt B, Ramasubbu K, Deswal A. Metformin use and mortality in ambulatory patients with diabetes and heart failure. *Circ Heart Fail.* 2011; 4:53-58

59. Razeghi P, Taegtmeier H. Activity of the AKT/GSK-3beta pathway in the failing human heart before and after left ventricular assist device support (letter to editor). *Cardiovasc Res.* 2004; 61:196-197

60. de Weger RA, Schipper ME, Siera-de Koning E, van der Weide P, van Oosterhout MF, Quadir R, Steenbergen-Nakken H, Lahpor JR, de Jonge N, Bovenschen N. Proteomic profiling of the human failing heart after left ventricular assist device support. *J Heart Lung Transplant.* 2011; 30:497-506

61. Handa N, Magata Y, Mukai T, Nishina T, Konishi J, Komeda M. Quantitative FDG-uptake by positron emission tomography in progressive hypertrophy of rat hearts in vivo. *Ann Nucl Med.* 2007; 21:569-576

VITA

Henry Cheng-Ju Wu was born in Taipei, Taiwan, the second of two sons, to Chen-Jung Thomas Wu and Li-Cheng Lillian Lee. After finishing high school at St. Stephen's Episcopal School in Austin, Texas in 2003, he continued his education in Washington University in St. Louis (St. Louis, Missouri). He earned a Bachelor of Arts degree with a major in biology and a one-class-shy-of-a-minor in mathematics. In May of 2007, he started his graduate education in the MD/PhD program at The University of Texas Medical School at Houston. He completed three years of medical school before beginning his PhD training at The University of Texas Health Graduate School of Biomedical Sciences. He will graduate in August 2015 and further his training by applying for graduate medical education.